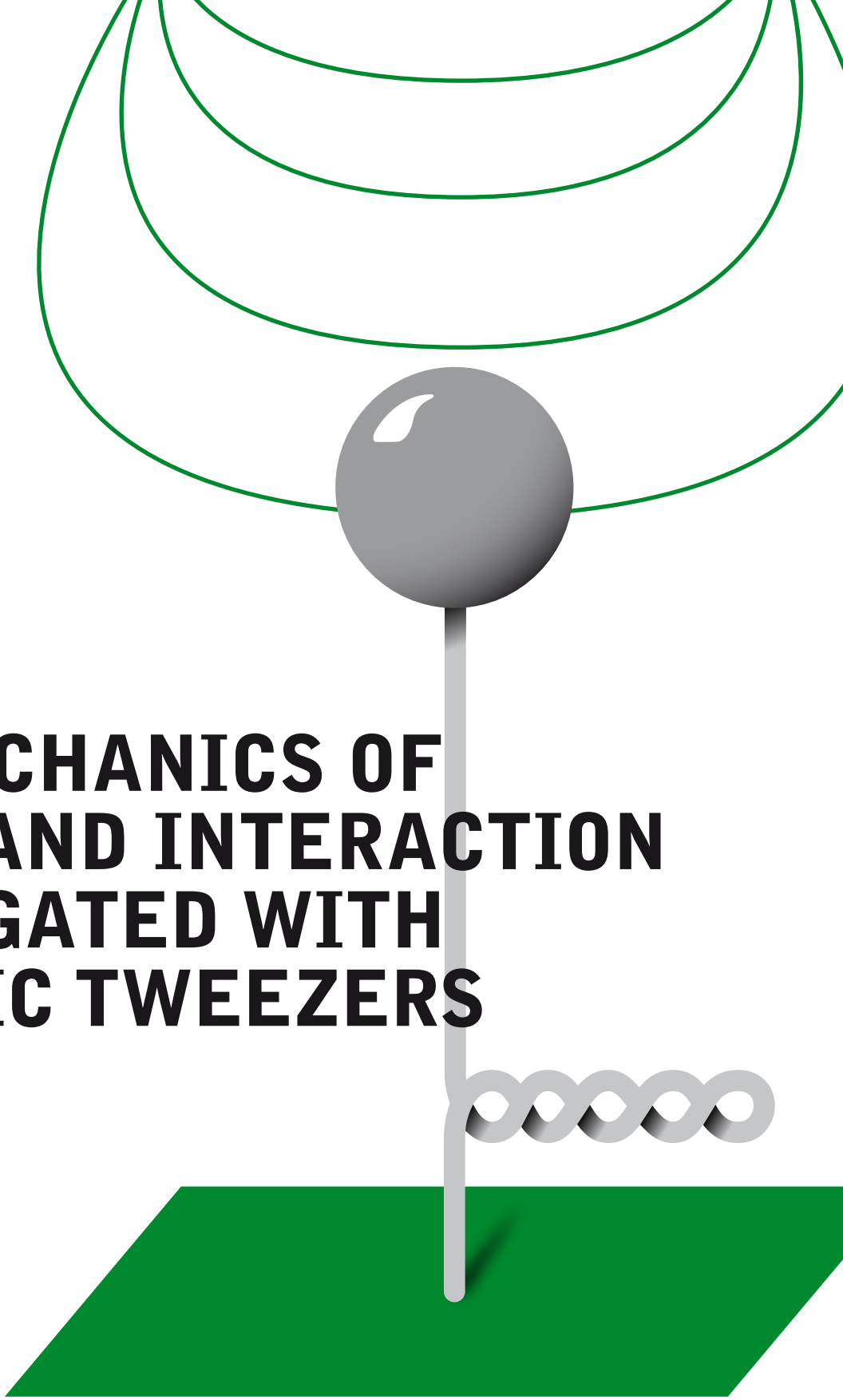

NANOMECHANICS OF DNA-LIGAND INTERACTION INVESTIGATED WITH MAGNETIC TWEEZERS

CUMULATIVE DISSERTATION

YING WANG

Dissertation zur Erlangung des Doktorgrades
Doktorin der Naturwissenschaften Dr. rer. nat.

Nanomechanics of DNA-Ligand Interaction Investigated with Magnetic Tweezers

vorgelegt von
M. Sc. Ying Wang
Bielefeld, 10.03.2017

Erster Gutachter: Prof. Dr. Phil. II Dario Anselmetti
Experimentelle Biophysik & angewandte Nanowissenschaften
Fakultät für Physik, Universität Bielefeld
Zweiter Gutachter: Prof. Dr. Phil. II Thomas Huser
Biomolekulare Photonik
Fakultät für Physik, Universität Bielefeld

Contents

List of publications

[I]. Rational Design of a Cytotoxic Dinuclear Cu_2 Complex That Binds by Molecular Recognition at Two Neighboring Phosphates of the DNA Backbone
T. Jany, A. Moreth, C. Gruschka, A. Sischka, A. Spiering, M. Dieding, Y. Wang, S. Haji Samo, A. Stammler, H. Bögge, G. Fischer von Mollard, D. Anselmetti, and T. Glaser. *Inorganic Chemistry*, Vol. 54, pp. 2679-2690, 2015. DOI: 10.1021/ic5028465

[II]. Nanomechanics of Fluorescent DNA Dyes on DNA Investigated by Magnetic Tweezers
Y. Wang, A. Sischka, V. Walhorn, K. Tönsing and D. Anselmetti. *Biophysical Journal*, Vol. 111, pp. 1604-1611, 2016. DOI: 10.1016/j.bpj.2016.08.042

[III]. Binding Mechanism of Fluorescent Dyes to DNA Characterized by Magnetic Tweezers
Y. Wang, H. Schellenberg, V. Walhorn, K. Tönsing and D. Anselmetti. *Materials Today: Proceedings*. 2017 (Accepted, in press).

[IV]. Binding Mechanism of PicoGreen to DNA characterized by Magnetic Tweezers and Fluorescence Spectroscopy
Y. Wang, H. Schellenberg, V. Walhorn, K. Toensing and D. Anselmetti. *European Biophysics Journal*. 2017 (Online first). DOI: 10.1007/s00249-017-1204-z.

[V]. Biophysical Characterization of the Association of Histones with Single-stranded DNA
Y. Wang, L. van Merwyk, K. Toensing, V. Walhorn, D. Anselmetti and X. Fernàndez-Busquets. *Biochimica et Biophysica Acta*. 2017 (Submitted).

Chapter 1

Introduction

"Life sciences" is an umbrella term which recaps several scientific disciplines that focus on the study of living organisms and the working principles of life. Despite the notion life sciences itself being rather new, several of the comprising scientific disciplines are performed for several hundred years. For instance, the term biophysics, which refers to the study of biological systems by means of physical methods, was introduced by Pearson in 1892 [1]. Even earlier, Young and Helmholtz already examined the hemodynamics and the transmission speed of the nerve signals carried along a nerve fiber, respectively, and can thereby be regarded as the first biophysicists [2–4].

Since the second half of the 20th century, with the emerging of the single molecule sensitive assays, biophysical sciences experienced a qualitative leap. The well-known optical tweezers (OT) and atomic force microscopy (AFM) were developed in the late 1980s. In the early 1990s, magnetic tweezers (MT) joined the team [5]. Notably, the applications of these techniques are all mechanical. In fact, the most classical physical term "force" is present as a key concept overall in biology. On the cellular level, for example, the interaction between the molecular motor actin and its physiological substrate myosin generates a force and thus results in the contraction of muscle cells [4]. In the perspective of receptor-ligand systems, with a tensile force a catch bond can occur within a certain force interval instead of a typical slip bond, i.e. the dissociation lifetime of the bond increases [6, 7]. Regarding a biopolymer as a receptor, the binding of ligands can induce conformational changes and thereby leads to tensions [8, 9]. For this reason, application and measurement of forces is always a meaningful method to observe and

investigate biological processes.

One of the most interesting observation objects is the carrier of the hereditary information deoxyribonucleic acid (DNA), which is a long biopolymer consisting of two helically wrapped phosphate strands that are bridged by nucleobases.

Applying forces on a DNA polymer with above mentioned single-molecule techniques, the single biomolecule can be extended and its physical characteristics like the length and rigidity can be revealed. Performing force-clamp experiments, the (nano)mechanical behavior of the biopolymer can be observed in real time. Magnetic tweezers differ themselves from other single-molecule techniques with two major unique advantages. Firstly, the extremely high force resolution of a few femto newton extends the low force region of the force spectra in the mechanical studies, leading to a considerably precise analysis of the elastic properties [10, 11]. Secondly, MT are capable of applying torque. Consequently, a single biomolecule can be twisted while the force response reveals information about the intramolecular structure [10, 12–17]. With the advanced magnetic torque tweezers developed by the Dekker Lab of Delft University of Technology, this torsional torque can even be measured in both magnitude and direction [17–20]. Furthermore, regarding proteins as biopolymers, the protein-protein interaction, i.e. the protein folding and unfolding, can also be observed with magnetic tweezers. For instance, Chen et al. reported lately an investigation about the unfolding mechanism of the actin crosslinking protein filamin A immunoglobulin-like repeats (IgFLNa) 20–21 [17, 21]. In cell studies, the elasticity of the cell membrane is also observable with magnetic tweezers via attaching magnetic particles on the cell surface [17, 22]. Very recently, two work groups (Schlierf group from Dresden University of Technology and Seidel group from University of Leipzig) have combined magnetic tweezers with the optical method fluorescence microscopy and realized a simultaneous bimodal measuring methodology [23, 24]. Due to these superiorities, magnetic tweezers are employed as the major tool in this work.

From a molecular perspective, DNA acts as a receptor for other binding partners, chemically called ligands, such as proteins and reagents. In this thesis, DNA-ligand systems involving the interaction of DNA with proteins, fluorophors and chemotherapeutic agents are investigated on the single molecule level by means of the single-molecule mechanoscopy. Using

the nanomechanical and structural properties of a bare DNA molecule as a reference, ligand induced influences on DNA can be deduced. Furthermore, the functionality of such ligands can be identified.

In general, DNA is a biological polymer consisting of nucleotides that encode all genetic information. In prokaryote cells, the genome is a (supercoiled) DNA plasmid which is located in the cytoplasm, together with other cellular components such as proteins, metabolites etc.. Eukaryote cells are much bigger and more complex and therefore bear a much larger genome. For example, the DNA of a human cell is about 2 m long [25]. Here, it is contained in the cell nucleus which has only a diameter of about several micrometers. The secret of holding DNA in such a small space is its packing with the help of histone proteins. Via the interaction with histones, DNA winds itself around these proteins and can thus be packed into a dense, highly organized chromosome conformation (chromatin). However, for biological processes like replication and transcription, DNA must be firstly freed from the chromosome form to the naked double stranded form, followed by a transition to the single-stranded structure. The role of the packing proteins histones in these processes is not well understood. Therefore, the possibility of the interaction between histones and single-stranded DNA is explored and discussed in this thesis.

In order to visualize DNA as well as the DNA-containing cell nucleus for an observation and investigation under a microscope, normally, DNA staining reagents are used. Many of these reagents are fluorescent dyes. Due to the luminescent functionality of their fluorophors, DNA containing samples can be visualized. However, the labeling of such dyes influences the structural and mechanical properties of DNA. In this thesis, the fluorescent dyes induced mechanical impacts on DNA are investigated. These studies may contribute to more accurate insights for DNA/cell researches choosing a more proper DNA reagent with an appropriate concentration.

In the perspective of genetics, the hereditary information carried by DNA determines the biological properties of an organism. Taking humans as an example, all features of appearance like body size, eye color and even number of teeth are the expression of the genetic information. Notably, predispositions to certain diseases, e.g. cancer, are also coded in the genes. In recent decades, the global population suffering from cancer continues to grow, which promotes the development of anticancer drugs. In this thesis,

a rational design of a potential anticancer drug with more efficient and stronger efficacy is described. Its interaction with DNA and thereby induced effects on cancer cells are explained as well.

Chapter 2

Background and theory

2.1 DNA

2.1.1 Chemical structure

Deoxyribonucleic acid (DNA) was discovered first by Miescher in 1869 which he at that time called "nuclein" [26]. Since DNA was found by Avery et al. as the carrier of hereditary information of life in 1944, it has become one of the best studied biological polymers [27]. Its chemical structure was firstly determined by Crick and Watson in 1953 inspired by Franklin's "Photo 51" [28, 29].

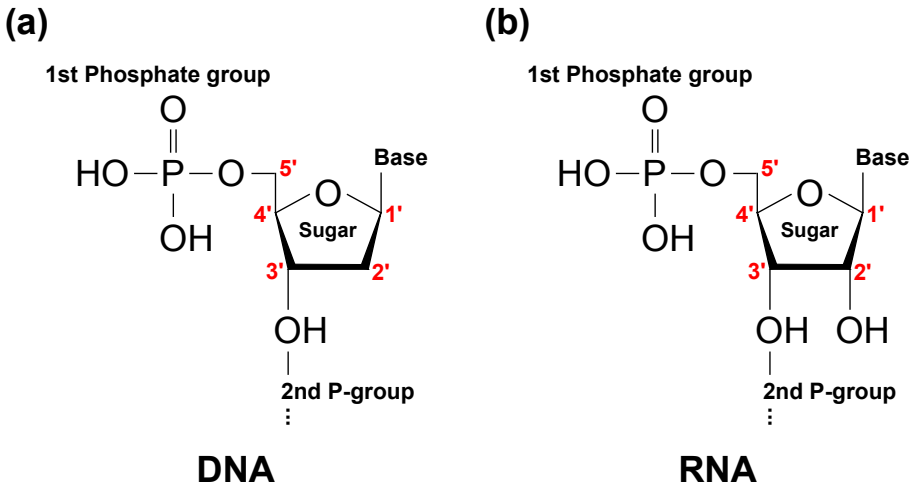

Figure 2.1: Chemical structure of a (**(a)** DNA- and **(b)** RNA-) nucleotide. It consists of a phosphate group, a sugar (**(a)** deoxyribose for DNA and **(b)** ribose for RNA) and a base.

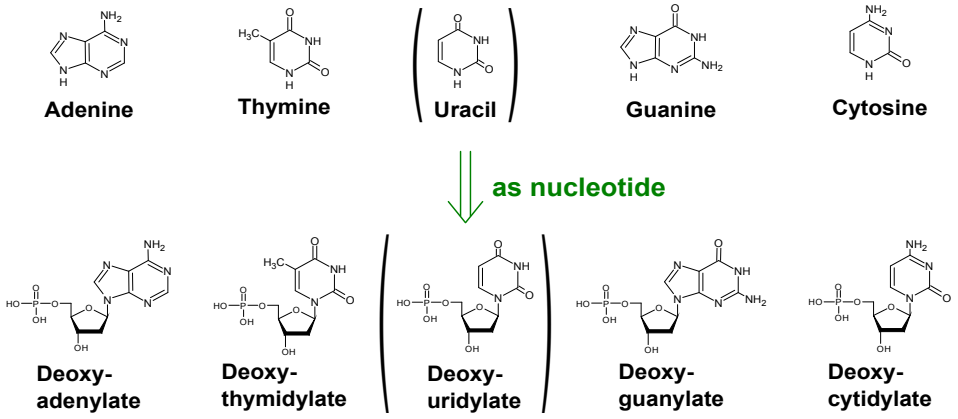

Figure 2.2: Chemical structures of the four heterocyclic bases adenine, thymine, guanine and cytosine, respectively. In RNA, thymine is replaced by uracil. Combined with phosphate group and sugar, they are named deoxyadenylate, deoxythymidylate, deoxyguanylate and deoxycytidylate, respectively. Deoxyuridylate is rarely found in natural DNA, however, it can be used to complement deoxyadenylate, e.g. in DNA functionalization.

Nowadays, DNA is well known as a polymer with many repetitive nucleotides consisting of a phosphate group (P-group), a sugar (deoxyribose) and an aromatic base (Fig. 2.1(a)). Through a phosphodiester bond, the phosphate group is connected to the 5'-carbon of the sugar whose 3'-carbon can be further bound to the next phosphate group of a neighboring nucleotide. As a result, a single-stranded polymer chain with a directionality of 5'-to-3' is formed. Bound to the 1'-carbon of the (deoxy)ribose is a base which carries hereditary information. There are four types of DNA bases in nature which are adenine (A), thymine (T), guanine (G) and cytosine (C) (Fig. 2.2), constituting nucleotides of deoxyadenylate (dA), deoxythymidylate (dT), deoxyguanylate (dG) and deoxycytidylate (dC), respectively. These bases are of two types: adenine and guanine belong to purines, whereas thymine and cytosine are pyrimidines. Each base type can bind specifically to one other base type complementarily through hydrogen bonds: adenine and thymine are connected by two hydrogen bonds while guanine and cytosine form three (Fig. 2.3). Two connected bases are called a base pair. Mostly, DNA is present in a fully-complemented, double-stranded form. Two complementary anti-parallel strands wind around each other resulting in a double helical conformation.

Besides DNA, ribonucleic acid (RNA) also plays an important role in

life. In replication and transcription processes, the genetic information of DNA is written into RNA. Similar to DNA, an RNA nucleotide consists of a phosphate group, a sugar (ribose) and an organic base. Instead of thymine, uracil (U) is present on the RNA polymer chain and is called uridylate as a nucleotide. Deoxyuridylate (dU) is barely found in natural DNA, however, it can be used to complement dA e.g. in DNA functionalization (see Section 3.2 for an application).

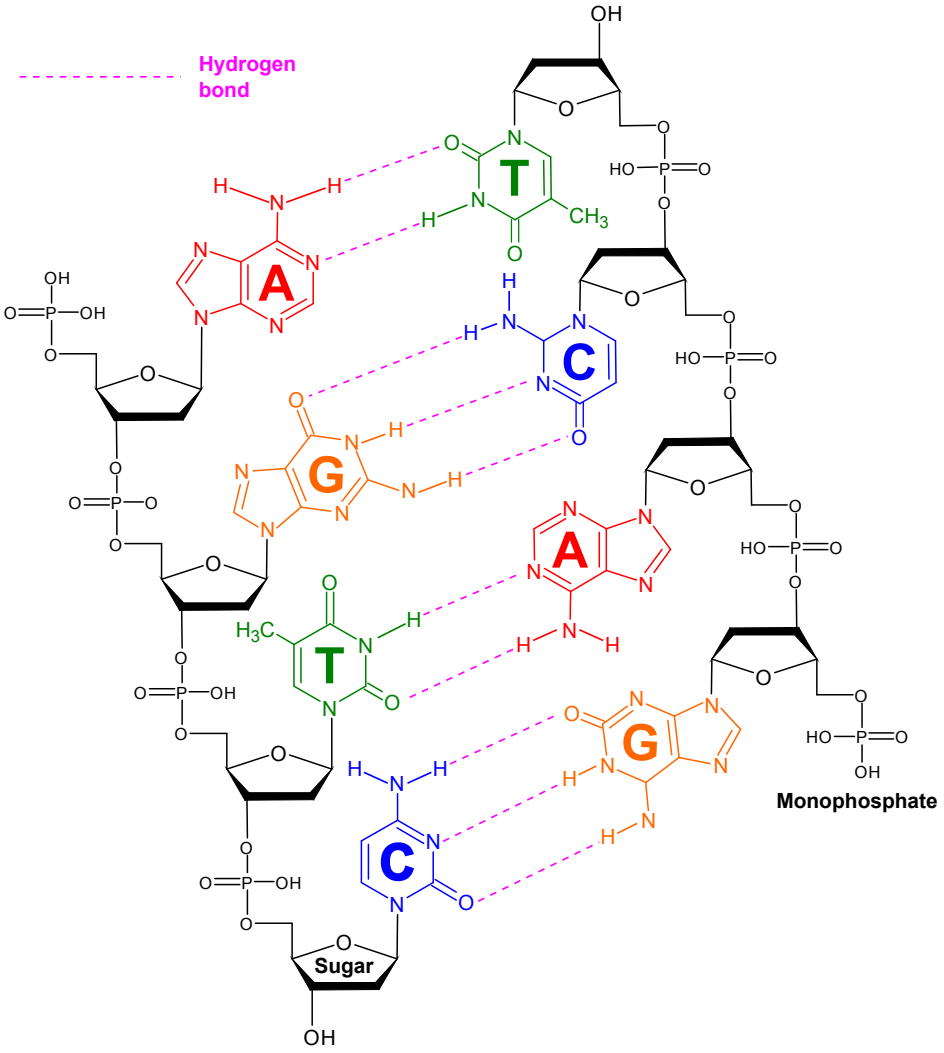

Figure 2.3: Each base type is complementary to one other base type. They bind to each other through hydrogen bonds (A = T and C ≡ G).

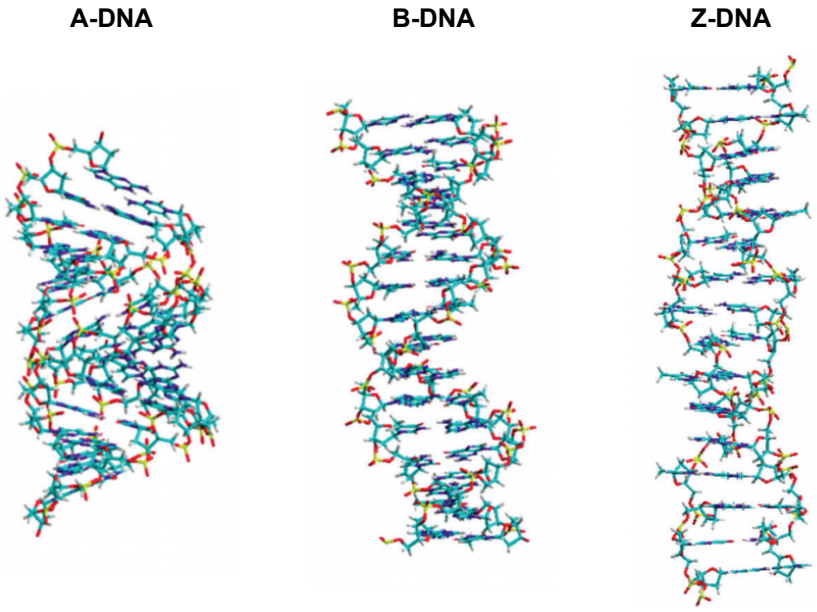

Figure 2.4: In nature, DNA can be found in three possible conformations: A-, B- and Z-DNA. (Source: [30], reuse with permission from *Royal Society of Chemistry*)

2.1.2 DNA conformation

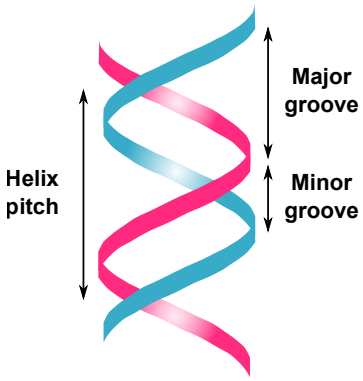

Figure 2.5: A helix pitch consists of about 10 base pairs which can be divided into a wide major groove and a narrow minor groove. The length of a helix pitch is about 3.4 nm.

Because of the different sequence-combinations of neighboring base pairs, DNA strands exist in several different conformations [31–39]. In nature, so far three possible conformations have been identified: B-DNA, A-DNA and Z-DNA (Fig. 2.4).

The majority of DNA found in functional cells exists in the B-like form. It is typical for mixed base sequences, whereas other conformations usually require special base sequences or special conditions to be realized [30, 37]. The DNA B-conformation, suggested firstly by Watson and Crick in 1953 [28], is a right-handed helix with a diameter of about 2 nm. A helical turn of 360° (called a helix pitch) consists of 10.5 base pairs, each of which occupies a

rotation of about 35.9° and a rise of 0.34 nm [40]. These 10.5 base pairs can be divided into two parts: a wide major groove and a narrow minor groove (Fig. 2.5). The major groove is favored by sequence-specific protein bindings while other sequence-nonspecific associations mostly occur in the minor groove [37, 39]. The lambda-DNA (λ-DNA) probed in this work possesses a B-conformation.

In absence of water, B-DNA can turn into an A-conformation. With certain purine/pyrimidine stretches (at least four purines/pyrimidines in a row), A-DNA can also occur in high hydration [37]. Like B-DNA, this conformation exhibits a right-handed double helix but with a helical winding of 32.7° per base pair. Each helix pitch consists of 10.7 base pairs where the rise of a base pair is equal to 0.26 nm. In contrast to B-DNA, the major groove of A-DNA is narrow and deep while the minor groove is wide and shallow [40]. Once, A-conformation was considered lacking biological function. However, DiMaio and coworkers have recently found a virus SIRV2 (Sulfolobus islandicus rod-shaped virus 2) surviving in extreme conditions (high temperature and acidity) with an A-conformation of its DNA [41]. Furthermore, association of certain proteins with B-DNA may also result in a conformation-transition to A-DNA [37, 42, 43].

Unlike the right-handed families, the left-handed Z-DNA appears for special DNA sequences, especially with alternating purine-pyrimidine tracts (e.g. CGCGCG) [30, 37]. The left-handed helix has a diameter of nearly 2 nm. Distinguished from B-/A-DNA, the Z-conformation possesses 2 base pairs as a repeating unit which rotates 60° left-handedly. The distance between two base pairs was characterized as 0.37 nm [40]. The minor groove of Z-DNA is narrow and deep, the major groove is hardly existent [37, 39]. Z-DNA was firstly characterized as a DNA-conformation with high salt-condition [34]. It has been later also understood as an underwound form of the double helix serving as a relaxation of torsional tension in negatively supercoiled B-DNA [39, 44].

2.1.3 Secondary structure

A secondary structure is mostly explored in native single-stranded DNA (ssDNA). In addition to above described DNA conformations, a DNA duplex may also be composed of one self-folded strand. Self-complementary sequences can fold upon themselves and generate stem-loop conformations.

Such a loop structure is called a hairpin [40]. Furthermore, some nearly self-complementary single strands may hybridize and form a duplex with internal loops. Such strands with internal loops prefer to entwine with each other despite of some consecutive mismatches [45]. As a result, single-stranded DNA in physiological conditions often exhibits a complicated cluster conformation.

2.1.4 Superhelical form

Like other macro-molecules, native DNA always seeks a configuration with minimum energy, corresponding to the double helix of B-conformation in physiological environment. Once DNA is bent and twisted, its deformation induces an energetic increase. Via a conformation transition like a plectonemic supercoiling, the DNA polymer is able to reduce the deformation-energy and thus remains in the state with minimum energy (Fig. 2.6) [46].

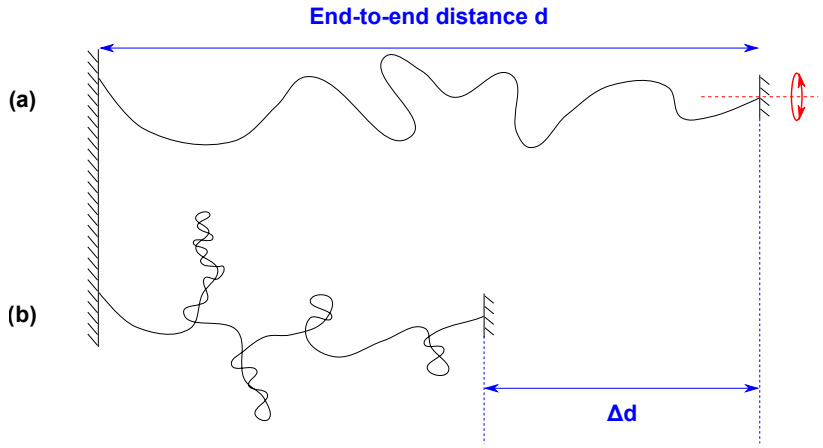

Figure 2.6: Schematic presentation of **(a)** B-DNA double helix; **(b)** Plectonemic supercoiling of the double helix. Through this conformational transition, the DNA polymer can reduce the increased energy introduced from bending, twisting etc. and thus retains the status of minimum energy. A supercoiling structure can be detected as a shortening of the DNA end-to-end distance Δd (see also Fig. 2.13, Sections 2.1.5 and 2.3.2).

In DNA replication and transcription processes, isomerase enzymes topoisomerases influence the topology of DNA and induce tension to the strands. In the configuration of a chromosome, the superhelical structure also has an important role in compressing long chains of DNA into a compact form. Considering the slight DNA unwinding introduced by drug-binding,

a plectonemic supercoiling is the simplest way to relax the torsional tension [40, 46, 47].

2.1.5 Physical characteristics

Electricity and stability

As described above, DNA polymers consist of multiple repetitive P-groups, sugars and heterocyclic bases. Adenine is connected with thymine/ uracil by a double hydrogen bond while guanine is bound to cytosine through a stronger triple hydrogen bond. These base pairs encode the genetic information and establish the internal bridging of both strands. In contrast, neighboring phosphate groups are covalently linked by sugars and thus build an outside phosphate backbone. In aqueous solution, the OH-groups of the phosphate groups are deprotonated, resulting in a negatively charged backbone that straightens the polymer due to the coulomb repulsion. The positively charged cations in the buffer or physiological solution screen the charges of the DNA backbone and thus weaken the repulsion between negatively charged phosphates. This effect leads to an effective reduction of the DNA net charge corresponding to less stabilized strands. The higher the salt concentration in the enviroment, the less stable, i.e. softer the DNA polymer becomes. In theoretical polymer models, this (bending-)stiffness is described by a charateristic length named *persistence length* (see also Section 2.3.2) [48–51]. A larger value of the persistence length corresponds to a stiffer DNA polymer with a lower environmental ionic strength.

Mechanical elasticity

Generally speaking, DNA is an elastic polymer which can be simulated as a spring whose mechanical elasticity (stiffness k) can be described by Hooke's law with applied force F and length change x (Fig. 2.7)

$$k = -\frac{F_{\text{restoring}}}{x} = \frac{F_{\text{applied}}}{x}. \tag{2.1}$$

For DNA, the extension of the "spring" d, equivalent to the distance between the two ends of the polymer, is termed *end-to-end distance* (Fig. 2.8(a)).

However, in fact the double-stranded polymer is much more complicated. Stretched by an external force, DNA shows three different elastic

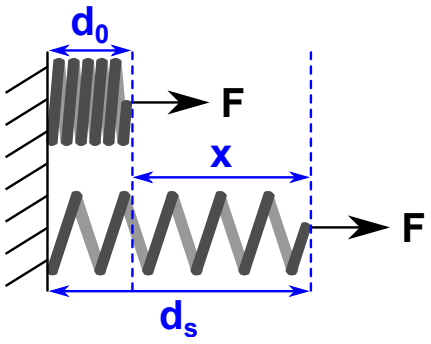

Figure 2.7: The elasticity/stiffness of a spring can be described by Hooke's law.

states corresponding to three force regimes. At small forces up to 10 pN, the polymer elasticity is purely entropic. By further increasing the force, the DNA polymer reaches the intrinsically elastic regime. At about 35 pN, the double helix is stretched straight realizing a base pair distance of 0.34 nm. In this case, the end-to-end distance is an important characteristic of the polymer, called *contour length* L. With even larger forces, the distance between two nucleotide base pairs is further extended. At forces larger than 65 pN, the DNA does not behave elastically any more, since the double strands are overstreched. A polymer deformation from B-DNA to S-DNA (stretched DNA [52]) occurs while the hydrogen bonds between each two nucleotide bases are successively broken. Eventually, the extension between two nucleotide base pairs is enlarged to 0.58 nm. The end-to-end distance in this case is a 1.7-fold of the DNA contour length L [53–56].

Not only overstreching can lead to a polymer deformation, twisting the double strands may also cause a structural change. Overwinding double-stranded DNA (dsDNA) with force over 3 pN results in a DNA deformation from B-DNA to P-DNA (Pauling-like DNA, see also Section 2.3.1) [10, 31, 56]. The elasticity of twisting processes is described in terms of the *torsional stiffness* C [11, 15, 16, 57]

$$C \propto \frac{L\sqrt{P}}{N}, \tag{2.2}$$

where L and P denote the contour- and persistence length of the DNA polymer. The buckling number N defines the crossover regime where double-stranded DNA can not settle torsional stress along the strand anymore. Instead, a configuration of topological plectonemes begins to form (see also Paper II).

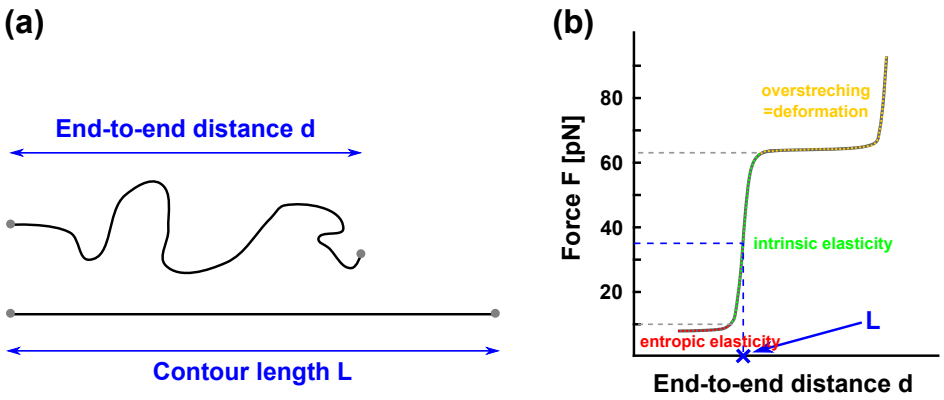

Figure 2.8: **(a)** The distance between two ends of the DNA polymer is named end-to-end distance. Stretched by a force of about 35 pN, the polymer reaches a straight form. The extension of this polymer conformation is described as contour length L, where the rise of a base pair is 0.34 nm. **(b)** Three force regimes correspond to three elastic behaviors of DNA polymer. With forces up to 10 pN, DNA double strands are extended purely entropically. Further increasing the force, the polymer behaves like a spring. From about 65 pN, a deformation from B-DNA to S-DNA occurs due to the overstreching.

2.2 Molecular recognition

2.2.1 Ligand-DNA interaction

The DNA polymer can act as a host molecule for DNA-binding agents such as proteins, drugs etc.. Here, the host molecule DNA is called receptor and the binding agent is referred to as ligand. As described above, sequence-specific proteins prefer binding to DNA major groove regions while the associations of sequence-nonspecific agents like drugs etc. occur predominantly in minor grooves. The interaction between DNA and its ligands is mostly a relatively weak, non-covalent, intermolecular binding, e.g. electrostatic affinity, hydrogen bond or van der Waals interaction.

Electrostatic interaction induces the binding between differently charged ions or functional groups of biological macromolecules. The binding energy E is inversely proportional to the distance between two interacting molecules r, i.e. $E \propto r^{-1}$.

The hydrogen bond is established between a hydrogen donor and a hydrogen acceptor. The hydrogen donor is always a strongly polar group such as OH or NH whereas a hydrogen acceptor is negatively charged due to

a free electron pair. Its binding energy varies from the 1.5-fold up to 15-fold of the thermal energy at room temperature (about 3 - 36 kJ mol^{-1}).

Van der Waals interaction can occur in three terms. Firstly, many biomolecules (dipoles) possess permanent dipole moments which results in an attractive or repulsive van der Waals force, also called Keesom force. Secondly, a permanent dipole can induce a dipole moment on an unpolar neighboring molecule, causing a Debye force. Thirdly, because of the fluctuation of the electron density of both interacting molecules, an instantaneously induced dipole moment can arise on both unpolar molecules. This caused attractive force is called London dispersion force. The binding energy of the van der Waals interaction depends on the distance between two interacting molecules with a relation of $E \propto r^{-6}$ [4, 58].

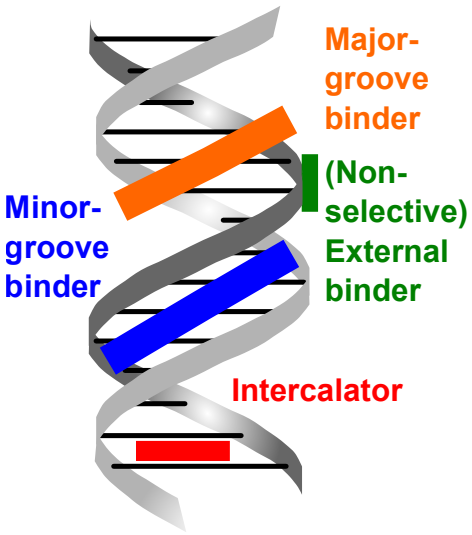

Figure 2.9: In the perspective of binding modes, ligands can be categorized into three major classes, which are non-selective external binder, intercalator and groove binder.

Regarding binding modes, DNA-ligand interactions can basically be categorized into three classes, which are non-selective adherence, intercalation and groove binding (Fig. 2.9). The corresponding ligands are called external binders, intercalators and groove binders.

In the non-selective adherence, positively charged chemical groups of the ligand adhere to the negatively charged DNA backbone via electrostatic attraction. In contrast, the intercalation binding is represented by certain heterocyclic groups of the ligand intercalating into the DNA double strands. The term groove binding refers to the ligand-DNA interaction in the groove regions of the DNA. Within this binding mode, one distinguishes further between major- and minor-groove binding. Whereas nucleo sequence-specific ligands typically associate with DNA in the major groove region, the sequence-nonspecific type usually binds to the minor groove of the double helix [40, 59].

Reaction kinetics

Molecular recognition as introduced before can be described quantitatively by the reaction kinetics of several reactants.

A time-dependent reaction between A and B,

$$\mathrm{A} + \mathrm{B} \xrightarrow{k} \mathrm{AB}$$

with a reaction rate v can be characterized by the temporal derivative of the reactants' concentration $\frac{\mathrm{d}[\mathrm{A}]}{\mathrm{d}t}$ and $\frac{\mathrm{d}[\mathrm{B}]}{\mathrm{d}t}$ [60]

$$v = -\frac{\mathrm{d}[\mathrm{A}]}{\mathrm{d}t} = -\frac{\mathrm{d}[\mathrm{B}]}{\mathrm{d}t} = \frac{\mathrm{d}[\mathrm{AB}]}{\mathrm{d}t}. \tag{2.3}$$

Introducing k as external condition dependent rate coefficient of the reaction, the equation can be expressed as

$$v = k[\mathrm{A}][\mathrm{B}]. \tag{2.4}$$

Basically, the interaction between ligand molecules and DNA can be seen as a simple reversible chemical reaction

$$\mathrm{L} + \mathrm{R} \underset{k_{\mathrm{off}}}{\overset{k_{\mathrm{on}}}{\rightleftharpoons}} \mathrm{LR},$$

where L represents the ligand, R the DNA as the receptor of the ligand and LR stands for the product of the ligand bound to DNA. k_{on} denotes the rate coefficient of the forward reaction and k_{off} that of the reverse reaction. This means that while some ligand molecules bind to DNA, a dissociation between other already bound ones occurs. Differing from the irreversible reaction, the reaction rate can only be discussed considering both reaction directions [61]

$$v = \frac{\mathrm{d}[\mathrm{LR}]}{\mathrm{d}t} = k_{\mathrm{on}}[\mathrm{L}][\mathrm{R}] - k_{\mathrm{off}}[\mathrm{LR}]. \tag{2.5}$$

When the equilibrium of the system is reached, the concentrations of reactants and their product no longer alter, leading to $v = 0$. According to Eq. 2.5, the ratio between k_{on} and k_{off} can be written as

$$\frac{k_{\mathrm{on}}}{k_{\mathrm{off}}} = \frac{[\mathrm{LR}]}{[\mathrm{L}][\mathrm{R}]} = \mathrm{K_a} = \mathrm{K_d^{-1}}, \tag{2.6}$$

which is defined as equilibrium constant of association K_a. Its inverse is called equilibrium constant of dissociation K_d [58]. Both K_a and K_d can be used as a measure of the binding affinity.

2.2.2 Specific binding

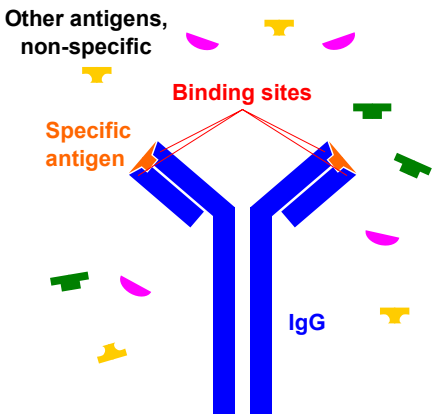

Figure 2.10: IgG has a "Y" shape whose two tips occupy two specific antigen binding sites each. Only antigens of proper size and shape can bind to IgG in a specific binding.

For important biological macromolecules like proteins, highly selective bindings on the proper receptors are necessary for the correct functioning. This can only work if the ligands recognize their partners very precisely among other molecules despite their possibly similar chemical structures. Therefore in 1894, Fischer suggested the *lock and key principle*. He postulated that every detail of the ligand molecules has to fit to the receptor, including complementary charges, their chemical structure and the molecular dimension [62]. Even the binding site must have a proper size and orientation. Such a highly selective binding is called *specific binding*.

The concept of a specific binding is essentially the affinity of this binding. In this thesis, two typical specific bindings are used to functionalize DNA polymers. One of them is the strongest known specific non-covalent binding, being between streptavidin (avidin) and biotin. Streptavidin is a protein purified from the bacterium Streptomyces avidinii. It has an extremely high affinity for biotin which is also known as vitamine B7. The binding affinity K_a between these two substances is about $10^{15}\,\mathrm{M}^{-1}$ [63]. The other used specific binding belongs to an antigen-immunoglobulin G-binding. Immunoglobulin G (IgG), belonging to the family of antibodies, is a large protein with a Y-shape. This protein can recognize specific agents (called antigens) and bind to them so that the infection or attack of such agents on cells can be blocked. On each tip of the "Y" are two specific binding sites which can only be bound by a certain antigen with proper

shape and size (Fig. 2.10). In this work, a sort of steroid digoxigenin acts as antigen where antidigoxigenin (anti-dig) works as antibody. The binding affinity K_a is about $10^9\,M^{-1}$ [64, 65].

2.3 Technique and theoretical models

2.3.1 Magnetic tweezers

Over the last decades, single-molecule force spectroscopy has been widely employed in biological applications. This powerful tool allows for an investigation of nanomechanical properties of individual biomolecules. Among the common force spectroscopic techniques, e.g. atomic force microscopy (AFM) and optical tweezers (OT), magnetic tweezers (MT) present their own advantages. As in typical applications with a common force spectroscopy, MT apply a longitudinal force on a probed single molecule which is immobilized on a functionalized surface. Furthermore, MT can achieve a full rotational control of the molecule by providing torque on the sample-molecule attached paramagnetic particle. In addition, MT allow to perform force-experiments with force as low as several femto newton (fN), which other single-molecule techniques cannot reach. Also, a real time detection of more than one molecule at the same time makes it possible to efficiently study temporary phenomena caused by intermolecular interaction with a statistical significance.

Experimental configuration

The used MT setup is a commercial system purchased from PicoTwist (Lyon, France) as schematically shown in Fig. 2.11 [13, 14]. Magnetic tweezers are essentially a microscope with a detection system mounted beneath the objective lens, a fluid cell and additionally a pair of permanent magnets. A red light-emitting diode (LED) illumination serves as the light source. Together with a 100× oil immersion objective, the observed images from the objective focal plane can be enlarged and recorded by a charge-coupled device (CCD) camera which is connected to a computer. A piezoelectric element can adjust the vertical position of the objective focal plane.

Above the objective, a custom-made flow cell is built on the sample holder. The flow cell is assembled with a glass coverslip occupying a hy-

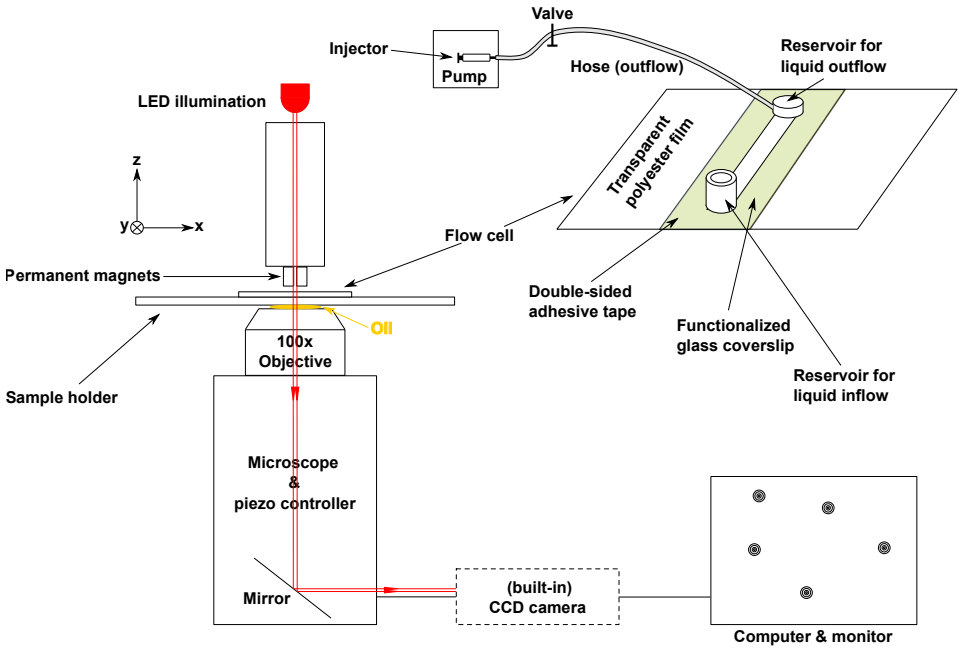

Figure 2.11: Schematic of MT configuration. MT are essentially a microscope system. The core parts of this instrument are a custom-made flow cell and the permanent magnets above it, which allows a longitudinal and rotational manipulation of sample molecules attached paramagnetic particles. The observed image from the objective focal plane can be recorded by a CCD camera and shown on a computer monitor.

drophobic surface, a double-sided adhesive tape cut in the middle and a transparent film. With these components, a chamber is accomplished in the middle of the flow cell. Single molecules can be immobilized between the surface and paramagnetic particles whose vertical position can be tracked by the detective system (for details see "Determination of bead position" below). The flow cell has two reservoirs for flushing in and out aqueous solution. The out-flow reservoir is connected to a pump generating a microfluidic system of the flow cell so that the solution in the chamber can be flushed in/out with a constant flow speed (for details see also Section 3.1).

Above the flow cell, a pair of permanent magnets with an air gap of $z_0 = 0.5\,\mathrm{mm}$ is located and exposes a horizontal (in $\vec{x}$ direction) external magnetic field $\vec{B}$ on the flow cell. This field serves as a magnetic trap allowing translational and torsional control on paramagnetic particles [15, 66, 67]. This magnetic field decreases rapidly in $\vec{z}$ direction away from the

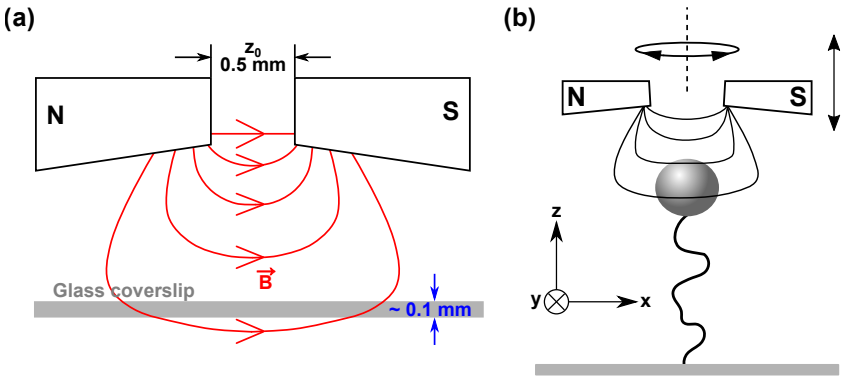

Figure 2.12: (a) A pair of permanent magnets is located over the flow cell with an air gap of 0.5 mm. The magnetic field is strongest in the air gap and decreases in the direction away from the magnets. **(b)** The magnetic field induces a force applying on the probed single molecule attached paramagnetic particle, which in this case is a bead. Moving the magnets vertically varies the induced magnetic force. Rotating the magnets, a torque is applied on the bead, which causes a twisting of the probed molecule.

magnets (Fig. 2.12(a)) with the relation (in first approximation)

$$B(z) = B_0 \exp\left(-\frac{z}{z_0}\right), \tag{2.7}$$

where B_0 is the maximum of the induced magnetic field in the air gap. The induced magnetic force is given by

$$\vec{F} = \frac{1}{2}\nabla(\vec{\mu} \cdot \vec{B}), \tag{2.8}$$

where $\vec{\mu}$ is the magnetic moment of the paramagnetic particle. For each z position, $\vec{F}$ can be seen as a constant force since the fluctuation of the magnetic particle in solution is several magnitudes smaller than the length scale of the magnetic field. Moving the magnets vertically (in $\vec{z}$ direction), the force on the paramagnetic particles can be changed. Similarly, rotating the magnets at a certain z position, a torque $\vec{\Gamma}$ will be generated on particles which can be written as

$$\vec{\Gamma} = \vec{\mu} \times \vec{B}, \tag{2.9}$$

causing a twisting of the probed molecule.

Typical sample model

As previously described, MT can apply forces as low as several fN on the paramagnetic particles (beads, typically). The maximum force is normally less than 100 pN, depending on the size of chosen paramagnetic beads. The force range is quite advantageous to perform experiments with biomolecules since most related non-covalent intermolecular bonds cannot hold larger forces [68–70]. A very interesting application of MT is to study nanomechanical properties of macropolymers like DNA. The DNA can be tethered between a functionalized surface and a paramagnetic bead (Fig. 2.12(b)). The most favorable beads are streptavidin-coated micro-sized beads, e.g. Dynabeads MyOne (⌀ 1 µm) and M270/M280 (⌀ 2.8 µm) (Thermo Fisher Scientific, Waltham, USA).

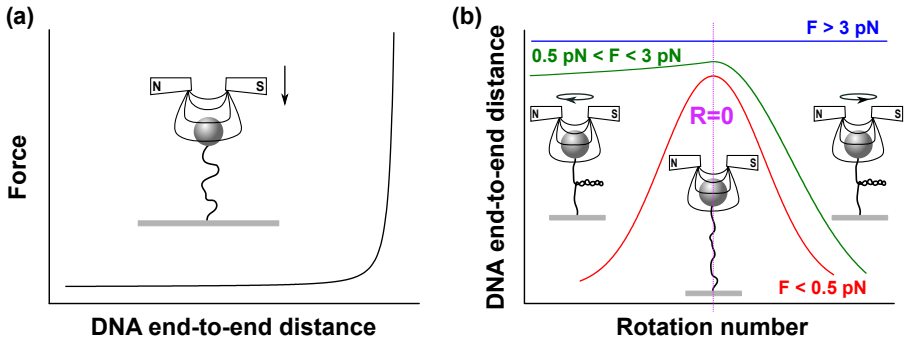

Figure 2.13: Typical measurements with MT. **(a)** The force-extension curve presents a stretching experiment. Moving the magnets to the flow cell, the increased magnetic force pulls the bead higher causing an extension of the DNA molecule. With force lower than 10 pN, the DNA stretching stays in an entropy dominant regime. **(b)** The hat curve presents a rotation experiment. Rotating the magnets with a stretching force up to 0.5 pN in counterclockwise direction, the double helix shows a positively supercoiled conformation. Twisted in the other direction, a negative plectonemic supercoiling is built.

Moving the magnets in negative z-direction, the induced magnetic force increases and pulls the bead higher, thereby extending the DNA molecule. Since the applied force is relatively low (in this work, mostly up to 10 pN), the DNA stretching stays in an entropy dominant regime [11] (Fig. 2.13(a)). Rotating the magnets under a low stretching force (<0.5 pN), a nick-free dsDNA will be twisted which creates plectonemic supercoilings in both rotation directions. The construction of these supercoilings are observed as a reduction of the effective DNA length and represented by a “hat curve”

(Fig. 2.13(b)). If a nick is present in the double helix, the DNA polymer can rotate around its sugar backbone in idle state and thus supercoilings cannot be introduced. In this case, the hat curve shows a rotation-independent constant DNA end-to-end distance. Increasing the stretching force up to 3 pN, an underwinding (negative supercoils) via rotation will not occur since the DNA molecule denatures (DNA melting), yet an overwinding (positive supercoils) can still be observed. At forces larger than 3 pN, the DNA overwinding disappears in the transition of the untwistable polymer to a P-conformation in order to reduce the applied torque [14, 17, 31].

Correction of applied force with Brownian Motion

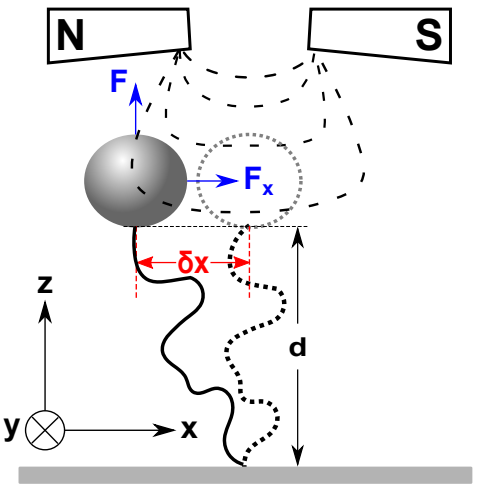

Figure 2.14: In aqueous solution, the DNA-bead setup fluctuates according to the theory of Brownian motion. Only the fluctuation in $\vec{x}$-direction δx along the magnetic field will be considered.

In principle, MT experiments as well as most researches in biological applications are built on the basis of studying biological phenomena and properties in vitro to understand the essence of life in vivo. In order to simulate a physiological environment of the sample object such as DNA molecules, the buffer system plays an important role. Since the whole sample setup is found in aqueous solution, the random Brownian Motion of the DNA-bead along the magnetic field should be taken into account. Accordingly, the magnetic force computed by Eq. 2.8 must be corrected.

Fig. 2.14 shows the schematic diagram of the DNA-bead setup in an aqueous environment. Here, F is the force acting on the bead in z-direction equivalent to the entropic force of DNA. Treating the DNA-bead as a pendulum, a restoring force by the DNA is applied if the bead leaves its equilibrium position. The distance to the equilibrium position can be written as the thermal fluctuation of the bead along the magnetic field in $\vec{x}$-direction δx. The restoring force F_x can be

written as

$$F_x = \frac{F}{d} \cdot \delta x = k \cdot \delta x, \tag{2.10}$$

where F/d indicates the stiffness of the elastic DNA polymer k. According to the equipartition theorem for the harmonic oscillator, the average potential energy $\langle E_p \rangle$ can be written as

$$\langle E_p \rangle = \frac{1}{2} k_{\mathrm{B}} T = \frac{1}{2} k \langle \delta x^2 \rangle, \tag{2.11}$$

where $k_{\mathrm{B}}T$ is the thermal energy with Boltzmann constant k_{B} and temperature T. The force acting on the bead F can be expressed as

$$F = \frac{k_{\mathrm{B}} T d}{\langle \delta x^2 \rangle}. \tag{2.12}$$

Measuring the DNA end-to-end distance d, or rather the bead position, and the variance of the fluctuation of the bead $\langle \delta x^2 \rangle$, the entropic force of the DNA polymer can be determined [13, 15, 17, 66, 67, 71–73].

Determination of bead position

During an MT experiment, real time images will be recorded by the CCD camera and presented on the connected computer monitor. In order to determine the bead's z-position corresponding to the DNA end-to-end distance, an image analysis is necessary. The change of the vertical position of the bead results in a shift of the focal plane of the objective. Using this principle, Gosse and Croquette have developed an image analysis method [71]. Firstly, images of diffraction rings of the bead at different observation planes are recorded as calibration profile (from both sides of the objective's focal plane, Fig. 2.15(a,b)). During the experiment, correlating the real time diffraction images to the calibration profile, the distance between bead and the focal plane can be tracked. Comparing the bead's position with the surface position which can be found using a bead fixed to the surface, the DNA end-to-end distance d can be determined (Fig. 2.15(c)). Recording and correlating the x-position of each frame taken by the CCD camera, $\langle \delta x^2 \rangle$ can be computed. Using Eq. 2.12, the entropic force of the DNA polymer can be yielded.

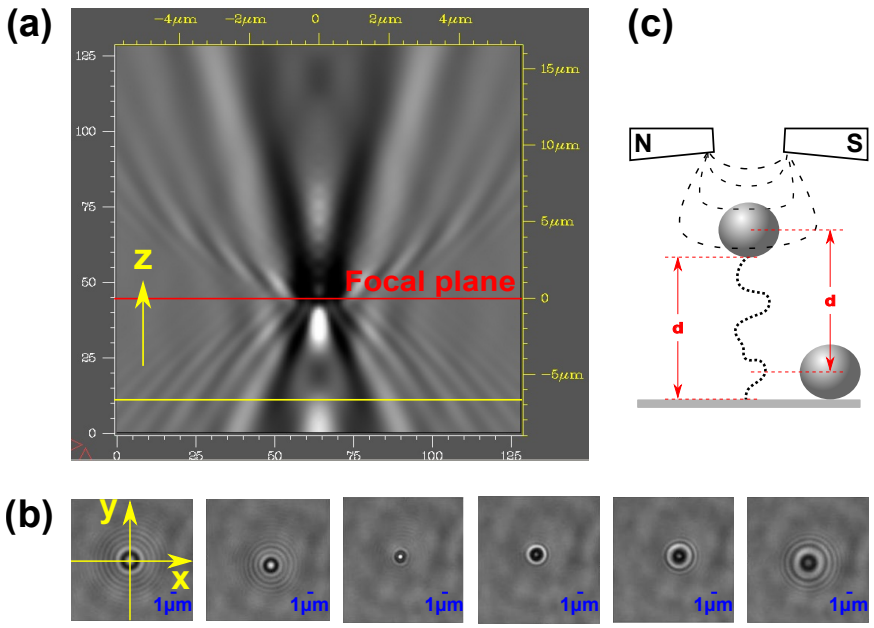

Figure 2.15: **(a)** Images of diffraction rings of the bead as calibration profile can be recorded. Moving the objective upwards from the yellow-line labeled position with unchanged bead-position, the diffraction rings of the bead can be observed as shown in **(b)**. **(c)** Correlating the diffraction pattern, the height of the bead can be tracked. Comparing with the surface position found using a fixed bead, the DNA end-to-end distance d can be determined.

2.3.2 Theoretical polymer models

Freely jointed model and freely rotating model

A DNA polymer in solution follows the thermal motion, therefore the elastic behavior is totally entropic. Whereas entropic force and DNA end-to-end distance can be computed in a relatively straightforward fashion, mechanical properties of the double helix such as contour length and bending stiffness can only be studied in a more indirect way. Therefore, theoretical models for elastic polymers are employed.

To simplify the situation, a polymer can be modeled as a simple chain assembled of N identical segments each with Kuhn length b. The total length of the polymer, called contour length, is thus $L = Nb$ [74]. The simplest model is the *freely jointed chain* (FJC) model proposed by Kuhn in 1936 [75]. In the FJC-model, the segments are considered independent and unoriented, and the polymer is allowed to cross itself (Fig. 2.16(a)). The force acts oppositely to the thermal agitation which disorders the segments.

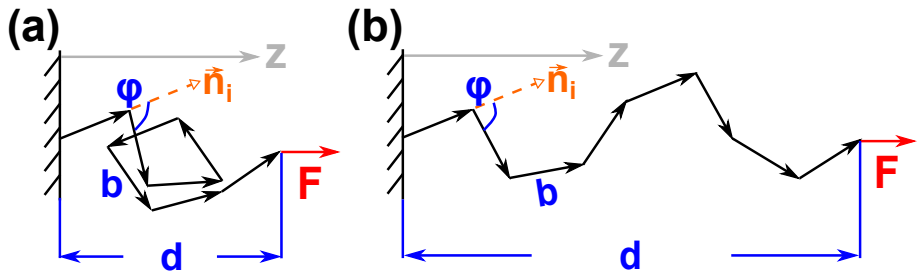

Figure 2.16: A polymer can be modeled as a simple chain. The polymer consists of N segments, each with Kuhn length b. The interaction between monomers is neglected. d indicates the end-to-end distance and the total length L of the polymer is $L = Nb$. **(a)** FJC-model. This model is based on a statistic random walk where the polymer is allowed to cross itself. **(b)** FRC- or WLC-model. The polymer is oriented in direction of the force.

The relation between the entropic force F and the end-to-end distance d is given by

$$d = L\left(\coth\frac{Fb}{k_\mathrm{B}T} - \frac{k_\mathrm{B}T}{Fb}\right). \tag{2.13}$$

In this model, a stiffer polymer is described by a larger Kuhn length b [5]. Considering the possibility that the Kuhn segments are stretchable and alignable under force, the FJC model can be extended to

$$d = L\left(\coth\frac{Fb}{k_\mathrm{B}T} - \frac{k_\mathrm{B}T}{Fb}\right)\left(1 + \frac{F}{K_0}\right) \tag{2.14}$$

introducing a material dependent parameter stretch modulus K_0 [5, 76–78].

Based on the FJC-model, the *freely rotating chain* (FRC) model was developed, replacing the random bond angle between consecutive segments by a fixed bond angle φ. Furthermore, the polymer follows a self-avoiding statistic motion (Fig. 2.16(b)) [79]. These two models fail to describe double-stranded DNA. However, in some ways, they are still good enough to analyze single-stranded DNA polymers.

Worm-like chain model

Whereas both FJC- and FRC-model consider polymers with rigid segments, the *worm-like chain* (WLC) or *Kratky-Porod chain* model describes the elastic behavior of a DNA polymer more precisely [80]. The WLC-model was proposed on the basis of both previous models regarding the polymer as a flexible rod. A characteristic parameter of the DNA bending stiffness

is the persistence length $P = b/2$ [10]. The F-d relation can be written as

$$\frac{FP}{k_{\mathrm{B}}T} = \frac{1}{4}\left(\left(1 - \frac{d}{L}\right)^{-2} - 1\right) + \frac{d}{L}, \tag{2.15}$$

where F, L, P, $k_{\mathrm{B}}T$ and d denote entropic force, DNA contour- and persistence length, thermal energy and DNA end-to-end distance, respectively. Excluding the possible DNA deformation at large forces, the WLC-model can only be used in the force regime with purely entropic elasticity (see also Section 2.1.5) with force up to 10 pN. Here, the failure probability is within 10% [5, 81].

To study the DNA stretched with force in the intrinsic elasticity regime, the extended WLC-model can be employed. Considering the DNA polymer as a stretchable rod, force and DNA contour length should be in positive linear correlation. The extended WLC-model for the force regime between 5 and 50 pN leads to

$$d = L\left(1 - \frac{1}{2}\left(\frac{k_{\mathrm{B}}T}{FP}\right)^{1/2} + \frac{F}{K_0}\right), \tag{2.16}$$

where K_0 denotes a material dependent parameter stretch modulus [53, 82, 83].

With a further increase of the force, the DNA molecule will be overstretched and a transition from the natural B-conformation to an S-conformation takes place [52, 53, 68, 84]. Since MT experiments in this work do not employ forces over 50 pN, the DNA overstretching will not be further discussed here.

Elasticity model of single-stranded DNA polymers

The FJC and WLC models describe well the elastic behavior of an ssDNA polymer stretched with large forces or in a highly salty environment (>3 M). In these cases, the intramolecular electrostatic interactions between monomers are negligible since the monomers are relatively separated or screened from each other, and the DNA can thus be considered as an ideal polymer. However, when the ssDNA polymer is stretched with low forces (<20 pN) in environmental cation concentrations c_{cation} from 20 mM up to 2 M, the ideal polymer models fail [85]. Therefore, a scaling model con-

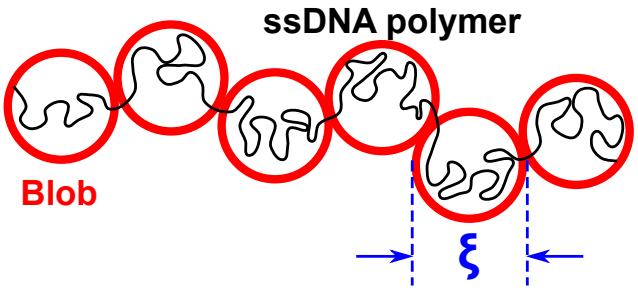

Figure 2.17: Regarding the intramolecular interactions between the monomers of the ssDNA, a scaling model can describe the polymeric elasticity better than the FJC and WLC models. In this model, the ssDNA with a segment length of b consists of several tensile blobs whose size is defined as ξ.

sidering the polymer as a polyelectrolyte composed of several tensile blobs was introduced in order to describe the polymeric elasticity more precisely (Fig. 2.17) [86–92]. Here, the defined tensile screening length ξ, i.e. the size of a single blob, is larger than the length of a single segment b. Normally, the intrastrand base-pairing and subsequent base-pair stacking cause a multitude of intramolecular interaction which make a qualitative description difficult [93]. In order to understand the elasticity of ssDNA more directly, here, only intramolecular electrostatic interactions between Kuhn segments are regarded.

The relation between the DNA end-to-end distance d and the stretching force F can be corrected to

$$d \propto F^{\alpha} \tag{2.17}$$

with α increasing from about 0.6 ($c_{\text{cation}} = 20\,\text{mM}$) up to 0.69 ($c_{\text{cation}} = 2\,\text{M}$) [85, 94]. The dependence of the Kuhn length b on the salt concentration c_{cation} can be expressed as $b \propto c_{\text{cation}}^{-\delta}$ with $\delta \approx 0.4\text{-}0.5$ [85, 95–97]. Introducing an excluded-volume [79, 98] parameter υ including all interactions between the monomers, the scaling model leads to

$$d \sim L \left(\frac{\upsilon}{b}\right)^{1/3} \left(\frac{F}{k_{\text{B}}T}\right)^{2/3}, \tag{2.18}$$

if the monomer interactions are significant [85].

Considering both electrostatic and structural contributions to the polymeric rigidity of the ssDNA, the Kuhn length can be written as sum $b = b_{\text{ele}} + b_{\text{str}}$. Regarding the fact that the sugar backbone of the ssDNA is freely

rotatable in idle state, the electrostatic contribution of the Kuhn length has a linear relation with the Debye length λ_{D} [85, 88, 91, 99]

$$b_{\mathrm{ele}} \sim \lambda_{\mathrm{D}} = \sqrt{\frac{\epsilon_0 \epsilon_{\mathrm{r}} k_{\mathrm{B}} T}{e^2 \sum c_i Z_i^2}}, \tag{2.19}$$

where ϵ_0 and ϵ_{r} denote the vacuum and material-dependent relative permittivity, respectively. The summation describes the doubled total ionic strength of all charges in the system with the molar concentration c_i and charge number Z_i of each charged ion. e is the elementary charge equal to $1.602 \times 10^{-19}\,\mathrm{C}$.

2.3.3 McGhee-von Hippel model

In order to discuss the mechanism of ligands interacting (intercalating) with DNA molecules, in 1974, McGhee and von Hippel proposed a theoretical model including estimating the binding affinity and the binding site size of ligand molecules [100]. The key formula of the *McGhee-von Hippel* model for a non-cooperative ligand is

$$\frac{\nu}{c_{\mathrm{f}}} = K_{\mathrm{a}} (1 - n\nu) \cdot \left(\frac{1 - n\nu}{1 - n\nu + \nu} \right)^{n-1}. \tag{2.20}$$

Here, ν, c_{f}, K_{a} and n represent binding density of the ligand molecules, concentration of free (unbound) ligands in solution, equilibrium constant of association for intercalation and binding site size of one ligand molecule, respectively. The binding density ν is defined as the concentration ratio between bound ligands and DNA (in basepair concentration)

$$\nu = \frac{[\text{bound ligands}]}{[\text{DNA}]} \tag{2.21}$$

with $0 < \nu \leq 1/n$. In this case, the binding of the ligand molecules follows the *nearest-neighbor exclusion principle* implying that between two intercalated molecules, at least one binding site must be unoccupied [101].

In 1992, Williams and coworkers presumed that ligand molecules introduce an elongation of the total molecule length intercalating in DNA double strands [102]. Based on this theory, Vladescu et al. transformed the

McGhee-von Hippel model and rewrote it as

$$\frac{\gamma}{c} = K_{\mathrm{a}} \frac{\Delta x}{x_{\mathrm{bp}}} \cdot \frac{\left(1 - \frac{n\gamma x_{\mathrm{bp}}}{\Delta x}\right)^n}{\left(1 - \frac{(n-1)\gamma x_{\mathrm{bp}}}{\Delta x}\right)^{n-1}}, \tag{2.22}$$

γ being the fractional elongation of DNA depending on the total ligand concentration c

$$\gamma = \frac{L(c) - L_0}{L_0}. \tag{2.23}$$

Δx is the DNA elongation induced by a single ligand molecule and x_{bp} is the rise of a (B-)DNA base pair equivalent to 0.34 nm [103]. Kleinmann et al. have developed this formula for bis-intercalators defining Δx as the DNA elongation induced by each binding site and expressed the model as [104]

$$\frac{\gamma}{c} = K_{\mathrm{a}} \frac{2\Delta x}{x_{\mathrm{bp}}} \cdot \frac{\left(1 - \frac{n\gamma x_{\mathrm{bp}}}{2\Delta x}\right)^n}{\left(1 - \frac{(n-1)\gamma x_{\mathrm{bp}}}{2\Delta x}\right)^{n-1}}. \tag{2.24}$$

Introducing a dimensionless geometrical factor a, indicating the number of binding sites that a ligand molecule occupies, the equilibrium binding model can be represented in the general form [9]

$$\frac{\gamma}{c} = K_{\mathrm{a}} \frac{a\Delta x}{x_{\mathrm{bp}}} \cdot \frac{\left(1 - \frac{n\gamma x_{\mathrm{bp}}}{a\Delta x}\right)^n}{\left(1 - \frac{(n-1)\gamma x_{\mathrm{bp}}}{a\Delta x}\right)^{n-1}}. \tag{2.25}$$

In the case of cooperative ligands, two different binding configurations are assumed. Configuration I is the one for non-cooperative ligand binding. Compared to configuration I, the intercalation of two ligand molecules in DNA in configuration II can be contiguous. The cooperativity factor ω, i.e. the probability ratio between these two binding configurations, is defined as

$$\omega = \frac{P_{\mathrm{conf.II}}}{P_{\mathrm{conf.I}}}. \tag{2.26}$$

A mathematical root term R is furthermore defined as

$$R = \sqrt{(1 - (n+1)\nu)^2 + 4\omega\nu(1 - n\nu)}, \tag{2.27}$$

excluding the unphysical situations like negative ω and ν as well as $\nu > 1/n$. Thus the McGhee-von Hippel model for cooperative ligands is expressed as

$$\frac{\nu}{c_\mathrm{f}} = K(1-n\nu)\cdot\left(\frac{(2\omega+1)(1-n\nu)+\nu-R}{2(\omega-1)(1-n\nu)}\right)^{n-1}\cdot\left(\frac{1-(n+1)\nu+R}{2(1-n\nu)}\right)^{2}, \tag{2.28}$$

where K is the nucleation constant corresponding to K_a in the non-cooperative model [105]. The association constant representing the cooperative interaction is here $K\omega$ instead [100].

Chapter 3

Sample preparation and object ligands

3.1 Flow cell

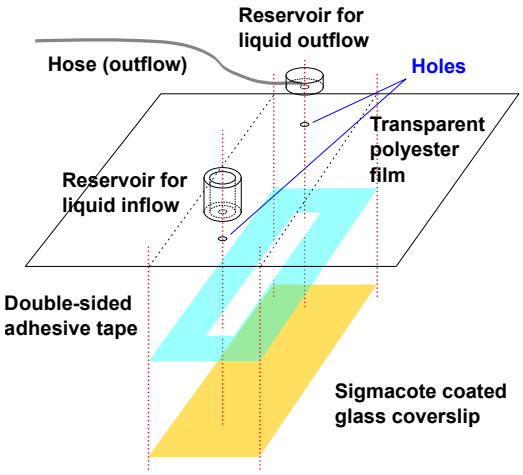

Figure 3.1: Assembly of the flow cell. Two holes in the transparent film are drilled for attaching reservoirs later. A glass coverslip is cleaned and coated with Sigmacote. It can be stuck to the film with a double-sided adhesive tape, which is cut in the middle to achieve a chamber. Two reservoirs made of PMMA are adhered over the holes where the flush-out reservoir is connected with a hose.

As described in Section 2.3.1, the flow cell of MT is assembled with a glass coverslip, a double-sided adhesive tape and a transparent film (Fig. 3.1).

Firstly, two holes are drilled in a 100 µm thick transparent polyester film (85 mm×60 mm, mod. 3560, Avery-Zweckform, Oberlaindern, Germany). Next, a glass coverslip (24 mm×60 mm, about 0.1 mm thick, Menzel glass, Thermo Fisher Scientific, Braunschweig, Germany) is cleaned and covalently coated with Sigmacote (Sigma-Aldrich, Munich, Germany) in a desiccator to produce a homogeneous hydrophobic surface. A double-

sided adhesive tape (acrylate, 70 µm thick, X-film, Lindlar, Germany) is cut in the middle to achieve a chamber and then stuck onto the transparent film. Adhering two reservoirs (polymethylmethacrylat, PMMA) over the holes using also drilled double-sided adhesive tapes, the flow cell is assembled. The flush-in reservoir works as a tank where the solution can be filled in while the flush-out reservoir is connected with a hose as previously described. As a result, the whole chamber occupies a volume of 5 mm×52 mm×70 µm with a hydrophobic surface (Fig. 3.2(a)). Lastly, two-components adhesive (5 min epoxy adhesive, Toolcraft, Conrad, Hirschau, Germany) is applied around the reservoirs to seal the flow cell ensuring a standing fluid when the valve is closed.

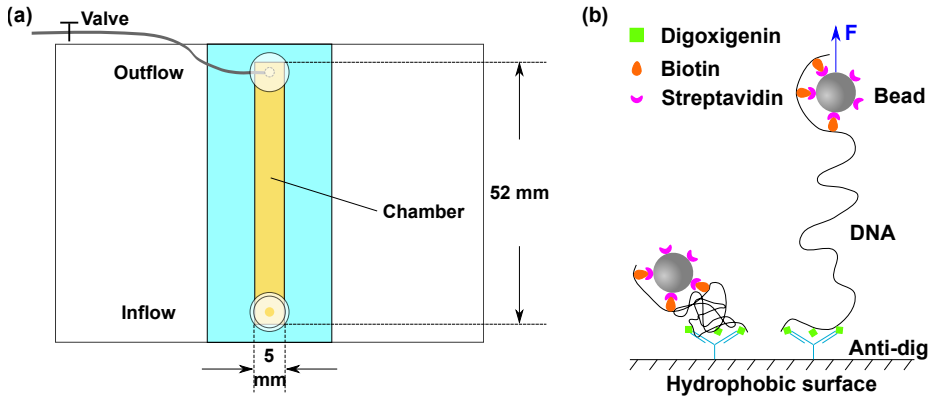

Figure 3.2: **(a)** The fluid chamber occupies a volume of 5 mm×52 mm×70 µm with a hydrophobic surface. **(b)** Anti-digoxigenin solution is flushed into the chamber and binds to the surface non-specifically so that the DNA end functionalized with digoxigenins can further bind to anti-dig.

To attach the DNA molecules on the surface with stable specific bonds, anti-digoxigenin (antibody IgG, 200 µg ml^{-1} solution, Roche, Mannheim, Germany) is flushed into the chamber and incubated for at least two hours at 37 °C. Through non-specific bonds, the Y-shaped proteins are adsorbed tightly to the surface (Fig. 3.2(b)).

In order to prevent possible unexpected non-specific adhesion during experiments, the chamber is passivated for at least 3 hours with a buffer containing 10 mM PBS (phosphate buffered saline, with 137 mM NaCl and 2.7 mM KCl, pH 7.4 at 25 °C, Sigma-Aldrich, Munich, Germany), 0.2 % BSA (bovine serum albumins, Sigma-Aldrich, Munich, Germany), 0.1 % Tween 20 (Sigma-Aldrich, Munich, Germany), 5 mM EDTA (ethylenediaminete-

traacetic acid, Sigma-Aldrich, Munich, Germany) and 10 mM NaN_3 (Sigma-Aldrich, Munich, Germany).

3.2 DNA samples

The DNA molecules for MT experiments must be functionalized. To accomplish stable bonds between the DNA and the surface/bead, specific chemical groups are introduced to the DNA molecules that serve as an anchor and provide a stable connection to the substrate. One DNA end is thus functionalized with digoxigenin and the other end is labeled with biotin (Fig. 3.2(b)).

3.2.1 Functionalization of lambda dsDNA

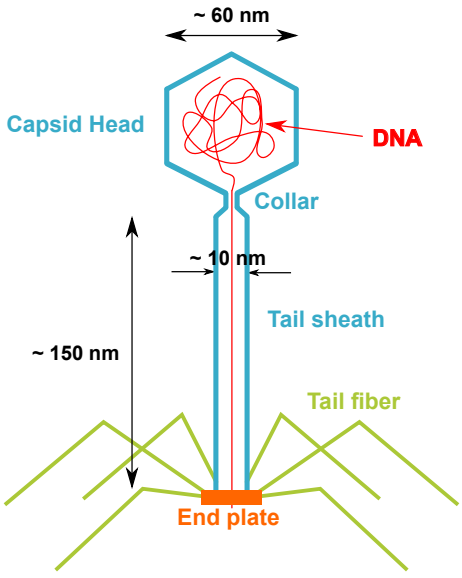

Figure 3.3: The lambda bacteriophage has a capsid head with diameter of about 60 nm, which contains DNA with a length of 48,502 base pairs. This head is made of proteins of several types. When the virus is adsorbed to a host cell, the so called lambda DNA can pass through the 150 nm long tail sheath and be injected into the cell.

Just as the name implies, lambda DNA (λ-DNA) is isolated from the lambda phage, which is a virus that infects the bacterial species Escherichia coli (E.coli). The lambda phage is essentially half protein and half DNA. It primarily consists of a capsid head with diameter of 50-60 nm and a tail which is about 150 nm long and ends in a fiber [106]. The head is made of proteins of several types and contains DNA. The bacteriophage can attach itself to E.coli by binding to the LamB receptor of the host cell. DNA can pass through the vertical tail sheath and be injected into the host cell, thereby infecting the bacterium. λ-DNA is named after the bacteriophage and exhibits a double-stranded B-form helical structure with a length of 48,502 base pairs. Taking into ac-

count that in B-conformation neighboring base pairs are 0.34 nm apart, the contour length of λ-DNA is computed as 16.5 µm [107]. The complete sequence was firstly published in 1982 by Sanger et al. [108]. In the capsid head of the bacteriophage, λ-DNA exists as a linear polymer and but shows a circular form after entering the host cell [109, 110]. In its linear form, λ-DNA has two sticky ends each with 12 bases cos(=cohesive) sequences which are complementary and essential for packaging.

As previously mentioned, MT can apply torque to nick-free single molecules in a controlled manner. Therefore, pre-handled (shortened and repaired) λ-DNA is used as double-stranded DNA model.

For the experiments underlying this thesis, linear λ dsDNA was purchased from New England Biolabs (48,502 bp, N_6-methyladenine-free, NEB, Ipswich, USA) and prepared according to a published [111] and an unpublished protocol (N. Bosaeus & S. Smith, 2009). Firstly, the DNA molecules are functionalized at both cos-sites with biotins applying dNTP (without dCTP, MetaBion, Steinkirchen, Germany), Klenow fragment (3'→5' exo-, NEB, Ipswich, USA) and biotin-14-dCTP (MetaBion, Steinkirchen, Germany). Next, T4-ligase (Thermo Fisher Scientific, Waltham, USA) is added to the mixture in order to connect all nucleotides. To reduce the probability of having nicks on the double strands which is proportional to its length, dsDNA molecules are then shortened. The restriction enzyme EagI (EagI HF, NEB, Ipswich, USA) is added to the DNA solution and cuts each molecule into three shorter fragments (19,944 bp, 16,710 bp and 11,848 bp, Fig. 3.4). The middle fragments are discarded due to their lack of biotin ends. Furthermore, dig-handles are modified via PCR (polymerase chain reaction). For PCR, 48,502 bp λ dsDNA molecules are bound with dNTP, dig-11-dUTP (Roche, Mannheim, Germany), forward- and backward-primers (MetaBion, Steinkirchen, Germany) as shown in Fig. 3.4. Cutting these modified DNA polymers by EagI, a large amount of short fragments with dig-ends are gained by replication. Mixing the dig-handles with the products from the former process, the DNA fragments are then functionalized at one end with biotins and at the other end with digoxigenins. PreCR mixture (PreCR Repair Mix, NEB, Ipswich, USA) are then used to repair all possible nicks on the double strands. Lastly, the sample DNA solution is softly purified in a centrifuge and subsequently stored in 10 mM PBS buffer at 4 °C until use.

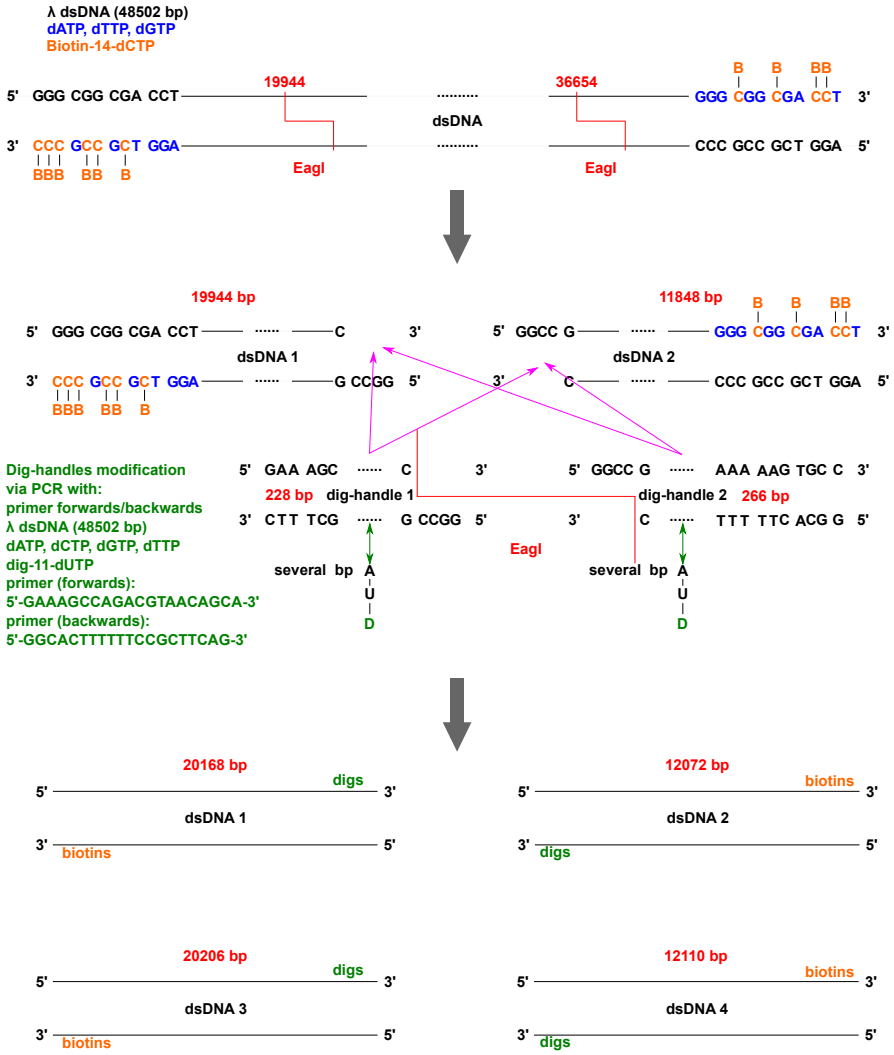

Figure 3.4: Illustration of the DNA modification for MT experiments. After adding biotins to the cos-sites of the linear dsDNA, the double strands are cut by the restriction enzyme EagI at two positions. Discarding the middle one, the two remaining fragments are labeled with several biotins. Applying the dig-handles produced via PCR to the biotin-labeled fragments, the DNA molecules are functionalized at both ends.

3.2.2 Functionalization of M13 ssDNA

As the single-stranded DNA model, DNA isolated from the bacteriophage M13 is employed. M13 was introduced to biological research in 1977 by Messing et al. [112]. It is a filamentous bacteriophage which specifically infects F-plasmid (fertility plasmid) contained male cells of the E.coli bacterium. The DNA within the capsid head is a circular, single-stranded polymer with a length of 7249 bases. Since the distance between two bases in single-stranded DNA is twice as long as the one of double-stranded DNA, thus corresponding to 0.68 nm, M13 ssDNA has a contour length of 4.9 µm [113]. A double-stranded form exists during the DNA replicational process. There are two sorts of M13mp phage DNA named M13mp18 and M13mp19. M13mp19 is almost identical to M13mp18, however it carries different genetic information due to the inverted multiple cloning site region (region of 6231-6288th base). The nucleotide sequences of M13mp18 were firstly determined by Yanisch-Perron and coworkers in 1985 [114], which were later corrected and completed by Ebright et al. in 1992 [115], Stewart in 2002 and Slatko in 2007 (both unpublished, NEB GenBank), respectively.

To perform the ssDNA experiments with MT, the M13 ssDNA is functionalized with biotin-/digoxigenin ends similarly as the λ dsDNA. The circular M13 ssDNA is linearized by coworkers of the Institute for Bioengineering of Catalonia (IBEC, Spain, for details see also Paper V). The primers used in the linearization process are then separated from the single strand. Three customized complementary oligonucleotides (chemically coupled with biotins/digoxigenins, Fig. 3.5, MetaBion, Steinkirchen, Germany) can hybridize with the single strand and realize both biotins-/digoxigenins-function-alized ends of the ssDNA. Until use, ssDNA is stored in the same way like λ dsDNA in 10 mM PBS buffer in a refrigerator at 4 °C.

3.3 MT buffer

MT buffer is used as the environmental buffer for all studies in this work. It is based on 10 mM PBS buffer (containing 137 mM NaCl and 2.7 mM KCl, pH 7.4 at 25 °C) with extra added 0.1 mg ml^{-1} BSA and 0.1 % Tween 20 as blocking agents against non-specific adherence. All substances introduced from Section 3.4 to Section 3.6 are diluted with MT buffer.

Figure 3.5: Three different oligonucleotides are attached to the single-stranded M13 DNA and thus functionalize it with biotin at one end and digoxigenin at the other end.

3.4 $Cu_2(OAc)_2$

The synthesis of $Cu_2(OAc)_2$ ($[(tom^{Me})\{Cu(OAc)\}_2]$) is performed by the Glaser group (Department of Chemistry at Bielefeld University). This cytotoxic dinuclear Cu_2 complex is synthesized as a new possible class of anticancer drugs which, unlike cisplatin (cisplatinum, $Cl_2H_6N_2Pt^{+2}$, [116]), does not bind to the nucleobases of DNA. Instead, via electrostatic interaction, this complex is able to attach itself to the DNA backbone.

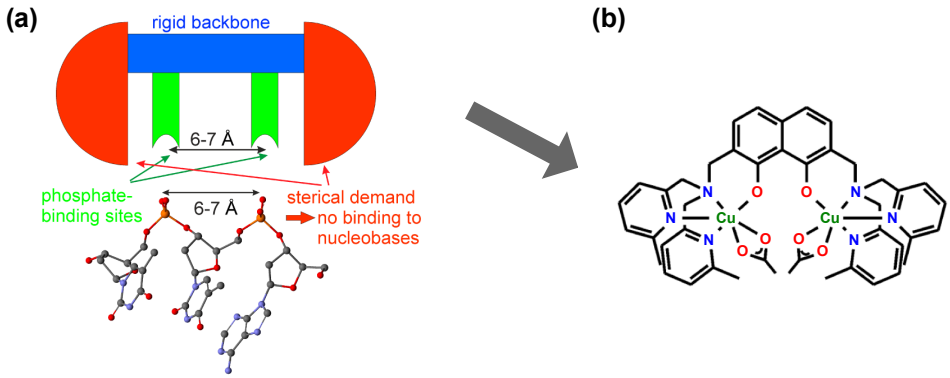

Figure 3.6: **(a)** The design concept of the dinuclear Cu_2 complex: binding to the DNA backbone. Between two metal ions is a distance of 6-7 Å corresponding to the distance between two neighboring phosphate groups of the DNA backbone. This distance is ensured through a rigid backbone. The spatial structure of the molecule prevents it from binding to nucleobases. **(b)** Chemical structure of $Cu_2(OAC)_2$. (Source: Paper I [117], open access)

The concept of the Cu_2 complex is presented in Fig. 3.6. Metal ions, Cu^{II} in this case, are employed here because of their positive charges which have a high affinity to the negatively charged DNA backbone. The distance between $Cu^{II}{}_2$ is about 6-7 Å corresponding to the distance between two neighboring phosphodiester groups. This distance is ensured through a rigid backbone accomplished with MOM_21 (2,7-diformyl-1,8-bis(methoxymethoxy)naphtha-lene, [118]). The two copper ions are thus preorganized to bind to (two) phosphate groups simultaneously. Two DPA^{Me} (di((6-methylpyridin-2-yl)-methyl)amine) serve as sterical blockers preventing the dinuclear complex binding to DNA nucleobases (Fig. 3.6(b)). After binding to the DNA backbone, the complex may introduce a hydrolytic phosphodiester cleavage on the polymer strands. In addition, this binding is irreversible resulting in a sterical hindrance to the association of DNA-polymerases.

Consequently, Cu_2 complexes hinder the DNA replication and transcription leading eventually to cell death (=cytotoxicity).

After the chemical synthesis, the $Cu_2(OAc)_2$ solution is lyophilized and for experiments dissolved and diluted in MT buffer to the required concentrations.

3.5 Fluorescent DNA binding dyes

Fluorescent DNA binding dyes are nowadays widely used to detect and image DNA molecules in biological applications. However, their association alters the nanomechanical properties of the DNA polymer like contour length and bending stiffness. The binding mechanisms of many of such dyes remain still unknown. In this thesis, the focus is on four fluorescent DNA binding dyes, YOYO-1, DAPI, DRAQ5 and PicoGreen. More precisely, their binding characteristics and related structural and nanomechanical influences on the DNA are studied.

3.5.1 YOYO-1

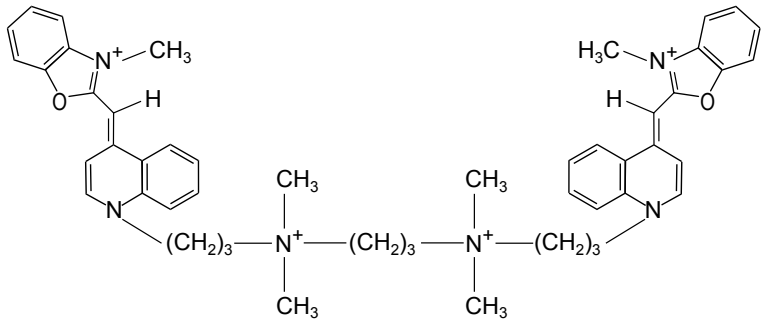

Figure 3.7: Chemical structure of YOYO-1 in solution.

YOYO-1 (1,1'-(4,4,7,7-tetramethyl-4,7-diazaundecamethylene)-bis-4-[3-methyl-2,3-dihydro-(benzo-1,3-oxazole)-2-methylidene]-quinolinium tetraiodide, [119]) is a tetracationic homodimer of oxazole yellow and belongs to the monomethine cyanine family. It can be excited with green light of 491 nm wavelength and shows then an emission maximum at a wavelength of 509 nm. YOYO-1 is one of the most widely used DNA binding dyes due to its photo-bleaching resistance and low background fluorescence of unbound dyes. Here, bound YOYO-1 molecules expose an over 1000-fold

stronger fluorescence emission than free dyes [120]. However, because of its cell-impermeability YOYO-1 can not be applied in cell-labeling. YOYO-1 is known as a bis-intercalator which locally untwists the DNA strands and thus induces a DNA elongation. Its influence on the bending stiffness of DNA is still under discussion. YOYO-1 iodide was purchased from Thermo Fisher Scientific (stock solution 1 mM in DMSO (dimethyl sulfoxide $(CH_3)_2SO$), Waltham, USA). For the conducted experiments, the stock solution is diluted with MT buffer to concentrations from 1 nM up to 10 µM.

3.5.2 DAPI

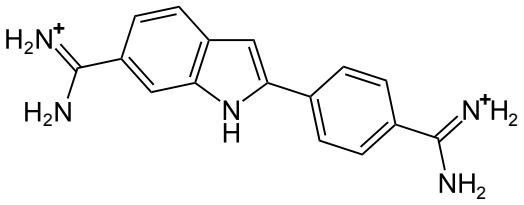

Figure 3.8: Chemical structure of DAPI in solution.

DAPI (4',6-diamidine-2-phenylindole dihydrochloride) is a classical, financially beneficial blue dye which belongs to the indol family. It is often chosen to stain chromosomes in the nucleus due to its cell-permeability. In aqueous solution, free DAPI can be excited by ultraviolet (UV) light at a wavelength of 340 nm and exhibits an emission maximum at a wavelength of 488 nm. Once bound to DNA, the excitation maximum exposes a peak shift of 24 nm ($\lambda_{ex} = 364$ nm) and a 20-fold increase of the fluorescence signal at a wavelength of 454 nm [121]. Since the excitation of the dye is in the UV spectral range, detecting living cells using DAPI interferes with the cell's viability and consequently limits the accessible observation time. DAPI is known as a DNA minor-groove binder which does not elongate the DNA molecule, however, it softens the polymer. DAPI was purchased from Sigma-Aldrich (Munich, Germany). The powder is dissolved in distilled water to a stock solution concentration of 2 mg ml^{-1} and diluted subsequently with MT buffer to concentrations from 1 nM up to 10 µM for experiments.

3.5.3 DRAQ5

In contrast to DAPI, the membrane-permeable dye DRAQ5 (deep red fluorescent antraquinone dye Nr. 5, 1,5-bis{[2-(di-methylamino) ethyl]amino} -4,8-dihydroxyanthracene-9,10-dione) has an excitation wavelength in the red spectral range (λ_{ex} = 646 nm) which is less harmful for living cells. DRAQ5 exhibits an emission maximum at the wavelength of 697 nm when bound to DNA [122]. Furthermore, it can be multiplexed with many other fluorophores and is thus an ideal choice for many fixed- and especially live-cell experiments. However, its binding mechanism is still not well understood. DRAQ5 was purchased from Thermo Fisher Scientific (stock solution 5 mM, Waltham, USA) and is diluted for experiments with MT buffer to cencentrations from 1 nM up to 10 µM. Preparation, incubation and experiments are performed in total darkness to ensure the association and avoid photo-bleaching as well.

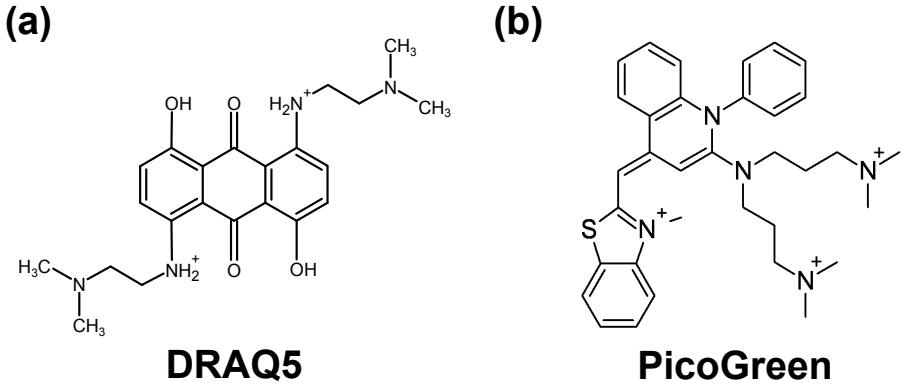

Figure 3.9: Chemical structures of **(a)** DRAQ5 [122] and **(b)** PicoGreen [123] in solution, respectively.

3.5.4 PicoGreen

PicoGreen (PG) ([2-[N-bis-(3-dimethylaminopropyl)-amino]-4-[2,3-dihydro-3-methyl-(benzo-1,3-thiazol-2-yl)-methylidene]-1-phenyl-quinolinium] +, [123]) can be used as an alternative dye for YOYO-1 which shares some similar characteristics. The membrane-impermeable dye can be excited with green light at a wavelength of 500 nm and shows an emission maximum at 523 nm. The free dyes in solution exhibit virtually no fluorescence but emit a 1000-fold stronger signal once bound to DNA. Therefore, a single dye con-

centration can be applied to a wide range of DNA concentrations. A large advantage of PG is its short incubation time of 2 to 5 minutes which so far no other fluorescent dye can reach. Furthermore, PG is expected to bind in an unselective manner [124]. PG was purchased from Thermo Fisher Scientific (in DMSO, Waltham, USA). The concentration of stock solution is unknown due to proprietary interests. Yet, by measuring the absorption of the solution with assuming an extinction coefficient of $E_{500} = 70{,}000\,\mathrm{M}^{-1}$ at room temperature [124, 125], the stock solution concentration is estimated as 0.3 mM (see also Papers III and IV).

3.6 Histones

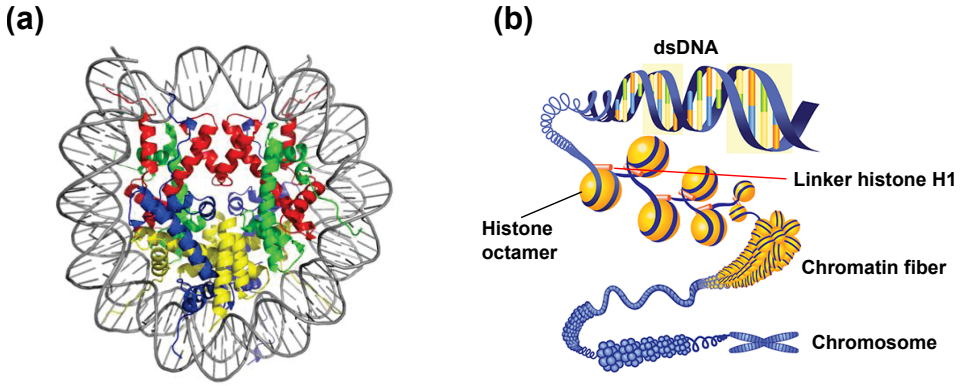

Figure 3.10: **(a)** Dimers of core histone proteins H2A (blue), H2B (yellow), H3 (red) and H4 (green) assemble a global octamer complex with diameter about 125 Å (Source: [126], open access). 147 base pairs of dsDNA are wrapped around it and the whole realizes a nucleosome formation. **(b)** Connected by linker sequences, nucleosomes reach a "beads on a string" formation. Bending linker DNA segments, nucleosomes fold up to produce a chromatin fiber, which next forms loops. The fiber loops are further compressed and coiled resulting in a compact chromosome structure. (Source: [127], public domain image)

Normally in eukaryotes, a cell nucleus is several micrometer in diameter. Notably, DNA contained in the nucleus is very long. For example, a human genome, i.e. the whole DNA in a human cell (except gametes) including 46 chromosomes, consists of about 6 billion base pairs corresponding to about 2 m [25]. To fit the meter-long DNA polymer within the cell nucleus, an extremely potent folding procedure is necessary. Therefore, the nucleic ds-DNA is packed into a nucleosome formation, involving the packing proteins

histones. There are five major families of histone proteins: linker histone protein H1 (instead, H5 in certain cells [128, 129]) as well as core proteins H2A, H2B, H3 and H4 [130]. Eight core histones, two of each kind, assemble a global octamer complex with a diameter of about 125 Å [131].

Due to the highly cationic tails of histone proteins, the negatively charged DNA backbone is attracted and binds to the histone octamer [132–134]. During replication and transcription processes in the cell, 147 base pairs of the dsDNA polymer are wrapped in 1.67 left-handed superhelical turns around each histone octamer complex, resulting in a nucleosome formation [135]. The nucleosomes are connected with linker sequences resulting in a "beads on a string" formation. Bending the linker DNA segment, H1/H5 histones further stabilize the complex and fold up the nucleosomes into a chromatin fiber with a diameter of 30 nm. The compact structure of a chromosome is accomplished by compressing and supercoiling the chromatin fibers (Fig. 3.10) [133, 136, 137].

The mixture of histone proteins (with a molecular weight of 130,268 Da [138]) was purchased from Worthington Biochemical Corporation (from calf thymus, unfractioned mixture, lyophilized, Lakewood, USA) and dissolved for experiments in distilled water with a concentration of stock solution of 10 µM. Further dilution is performed with MT buffer to required concentrations.

Chapter 4

Discussions and reprints of publications

4.1 Paper I

Regarding the high mortality and morbidity rate of cancer diseases, developing new and more effective anticancer drugs with less side effects is of high relevance. On the molecular level, drugs present their functions via interacting with DNA molecules in cell nuclei as binding ligands. Thereby, their binding mode and mechanism decide the heal efficacy of a cytotoxic agent. For example, anthracyclines like mitoxantrone (1,4-dihydroxy-5,8-bis[2-(2-hydroxyethylamino)ethylamino]anthracene-9,10-dione, [139]) intercalate sequence-specifically into the DNA double strands in a reversible mode [140]. Such a specific binding mechanism restricts the efficiency of its cytotoxic function to a certain extent. The widely used platinum-based agent cisplatin binds selectively to the nucleobases of the DNA. A strong cytotoxicity is represented by its molecular recognition of RNA-polymerases that consequently interferes with the DNA transcription. However, due to its selective binding mode, a large dose of cisplatin is required in the therapy resulting in strong side effects like kidney damage. Therefore, there is a demand of new classes of anticancer drugs that establish other binding modes which are permanent and less specific/selective. In this paper, rational design and synthesis of a new cytotoxic complex are described.

The basic idea is to attach the cytotoxic complex to the DNA backbone through electrostatic interaction between positively charged metal ions and

the negatively charged DNA backbone. Firstly, via a rigid backbone, two Cu^{II} (=Cu^{2+}) ions are held with a distance of 6-7 Å corresponding to the distance between two neighboring phosphodiester groups. As a result, both copper ions are able to bind to the DNA polymer simultaneously. Secondly, using sterical blockers, the association of the complex with DNA nucleobases is excluded. Lastly, the complex should bind to DNA irreversibly and thus sterically hinder the DNA biological functions involving DNA-polymerases like replication and transcription.

After the successful synthesis of the Cu_2 complex, its binding to the DNA strand was experimentally verified. In bulk and single-molecule studies of the DNA-$Cu_2(OAc)_2$ interaction, a reduction of the DNA length was detected. This indicates a DNA intrastrand interaction and proves a successful $Cu^{II}{}_2$ binding to DNA. In rare cases, the hat curves of the DNA overwinding experiments with magnetic tweezers exhibit a sudden increase of the effective DNA length after which a nicked DNA structure was observed. These results suggest a hydrolytic phosphodiester cleavage of the DNA backbone induced by the binding of the Cu_2 complex.

In PCR experiments, the Cu_2 complex was proved to prevent the interaction between DNA and DNA-polymerases. Consequently, due to this cytotoxicity, the DNA synthesis and related biological replication and transcription processes are effectively hindered. This leads to a restraint of the proliferation and the growth of the cancer/tumor cells, furthermore the cell death. In living cell experiments, Cu_2 complex was found to possess a stronger cytotoxicity compared to cisplatin and therefore can supply a potentially better healing effect with a smaller dose. Due to the non-specific but permanent binding of the Cu_2 complex, the potential drug should be able to provide a faster and long-term efficacy.

Paper I

Rational Design of a Cytotoxic Dinuclear Cu_2 Complex That Binds by Molecular Recognition at Two Neighboring Phosphates of the DNA Backbone

T. Jany, A. Moreth, C. Gruschka, A. Sischka, A. Spiering, M. Dieding, **Y. Wang**, S. Haji Samo, A. Stammler, H. Bögge, G. Fischer von Mollard, D.Anselmetti and T. Glaser. *Inorganic Chemistry*, Vol. 54, pp. 2679-2690, 2015.

Abstract: The mechanism of the cytotoxic function of cisplatin and related anticancer drugs is based on their binding to the nucleobases of DNA. The development of new classes of anticancer drugs requires establishing other binding modes. Therefore, we performed a rational design for complexes that target two neighboring phosphates of the DNA backbone by molecular recognition resulting in a family of dinuclear complexes based on 2,7-disubstituted 1,8-naphthalenediol. This rigid backbone preorganizes the two metal ions for molecular recognition at the distance of two neighboring phosphates in DNA of 6-7 Å. Additionally, bulky chelating pendant arms in the 2,7-position impede nucleobase complexation by steric hindrance. We successfully synthesized the $Cu^{II}{}_2$ complex of the designed family of dinuclear complexes and studied its binding to dsDNA by independent ensemble and single-molecule methods like gel electrophoresis, precipitation and titration experiments followed by UV-vis spectroscopy, atomic force microscopy (AFM), as well as optical tweezers (OT) and magnetic tweezers (MT) DNA stretching. The observed irreversible binding of our dinuclear $Cu^{II}{}_2$ complex to dsDNA leads to a blocking of DNA synthesis as studied by polymerase chain reactions and cytotoxicity for human cancer cells.

Authors' contributions:
Design of the study: T.G., D.A. and G.FvM.
Synthesis of samples: T.J. and C.G.
Biochemical measurements: A.M. and C.G.
Single-Crystal X-ray Diffraction Analysis: A.St. and H.B.
Design and performance of experiments, data-analysis (AFM): M.D.
Design and performance of experiments, data-analysis (OT): A.Si, A.Sp. and S.HS.
Design and performance of experiments, data-analysis (MT): A.Si. and ***Y.W.***
Writing the manuscript: T.G., D.A. and G.FvM

Inorganic Chemistry

Article

pubs.acs.org/IC

Rational Design of a Cytotoxic Dinuclear Cu_2 Complex That Binds by Molecular Recognition at Two Neighboring Phosphates of the DNA Backbone

Thomas Jany,[†] Alexander Moreth,[‡] Claudia Gruschka,[†] Andy Sischka,[§] Andre Spiering,[§] Mareike Dieding,[§] Ying Wang,[§] Susan Haji Samo,[§] Anja Stammler,[†] Hartmut Bögge,[†] Gabriele Fischer von Mollard,[‡] Dario Anselmetti,[§] and Thorsten Glaser*[,†]

[†]Lehrstuhl für Anorganische Chemie I, Chemistry Department, [‡]Lehrstuhl für Biochemie III, Chemistry Department, and [§]Experimentelle Biophysik, Physics Department, Bielefeld University, Universitätsstrasse 25, 33615 Bielefeld, Germany

Supporting Information

ABSTRACT: The mechanism of the cytotoxic function of cisplatin and related anticancer drugs is based on their binding to the nucleobases of DNA. The development of new classes of anticancer drugs requires establishing other binding modes. Therefore, we performed a rational design for complexes that target two neighboring phosphates of the DNA backbone by molecular recognition resulting in a family of dinuclear complexes based on 2,7-disubstituted 1,8-naphthalenediol. This rigid backbone preorganizes the two metal ions for molecular recognition at the distance of two neighboring phosphates in DNA of 6−7 Å. Additionally, bulky chelating pendant arms in the 2,7-position impede nucleobase complexation by steric hindrance. We successfully synthesized the Cu^{II}_2 complex of the designed family of dinuclear complexes and studied its binding to dsDNA by independent ensemble and single-molecule methods like gel electrophoresis, precipitation, and titration experiments followed by UV−vis spectroscopy, atomic force microscopy (AFM), as well as optical tweezers (OT) and magnetic tweezers (MT) DNA stretching. The observed irreversible binding of our dinuclear Cu^{II}_2 complex to dsDNA leads to a blocking of DNA synthesis as studied by polymerase chain reactions and cytotoxicity for human cancer cells.

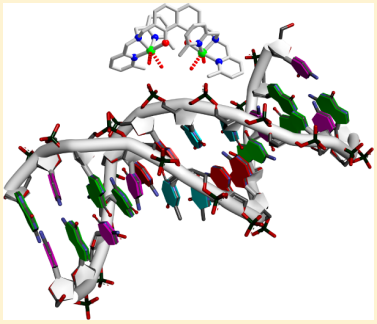

INTRODUCTION

Nucleic acids are polymers from condensation of phosphoric acid with alcohol groups of ribose (RNA) or desoxyribose (DNA) that possess heterocyclic purine and pyrimidine bases as side chains.[1] Thus, these polyphosphodiesters offer several potential binding sites for metal ions. Each phosphate group contributes one negative charge to the overall charge of the polymer that is electrostatically balanced by a layer of alkali metal and Mg^{II} ions. On the other hand, transition metal ions often bind specifically by coordination to nucleobases and phosphates, while coordination to the sugar moieties is rare.[2] Another way metal complexes can bind to the nucleobases of DNA is by intercalation of a planar aromatic functionality between the base pairs of double-helical DNA.[3] The glycopeptide antibiotic bleomycine is a prominent example for an interaction of a metal complex with nucleic acids, which offers therapeutical applications.[4] A prominent example for binding to the nucleobases is the major anticancer drug cisplatin (*cis*-$[PtCl_2(NH_3)_2]$). Upon cellular uptake, cisplatin binds to DNA preferentially via a 1,2-intrastrand binding d(GpG) at N7 of purine bases with guanine is favored over adenine,[5,6] resulting in a strong bending of the DNA.[6,7] This interferes with the molecular recognition of essential proteins for transcription, as RNA polymerases,[8,9] which is supposed to cause the cytotoxicity of cisplatin. As a single drug or in combination with other drugs, cisplatin is used in the treatment for testicular, bladder, ovarian, head and neck, cervical, and lung cancers.[8,10] The application of cisplatin is limited by acquired resistance to cisplatin[11] and by severe side effects in normal tissues. In particular, nephrotoxicity is a major factor that limits the use and efficiency of cisplatin in cancer therapy.[12] To overcome the limitations of cisplatin and to broaden the range of treatable tumors, a lot of efforts have been devoted to improve cisplatin.[13] Many analogs of cisplatin have been synthesized resulting in second-generation cisplatin drugs like oxaliplatin and carboplatin.[14]

In addition to the binding at the nucleobases, the phosphates of the DNA backbone are known to be the target of the metal active sites of enzymes such as nucleases. These metalloenzymes catalyze the hydrolytic cleavage of the phosphoester bonds that are thermodynamically unstable toward hydrolysis but kinetically highly inert.[15,16] The active sites consist of one or more metal ions that provide several pathways to accelerate hydrolysis as Lewis-acid activation, leaving group stabilization or providing a metal-bound hydroxide as nucleophile. This reactivity usually implies the formation of a metal−phosphate oxygen bond during the catalytic cycle. However, this bond

Received: November 28, 2014
Published: February 4, 2015

DOI: 10.1021/ic5028465
Inorg. Chem. 2015, 54, 2679−2690

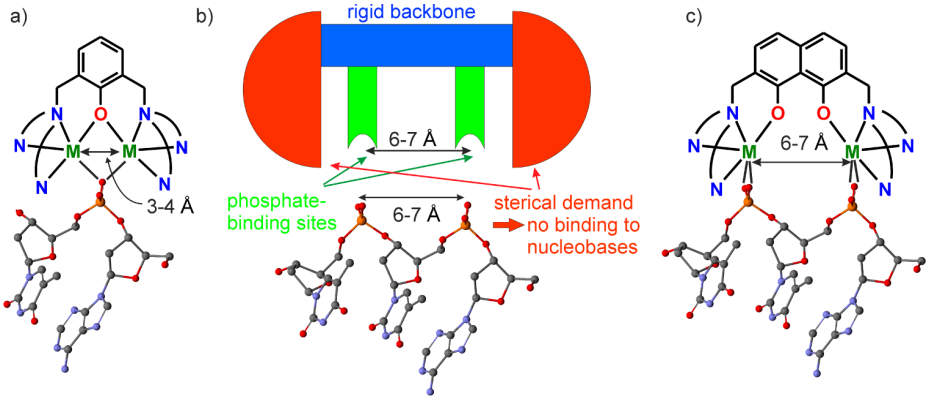

Figure 1. (a) Family of dinuclear complexes with hydrolytic reactivity based on dinucleating Robson ligands with a central phenolate. Two metal ions coordinate to one DNA phosphate. (b) Design concept for a dinuclear complex binding to two neighboring phosphates of the DNA backbone. (c) Molecular realization by a family of dinuclear complexes based on 2,7-disubstituted 1,8-naphthalenediol ligands. Please note that the two metal ions cannot coordinate to one DNA phosphate but are preorganized to coordinate to two neighboring DNA phosphates.

must be labile enough to be cleaved in the catalytic cycle to enable product release. This reactivity has stimulated intense research to mimic structure and function of the active sites of these nucleases and closely related phosphatases by biomimetic model complexes.[17] A prominent family of dinuclear model complexes (e.g., with Cu^{II}) that not only mimic the hydrolytic cleaving reactivity of nucleases but also of peptidases has been synthesized using phenol-based, dinucleating Robson ligands with pendant chelating arms in the 2,6-position (Figure 1a).[16,18,19] A main mode of action is a bridging coordination of one phosphate to both metal ions (Lewis-acid activation) facilitated by a metal−metal distance of 3−4 Å with one metal ion providing a bound hydroxide as nucleophile.

There has been recent success in the field by increasing the level of complexity to incorporate details of the second coordination sphere in the active sites.[20] These developments include the combination of a hydrolytically active metal site with DNA binding groups such as amine and guanidine groups for hydrogen bonding, positively charged residues for electrostatic interactions, or minor-groove binding motives.[21]

However, the hydrolytic cleavage of the bound phosphoester destroys the DNA−metal complex that foils the formation of a stable metalated DNA adduct. Therefore, a metal complex as efficient binder to DNA phosphates must provide a strong thermodynamic and kinetic driving force with low hydrolytic activity. Herein, we report on the rational design of a dinuclear complex family that is supposed to bind to two neighboring phosphates of the DNA backbone by molecular recognition without having an unwanted hydrolytic activity. We demonstrate the irreversible binding ability of the dinuclear Cu^{II}_2 complex to DNA by several independent biochemical, spectroscopic, and single-molecule methods. Furthermore, we show that this compound inhibits DNA synthesis and is cytotoxic to human cancer cells at the same concentration, which provides evidence that DNA binding causes the inhibition of DNA synthesis that leads to the death of the cancer cells.

EXPERIMENTAL SECTION

General Considerations. Solvents and starting materials were of the highest commercially available purity and used as received. All reactions were carried out under an argon atmosphere. The synthesis of MOM_2**1** was described previously.[22] Bis((6-methylpyridin-2-yl)methyl)amine has been synthesized according to a modified literature procedure.[23] Infrared spectra (400−4000 cm^{-1}) of solid samples were recorded on a Shimadzu FTIR-8300 or a Shimadzu FTIR 8400S spectrometer as KBr disks. ESI and MALDI-TOF mass spectra were recorded on a Bruker Esquire 3000 ion trap mass spectrometer and a PE Biosystems Voyager DE mass spectrometer, respectively. For acquisition of high-resolution mass spectra a Bruker APEX III FT-ICR has been used. ^1H and ^{13}C NMR spectra were recorded on a Bruker Avance 600 spectrometer using the solvent as an internal standard. The assignments of the NMR resonances were supported by 2D HMBC and HMQC spectroscopy. Elemental analyses were carried out on a LECO CHN-932 or a HEKAtech Euro EA elemental analyzer. UV−vis−NIR absorption spectra of solutions were measured on a Shimadzu UV-3101PC spectrophotometer in the range 190−3200 nm at ambient temperatures. Temperature-dependent magnetic susceptibilities were measured by using a SQUID magnetometer (MPMS XL-7 EC, Quantum Design) in a static field of 1 T in the range 2−290 K. For calculations of the molar magnetic susceptibilities, χ_m, the measured susceptibilities were corrected for the underlying diamagnetism of the sample holder and the sample by using tabulated Pascal's constants. The JulX program package was used for spin-Hamiltonian simulations and fitting of the data by a full-matrix diagonalization approach.[24]

Synthesis of 2,7-Bis(*N*,*N*-di((6-methylpyridin-2-yl)methyl)-aminomethyl)-1,8-bis(methoxymethoxy)naphthalene (MOM_2tom^{Me}). Solid $Na[BH(OAc)_3]$ (1.11 g, 5.25 mmol) is added to a solution of 2,7-diformyl-1,8-bis(methoxymethoxy)naphthalene (MOM_2**1**) (532 mg, 1.75 mmol) and di((6-methylpyridin-2-yl)-methyl)amine (DPA^{Me}) (795 mg, 3.50 mmol) in 1,2-dichloroethane (70 mL). The resulting suspension is stirred for 18 h at room temperature and then for 4 h at 50 °C. The reaction is quenched by addition of NH_4OH solution (1 M, 350 mL). The aqueous layer is extracted with CH_2Cl_2 (6 × 70 mL), and the organic extracts are combined, dried over Na_2SO_4, and concentrated in vacuo, resulting in a yellow oil of high viscosity. The crude product is purified by column chromatography (basic aluminum oxide, THF). Yield: 1.01 g (1.39 mmol, 79%). ^1H NMR (600 MHz, $CDCl_3$): δ/ppm =7.73 (d, J = 8.5 Hz, 2 H, H10), 7.52 (t, J = 7.7 Hz, 4 H, H4), 7.56 (d, J = 8.5 Hz, 2 H, H11), 7.45 (d, J = 8.5 Hz, 4 H, H5), 6. 96 (d, J = 7.7 Hz, 4 H, H3), 4.94 (s, 4 H, H15), 3.98 (s, 4 H, H8), 3.83 (s, 8 H, H7), 3.48 (s, 6 H, H16), 2.49 (s, 12 H, H1). ^{13}C NMR (125 MHz, $CDCl_3$): δ/ppm = 159.6 (C2), 157.5 (C6), 150.1 (C14), 136.6 (C4), 136.2 (C12), 130.1 (C9), 127.4 (C10), 124.8 (C11), 121.4 (C3), 121.2 (C13), 119.5 (C5), 101.2 (C15), 60.5 (C7), 58.0 (C16), 52.6 (C8), 24.5 (C1). HR-ESI-MS ($CHCl_3$/MeOH m/z): calcd for $[M + H]^+$ $C_{44}H_{51}N_6O_4$ 727.39663, found 727.39477; calcd for $[M + Na]^+$ $C_{44}H_{50}N_6O_4Na$ 749.37858, found 749.37649. UV−vis (CH_3CN): $\tilde{\nu}$/cm^{-1} (ε/10^3 M^{-1} cm^{-1}): 42 400 (73.5), 37 500 (25.1), 30 260 (1.79). IR (KBr): $\tilde{\nu}$/cm^{-1} = 3441 s, 3416 s, 3059 w, 3007 w, 2922 m, 2852 w, 2824 w, 1591 s,

DOI: 10.1021/ic5028465
Inorg. Chem. 2015, 54, 2679−2690

1577 s, 1474 s, 1433 s, 1358 m, 1329 m, 1157 s, 1020 s, 955 s, 926 s, 788 s.

Chart 1

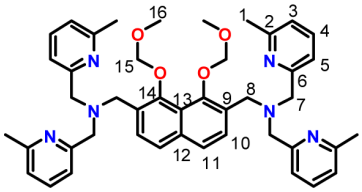

Synthesis of [(tom^{Me}){Cu(OAc)}$_2$] ($Cu_2(OAc)_2$). A solution of MOM_2tom^{Me} (370 mg, 0.509 mmol) in MeOH (35 mL) is added dropwise to a solution of copper acetate ($Cu(OAc)_2 \cdot H_2O$) (208 mg, 1.04 mmol) in MeOH (35 mL). The greenish-blue solution is stirred for 25 h at 40 °C, resulting in a color change to a greenish-black. The solvent is removed under vacuum. Upon slow diffusion of Et_2O into a solution of the residue in CH_3CN/H_2O (14:1), blue crystals were obtained. Yield: 314 mg (0.300 mmol, 60%). ESI-MS (MeOH, m/z): 382.1 $[M - 2OAc]^{2+}$, 881.2 $[M + H]^+$. IR (KBr): $\tilde{\nu}/cm^{-1}$ = 3397 m br, 3067 w, 3055 w, 3011 w, 3011 w, 2970 w, 2926 w, 2859 w, 1611 s, 1584 s, 1530 m, 1472 m, 1449 m, 1395 s, 1375 s, 1341 m, 1288 w, 1271 w, 1254 w, 1219 w, 1200 w, 1165 w, 1142 w, 1099 w, 1078 w, 1055 m, 1022 w, 1001 w, 968 w, 876 w, 831 m, 787 m, 679 m, 648 w, 621 w, 586 w, 567 w, 523 w, 502 w, 469 w. UV-/Vis (CH_3CN): $\tilde{\nu}/cm^{-1}$ (10^3 ε/M^{-1} cm^{-1}): 42 100 sh (45.1), 27 900 (9.9), 23 900 (0.54), 18 500 (0.34), 14 800 (0.34). Anal. Calcd for $C_{44}H_{63}N_6Cu_2O_{14.5}$ [(tom^{Me}){Cu(OAc)}$_2$]·8.5 H_2O): C, 51.06; H, 6.14; N, 8.12. Found: C, 51.14; H, 6.03; N, 7.74

Single-Crystal X-ray Diffraction. A crystal of [(tom^{Me}){Cu(OAc)}$_2$]·9.75H_2O·CH_3CN was measured at 100(2) K on a Bruker Kappa APEXII diffractometer (four-circle goniometer with 4K CCD detector, Mo Kα radiation, focusing graphite monochromator). Crystal and refinement data: M = 1098.66 g mol^{-1}, $C_{46}H_{68.50}Cu_2N_7O_{15.75}$, orthorhombic, space group $P2_12_12_1$, a = 10.9107(16) Å, b = 15.793(2) Å, c = 31.758(5) Å, V = 5472.3(14) Å^3, Z = 4, ρ = 1.334 g/cm^3, μ = 0.847 mm^{-1}, F (000) = 2310, crystal size = 0.37 × 0.23 × 0.14 mm^3, 57 003 reflections (3.43 < Θ < 27.00°) collected, 11 883 reflections unique. Absolute structure parameter = −0.003 (10), R = 0.0436 for 10 494 reflections with $I > 2\ \sigma(I)$, R = 0.0521 for all reflections. Crystallographic data are deposited at the Cambridge Crystallographic Data Centre as supplementary publication no. 936123 ($Cu_2(OAc)_2$). These data can be obtained free of charge from the Cambridge Crystallographic Data Centre via www.ccdc.cam.ac.uk/data_request/cif.

Atomic Force Microscopy. λ-DNA (400 pM λ-DNA equivalent to 40 μM DNA bases/phosphates) was incubated with 50 and 200 μM $Cu_2(OAc)_2$ for 15 min at room temperature in TRIS buffer (150 mM KCl, 10 mM Tris/HCl, pH 8.0) as well as in double-distilled ultrapure water (18.2 MΩcm). A 10 μL amount of the solution was incubated for 15 min on freshly cleaved mica, subsequently rinsed by ultrapure water (18.2 MΩcm), and carefully dried in a nitrogen steam. AFM measurements were performed with a commercial instrument (Nanoscope V, Multimode, Bruker) at room temperature under ambient conditions in tapping mode of operation using single-crystal Si-cantilevers (Bruker).

DNA Overstretching with Optical Tweezers. Streptavidin-coated polystyrene microspheres (Spherotech, IL) with a diameter of 3.05 μm (0.5% w/v) were diluted 1:1000 in 150 mM NaCl, 10 mM Tris/HCl at pH 8.0 and introduced into the sample chamber.[25] One bead was trapped with the optical tweezers,[26] handed over to the glass micropipette, and held tightly by applying low pressure. A second bead was then trapped remaining inside the optical trap. λ-DNA was biochemically functionalized[27] on both ends with several biotins to ensure tethering to the beads. The functionalized λ-DNA (15 pM in 150 mM NaCl, 10 mM Tris/HCl at pH 8.0) was then introduced into the sample chamber to allow immobilization between the two beads.[27] Then a first λ-DNA overstretching experiment was done with a velocity of 1 μm/s to an end-to-end distance of ∼18 μm and immediately relaxed. Comparison with the literature-based dsDNA reference elasticity curve (transitional/melting plateau at ∼64 pN) ensured that only one single DNA molecule is bound between the microbeads. This force/extension curve serves as a reference. In a second step, a solution of 6 μM $Cu_2(OAc)_2$ in 150 mM NaCl, 10 mM Tris/HCl at pH 8.0 was added into the sample chamber. After a typical waiting time of at least 2 min, where $Cu_2(OAc)_2$ is supposed to bind to the DNA strand, subsequent DNA overstretching experiments were performed. All experiments were conducted at 20 °C.

DNA Torsional Stretching with Magnetic Tweezers. We used a commercial magnetic tweezers instrument (Picotwist, Lyon, France) where the magnetic bead position is determined by an optical microscopic setup with a CCD camera. 4.2 μm short double-stranded DNA fragments were functionalized with multibiotins at one end and multidigoxigenins at the other end for magnetic tweezers (MT) experiments. These DNA fragments were immobilized via several antidigoxigenins at the bottom cell wall and via their biotins on streptavidin-coated paramagnetic beads (MyOne, Dynabeads, Life-Technologies). All MT experiments were conducted in adapted PBS buffer (137 mM NaCl, 27 mM KCl, at pH 7.4; 0.1% BSA, 0.1% TWEEN 20). Typical incubations times were 30 (digoxigenin) and 15 min (biotin). The multiple surface binding ensures a torsionally constraint immobilization of the DNA fragment which is of crucial importance for the experiment. Successful multivalency binding and a nick-free DNA can be confirmed by optically inspecting the rotation of the DNA-bead complex via external magnetic field rotation. A proper preparation induces DNA plectonemic superspiralization and shortening of the DNA. All MT experiments were conducted at 25 °C.

Plasmid Binding of $Cu_2(OAc)_2$ and Analysis by Agarose Gel Electrophoresis. pBluescript SK$^+$ plasmid DNA (2960 base pairs, bp) was isolated from *E. coli* strain XL1 blue. A 1.25 μg amount of plasmid DNA (100 μM DNA bases/phosphates) was incubated in 20 mM HEPES pH = 7.5 without addition, with $Cu_2(OAc)_2$, copper chloride ($CuCl_2 \cdot 2H_2O$), or MOM_2tom^{Me} for 1 h at 37 °C. To obtain corresponding concentrations of copper ions the molar concentration of copper chloride was 2-fold higher than that of $Cu_2(OAc)_2$. The DNA was separated by agarose gel electrophoresis in TBE buffer (89 mM Tris base, 89 mM boric acid, 2 mM EDTA), stained with ethidium bromide, and viewed under UV light. Digital pictures were quantified to determine the fraction of supercoiled, open-circular, and linear plasmid DNA. Cleavage of a single phosphodiester bond in a supercoiled plasmid induces relaxation into the open-circular form. A plasmid is linearized by cleavage of both strands in close proximity, for example, by the restriction enzyme *Eco*RI.

Quantification of DNA Binding of $Cu_2(OAc)_2$. A 20 μg amount of pBluescript SK$^+$ plasmid DNA (600 μM DNA bases/phosphates) was incubated in 20 mM HEPES pH 7.5 without addition or with 100 μM to 3 mM $Cu_2(OAc)_2$ for 1 h at 37 °C in a total volume of 100 μL. DNA was precipitated by addition of $NaClO_4$ to 75 mM and ethanol to 70% final concentration for 3 days at −20 °C.[28] DNA was pelleted by centrifugation for 20 min with 13 000 rpm in a microcentrifuge, rinsed with 70% ethanol, and resuspended in 100 μL of 20 mM HEPES pH 7.5. Absorption at 356 nm was determined in a UV−vis spectrometer to calculate the concentration of Cu_2^{2+}. The DNA precipitation efficiency was determined from samples without $Cu_2(OAc)_2$ by absorption at 260 nm and used for correction of the binding data.

PCR. A 380 bp insert was amplified from the plasmid pBK38 encoding mouse vti1b using the oligonucleotide primer GGAATTCATGGCCGCCTCCGCCGC and CGGGATCCTATTGAGACTGTAGTCGATTC.[29] About 2.3 ng of plasmid DNA (0.34 μM DNA bases/phosphates), 0.1 μM primer (together 5.3 μM DNA bases/phosphates), 250 μM dNTPs, and various concentrations of metal complexes were used per reaction. Taq DNA polymerase was used for DNA amplification. After 17 PCR cycles the reaction products were analyzed by agarose gel electrophoresis.

Survival of HeLa Cells. Two thousand five hundred HeLa cells were plated in 96-well plates in DMEM medium with 5% FCS and

DOI: 10.1021/ic5028465
Inorg. Chem. 2015, 54, 2679−2690

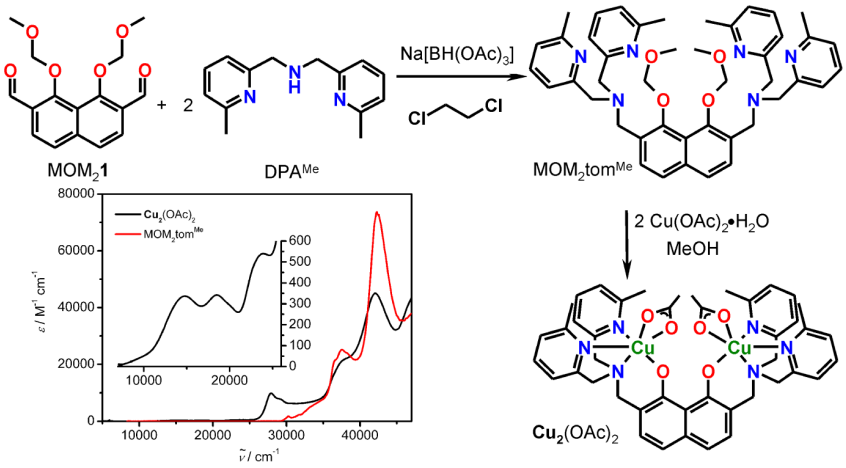

Figure 2. Synthesis of the targeted complex $\mathbf{Cu_2}(OAc)_2$. (Inset) Electronic absorption spectra of $\mathbf{Cu_2}(OAc)_2$ and MOM_2tom^{Me} measured in CH_3CN solutions at ambient temperatures.

incubated for 24 h at 37 °C 5% CO_2. The cells were further incubated for 3 days without addition or with the indicated concentrations of metal complexes in triplicates. Cells were inspected with a microscope. Cell survival was assayed with sulforhodamine B according to published procedures.[30] Briefly, cells were fixed with trichloroacetic acid and stained with 0.4% sulforhodamine B in 1% acetic acid. Cells were washed and dried. Bound sulforhodamine B was solubilized with 10 mM Tris base and the absorption at 564 nm determined in an ELISA plate reader. Sulforhodamine B binds to proteins and therefore is an established way to measure cell proliferation and survival. Averages of 3 wells for each condition were calculated in three independent experiments and compared to untreated controls set as 100% survival. Similar results were obtained by testing cell survival with the XTT assay, which measures metabolic reduction of a tetrazolium reagent to a formazan.

RESULTS AND DISCUSSION

Rational Design of a Complex Family Binding Neighboring Phosphates of DNA. Inspired (i) by the cytotoxicity of cisplatin due to its strong binding to the nucleobases of DNA and (ii) by the hydrolytic cleaving ability of transition metal ions of nucleases and their model complexes due to coordination to the phosphates of DNA we designed a new lead motif that binds by molecular recognition to the phosphate backbone of DNA and not to the nucleobases. The freedom in the choice of the metal ion allows controlling the reactivity of these complexes to exhibit either hydrolytic activity or a strong binding affinity to DNA without hydrolytic activity.

In order to achieve coordination of a metal complex to the phosphates of the DNA backbone the complex and ligand design must on one hand involve a source of molecular recognition for the phosphate groups and on the other hand impede complexation with the nucleobases that are located in the minor and major groove and thus less exposed. We are following the multivalence principle, which states that several preorganized binding sites connected by a rigid backbone are not only enthalpically but also entropically favored as only the first binding event costs loss of degrees of freedom.[31] In this respect, our concept relies on the molecular recognition of two neighboring phosphodiester groups by a dinuclear metal complex, in which a rigid ligand backbone predefines the metal−metal distance to ∼6−7 Å, the distance of two neighboring phosphates in the DNA backbone (Figure 1b). Furthermore, the coordination environment must provide some sterical hindrance to prevent a potential competing binding to the less exposed nucleobases. Inspired by the success of the complexes of phenol-based Robson ligands (Figure 1a), whose metal−metal distances of 3−4 Å preorganize the metal ions to bind both to the same phosphate,[16,18,19] we came up with the idea to create an extended ligand system based on 1,8-naphthalenediol that would be able to enforce metal−metal distances of 6−7 Å with sterically demanding pendant arms in the 2,7-position (Figure 1c). Furthermore, this rigid backbone prohibits coordination of both metal ions to the same phosphate. It should be noted that a dinuclear Cu^{II} complex, whose ligand compartments are connected by a flexible 1,8-naphthalene spacer, was reported recently,[32] but a binding of both Cu^{II} ions to one phosphate has been proposed due to the strong flexibility. Variation of the metal ions (divalent vs trivalent, 3d vs 4d vs 5d) may allow a fine tuning of the kinetic and thermodynamic stability so that potentially a new family of DNA-binding molecules evolves that can be cytotoxic to cancer cells. The variation of the binding mode in comparison to cisplatin-based drugs may provide access to the treatment of different cancer types with different toxicity.

Herein, we present the synthesis of the first complex of this new family with Cu^{II} ions. The kinetically labile Cu^{II} ion has a thermodynamic driving force for DNA complexation. Binding constants of Cu^{II} complexes that catalyze the hydrolytic cleavage of DNA have been reported in the order of 10^3−10^4.[33] Although Cu^{II} complexes of tridentate ligands are active in hydrolytic cleavage of phosphoesters, those of tetradentate ligands are less active. This reactivity difference may be related to the Jahn−Teller effect that usually results in a tetragonal elongated coordination environment for Cu^{II} complexes. A tridentate ligand provides two coordination sites: one for phosphate binding (Lewis-acid activation) and one for hydroxide binding (providing the reactive nucleophile). On the other hand, a tetradentate ligand provides only one coordination site of significant binding energy (not in the Jahn−Teller axis) open either for phosphate binding or for hydroxide binding resulting in the reduced hydrolytic reactivity. Furthermore, it has been proposed that endogenous metals like copper may be equally effective but less toxic than platinum complexes.[34]

Synthesis and Characterization. We already established a streamlined synthesis of 2,7-diformyl-1,8-naphthalenediol

DOI: 10.1021/ic5028465
Inorg. Chem. 2015, 54, 2679−2690

(H_2**1**)[22] and applied it for the preparation of a trinucleating ligand via Schiff-base condensation with 2 equiv of *N*,*N*-dimethylethylenediamine.[35] It should be noted that analogous ligands have recently been used for the preparation of efficient olefine polymerization catalysts.[36] Initially, we attempted a reductive amination of the free diol H_2**1** with DPA^{Me}, which was not successful. However, the reductive amination of the MOM-protected precursor MOM_2**1** with DPA^{Me} using Na[$BH(OAc)_3$] afforded the protected ligand MOM_2tom^{Me} (Figure 2).

While MOM-protecting groups are easy to cleave with Brønsted acids, this route proved to be not applicable for MOM_2tom^{Me} due to the six basic nitrogen atoms, which underwent protonation followed by precipitation before cleavage. We thus thought that a metal ion that is already coordinated in the N_3 ligand compartment of MOM_2**1** could act as a Lewis acid for MOM deprotection as it has been observed for thioethers.[37] In this respect, reaction of MOM_2**1** with copper acetate at 40 °C resulted in the clean MOM deprotection, and the targeted complex [(tom^{Me}){Cu$(OAc)_2$}$_2$] (= **Cu$_2$**$(OAc)_2$) has been isolated (Figure 2). Complex formation can be monitored by UV−vis spectroscopy, as a prominent aryloxide → Cu^{II} LMCT transition at 27 900 cm^{-1} appears for the deprotected complex accompanied by d−d transitions in the range 14 000−25 000 cm^{-1} (Figure 2 inset).

The molecular structure of **Cu$_2$**$(OAc)_2$ has been established by single-crystal X-ray diffraction and is shown in different orientations in Figure 3. A thermal ellipsoid plot is provided in

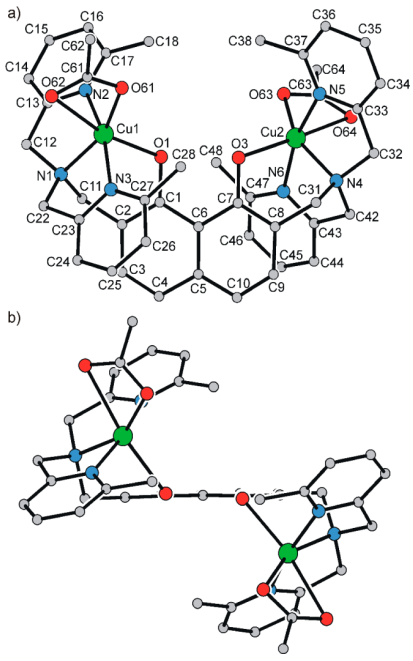

Figure 3. Molecular structure of **Cu$_2$**$(OAc)_2$ in crystals of **Cu$_2$**$(OAc)_2$·$9.75H_2O$·CH_3CN in two different orientations (a and b) and labeling scheme used (b). Hydrogen atoms are omitted for clarity.

Figure S1, Supporting Information, and selected interatomic distances and angles are summerized in Table 1. Two Cu^{II} ions are coordinated in the N_3O compartments of the deprotected ligand $(tom^{Me})^{2-}$. The octahedral coordination environments are saturated by bidentate OAc^- ligands. One oxygen donor of the acetate (Cu−O = 2.58 and 2.55 Å) and the aryloxides of the

Table 1. Selected Interatomic Distances (Angstroms) and Angles (degrees) for $Cu_2(OAc)_2$·$9.75H_2O$·CH_3CN

Cu1−O1	2.284(2)	O62−Cu1−N1	99.07(10)
Cu1−O61	1.968(2)	O62−Cu1−N2	90.60(10)
Cu1−O62	2.580(3)	O62−Cu1−N3	92.16(10)
Cu1−N1	2.015(3)	N1−Cu1−N2	82.41(12)
Cu1−N2	2.043(3)	N1−Cu1−N3	82.34(11)
Cu1−N3	2.057(3)	N2−Cu1−N3	164.75(12)
Cu2−O3	2.309(2)	O3−Cu2−O63	117.34(8)
Cu2−O63	1.966(2)	O3−Cu2−O64	171.78(8)
Cu2−O64	2.555(2)	O3−Cu2−N5	92.81(9)
Cu2−N4	2.015(3)	O3−Cu2−N4	92.29(9)
Cu2−N5	2.015(3)	O3−Cu2−N6	90.47(9)
Cu2−N6	2.030(3)	O63−Cu2−N5	96.37(10)
O1−C1	1.362(4)	O63−Cu2−N4	150.30(10)
O3−C7	1.361(4)	O63−Cu2−N6	93.77(10)
O61−C61	1.273(4)	O63−Cu2−O64	56.71(9)
O62−C61	1.254(4)	O64−Cu2−N5	93.55(10)
O63−C63	1.273(4)	O64−Cu2−N4	93.61(9)
O64−C63	1.251(4)	O64−Cu2−N6	84.54(9)
		N4−Cu2−N5	83.30(11)
O1−Cu1−N1	93.93(10)	N4−Cu2−N6	83.44(11)
O1−Cu1−N2	90.18(10)	N5−Cu2−N6	166.46(11)
O1−Cu1−N3	90.49(9)	O61−C61−O62	121.8(3)
O1−Cu1−O61	110.82(9)	O62−C61−C62	120.6(3)
O1−Cu1−O62	166.96(9)	O61−C61−C62	117.6(3)
O61−Cu1−O62	56.16(9)	O63−C63−O64	122.1(3)
O61−Cu1−N1	155.20(11)	O64−C63−C64	121.1(3)
O61−Cu1−N2	95.45(11)	O63−C63−C64	116.8(3)
O61−Cu1−N3	98.55(10)		

naphthalenediol (Cu−O = 2.28 and 2.31 Å) are coordinated in the Jahn−Teller axes of the Cu^{II} ions. The two Cu^{II} ions are not in the naphthalene plane but oriented to opposite sides relative to the naphthalene plane (Figure 3b) demonstrating some degree of flexibility of the Cu^{II} polyhedra especially at the benzylic carbon atoms. The 1,8-naphthalenediol backbone affords an intramolecular Cu−Cu distance of 6.32 Å. The labile acetates are at the potential binding sites for the DNA phosphate oxygen donor atoms. The O···O distances between the two acetates are 7.02, 8.88, 8.91, and 10.85 Å. These distances in conjunction with the flexibility at the benzylic carbon atoms hint at the capability of **Cu$_2$**$^{2+}$ to coordinate to two neighboring phosphates of the DNA backbone by molecular recognition.

The magnetic measurements reveal an almost temperature-independent effective magnetic moment, μ_{eff}, of 2.65 μ_B (Figure 4). Simulations using the adequate spin Hamiltonian ($H = -2JS_1S_2$) for dinuclear Cu^{II}_2 complexes provide a good reproduction of the experimental data with an almost vanishing coupling constant $J = -0.1$ cm^{-1}. This small coupling behavior is consistent with the Cu−O^{ar} bonds being in the Jahn−Teller axes. Thus, despite the long Cu−O^{ar} bonds, the magnetic d($x^2 - y^2$) orbitals are of δ symmetry with respect to the Cu−O^{ar} bonds and thus nonbonding.

As a prerequisite for studying the interaction with DNA under physiological conditions, **Cu$_2$**$(OAc)_2$ is highly soluble in water and buffer solutions. We attribute this to a loss of bound acetate resulting in a hydrated form of **Cu$_2$**$^{2+}$. As crystallization of **Cu$_2$**$^{2+}$-bound DNA seems to be elusive due to the sequence-unspecific binding of **Cu$_2$**$^{2+}$ to DNA providing only statistical mixtures of **Cu$_2$**$^{2+}$-bound DNA, we evaluated the binding of

DOI: 10.1021/ic5028465
Inorg. Chem. 2015, 54, 2679−2690

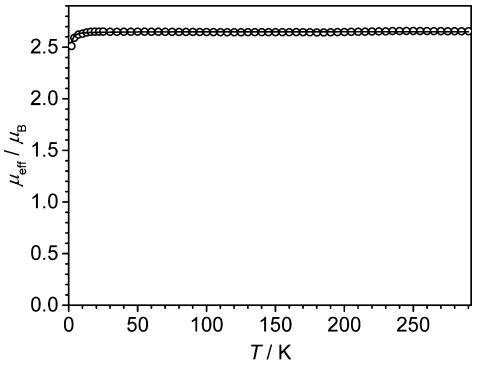

Figure 4. Temperature dependence of μ_{eff} for $Cu_2(OAc)_2$. Solid line corresponds to the best fit to the spin Hamiltonian using $J = -0.1$ cm^{-1}, $g = 2.163$.

Cu_2^{2+} to DNA by independent biochemical, spectroscopic, and single-molecule methods.

Interaction with DNA Studied by Gel Electrophoresis. Although the dinuclear copper complex was chosen as the first complex of this family of complexes to strongly bind to DNA and not to exhibit a strong hydrolytic cleavage ability, we first tested the ability of $Cu_2(OAc)_2$ for hydrolytic cleavage. In this respect, plasmid DNA (100 μM DNA phosphates) was incubated with $Cu_2(OAc)_2$ and studied by agarose gel electrophoresis. Addition of copper chloride or MOM_2tom^{Me} was studied as reference (Figure 5). Circular plasmid DNA can adopt different topoisomers. The supercoiled plasmid is a tense topoisomer that results from partial unwinding and is the predominant form in bacteria. It migrates fastest on an agarose gel due to its compactness. The supercoiled topoisomer of our 3 kb (kilo base pairs) plasmid had a similar mobility as the 2 kb linear marker fragment. If one phosphodiester bond is hydrolyzed, a nick is introduced and the supercoiled plasmid relaxes into the open-circular form, which migrates slower on agarose gels similar to the 4 kb linear marker fragment. If both DNA strands are hydrolyzed in close proximity the circular plasmid is converted into the linear form as observed after digestion with the restriction enzyme *Eco*RI (Figure 5, Eco).

While 5% open-circular plasmid DNA were already present without addition (0 μM), 10−50 μM $Cu_2(OAc)_2$ increased the share of open-circular plasmid DNA slightly but significantly to 12−14% (Figure 5, quantification in Figure S2a, Supporting Information). Addition of comparable concentrations of copper chloride or MOM_2tom^{Me} did not alter the amount of open-circular plasmid DNA. The linear form was not observed after addition of $Cu_2(OAc)_2$, indicating that Cu_2^{2+} did not cause massive hydrolysis. This indicates that Cu_2^{2+} hydrolyzes DNA with very low frequency. Although this is only a weak acceleration of hydrolytic phosphodiester cleavage, it is a clear indication that Cu_2^{2+} binds to the phosphate backbone of DNA.

Most interestingly, an unknown behavior has been observed for concentrations above 100 μM $Cu_2(OAc)_2$. As can be seen in Figure 5, the dark spots from the ethidium fluorescence, which indicate the location of the DNA, persisted in the loading pocket for concentrations of 100 and 200 μM. This indicates that the DNA was not entering the gel. Moreover, at 500 μM no ethidium fluorescence was observed, although a DNA−Cu_2^{2+} precipitate could be observed in the loading pocket

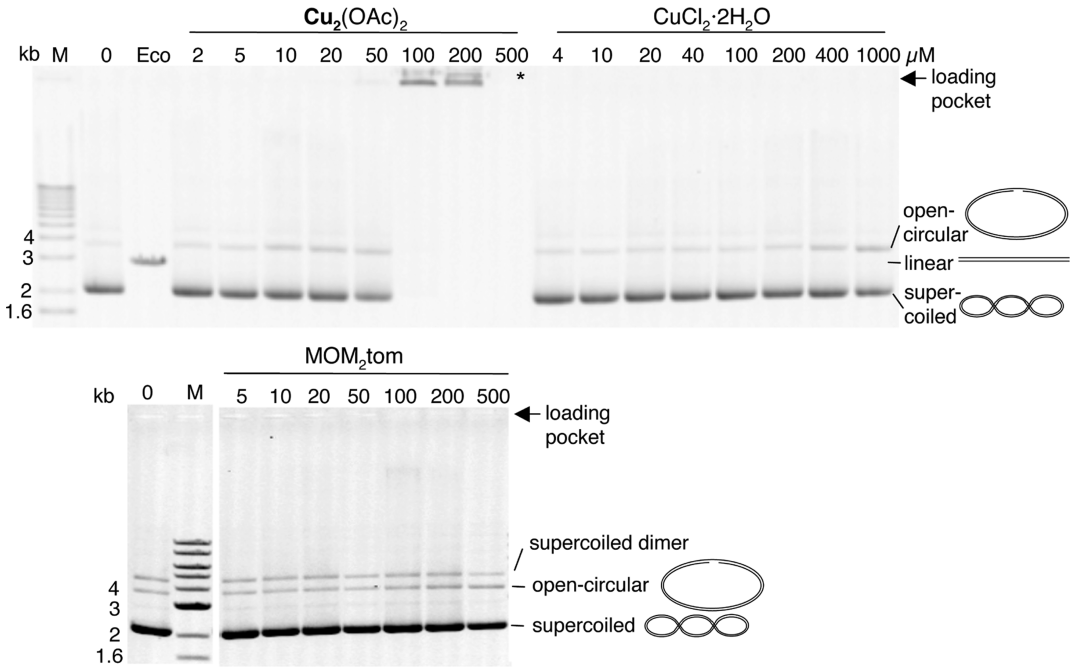

Figure 5. Interaction of $Cu_2(OAc)_2$ with plasmid DNA. Plasmid DNA incubated with the indicated concentrations of $Cu_2(OAc)_2$, copper chloride ($CuCl_2 \cdot 2H_2O$), or MOM_2tom^{Me} for 1 h at 37 °C was separated by agarose gel electrophoresis after transfer into the loading pockets (arrows) and DNA stained with ethidium. DNA hydrolysis in the supercoiled topoisomer leads to the slight increase in the amount of open-circular DNA observed at 10−50 μM $Cu_2(OAc)_2$. The mobility of the DNA is lost above at 100 μM $Cu_2(OAc)_2$, because it does not leave the loading pocket. (*) Plasmid DNA is present but could not be detected with ethidium. (0) no additions; (Eco) plasmid DNA linearized by the restriction enzyme *Eco*RI; (M) marker; kb kilo base pairs.

DOI: 10.1021/ic5028465
Inorg. Chem. 2015, 54, 2679−2690

(Figure 5 asterisk). By contrast, neither copper chloride nor MOM_2tom^{Me} did prevent the migration of the DNA.

The aromatic dye bromphenol blue was present in the loading buffer to monitor the progress of the electrophoresis in an additional experiment. Only in the presence of 100−500 μM $\mathbf{Cu_2}(OAc)_2$ bromphenol blue stayed in the loading pocket (Figure S2b, Supporting Information). This indicates that an immobile aggregate of DNA, $\mathbf{Cu_2}^{2+}$, and bromphenol blue has formed. Even in the absence of bromphenol blue precipitates were visible in the loading pockets of the gel at 500 μM $\mathbf{Cu_2}(OAc)_2$ or above in the presence of 100 μM DNA bases/phosphates. These data indicate that DNA is aggregated by $\mathbf{Cu_2}^{2+}$ at high concentrations and not able to enter the agarose gel.

The observation that DNA is not entering the gel may be explained either by an increased size of the DNA so that it is too large to pass through the gel or by a charge neutrality so that the electric field in the gel electrophoresis experiment does not attract the DNA to enter the gel. The latter would indicate that all negatively charged phosphates of the DNA are complexed by a Cu^{II} ion of $\mathbf{Cu_2}^{2+}$. However, this should be a gradual effect with increasing concentration of $\mathbf{Cu_2}^{2+}$, but no indication of a reduced velocity of DNA migration can be detected at lower concentrations. This implies that the presence of $\mathbf{Cu_2}^{2+}$ at high concentration induces the formation of a firm DNA network, so that the resulting conglomerate is too large to pass through the gel.

DNA Binding Studies in Solution by UV−Vis and NMR Spectroscopies. As the gel electrophoresis experiments showed not only that $\mathbf{Cu_2}(OAc)_2$ possesses only a moderate hydrolytic activity but also that there is also a significant binding of $\mathbf{Cu_2}^{2+}$ that unexpectedly causes interconnection of DNA plasmids, we wanted to quantify this DNA binding. In this respect, we incubated the plasmid DNA (600 μM DNA phosphates) with various amounts of $\mathbf{Cu_2}(OAc)_2$ (100−3000 μM). The $\mathbf{Cu_2}^{2+}$-bound DNA was precipitated by 70% ethanol and 75 mM $NaClO_4$. NaOAc in the standard DNA precipitation protocol was replaced by $NaClO_4$ because ClO_4^- does not complex Cu^{II} in contrast to OAc^-. Pellets were washed and redissolved in either buffer or water, and the absorption at 356 nm (28 100 cm^{-1}) was measured by UV−vis spectroscopy. $\mathbf{Cu_2}(OAc)_2$ shows a strong absorbance at this wavelength (Figure 2 inset), while absorption of DNA is negligible. However, the redissolved pellets exhibited a significant background absorption at high wavelengths, where no DNA absorption is feasible. This background absorption is more intense than the Cu^{II} d−d bands and does not possess their characteristic signature. Moreover, this background absorption increased with increased $\mathbf{Cu_2}(OAc)_2$ concentrations. We assign this background to scattering effects from nanosized objects. The only nanosized objects present are the DNA molecules, but they are not large enough for the scattering observed. The increased scattering by increased $\mathbf{Cu_2}(OAc)_2$ concentration corroborates the results observed by gel electrophoresis that $\mathbf{Cu_2}^{2+}$-bound DNA molecules interconnect.

In another attempt to quantify this DNA binding, we performed titration experiments of $\mathbf{Cu_2}(OAc)_2$ with DNA.[38] DNA binding by intercalation is indicated in these experiments by an intensity decrease of the intercalating chromophore. In our experiments using low DNA concentrations, a significant intensity increase of the absorption of $\mathbf{Cu_2}^{2+}$ at 28 100 cm^{-1} (356 nm) was observed providing strong evidence for a nonintercalating binding mode. However, at moderate to high DNA concentrations, a strong scattering background prevented a quantitative analysis of the DNA binding. Efforts to separate the scattering background led to different results for various titration experiments. Thus, the strong interconnecting tendency of $\mathbf{Cu_2}^{2+}$-bound DNA prevented further analysis of this binding.

The same holds true for NMR experiments. ^{31}P NMR has been proven as a valuable tool to examine the binding of paramagnetic metal ions to the phosphates of DNA.[39] However, even at such low DNA concentrations that needed 3 days acquisition time on a 600 MHz NMR spectrometer for the $\mathbf{Cu_2}^{2+}$-free reference measurements a precipitate resulted by adding $\mathbf{Cu_2}^{2+}$ (1:10 ratio). Thus, NMR measurements in solution for further evaluation of this binding are also prevented.

DNA binding by AFM Imaging. Although conventional methods for studying DNA binding provide strong evidence for a strong binding of $\mathbf{Cu_2}^{2+}$, these methods do not allow a more detailed study as $\mathbf{Cu_2}^{2+}$-bound DNA seems to induce intermolecular DNA entanglements. Thus, we applied single-molecule methods, namely, atomic force microscopy (AFM), optical tweezers (OT), and magnetic tweezers (MT) DNA stretching experiments, to investigate this binding in more detail. First, we investigated the DNA binding properties of $\mathbf{Cu_2}(OAc)_2$ by AFM imaging.[40] Linear λ-DNA was incubated with 50 and 200 μM $\mathbf{Cu_2}(OAc)_2$ and imaged by AFM in tapping mode of operation under ambient conditions. In Figure 6, representative AFM images of the untreated reference λ-DNA (Figure 6a) as well as $\mathbf{Cu_2}(OAc)_2$-treated λ-DNA samples (Figure 6b and 6c) are shown.

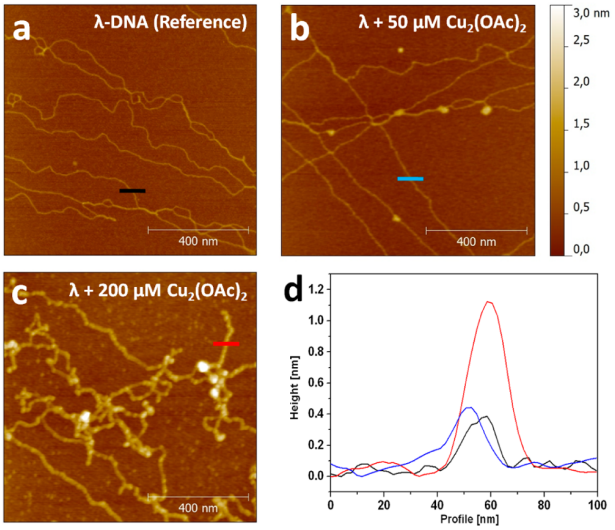

Figure 6. DNA binding of $\mathbf{Cu_2}(OAc)_2$ studied by AFM. (a−c) AFM topography images (1 μm × 1 μm) with a z scale of 3.0 nm. (a) Untreated linear λ-DNA (Reference). (b) $\mathbf{Cu_2}(OAc)_2$-treated λ-DNA (50 μM) with local intra- and interstrand entanglements. (c) $\mathbf{Cu_2}(OAc)_2$-treated λ-DNA (200 μM) exhibiting fully complexed DNA with local intra- and interstrand coiling induced by interaction with the metal complex. It should be noted that the bright spots do not represent the copper complexes alone but copper complex-induced DNA coils and knots. (d) AFM topography cross sections as indicated in a−c displaying an effective corrugation height of 0.4−0.5 and 1.2 nm for untreated λ-DNA and the $\mathbf{Cu_2}^{2+}$-bound DNA, respectively. Local entanglements can be as large as 3.0−4.0 nm.

DOI: 10.1021/ic5028465
Inorg. Chem. 2015, 54, 2679−2690

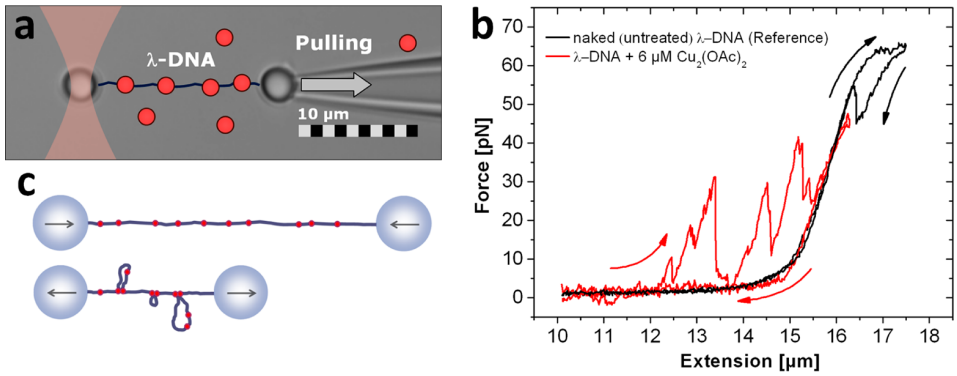

Figure 7. DNA stretching experiments with optical tweezers (OT). (a) OT micrograph setup: One single λ-DNA is immobilized between two microbeads (one is fixed by a micropipette and the other inside the optical trap). (b) Force–extension curves with untreated λ-DNA (black curve) and $Cu_2(OAc)_2$-treated λ-DNA (red curve). In contrast to the reference curve where a significant increase of the force can be discerned at an extension approaching the molecular contour length, a multipeak signature can be detected for $Cu_2(OAc)_2$-treated λ-DNA. (c) Molecular model that attributes these peaks to $Cu_2(OAc)_2$-induced DNA–intrastrand interactions and local DNA entanglements that shorten the global molecular contour length and resist a maximum force before they break.

Whereas native λ-DNA exhibits a linear and smooth appearance, distinct corrugations and aggregation spots can be discerned in Figure 6b and 6c, indicating Cu_2^{2+} binding with local DNA entanglements or partial folding of dsDNA. In Figure 6c the complete DNA strand is affected by the Cu_2^{2+} binding, which could also be quantified by the measured effective height of the complexed DNA strand as shown in Figure 6d. Whereas native λ-DNA usually displays an effective corrugation height of 0.4–0.5 nm, the DNA height at high Cu_2^{2+} concentration increases to 1.2 nm with distinct aggregative spots, yielding a height of up to 3.0–4.0 nm. Since this observation could be made using either Tris buffer or ultrapure water as the solvent and the samples were rigorously washed after the incubation steps (what can also be inferred from Figure 6a) we can exclude salt aggregation effects of the buffer. These single-molecule measurements corroborate the observations from the gel electrophoresis and the solution spectroscopic experiments that the complex Cu_2^{2+} strongly interacts with DNA. Furthermore, our AFM experiments support Cu_2^{2+}-induced DNA intra- and interstrand interactions and bridging as it was concluded from the gel electrophoresis and the solution spectroscopic experiments.

DNA Binding by Optical Tweezers Nanomechanics. In addition to AFM, we investigated the interaction of $Cu_2(OAc)_2$ with dsDNA by molecular stretching experiments with optical tweezers (OT). Here, one single λ-DNA molecule was functionalized on both ends with multibiotins, immobilized between two streptavidin-coated polystyrene microbeads, and subsequently mechanically (over)stretched in force spectroscopy experiments by OT (Figure 7a).[25,41] These nanomechanical experiments allow insights into the structure and force mechanics of long biopolymers and their interplay with binding agents.[25] Reference force/extension experiments exhibit a smooth, nonlinear force increase when stretching the untreated λ-DNA (Figure 7b). A measurable force starts to significantly increase at an extension approaching the molecular contour length of 16.4 μm (Figure 7b, black curve). The plateau that is reached at 64 pN is due to the onset of local melting processes that occur during overstretching.[42] After relaxing the DNA molecule again, the force–extension curve compares almost with the one from the extensional process with the exception of a small hysteretic regime reflecting nonequilibrium processes during the first stages of rehybridization.

Upon adding a solution of 6 μM $Cu_2(OAc)_2$ and waiting typically a few (>2) minutes, the very same DNA molecule was stretched and relaxed again (Figure 7b, red curve). Now, several peaks can readily be discerned in the stretching curve. Each of these peaks can be attributed to Cu_2^{2+}-induced DNA–intrastrand interactions and local DNA entanglements that shorten the global molecular contour length and resist a maximum force before they break (Figure 7c), conceptually very similar to protein unfolding experiments with AFM.[43] These force peak values are typically between 10 and 40 pN, which are in the range of 3–6 times the force of a hydrogen bond.[44] This may lead to the conclusion that Cu_2^{2+}-bound DNA molecules are attracting and binding each other by π–π stacking interactions of the aromatic rings of their naphthalene backbone and/or their pyridyl rings of the pendant arms. Importantly, the corresponding relaxation curves always remained perfectly superimposed with the reference relaxation curve. This observation fully complies with the AFM observation, where the binding of Cu_2^{2+} to dsDNA also induces distinct local entanglements of the DNA. Interestingly, during immediate, subsequent, and ongoing stretching experiments the same overall "multipeak" signature can be detected again, however, appearing at different extension lengths. This of course can be explained by a permutation of the DNA–intrastrand interaction mediated by statistically distributed Cu_2^{2+} binding along the DNA strand. It is worth noting that removing the Cu_2^{2+} solution and additional rinsing with buffer or ultrapure water did not alter the multipeak signature at all, pointing to a firm and irreversible binding of Cu_2^{2+} to DNA.

In order to relate the observed phenomenon unequivocally to the binding of Cu_2^{2+} to DNA, control experiments with copper(II) acetate instead of $Cu_2(OAc)_2$ in comparable concentrations have been conducted. They did not show any force peaks during DNA stretching and no deviation from the original force–extension curve of the untreated λ-DNA (data not shown).

DNA Binding by Magnetic Tweezers. In addition to our AFM and OT experiments we conducted magnetic tweezers (MT) experiments on single torsionally constrained short DNA fragments. Such experiments allow nanomechanical force

DOI: 10.1021/ic5028465
Inorg. Chem. 2015, 54, 2679–2690

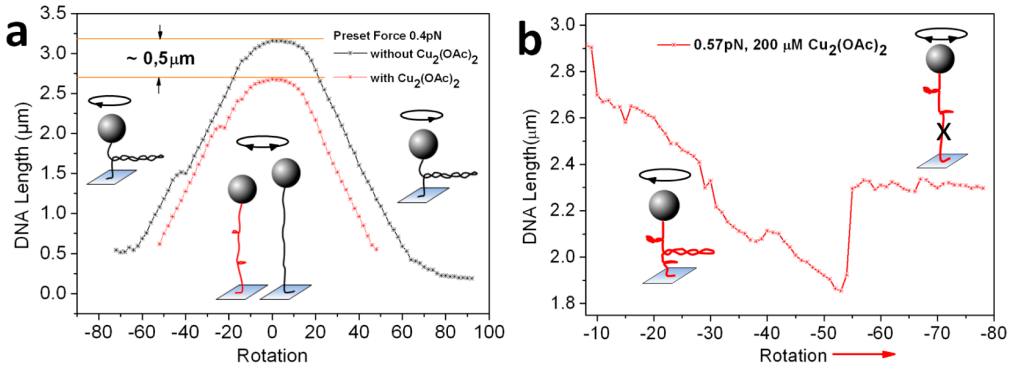

Figure 8. DNA stretching experiments with magnetic tweezers (MT). (a) MT "hat" curve showing the effective length reduction of a torsionally constrained, 3.25 μm long DNA with plectonemic superspiralization due to DNA overwinding (black curve). Upon adding 200 μM $\mathbf{Cu_2}(OAc)_2$ a similar hat curve with a ~0.5 μm smaller effective length could be measured (red curve). (b) In rare cases hydrolytic phosphodiester cleavage of the DNA backbone and introduction of a DNA nick could be observed. During DNA overwinding, suddenly the effective DNA length increased to a certain value that could not any more be affected by further rotation.

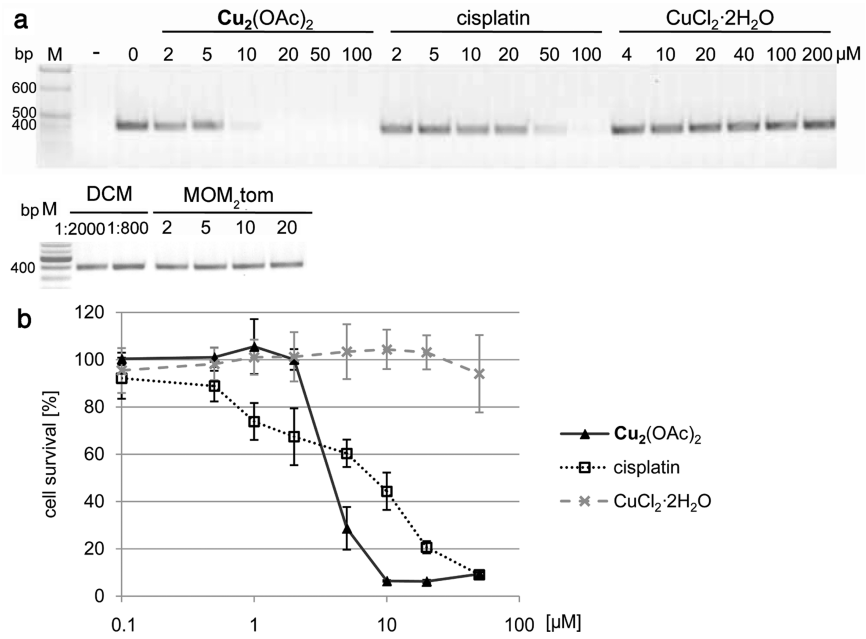

Figure 9. Inhibition of DNA synthesis by $\mathbf{Cu_2}(OAc)_2$ and cytotoxicity of $\mathbf{Cu_2}(OAc)_2$ in human cancer cells. (a) PCR reactions with the indicated additions were analyzed by agarose gel electrophoresis. Ten micromolar $\mathbf{Cu_2}(OAc)_2$ inhibited the DNA polymerase, while copper chloride ($CuCl_2 \cdot 2H_2O$) or MOM_2tom^{Me} were without effect: (−) no DNA; (M) marker; (bp) base pairs; (DCM) dichloromethane was added in the indicated concentration because it was used as a solvent for MOM_2tom^{Me}. (b) Survival of HeLa cells incubated with the indicated additions was analyzed photometrically after 3 days by staining of proteins with sulforhodamine B. Values without additions were set to 100% and used for normalization. Ten micromolar $\mathbf{Cu_2}(OAc)_2$ killed HeLa cells. Shown are means ± SD, n = 3.

spectroscopy experiments with single DNA strands introducing torsional molecular overwinding and manipulative superspiralization.[45] After having immobilized a DNA fragment via their ends between a surface and a superparamagnetic bead (Figure 8a, inset) an external magnetic field is applied, which extends the DNA in the axial direction.

In addition to this axial magnetic force the magnetic field exerts also a radial force component that interacts with the magnetic dipole of the superparamagnetic bead and allows a controlled rotational motion of the bead in both directions. In case of a (i) torsionally constrained DNA immobilization and (ii) nick-free double-stranded DNA structure, the DNA gets overwound and undergoes plectonemic superspiralization accompanied by a reduction of the effective length (= distance surface−bead). This can be seen in Figure 8a (black curve), where such a characteristic "hat" curve is shown.[45] In this experiment the preset stretching force was set to 0.4 pN, leading to an effective contour length of 3.25 μm. Upon adding 200 μM $\mathbf{Cu_2}(OAc)_2$ the same experiment was conducted again, which resulted in a similar "hat" curve that was, however, shifted by ~0.5 μm to smaller effective lengths. This length reduction can be explained as a successful binding of $\mathbf{Cu_2}^{2+}$ to DNA accompanied by DNA−intrastrand interaction as it has also been detected in our OT experiments. In contrast to OT, where those intrastrand interactions (10−40 pN) could be broken up by an external OT force, the limited maximum force in MT (~20 pN) prevented a complete disentanglement of the DNA, therefore resulting in an overall effective length

DOI: 10.1021/ic5028465
Inorg. Chem. 2015, 54, 2679−2690

reduction. In rare cases, long-term MT experiments on the very same $Cu_2(OAc)_2$-treated DNA molecule yielded evidence of rare hydrolytic phosphodiester cleavage of the DNA backbone (Figure 8b) as discussed above in our gel electrophoresis experiments. There, during DNA overwinding, suddenly the effective DNA length increased to a certain value that could not any more be affected by further rotation (clock or counterclockwise). This phenomenon can be explained by the introduction of a nick in a DNA strand as a result of a hydrolytic phosphodiester cleavage conceptually similar to the functional activity of topoisomerases as it could be also detected by MT.[46] The result is an abolished torsional constriction of the DNA leaving the biopolymer in an idle state where no torsional forces can be applied to (Figure 8b, inset).

Inhibition of DNA synthesis. The binding of Cu_2^{2+} to DNA should prevent the interaction of DNA with DNA polymerases due to sterical hindrances and therefore should prevent DNA synthesis. A very efficient way to use DNA polymerases for the synthesis of DNA in test tubes is the polymerase chain reaction (PCR). A template DNA is amplified using two oligonucleotide primers, which hybridize with the DNA as the starting point for the Taq DNA polymerase. DNA is amplified in repeated cycles of denaturation of double-stranded DNA, primer binding, and DNA synthesis. In order to evaluate the effect of Cu_2^{2+}-bound DNA on DNA synthesis, polymerase chain reactions were performed in the presence of $Cu_2(OAc)_2$, copper chloride, MOM_2tom^{Me}, or cisplatin (Figure 9a). A DNA fragment of about 400 bp was amplified in the absence of additions (Figure 9a, 0). Interestingly, the PCR reaction was strongly affected at 10 μM $Cu_2(OAc)_2$, and DNA was not amplified at 20 μM or above. Neither copper chloride nor MOM_2tom^{Me} affected DNA synthesis at these concentrations, excluding nonspecific effects of Cu^{II} or MOM_2tom^{Me} on the DNA polymerase. Comparably, 50 μM cisplatin was required for strong inhibition of the DNA polymerase. These experiments prove that Cu_2^{2+} inhibits DNA synthesis at lower concentrations than cisplatin. This inhibition can be caused by the binding of Cu_2^{2+} to DNA, but these experiments do not allow us to exclude that inhibition is caused by an interaction of Cu_2^{2+} with the DNA polymerase.

Cytotoxicity to Human Cancer Cells. As the PCR experiments show that Cu_2^{2+} is a potent inhibitor of DNA synthesis under those conditions, we tested its cytotoxicity. Equal numbers of HeLa human cancer cells were seeded into 96-well plates and allowed to grow for 24 h. Afterward, they were incubated for 3 days without additions or with 0.1−50 μM $Cu_2(OAc)_2$, copper chloride, or cisplatin. Cell survival was assayed microscopically (Figure S3, Supporting Information). Healthy cells are attached to the surface and spread out. Healthy HeLa cells covered a large fraction of the well in cells incubated with copper chloride or 0.5 or 2 μM $Cu_2(OAc)_2$. By contrast, hardly any healthy cells were seen after incubation with 10 or 20 μM $Cu_2(OAc)_2$, but round stressed or dead cells were visible. As a quantitative measure for cell numbers their proteins were stained with sulforhodamine B and the absorption measured photometrically in an ELISA plate reader (Figure 9b). HeLa cells survived 2 μM $Cu_2(OAc)_2$ but were killed by 10 μM. Cisplatin had a more gradual effect on HeLa cells with cytotoxic effects starting at 1 μM and maximal effects at 20 μM. Similar results were obtained by testing cell survival with the XTT assay (data not shown), which measures metabolic reduction of a tetrazolium reagent to a formazan. As concentrations of 10 μM Cu_2^{2+} inhibited DNA synthesis and resulted in complete cell death, our data suggest that (i) Cu_2^{2+} is membrane permeable, which is a prerequisite for developing novel anticancer drugs, and (ii) binding of Cu_2^{2+} to DNA inhibits DNA polymerase and is the reason for cell death in HeLa cells.

CONCLUSIONS

In summary, we developed by rational design a new dinuclear complex family with the objective of binding to two neighboring phosphates in the backbone of dsDNA yielding a cytotoxic effect to human cancer cells in analogy to the nucleobase-binding family of cisplatin anticancer drugs. Several independent experiments at the single-molecule level and ensemble experiments in solution provide strong evidence for a severe, irreversible binding of the dinuclear $Cu_2(OAc)_2$ complex to DNA. It should be noted that crystallization of a Cu_2^{2+}-bound DNA is elusive as Cu_2^{2+} does not bind to DNA in a sequence-specific manner. Thus, only statistical mixtures of Cu_2^{2+}-bound DNA molecules are present in solution that cannot crystallize. Therefore, only the application of a combination of biochemical, spectroscopic, and single-molecule methods allows obtaining insight into the binding of Cu_2^{2+} to DNA.

The strong inhibition of DNA synthesis and the strong cytotoxicity effects of $Cu_2(OAc)_2$ compared to cisplatin presupposes an efficient Cu_2^{2+}-DNA interaction in vitro and in living cells. The weak but measurable ability of Cu_2^{2+} to cleave DNA demonstrates its binding capability to the DNA phosphates, where the phosphate oxygen atoms on the DNA surface are pointing outward. Cu_2^{2+} binding to these phosphate oxygen atoms results in a decoration of the DNA surface with naphthalene rings making the hydrophilic DNA backbone more hydrophobic. In these aqueous solutions $\pi-\pi$ or other van-der-Waals-like interactions of the naphthalene rings of phosphate-bound Cu_2^{2+} enable intramolecular DNA entanglements as evidenced by the knot and coil formations by AFM and OT stretching experiments. Intermolecular DNA entanglements could be evidenced in gel electrophoresis experiments and by the strong scattering effects in UV−vis spectroscopy experiments. Currently, we are investigating the influence, binding, and cytotoxicity of various other metal ions in $[(tom^{Me})M_2]^{n+}$ for binding to DNA and their potential for oncogenic applications.

ASSOCIATED CONTENT

Supporting Information

Thermal ellipsoid plot, quantification of gel electrophoresis, microscopy pictures of HeLa cell death studies, NMR spectra. This material is available free of charge via the Internet at http://pubs.acs.org.

AUTHOR INFORMATION

Corresponding Author

*E-mail: thorsten.glaser@uni-bielefeld.de.

Notes

The authors declare no competing financial interest.

ACKNOWLEDGMENTS

Financial support by the Deutsche Forschungsgemeinschaft within the Collaborative Research Center SFB613 (project A9) and Bielefeld University is gratefully acknowledged.

DOI: 10.1021/ic5028465
Inorg. Chem. 2015, 54, 2679−2690

REFERENCES

(1) (a) Lippert, B. *Coord. Chem. Rev.* **2000**, *200*−*202*, 487−516. (b) Derose, V. J.; Burns, S.; Kim, N.-K.; Vogt, N. In *Comprehensive Coordination Chemistry II*; McCleverty, J. A., Meyer, T. J., Eds.; Elsevier, Ltd.: Oxford, 2004; Vol. *8*, pp 787−813. (c) In *Nucleic Acid-Metal Ion Interactions*; Hud, N. V., Ed.; Royal Society of Chemistry: Cambridge, 2008. (d) In *Interplay between metal ions and nucleic acids*; Sigel, A., Sigel, H., Sigel, R. K. O., Eds.; Springer: Dordrecht, New York, 2012.

(2) (a) Scott, W. G.; Murray, J. B.; Arnold, J. R. P.; Stoddard, B. L.; Klug, A. *Science.* **1996**, *274*, 2065−2069. (b) Rulisek, L.; Sponer, J. *J. Phys. Chem. B* **2003**, *107*, 1913−1923. (c) Alexandre, S. S.; Murta, B. J.; Soler, J. M.; Zamora, F. *Phys. Rev. B* **2011**, *84*, 045413. (d) Sigel, H.; Amsler, P. E. *J. Am. Chem. Soc.* **1976**, *98*, 7390−7400. (e) Cartwright, B. A.; Goodgame, D.; Jeeves, I.; Skapski, A. C. *Biochim. Biophys. Acta* **1977**, *477*, 195−198. (f) Fischer, B. E.; Bau, R. *Inorg. Chem.* **1978**, *17*, 27−34.

(3) Erkkila, K. E.; Odom, D. T.; Barton, J. K. *Chem. Rev.* **1999**, *99*, 2777−2795.

(4) Claussen, C. A.; Long, E. C. *Chem. Rev.* **1999**, *99*, 2797−2816.

(5) (a) Fichtinger-Schepman, A. M. J.; Vanderveer, J. L.; Denhartog, J. H. J.; Lohman, P. H. M.; Reedijk, J. *Biochemistry.* **1985**, *24*, 707−713. (b) Sherman, S. E.; Gibson, D.; Wang, A. H. J.; Lippard, S. J. *Science* **1985**, *230*, 412−417.

(6) Yang, D.; von Boom, S. S. G. E.; Reedijk, J.; Van Boom, J. H.; Wang, A. H.-J. *Biochemistry.* **1995**, *34*, 12912−12920.

(7) (a) Takahara, P. M.; Rosenzweig, A. C.; Frederick, C. A.; Lippard, S. J. *Nature* **1995**, *377*, 649−652. (b) Takahara, P. M.; Frederick, C. A.; Lippard, S. J. *J. Am. Chem. Soc.* **1996**, *118*, 12309−12321. (c) Gelasco, A.; Lippard, S. J. *Biochemistry.* **1998**, *37*, 9230−9239.

(8) Jamieson, E. R.; Lippard, S. J. *Chem. Rev.* **1999**, *99*, 2467−2498.

(9) (a) Pinto, A. L.; Lippard, S. J. *Proc. Natl. Acad. Sci. U.S.A.* **1985**, *82*, 4616−4619. (b) Suo, Z.; Lippard, S. J.; Johnson, K. A. *Biochemistry.* **1999**, *38*, 715−726. (c) Wang, D.; Lippard, S. J. *Nat. Rev. Drug Discovery* **2005**, *4*, 307−320. (d) Jung, Y.; Lippard, S. J. *Chem. Rev.* **2007**, *107*, 1387−1407. (e) Tornaletti, S.; Patrick, S. M.; Turchi, J. J.; Hanawalt, P. C. *J. Biol. Chem.* **2003**, *278*, 35791−35797. (f) Jung, Y. W.; Lippard, S. J. *J. Biol. Chem.* **2003**, *278*, 52084−52092.

(10) (a) Galanski, M. *Recent Pat. Anti-Cancer Drug Discovery* **2006**, *1*, 285−295. (b) In *Cisplatin-Chemistry and Biochemistry of a Leading Anticancer Drug*; Lippert, B., Ed.; Wiley VCH: New York, 1999. (c) Timerbaev, A. R.; Hartinger, C. G.; Aleksenko, S. S.; Keppler, B. K. *Chem. Rev.* **2006**, *106*, 2224−2248.

(11) Galluzzi, L.; Senovilla, L.; Vitale, I.; Michels, J.; Martins, I.; Kepp, O.; Castedo, M.; Kroemer, G. *Oncogene* **2012**, *31*, 1869−1883.

(12) (a) Pabla, N.; Dong, Z. *Kidney Int.* **2008**, *73*, 994−1007. (b) Miller, R. P.; Tadagavadi, R. K.; Ramesh, G.; Reeves, W. B. *Toxins* **2010**, *2*, 2490−2518.

(13) Ho, Y. P.; Au-Yeung, S. C. F.; To, K. K. W. *Med. Res. Rev.* **2003**, *23*, 633−655.

(14) (a) Lerman, L. S. *J. Mol. Biol.* **1961**, *3*, 18−30. (b) Kelland, L. *Nat. Rev. Cancer.* **2007**, *7*, 573−584.

(15) (a) Wilcox, D. E. *Chem. Rev.* **1996**, *96*, 2435−2458. (b) Cowan, J. A. *Chem. Rev.* **1998**, *98*, 1067−1087.

(16) Weston, J. *Chem. Rev.* **2005**, *105*, 2151−2174.

(17) (a) Gajewski, E.; Aruoma, O. I.; Dizdaroglu, M.; Halliwell, B. *Biochemistry* **1991**, *30*, 2444−2448. (b) Parkin, G. *Chem. Rev.* **2004**, *104*, 699−767. (c) Aoki, S.; Kimura, E. *Chem. Rev.* **2004**, *104*, 769−787. (d) Liu, C.; Wang, M.; Zhang, T.; Sun, H. *Coord. Chem. Rev.* **2004**, *248*, 147−168. (e) Liu, C.; Wang, L. *Dalton Trans.* **2009**, 227−239.

(18) Williams, N. H.; Takasaki, B.; Wall, M.; Chin, J. *Acc. Chem. Res.* **1999**, *32*, 485−493.

(19) Mitic, N.; Smith, S. J.; Neves, A.; Guddat, L. W.; Gahan, L. R.; Schenk, G. *Chem. Rev.* **2006**, *106*, 3338−3363.

(20) (a) Desbouis, D.; Troitsky, I. P.; Belousoff, M. J.; Spiccia, L.; Graham, B. *Coord. Chem. Rev.* **2012**, *256*, 897−937. (b) Mancin, F.; Scrimin, P.; Tecilla, P. *Chem. Commun.* **2012**, *48*, 5545−5559. (c) Zhao, M.; Wang, H.-B.; Ji, L.-N.; Mao, Z.-W. *Chem. Soc. Rev.* **2013**, *42*, 8360−8375. (d) de Souza, B.; Heying, R.; Bortoluzzi, A. J.; Domingos, J. B.; Neves, A. *J. Mol. Catal. A: Chem.* **2015**, *397*, 76−84.

(21) Tjioe, L.; Meininger, A.; Joshi, T.; Spiccia, L.; Graham, B. *Inorg. Chem.* **2011**, *50*, 4327−4339.

(22) Glaser, T.; Liratzis, I. *Synlett* **2004**, *4*, 735−737.

(23) Komatsu, K.; Kikuchi, K.; Kojima, H.; Urano, Y.; Nagano, T. *J. Am. Chem. Soc.* **2005**, *127*, 10197−10204.

(24) The program package JulX was used for spin-Hamiltonian simulations and fittings of the data by a full-matrix diagonalization approach. Bill, E. Unpublished results.

(25) Sischka, A.; Toensing, K.; Eckel, R.; Wilking, S. D.; Sewald, N.; Ros, R.; Anselmetti, D. *Biophys. J.* **2005**, *88*, 404−411.

(26) Sischka, A.; Kleimann, C.; Hachmann, W.; Schaefer, M. M.; Seuffert, I.; Toensing, K.; Anselmetti, D. *Rev. Sci. Instrum.* **2008**, *79*, 063702.

(27) Sischka, A.; Eckel, R.; Toensing, K.; Ros, R.; Anselmetti, D. *Rev. Sci. Instrum.* **2003**, *74*, 4827−4831.

(28) Vandenplas, S.; Wiid, I.; Groblerrabie, A.; Brebner, K.; Ricketts, M.; Wallis, G.; Bester, A.; Boyd, C.; Mathew, C. *J. Med. Genet.* **1984**, *21*, 164−172.

(29) Antonin, W.; Riedel, D.; von Mollard, G. F. *J. Neurosci.* **2000**, *20*, 5724−5732.

(30) Skehan, P.; Storeng, R.; Scudiero, D.; Monks, A.; McMahon, J.; Vistica, D.; Warren, J. T.; Bokesch, H.; Kenney, S.; Boyd, M. R. *J. Natl. Cancer Inst.* **1990**, *82*, 1107−1112.

(31) Mammen, M.; Choi, S. K.; Whitesides, G. M. *Angew. Chem., Int. Ed.* **1998**, *37*, 2755−2794.

(32) Young, M. J.; Chin, J. *J. Am. Chem. Soc.* **1995**, *117*, 10577−10578.

(33) (a) Anbu, S.; Kandaswamy, M.; Varghese, B. *Dalton Trans.* **2010**, *39*, 3823−3832. (b) Zhang, Q.; Liu, J.; Chao, H.; Xue, G.; Li, L. *J. Inorg. Biochem.* **2001**, *83*, 49−55. (c) Wang, Y.; Xiao, W.; Mao, J. W.; Zhou, H.; Pan, Z. Q. *J. Mol. Struct.* **2013**, *1036*, 361−371. (d) Anbu, S.; Kandaswamy, M.; Suthakaran, P.; Murugan, V.; Varghese, B. *J. Inorg. Biochem.* **2009**, *103*, 401−410. (e) Arjmand, F.; Muddassir, M. *J. Photochem. Photobiol. B, Biol.* **2010**, *101*, 37−46.

(34) Tardito, S.; Bussolati, O.; Gaccioli, F.; Gatti, R.; Guizzardi, S.; Uggeri, J.; Marchio, L.; Lanfranchi, M.; Franchi-Gazzola, R. *Histochem. Cell Biol.* **2006**, *126*, 473−482.

(35) Glaser, T.; Liratzis, I.; Froehlich, R.; Weyhermueller, T. *Chem. Commun.* **2007**, 356−358.

(36) (a) Salata, M. R.; Marks, T. J. *J. Am. Chem. Soc.* **2008**, *130*, 12−13. (b) Rodriguez, B. A.; Delferro, M.; Marks, T. J. *J. Am. Chem. Soc.* **2009**, *131*, 5902−5919.

(37) (a) Becher, J.; Toftlund, H.; Olesen, P. H. *Chem. Commun.* **1983**, 740−742. (b) Anderson, O. P.; Becher, J.; Frydendahl, H.; Taylor, L. F.; Toftlund, H. *J. Chem. Soc., Chem. Commun.* **1986**, 699−701. (c) Bouwman, E.; Henderson, R. K.; Powell, A. K.; Reedijk, J.; Smeets, W. J. J.; Spek, A. L.; Veldman, N.; Wocadlo, S. *Dalton Trans.* **1998**, 3495−3499.

(38) (a) Li, H. J.; Crothers, D. M. *J. Mol. Biol.* **1969**, *39*, 461−477. (b) Schmechel, D. E.; Crothers, D. M. *Biopolymers* **1971**, *10*, 465−480. (c) Jennette, K. W.; Lippard, S. J.; Vassiliades, G. A.; Bauer, W. R. *Proc. Natl. Acad. Sci. U.S.A.* **1974**, *71*, 3839−3843. (d) Wolfe, A.; Shimer, G. H.; Meehan, T. *Biochemistry.* **1987**, *26*, 6392−6396. (e) Dougherty, G.; Pigram, W. J. *Crit. Rev. Biochem. Mol. Biol.* **1982**, *12*, 103−132.

(39) (a) Kotowycz, G. *Can. J. Chem.* **1974**, *52*, 924−929. (b) Eichhorn, G. L.; Clark, P.; Becker, E. D. *Biochemistry.* **1966**, *5*, 245−253. (c) Granot, J.; Feigon, J.; Kearns, D. R. *Biopolymers* **1982**, *21*, 181−201. (d) Banville, D. L.; Wilson, W. D.; Marzilli, L. G. *Inorg. Chem.* **1985**, *24*, 2479−2483.

(40) (a) Coury, J. E.; Anderson, J. R.; McFail-Isom, L.; Williams, L. D.; Bottomley, L. A. *J. Am. Chem. Soc.* **1997**, *119*, 3792−3796. (b) Arbuse, A.; Font, M.; Martínez, M. A.; Fontrodona, X.; Prieto, M. J.; Moreno, V.; Sala, X.; Llobet, A. *Inorg. Chem.* **2009**, *48*, 11098−11107. (c) Onoa, G. B.; Cervantes, G.; Moreno, V.; Prieto, M. J. *Nucleic Acids Res.* **1998**, *26*, 1473−1480. (d) Gamba, I.; Salvadó, I.; Rama, G.; Bertazzon, M.; Sánchez, M. I.; Sánchez-Pedregal, V. M.; Martínez-Costas, J.; Brissos, R. F.; Gamez, P.; Mascareñas, J. L.;

DOI: 10.1021/ic5028465
Inorg. Chem. 2015, 54, 2679−2690

Vázquez López, M.; Vázquez, M. E. *Chem.—Eur. J.* **2013**, *19*, 13369−13375.
(41) Heller, I.; Hoekstra, T. P.; King, G. A.; Peterman, E. J. G.; Wuite, G. J. L. *Chem. Rev.* **2014**, *114*, 3087−3119.
(42) King, G. A.; Gross, P.; Bockelmann, U.; Modesti, M.; Wuite, G. J. L.; Peterman, E. J. G. *Proc. Natl. Acad. Sci. U.S.A.* **2013**, *110*, 3859−3864.
(43) Rief, M. *Science* **1997**, *276*, 1109−1112.
(44) Bockelmann, U.; Thomen, P.; Essevaz-Roulet, B.; Viasnoff, V.; Heslot, F. *Biophys. J.* **2002**, *82*, 1537−1553.
(45) Strick, T.; Allemand, J.; Bensimon, D.; Croquette, V. *Biophys. J.* **1998**, *74*, 2016−2028.
(46) Strick, T. R.; Croquette, V.; Bensimon, D. *Nature* **2000**, *404*, 901−904.

DOI: 10.1021/ic5028465
Inorg. Chem. 2015, 54, 2679−2690

4.2 Papers II-IV

Fluorescent dyes are nowadays broadly used in many biotechnological applications. Using their specific fluorescent properties, visualization and detection of stained samples like cells and DNA can be realized in separation gels or fluorescence microscopy. However, their binding alters the nanomechanical behavior and structural properties of DNA polymers, which furthermore affects DNA associated biological processes such as replication and transcription. Although many interaction modes have already been identified, their influences on the mechanical level like elongation, softening and unwinding are often poorly understood. In these three papers, the (nano)mechanisms of four fluorescent DNA dyes (YOYO-1, DAPI, DRAQ5 and PicoGreen) binding to DNA are investigated by molecular recognition on the molecular level. Furthermore, the so far unknown binding modes of DRAQ5 and PicoGreen are identified.

The first dye YOYO-1 is one of the most used fluorescent DNA binding dyes because of its photobleaching-resistance and little background fluorescence, i.e. unbound dye molecules in solution exhibit virtually no luminescence. Once bound to DNA, a more than 1000-fold stronger fluorescence emission of YOYO-1 can be observed. Although YOYO-1 is known (bis-) intercalating into DNA double strands, its impact on mechanical properties of DNA is still under debate. The fact that intercalators elongate DNA molecules is already identified, yet whether they soften DNA polymers or not is still obscure. Employing magnetic tweezers and performing single-molecule experiments, such features can be investigated. Observing the stretching processes of the DNA polymer with and without the presence of YOYO-1, force-extension curves were collected. The data were fitted with the *worm-like-chain model* in order to estimate the DNA contour- and persistence length. As a result, a DNA elongation induced by the YOYO-1 intercalation is obvious, corresponding to other publications. The increment of the DNA contour length lies in the range from 2.3 % to 58 % at dye concentrations from 1 nM to 10 µM. In contrast, the DNA persistence length remained almost constant independent of the dye concentration. Looking into other recent publications, reports of the influence of YOYO-1 binding on the bending stiffness of DNA are not consistent. Several works suggested that the association of YOYO-1 reduces the net charge of the DNA back-

bone, thereby softening the DNA polymer. However, several other works reported minute or no changes of the DNA persistence length. When regarding the experimental environments under which these experiments were conducted, it can be concluded:

i. Beneath the saturation dye concentration, YOYO-1 intercalates specifically into DNA double strands which stiffens the DNA polymer. On the other hand, the electrostatic interaction between the negatively charged DNA backbone and the positively charged dye molecule creates an electrostatic shielding and thus softens the DNA molecule. These two effects cancel each other, leading to an unchanged persistence length of the DNA molecule;

ii. Beyond the saturation dye concentration, a large number of excess dye molecules adhere nonspecifically on the DNA backbone. Therefore, the DNA rigidity is reduced.

Based on these points, through analyzing the association of a typical intercalator agent YOYO-1, intercalators can be generally identified to elongate the DNA molecule but not to affect its bending stiffness. As a matter of fact, the essential reason of the DNA elongation is the intercalation induced unwinding of the double helix. Twisting the target DNA molecule using magnetic tweezers, the phenomenon of plectonemic supercoiling can be recorded as commonly called "hat curves". In presence of YOYO-1 with different concentrations, a shift of the hat curves to negative rotation numbers was observed, which implies that the rotation number at which the DNA polymer was free from the torsional tension is decreased. Analyzing the relation between the change of this rotation number and the DNA elongation, the induced untwisting of the DNA double strands was estimated as 32° per intercalated YOYO-1 molecule. The impact on the DNA torsional elasticity was also found. As a consequence of the YOYO-1 binding, the torsional stiffness of the DNA molecule decreased by a factor of 4.2 (5 µM YOYO-1). Furthermore, with the approximation of the data to the *McGhee-von Hippel model*, the characteristic binding constants of the YOYO-1 association to DNA were determined. Regarding the experimental environment, YOYO-1 binds to DNA specifically with an equilibrium constant of association of $10^6\,\mathrm{M}^{-1}$. Each bound YOYO-1 molecule occupies a binding site size of

about 3.2 base pairs. The DNA molecule is extended by each intercalated dye molecule for about 0.72 nm due to the unwinding.

The second investigated fluorescent dye is DAPI. The classical blue dye DAPI is a widely applied fluorescent DNA stain due to its financial advantage and cell membrane permeability. DAPI is known as a typical minor-groove binder that binds selectively to AT-rich regions of the DNA. Performing force-extension measurements and analyzing the data, DAPI was found to reduce the persistence length of the DNA polymer without altering the contour length. Based on the analysis of DAPI, the binding-induced influences of minor-groove binders can be summarized to softening the DNA polymer but not impacting its length. Furthermore, in DNA rotation experiments, DAPI was proved not being able to unwind the double helix. However, DAPI still slightly influences the DNA torsional stiffness, decreasing it by a factor 1.4 (10 µM DAPI).

The third probed fluorescent DNA stain is DRAQ5. This dye becomes more and more popular due to its cell-permeability and the long excitation wavelength in the red spectral range, which is less harmful for living cells compared to UV light (DAPI). Still, its binding mode and the mechanical impact on samples are not well explored. Therefore, in these works, such characteristics were studied based on the reference-observations on the intercalator YOYO-1 and the minor-groove binder DAPI. Force-extension experiments on DNA molecules were performed with different DRAQ5 concentrations using the zero-concentration as control measurement. At low dye concentrations up to 500 nM, there was no shift of the curves indicating an unchanged DNA contour length. In contrast, fitting the data with the WLC model, a reduction of the persistence length was observed, suggesting a softening effect of the DRAQ5 binding. Regarding the reference studies described above, DRAQ5 can be categorized as a minor-groove binder. Further increasing the dye concentration, an opposite phenomenon occurred. At high concentrations (> 500 nM), an elongation of the DNA molecules was observed while the DNA persistence length remained constant. This result indicated an intercalator-like binding mode of DRAQ5. Based on the observations above, DRAQ5 seems to have a bi-modal binding mode. In order to prove this hypothesis, twisting experiments were also executed. At low concentrations (< 500 nM), the hat curves remained unaffected suggesting no unwinding due to DRAQ5 binding. These observations match the char-

acteristics of the minor-groove binding. At high concentrations (> 500 nM), a shift of the hat curves was observed, exposing an unwinding effect due to the dye intercalation. With a further analysis, an untwisting angle of about 13° per intercalated DRAQ5 dye molecule was determined. In addition, the association of DRAQ5 softens the DNA torsional rigidity by a factor of 4.4 (10 µM DRAQ5). Thus far, it can be concluded that the DNA binding dye DRAQ5 has a bi-modal binding mode:

i. It binds primarily as minor-groove binder at low concentrations;

ii. Secondly, the mono-intercalation dominates when the dye concentration is beyond the threshold concentration (500 nM).

Using the *McGhee-von Hippel model*, the equilibrium constant of association of DRAQ5 was estimated as $10^5\,\mathrm{M}^{-1}$. The binding site size of each DRAQ5 molecule was found as 3.1 base pairs. The DNA elongation per intercalated dye molecule was determined as 0.24 nm.

The last studied fluorescent dye is PicoGreen. PicoGreen can be seen as an alternative to cyanine dyes like YOYO-1. Besides most similar characteristics compared to YOYO-1, a quite short incubation time of 2 to 5 min is a major benefit of this dye. Little is known about its binding mode and other characteristics like the binding affinity etc.. PicoGreen is suggested to have a bi-modal binding mode. However, whether both modes occur simultaneously or successively is still under discussion. Based on this situation, nanomechanical single-molecule experiments on DNA molecules in the presence of PicoGreen were performed. Analyzing the data of the force-extension experiments, no change of the DNA contour- and persistence length was observed at low dye concentrations (up to 100 nM). This result suggested that the applied dye concentrations were too low to show any effect. The reason for this might be that the cations and proteins in the experimental buffer impair the interaction between DNA and the dye molecules [124]. When increasing the dye concentration, an obvious shift of the force-extension curves indicating larger DNA contour lengths was detected, which categorized PicoGreen as an intercalator. Simultaneously, a decrease of the persistence length was also observed, rather suggesting a minor-groove binding. Regarding the chemical structure of PicoGreen, it seems likely that the phenyl quinolinium aromatic system of the PicoGreen intercalates into DNA double strands while the dimethylaminopropyl binds

to the minor-groove at the same time. Here, PicoGreen is therefore suggested as a simultaneous intercalator and minor-groove binder. Upon the intercalation, the unwinding angle per intercalated dye molecule of 21° was quantified by twisting experiments. Since the association of PicoGreen with DNA molecules is strongly environment-dependent, the characteristic binding constants of PicoGreen were explored with both bulk (fluorescence spectroscopy) and single-molecule studies (magnetic tweezers). The results of both studies matched and presented the equilibrium constant of association of PicoGreen in the applied experimental environment as $10^6\,\mathrm{M}^{-1}$. Its binding site size was estimated as 2.3 base pairs and the elongation per intercalated dye was quantified as 0.38 nm as well.

Paper II

Nanomechanics of Fluorescent DNA Dyes on DNA Investigated by Magnetic Tweezers

Y. Wang, A. Sischka, V. Walhorn, K. Tönsing and D. Anselmetti. *Biophysical Journal*, Vol. 111, pp. 1604-1611, 2016.

Abstract: Fluorescent DNA dyes are broadly used in many biotechnological applications for detecting and imaging DNA in cells and gels. Their binding alters the structural and nanomechanical properties of DNA and affects the biological processes that are associated with it. Although interaction modes like intercalation and minor groove binding already have been identified, associated mechanic effects like local elongation, unwinding, and softening of the DNA often remain in question. We used magnetic tweezers to quantitatively investigate the impact of three DNA-binding dyes (YOYO-1, DAPI, and DRAQ5) in a concentration-dependent manner. By extending and overwinding individual, torsionally constrained, nickfree dsDNA molecules, we measured the contour lengths and molecular forces that allow estimation of thermodynamic and nanomechanical binding parameters. Whereas for YOYO-1 and DAPI the binding mechanisms could be assigned to bis-intercalation and minor groove binding, respectively, DRAQ5 exhibited both binding modes in a concentration-dependent manner.

Authors' contributions:
Design of the study: D.A., K.T. and A.S.
Preparation of samples: K.T. and ***Y.W.***
Design and performance of experiments: ***Y.W.***
Data-analysis: ***Y.W.****, A.S. and V.W.*
Writing the manuscript: ***Y.W.****, V.W. and D.A.*

Biophysical Journal
Article

Biophysical Society

Nanomechanics of Fluorescent DNA Dyes on DNA Investigated by Magnetic Tweezers

Ying Wang,[1] Andy Sischka,[1] Volker Walhorn,[1] Katja Tönsing,[1] and Dario Anselmetti[1,*]
[1]Experimental Biophysics, Physics Faculty, Bielefeld University, Bielefeld, Germany

ABSTRACT Fluorescent DNA dyes are broadly used in many biotechnological applications for detecting and imaging DNA in cells and gels. Their binding alters the structural and nanomechanical properties of DNA and affects the biological processes that are associated with it. Although interaction modes like intercalation and minor groove binding already have been identified, associated mechanic effects like local elongation, unwinding, and softening of the DNA often remain in question. We used magnetic tweezers to quantitatively investigate the impact of three DNA-binding dyes (YOYO-1, DAPI, and DRAQ5) in a concentration-dependent manner. By extending and overwinding individual, torsionally constrained, nick-free dsDNA molecules, we measured the contour lengths and molecular forces that allow estimation of thermodynamic and nanomechanical binding parameters. Whereas for YOYO-1 and DAPI the binding mechanisms could be assigned to bis-intercalation and minor groove binding, respectively, DRAQ5 exhibited both binding modes in a concentration-dependent manner.

INTRODUCTION

Fluorescent DNA dyes are broadly used in biology and biomedicine to detect and image DNA in separation gels or in fluorescence light microscopy. The specific interaction of these dyes with DNA affects the nanomechanical behavior and the structural properties of DNA, interfering with many of the well-known DNA associated processes like transcription and replication. Although a number of different interaction modes have been identified, the associated molecular mechanics like elongation, untwisting, and softening of the DNA polymer are often poorly understood and debated. In this work we chose three commonly used fluorescent stains (YOYO-1, DAPI, and DRAQ5) and investigated the nanomechanical effects of the DNA-binding dyes using magnetic tweezers (MTs). The green-fluorescent DNA dye YOYO-1 is a tetracationic homodimer of oxazole yellow and belongs to the monomethine cyanine family. It is one of the most commonly used nucleic acid dyes and shows virtually no fluorescence in solution but in contrast a more than 1000-fold increase of fluorescent intensity when bound to DNA (1). YOYO-1 is known to interact with DNA as a bis-intercalator, which leads to a local unwinding the double helix and a considerable lengthening of the DNA strand. The reported elongation varies from 18% to 50% (2–7). The associated unwinding angle of YOYO-1 has been measured in MT experiments to 24° by Günther et al. (8), whereas Johansen et al. measured an angle of 106° by NMR (9). A further debate was related to how YOYO-1 influences the bending stiffness or softening of the biopolymer. Quake et al. reported a 32% persistence-length increase of DNA with optical tweezers (3), whereas two other groups have measured reduction of 70% with the same methodology (4,5). Shi et al. have used entropic force microscopy and observed a reduction of 9% of the persistence length (7). By using atomic force microscopy (AFM) in solution, Maaloum et al. reported a reduction of 44% (6), whereas Kundukad et al. suggested a more or less constant persistence length under ambient conditions (10). Recently, Günther et al. (8) employed MTs to perform single-molecule stretching experiments and concluded that the persistence length of dsDNA remained almost constant during intercalation with YOYO-1.

Although YOYO-1 is regarded as an efficient and photobleaching-resistant DNA dye, it is cell-impermeable, which means that it cannot be applied in live- and fixed-cell experiments. Therefore, the classical blue DNA dye DAPI, which belongs to the indol family, is the dye of choice for staining the chromosomes in the nucleus of fixed and living cells. It could be shown that the binding of DAPI to DNA leads to a

Submitted June 8, 2016, and accepted for publication August 26, 2016.
*Correspondence: dario.anselmetti@physik.uni-bielefeld.de
Editor: Keir Neuman
http://dx.doi.org/10.1016/j.bpj.2016.08.042

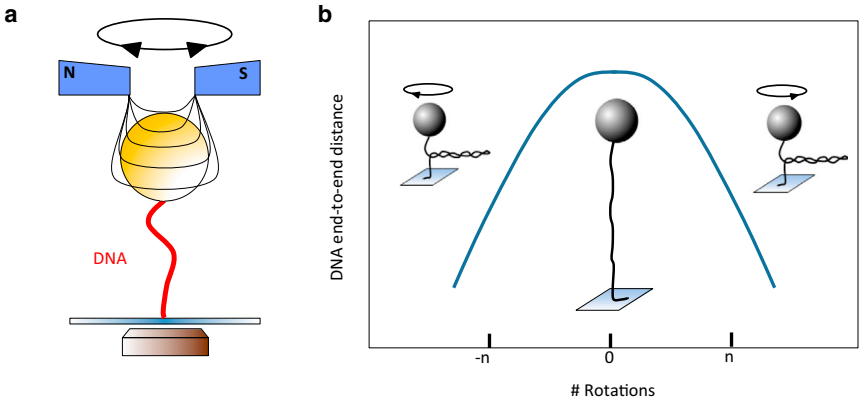

FIGURE 1 Schematic of magnetic tweezers. (*a*) A single dsDNA molecule is attached between a surface and a micrometer-sized magnetic bead that is trapped and manipulated in a variable, external magnetic field. (*b*) Supercoiling curve (*hat curve*) of dsDNA is shown. By rotating a magnetic bead, mechanical torque is applied to the DNA molecule and the end-to-end distance is reduced. Hat curves can be divided into two regimes: for a number of twists, R, smaller than the buckling number, N, the torque is released along the double strands (torsional elastic regime). At higher rotation numbers, $R > N$, the torsional stress is released by the formation of plectonemes that leads to a substantial topological shortening of the DNA end-to-end distance (plectonemic regime). To see this figure in color, go online.

20-fold increase of the fluorescence (11). However, since DAPI can only be excited with ultraviolet (UV) light, exposition of this fluorescent dye interferes with the viability of the probed cells and somewhat limits the accessible observation time. DAPI is known as a DNA minor groove binder that binds preferentially to AT-rich regions and theoretically influences the bending rigidity of DNA (12–14). In a recent AFM study, Japaridze et al. (15) reported that upon DAPI staining the contour length of dsDNA remains unchanged, whereas, the persistence length considerably decreased up to 42%.

In contrast to DAPI, DRAQ5 (deep red fluorescent antraquinone dye Nr. 5) is less harmful for living cells due to the long excitation wavelength in the red spectral range (647 nm) (16). Furthermore it is membrane-permeable and it can be multiplexed with many other fluorophores. Consequently, it is an ideal choice for many live-cell experiments. Yet, the binding mode of DRAQ5 to DNA is still debated. Japardize et al. (15) and Martin et al. (17) suggested DNA intercalation as the dominating binding mechanism whereas Njoh et al. (18) concluded in their molecular docking studies that the binding mode can adequately be described by AT preferred engagement in the DNA minor groove. A more competitive bi-mechanistic interaction was suggested by Islam et al. (19) in their theoretical modeling experiments, however, without experimentally investigating further associated nanomechanical properties.

In this work, we investigated the DNA binding properties of DRAQ5 by means of MT extension and overwinding experiments within a force regime from 5×10^{-3} pN up to 10 pN. The well-known bis-intercalator YOYO-1 and the minor groove binder DAPI served as a reference to interpret and quantify the influence of DRAQ5 association on the structural and nanomechanical properties of dsDNA. Within this mechanistic picture we found that DRAQ5 exposes a bimodal binding behavior. Our results consistently indicate that at concentrations below 0.5 μM, DRAQ5 binds as a minor groove binder whereas at higher dye concentrations intercalation dominates.

MATERIALS AND METHODS

DNA sample preparation

We prepared λ-DNA fragments (New England BioLabs, Frankfurt, Germany) that were functionalized at one end with several biotins (Biotin-14-dCTP, Metabion, Steinkirchen, Germany) and on the other side with several digoxigenins (Dig-11-dUTP, Hoffmann-LaRoche, Penzberg, Germany) according to a recently published protocol (20). The fragments were repaired with PreCR Repair Mix (New England BioLabs, Frankfurt, Germany) and stored in 10 mM PBS buffer (137 mM NaCl + 2.7 mM KCl (pH 7.4) at 25°C) at 4°C. The DNA fragments were attached via several antidigoxigenins to the surface of a glass cover slip of a custom-made flow cell. As a handle, streptavidin-coated magnetic beads with a diameter of 1 μm (Dynabeads MyOne Streptavidin C1, Life Technologies, Carlsbad, CA) were attached to the other DNA side. For that, the magnetic beads (5 mg/ml) were gently mixed with DNA fragments (60 pM) into the MT buffer and incubated for 15 min. Before every experiment we verified the structural integrity of each probed DNA-molecule (nick-free) and its torsionally constrained immobilization, and we acquired a reference hat curve by MT overwinding experiments. Moreover we verified the contour length by means of stretching experiments (21).

Fluorescent dyes

In the experiments we used three fluorescent dyes, namely YOYO-1, DAPI, and DRAQ5. YOYO-1 iodide was purchased from Life Technologies (stock solution 1 mM). DAPI was obtained from Sigma-Aldrich (Seelze, Germany; stock solution 1 mg/500 μl). DRAQ5 was acquired from Thermo Fisher Scientific (Ulm, Germany; stock solution 5 mM). Before the experiments all three stock solutions were diluted with the MT buffer to concentrations from 1 nM to 10 μM.

Magnetic tweezers analysis

The used MT setup is a commercial system (PicoTwist, Lyon, France) and has been described previously (21–23) (Fig. 1 *a*). The DNA-functionalized beads were filled into the chamber of the flow cell, whose surface was functionalized with antidigoxigenins (0.2 mg/ml, at 37°C for 2 h) and allowed to rest for 20–30 min. Then, the flow cell was flushed with the MT buffer so that unbound DNA-beads were removed. All force-extension experiments have been taken from 5×10^{-3} pN up to an upper force limit of 10 pN. The overwinding experiments were performed with a preset force of 0.2 pN. The DNA was stained within the fluid cell by means of flushing the fluorescent dyes into the chamber with stepwise increasing concentrations. To exchange the buffer completely a multitude of the fluid cell

volume was infused. Furthermore, the DNA was incubated for another 20 min to achieve thermodynamical equilibrium. To avoid crosstalk of different dyes, we replaced the complete flow cell after every experimental series. All experiments were performed in the MT buffer at 25°C. Of note, we took special attention that DRAQ5 that was incubated in total darkness according to the instructions of the manufacturer.

MT buffer

All the experiments were performed with the MT buffer that contained 10 mM phosphate buffered saline (137 mM NaCl + 2.7 mM KCl (pH 7.4) at 25°C) with 0.1 mg/ml additional bovine serum albumin (Sigma-Aldrich) and 0.1% Tween 20 (Sigma-Aldrich).

Analysis of the data

The molecular stretching curves were fitted with the following worm-like chain (WLC) model:

$$\frac{FP}{k_{\mathrm{B}}T} = \frac{1}{4}\left(\left(1-\frac{d}{L}\right)^{-2} - 1\right) + \frac{d}{L}, \qquad (1)$$

for each dye concentration (24,25). Here, F, P, $L(c)$, $k_{\mathrm{B}}T$, and d denote the pulling force, the persistence length as a function of the dye concentration, the contour length, the thermal energy, and the DNA molecular extension (end-to-end distance), respectively. Furthermore, the correlation between the fractional DNA elongation γ and dye concentrations c were analyzed by fitting it with the following McGhee–von Hippel model (26):

$$\frac{\gamma}{c} = a\,K_a\frac{\Delta x}{x_{bp}} \cdot \frac{\left(1-\frac{n\,\gamma\,x_{bp}}{a\,\Delta x}\right)^{n}}{\left(1-\frac{(n-1)\,\gamma\,x_{bp}}{a\,\Delta x}\right)^{n-1}}, \qquad (2)$$

where K_a is the equilibrium constant of association for intercalation, n is the binding site size per dye molecule, x_{bp} is the reference distance between two base pairs ($x_{bp} = 0.34$ nm), Δx is the DNA elongation due to one binding site of an intercalated dye, and a is a dimensionless geometrical factor for intercalators like DRAQ5 ($a = 1$) and bis-intercalators like YOYO-1 ($a = 2$).

RESULTS AND DISCUSSIONS

To investigate the impact of dye association on the nanomechanic properties of DNA we used a joined approach of MT-based extension and overwinding experiments. MTs allow the exact determination of the DNA end-to-end distance, contour, and persistence length at full control of the DNA helical twist. First, we performed extension experiments while the twist was adjusted in such a way that the DNA remained in the torsionally relaxed state in which it exposes the maximum end-to-end length. The DNA was incubated within the MT fluid cell at various dye concentrations for 20 min. We started with concentrations as low as 1 nM to inhibit artifacts due to unspecific adhesion. The stained DNA molecules were extended at zero twist to acquire force-extension curves with a maximum force up to 10 pN (Fig. 2, *a*, *c*, and *e*). After each extension step we allowed the molecular system to settle down for ~5 s before the force and end-to-end distance were acquired with an integration time of ~1 min. The force-extension data was approximated to the WLC model to estimate the DNA contour and persistence length and also to the McGhee–von Hippel model to evaluate the equilibrium constant of association, the induced length increase per associated dye, and the binding site size in base pairs per dye molecule, respectively.

Contour and persistence length

By analyzing the YOYO-1 bis-intercalator we found a successive shift of the force-extension curves toward larger contour lengths ranging from elongations of 2.3% to 58% at dye concentrations from 1 nM to 10 μM (Fig. 2 *a*). This finding is in full accordance with recently published results (5). In contrast, the DNA persistence length remained unchanged at ~50 nm independent of the dye concentration (Fig. 2 *b*). Interestingly, reports on the impact of YOYO-1 association on the persistence length are not very consistent. Kundukad and co-workers outlined the key data of various publications that were acquired with different experimental techniques such as optical tweezers or MTs, AFM, and entropic force microscopy (10). There, minute or no changes of the persistence length nicely matching our findings stand in contrast to publications reporting on a significant decrease (up to 70%). Though, when regarding the experimental conditions under which these data are obtained, a consistent scheme can be found: whenever the DNA is incubated with YOYO-1 below the saturation concentration (i.e., less than one YOYO-1 per four base pairs), no or only a small change of the persistence length was observed (8,10). In contrast, when measurements have been performed with a large excess of dye molecules the DNA becomes more flexible, which corresponds to a decrease of the persistence length (3–6). We ascribe this to an additional unspecific adhesion like mono-intercalated YOYO-1 and electrostatic interaction between the negatively charged DNA backbone and the positively charged dye molecule that generates an electrostatic shielding and thus reduces the DNA stiffness (27).

Furthermore, we also tested the minor groove binder DAPI in a concentration-dependent manner. According to our data, DAPI binding to DNA has virtually no influence on the contour length that can be deduced from the evolution of the force-extension curves (Fig. 2 *c*). We furthermore fitted our data to the WLC molecular elasticity model (Eq. 1) and found no obvious elongation. However, we observed a progressive but moderate reduction of the persistence length from 48 to 44 nm for increasing dye concentrations (Fig. 2 *d*), which is consistent with recent results (15). As a consequence, we can conclude that minor groove binding leads to a moderate softening of the dsDNA.

By knowing the influence of intercalation and minor groove binding on DNA nanomechanics, we now analyzed the binding mode of the DNA dye DRAQ5. Interestingly,

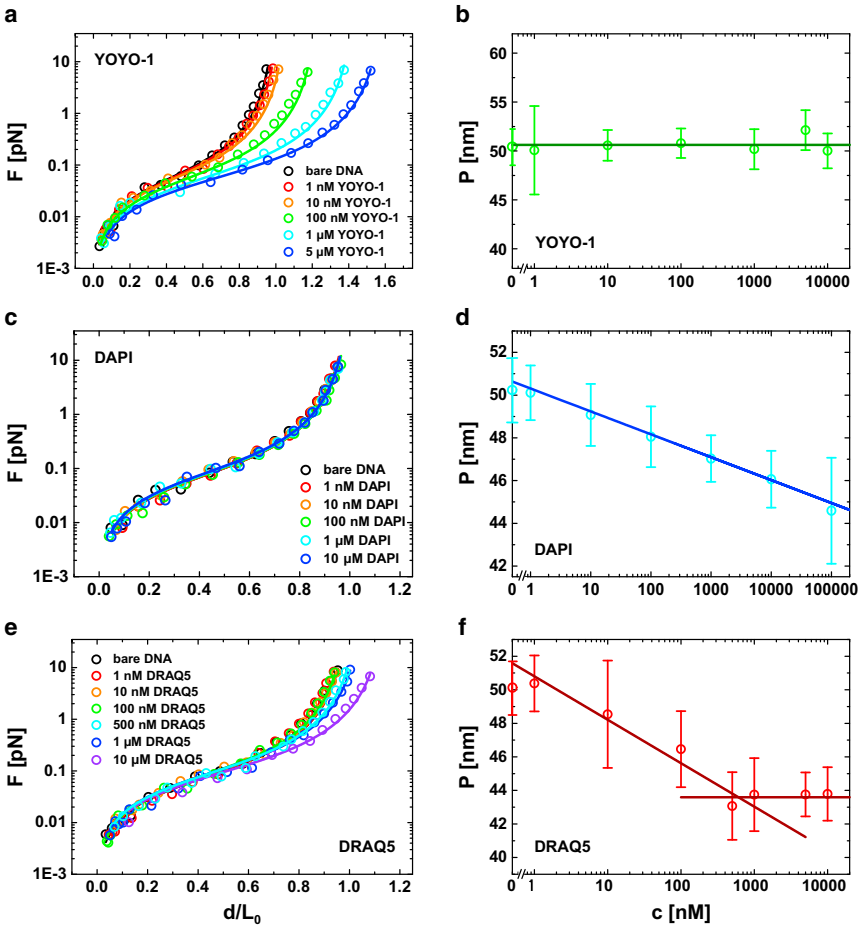

FIGURE 2 Force-extension curves of bare and dye-complexed dsDNA (*left column*) for (*a*) YOYO-1, (*c*) DAPI, and (*e*) DRAQ5. Open circles represent experimental data whereas solid lines stand for WLC fits. Persistence length in dependence of dye concentration is shown (*b*, *d*, and *f*). To see this figure in color, go online.

DRAQ5 exhibits characteristics of both, minor groove binding and intercalation (Fig. 2 *e*). At low dye concentrations (<0.5 μM), we merely observed a decrease of the persistence length from ~50 to 43 nm while the contour length remained constant (Fig. 2 *f*). In accordance with our previous findings this clearly indicates a minor-groove-like binding mechanism. By further increasing the dye concentration we found an incremental shift of the force-extension curves toward a higher contour length (Fig. 2 *e*). Similar to the results obtained for YOYO-1, this indicates an intercalator-like binding mode. Noteworthy, the increase of the contour length is rather moderate. We estimated the maximum increase to be 14% at a dye concentration of 10 μM. Moreover, the persistence length did not vary anymore at high DRAQ5 concentrations (Fig. 2 *f*).

Fractional elongation and association constant

As shown before, intercalation induces an increase of the DNA contour length. This elongation can be used to further validate and quantify the intercalating character of a bond. We plotted the fractional elongation $\gamma(c) = (L(c) - L_0)/L_0 = \Delta L/L_0$ as a function of the dye concentration c. Here L_0 denotes the contour length of bare DNA whereas $L(c)$ is the DNA contour length as a function of the dye concentration. We approximated $\gamma(c)$ to the McGhee–von Hippel model (Eq. 2) to determine the equilibrium constant of association K_a, the binding site size per dye molecule n in base pair, and the DNA elongation per intercalated dye molecule $a \times \Delta x$, respectively (Fig. 3, *a* and *c*). Because DAPI as a typical minor groove binder does not affect the contour length, this analytical approach is not applicable (Fig. 3 *b*).

For YOYO-1 the equilibrium constant K_a was calculated to be $(3.58 \pm 0.103) \times 10^6$ M^{-1}, which is nicely supported by previously published data (5). The apparently reduced affinity can be attributed to elution effects caused by the high salt concentration of the PBS buffer (137 mM NaCl + 2.7 mM KCl) (28). The binding site size was estimated as $n = 3.22 \pm 0.3$ bp/dye. This comparably large value reflects the fact that bis-intercalation inhibits the occupation of adjacent base pair voids (29). This negative cooperativity is referred to as "nearest neighbor exclusion principle" (30). The DNA elongation per intercalated molecule was $2 \cdot \Delta x = 0.72 \pm 0.082$ nm/dye.

Analogously, we analyzed the DNA elongation by DRAQ5 binding within the intercalating regime ($c > 0.5\mu$M). Here we

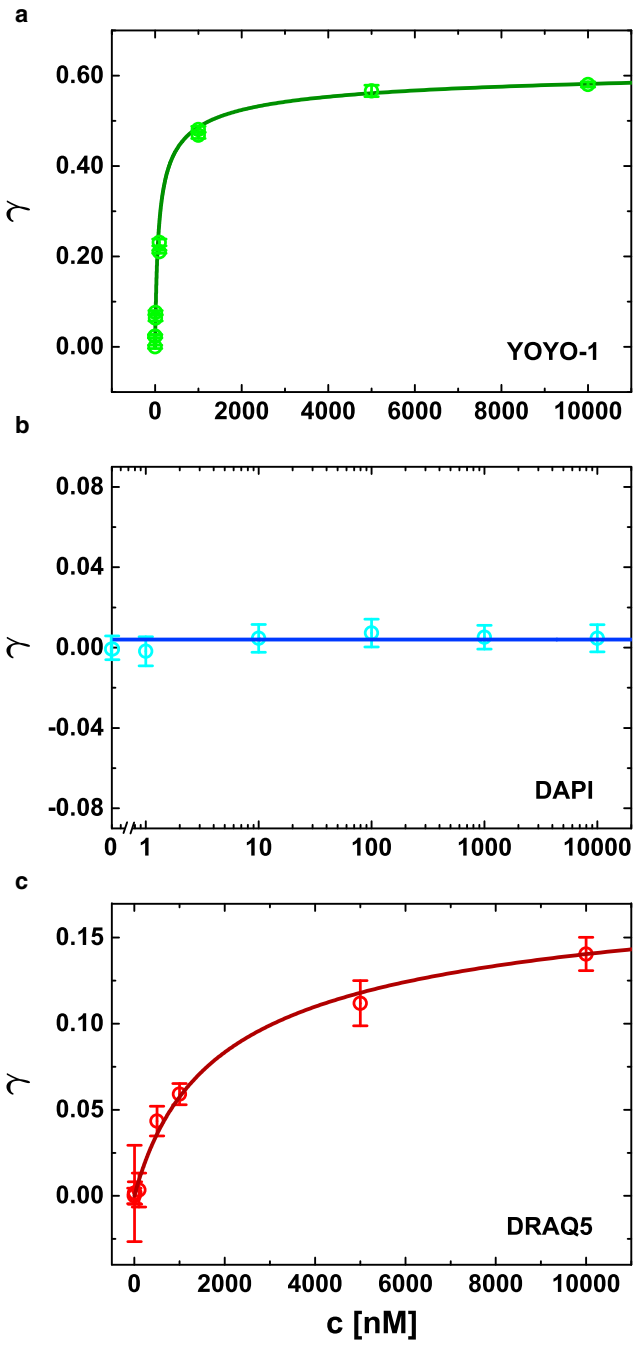

FIGURE 3 Plots of the fractional elongation $\gamma(c)$ of (*a*) YOYO-1, (*b*) DAPI, and (*c*) DRAQ5. Experimental data (*open circles*) are approximated to the McGhee–von Hippel model (*solid line in a* and *c*). To see this figure in color, go online.

estimated an equilibrium constant of association of $K_a = (1.40 \pm 0.123) \times 10^5\ \mathrm{M}^{-1}$ which, compared with YOYO-1, is more than one magnitude smaller than for YOYO-1. Furthermore, we estimated a binding site size of 3.13 ± 0.286 bp/dye. Compared with a mono-intercalator such as ethidium bromide (~2 bp/dye), one would expect a smaller binding site size (31,32). However, as DRAQ5 exposes nonuniform binding characteristics, the McGhee–von Hippel model might be of limited applicability. Probably, minor groove and intercalative binding interfere with each other: apparently, minor groove binding is favored in the first place until a certain degree of binding sites is occupied. Then, intercalative binding dominates. Hence, the amount of free intercalative binding sites is reduced due to previous minor groove association that in turn inhibits a high intercalation density along the dsDNA. Therefore, the estimated binding-site size appears larger than expected.

The intercalation of DRAQ5 to DNA seems to be a less-pronounced secondary binding mode. In line with this finding is also a comparably small elongation per (intercalative) bond. We found a lengthening per dye molecule of $\Delta x = 0.24 \pm 0.020$ nm/dye, which is nearly identical to data obtained for ethidium bromide ($\Delta x = 0.25$ nm/dye) (31).

Dye-induced unwinding

A crucial feature of MTs is the ability to apply torque to single molecules. When rotating magnetic beads, attached DNA molecules are twisted in a controlled manner and plectonemic strands can be produced. These induced conformational changes are often displayed as DNA supercoil curves that expose the end-to-end distance d versus the number of applied turns R (Fig. 1 *b*). Commonly, these are also referred to as "hat curves." In the low-force range (~ <0.5 pN), bare dsDNA exposes a symmetric torsional behavior (33). There, the peak of the hat curve denotes the rotational relaxed state where the DNA exposes the maximum end-to-end distance. Starting from here, the hat curve can be divided into two regimes (Fig. 1 *b*). At low rotation numbers the torque that is built up by the intrinsic torsional elasticity (torsional elastic regime) of the DNA double strand goes along with a slight decrease of the end-to-end distance. In contrast, at higher rotation numbers the torque induces buckling of the DNA double helix that leads to the formation of topological plectonemes and a significant reduction of the end-to-end length. The rotation number at the transition of these regimes is often referred to as buckling number N (Fig. 1 *b*) (34).

To strengthen the results of our extension measurements we acquired overwinding curves at pulling forces of 0.2 pN for all three ligands (Fig. 4, *a*, *c*, and *e*). First, YOYO-1 was applied to torsional fixed but relaxed ($R = 0$) dsDNA with a stepwise increasing concentration. The acquired hat curves expose a successive shift to negative rotation numbers and an increasing end-to-end distance that indicates a gradual unwinding of the dsDNA (Fig. 4 a). Evidently, YOYO-1 intercalation induces a supercoiling that can be removed by applying rotations in the (negative) counterdirection (6,8,10). We estimated the untwisting angle per dye molecule θ as follows:

$$\theta = \frac{\Delta R}{\#} = \frac{\Delta R}{\Delta L} \cdot (a \cdot \Delta x), \tag{3}$$

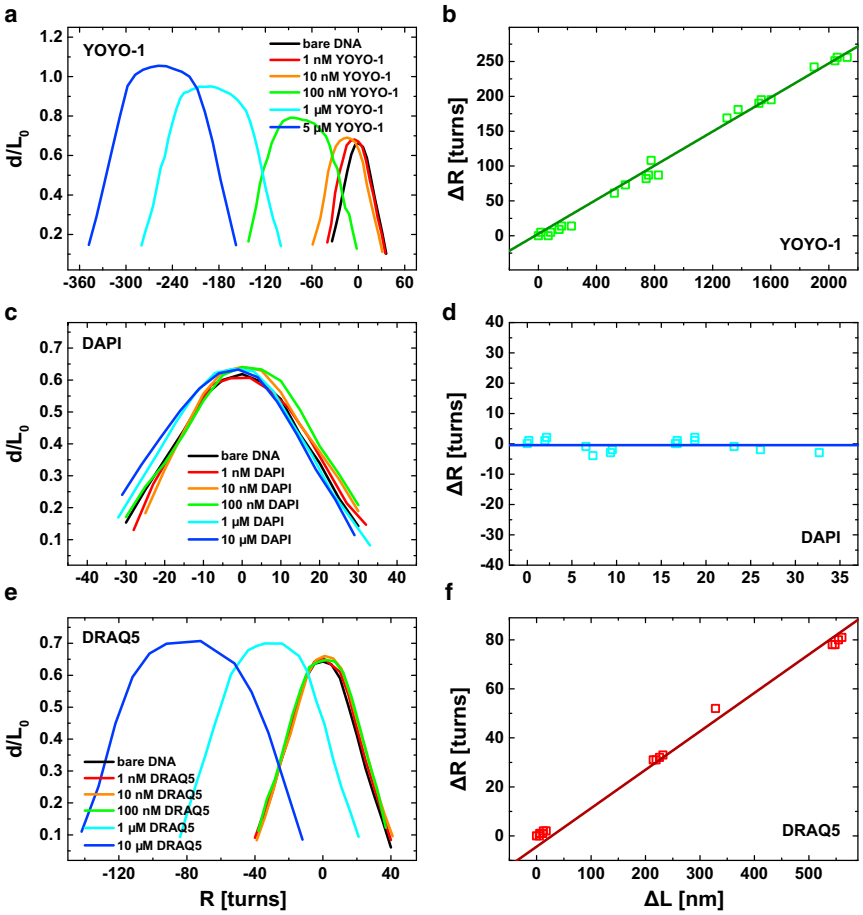

FIGURE 4 Supercoiling curves (*hat curves*) of dsDNA complexed with (*a*) YOYO-1, (*c*) DAPI, and (*e*) DRAQ5. The data were acquired at a load of 0.2 pN. (*b*, *d*, and *f*) Linear approximation of the rotation-elongation plots allows to estimate the unwinding angle per intercalated dye. The error of ΔL was found in the order of 10 nm where ΔR occupied an error of about $\pm$ 1 turn. To see this figure in color, go online.

where ΔR quantifies the unwinding at different dye concentrations c, and # is the corresponding number of intercalated dye molecules. The latter is calculated by the difference of the DNA contour length ΔL divided by lengthening per dye molecule $a \times \Delta x$. Both quantities have been estimated in the experiments before. We plotted ΔR versus ΔL and estimated by θ approximating the slope of the plot (Fig. 4, *b*, *d*, and *f*). As a result, we obtained an angle of 0.088 ± 0.0411 turns per dye corresponding to $\theta = 31.68 \pm 14.79^\circ$ per dye for YOYO-1.

In contrast, supercoil curves that have been acquired upon association of the minor groove binder DAPI hardly differ from those acquired with bare DNA (Fig. 4 *d*). We neither observed a rotational shift nor a significant increase of the end-to-end distance. This finding verifies that DAPI minor groove binding does not induce supercoiling to dsDNA and therefore elongation due to unwinding cannot be observed.

The results of the rotation experiments of DRAQ5, which are presented in Fig. 4 *e*, reveal features of both, minor groove binding and intercalation. At dye concentrations below 0.5 μM, DRAQ5 associates to DNA like a minor groove binder that can be seen from the overlaying hat curves (Fig. 4 *e*). At higher dye concentrations, the hat curves yield a substantial shift to negative rotation numbers and a slight increase of the end-to-end distance indicating an intercalation-like binding mechanism. Notably, as intercalation apparently is a less-distinct secondary binding mode, the increase of the molecule end-to-end distance as compared with YOYO-1 is rather small (Fig. 4 *e*). We calculated the unwinding angle within the intercalation regime as described before and estimated an unwinding of 0.036 ± 0.0127 turns per dye that is equivalent to $\theta = 12.99 \pm 4.58^\circ$ per dye (Fig. 4 *f*). However, the exact quantity of θ might be affected by potential crosstalk between minor groove binding and intercalation as the lengthening per dye molecule Δx (Eq. 3) was estimated by the McGhee–von Hippel model (Eq. 2).

Effects on torsional elasticity

Disregarding the shift to negative rotation numbers and an increase of the end-to-end distance that has been discussed above, we furthermore observed a substantial broadening of the hat curves within the intercalation regime that can be interpreted alongside within the picture of torsional elasticity and the formation of topological plectonemes. There, the buckling number N defines the crossover regime where the

ability of dsDNA to settle torsional stress along the strand is exhausted and topological plectonemes are formed instead. For YOYO-1 the buckling number shifted from $N = 6$ for bare dsDNA to $N = 40$ at a concentration of 5 μM. Notably, N was determined with respect to the new shifted center of the hat curve. Furthermore, the hat curves continuously flatten within the torsional elastic regime for increasing dye concentrations (Fig. 4 *a*). In contrast, the plectonemic regime ($R > N$) is virtually unchanged throughout the whole experiment. The shift of the buckling transition to higher rotation numbers together with the flattening of the hat curves indicates that YOYO-1 binding softens dsDNA, i.e., the ability to release torque along the double strands is enhanced. Hence, more twists have to be applied until buckling and the formation of plectonemes are induced. To quantify the effect of intercalation we analyzed our data within the following simplified torsional elasticity model (23,32,34):

$$\frac{C(c)}{C_0} = \frac{L(c)}{L_0} \cdot \frac{N_0}{N(c)} \sqrt{\frac{P(c)}{P_0}}, \tag{4}$$

where the torsional elasticity of dsDNA in the presence and absence of dye molecules are denoted by $C(c)$ and C_0, respectively. Similarly, L, P, and N represent the contour length, the persistence length, and the buckling number, respectively. At a YOYO-1 concentration of $c = 5$ μM we observed a relative lengthening of $L(c)/L_0 \approx 1.59$ and a virtually unchanged persistence length $P(c)/P_0 \approx 1$. Moreover a significantly reduced relative torsional elasticity of $C(c)/C_0 \approx 0.24$ was discerned. These results are consistent with recently published data on the (mono-) intercalator ethidium bromide (32).

In contrast, DAPI minor groove binding has only a very small impact on the shape of the hat curves. At a concentration of $c = 10$ μM, the rotation-extension curve yields only a minimal shift of the buckling number ($N = 6 -> N = 8$) and a slight broadening of the torsional elastic regime (Fig. 4 *c*). As DAPI does not unwind the dsDNA, we did not observe any lengthening of the DNA contour ($L(c)/L_0 \approx 1$). Nevertheless, the reduction of the bending stiffness (persistence length) that we have seen in the extension experiments ($P(c)/P_0 \approx 0.88$) has a considerable effect on the torsional elasticity. Accordingly, we estimated a torsional softening by a factor of 1.42 ($C(c)/C_0 \approx 0.70$).

On the basis of these findings we can interpret the results of DRAQ5 association on the torsional elasticity of dsDNA. In the primary, minor groove binding mode ($c < 0.5$ μM) the DNA softens due to the decrease of the persistence length ($P(c)/P_0 \approx 0.86$), whereas the shift of the buckling number and the elongation of the contour length can be neglected. Evidently, the torsional softening due to minor groove binding is rather moderate (by a factor of 1.61), which is consistent with the results found for DAPI.

At dye concentrations above 0.5 μM, where DRAQ5 intercalation dominates, the persistence length stays constant and the buckling number increases significantly ($N = 6 -> N = 28$). Furthermore, we observed an increase of the contour length ($L(c)/L_0 \approx 1.15$). Yet, this effect is unincisive, which probably is due to the fact that intercalation itself is a less-pronounced binding mode. Finally, minor groove binding and intercalation of DRAQ5 at the concentration of 10 μM lead to a decrease of the torsional stiffness by a factor of 4.35 ($C(c)/C_0 \approx 0.23$).

CONCLUSIONS

In summary, we investigated the nanomechanical effects on dsDNA due to dye association. Therefore, we used MTs to perform various force-extension and rotation-extension experiments in a concentration-dependent manner.

In case of the bis-intercalator YOYO-1 we found a significant increase of the contour length that we could attribute to a gradual unwinding of the DNA double helix. In contrast the persistence length remained virtually unchanged independent of the YOYO-1 concentration. Presuming mono-intercalation and unspecific adhesion of YOYO-1 to the dsDNA backbone, we could provide a consistent explanation for disparate reports concerning the impact of intercalation on the persistence length. We furthermore approximated our data according to the McGhee–von Hippel model and estimated the binding site size per dye molecule, the induced elongation per dye, and the equilibrium constant of association that are well supported by recently published works.

The minor groove binder DAPI caused no significant elongation of the DNA contour length that is also supported by our rotation extension experiments, where we could not find evidence of DNA unwinding. In contrast, the persistence length decreased substantially upon increasing the DAPI concentration that is in agreement with recently published data.

On the basis of these results we categorized the characteristic phenomena of intercalation and minor groove binding, respectively. Within this scheme we analyzed the DRAQ5 binding data and consistently identified a bimodal association behavior: at low dye concentrations DRAQ5 associates to DNA as a minor groove binder. We observed a decrease of the persistence length but neither an increase of the contour length nor an unwinding of the DNA double helix.

At high DRAQ5 concentrations, we found an intercalator-like behavior, i.e., the lengthening of the DNA due to unwinding at a constant persistence length. In the rotation extension experiments dsDNA decorated with DRAQ5 significant broadening of the hat curves that also clearly indicate intercalation. Furthermore, we estimated a threshold concentration at which the primary minor groove binding declines and intercalation becomes the dominant binding mode.

Finally, we estimated the effect of dye association on the torsional elasticity within the framework of a simplified model. Interestingly, both minor groove binding and intercalation induce a reduction of the dsDNA torsional stiffness. Yet, softening due to intercalation is the major contribution whereas minor groove binding plays only a minor role. In full accordance with our previous results the reduction of the dsDNA elasticity due to DRAQ5 binding can be divided into two "softening regimes": at low concentrations of DRAQ5 (in the minor groove binding regime) torsional softening is less pronounced whereas in the intercalation regime the torsional elasticity drops by a factor of four.

SUPPORTING MATERIAL

Two figures and one table are available at http://www.biophysj.org/biophysj/supplemental/S0006-3495(16)30765-2.

AUTHOR CONTRIBUTIONS

D.A., K.T., and A.S. designed the research. K.T. contributed substantially to the sample preparation. Y.W. performed all measurements. Y.W., A.S., and V.W. analyzed the data. Y.W., V.W., and D.A. wrote the manuscript.

REFERENCES

1. Rye, H. S., S. Yue, …, A. N. Glazer. 1992. Stable fluorescent complexes of double-stranded DNA with bis-intercalating asymmetric cyanine dyes: properties and applications. *Nucleic Acids Res.* 20:2803–2812.
2. Perkins, T. T., D. E. Smith, and S. Chu. 1997. Single polymer dynamics in an elongational flow. *Science.* 276:2016–2021.
3. Quake, S. R., H. Babcock, and S. Chu. 1997. The dynamics of partially extended single molecules of DNA. *Nature.* 388:151–154.
4. Sischka, A., K. Toensing, …, D. Anselmetti. 2005. Molecular mechanisms and kinetics between DNA and DNA binding ligands. *Biophys. J.* 88:404–411.
5. Murade, C. U., V. Subramaniam, …, M. L. Bennink. 2009. Interaction of oxazole yellow dyes with DNA studied with hybrid optical tweezers and fluorescence microscopy. *Biophys. J.* 97:835–843.
6. Maaloum, M., P. Muller, and S. Harlepp. 2013. DNA-intercalator interactions. structural and physical analysis using atomic force microscopy in solution. *Soft Matter.* 9:11233–11240.
7. Shi, N., and V. M. Ugaz. 2014. An entropic force microscope enables nanoscale conformational probing of biomolecules. *Small.* 10:2553–2557.
8. Günther, K., M. Mertig, and R. Seidel. 2010. Mechanical and structural properties of YOYO-1 complexed DNA. *Nucleic Acids Res.* 38:6526–6532.
9. Johansen, F., and J. P. Jacobsen. 1998. ^{1}H NMR studies of the bis-intercalation of a homodimeric oxazole yellow dye in DNA oligonucleotides. *J. Biomol. Struct. Dyn.* 16:205–222.
10. Kundukad, B., J. Yan, and P. S. Doyle. 2014. Effect of YOYO-1 on the mechanical properties of DNA. *Soft Matter.* 10:9721–9728.
11. Barcellona, M. L., G. Cardiel, and E. Gratton. 1990. Time-resolved fluorescence of DAPI in solution and bound to polydeoxynucleotides. *Biochem. Biophys. Res. Commun.* 170:270–280.
12. Parolin, C., A. Montecucco, …, G. Palu. 1990. The effect of the minor groove binding agent DAPI (2-amidino-diphenyl-indole) on DNA-directed enzymes: an attempt to explain inhibition of plasmid expression in *Escherichia coli* [corrected]. *FEMS Microbiol. Lett.* 68:341–346.
13. Tanious, F. A., J. M. Veal, …, W. D. Wilson. 1992. DAPI (4′,6-diamidino-2-phenylindole) binds differently to DNA and RNA: minor-groove binding at AT sites and intercalation at AU sites. *Biochemistry.* 31:3103–3112.
14. Eriksson, S., S. K. Kim, …, B. Nordén. 1993. Binding of 4′,6-diamidino-2-phenylindole (DAPI) to AT regions of DNA: evidence for an allosteric conformational change. *Biochemistry.* 32:2987–2998.
15. Japaridze, A., A. Benke, …, G. Dietler. 2015. Influence of DNA binding dyes on bare DNA structure studied with atomic force microscopy. *Macromolecules.* 48:1860–1865.
16. Thomas, J. A. 2015. Optical imaging probes for biomolecules: an introductory perspective. *Chem. Soc. Rev.* 44:4494–4500.
17. Martin, R. M., H. Leonhardt, and M. C. Cardoso. 2005. DNA labeling in living cells. *Cytometry A.* 67:45–52.
18. Njoh, K. L., L. H. Patterson, …, P. J. Smith. 2006. Spectral analysis of the DNA targeting bisalkylaminoanthraquinone DRAQ5 in intact living cells. *Cytometry A.* 69:805–814.
19. Islam, S. A., S. Neidle, …, J. R. Brown. 1985. Comparative computer graphics and solution studies of the DNA interaction of substituted anthraquinones based on doxorubicin and mitoxantrone. *J. Med. Chem.* 28:857–864.
20. Cheng, W. Protocol to generate half LAMBDA DNA for optical/magnetic tweezer.http://tweezerslab.unipr.it/cgi-bin/mt/documents.pl/Show?_id=ab03&sort=DEFAULT&search=&hits=23. Accessed November 4, 2015.
21. Strick, T. R., J.-F. Allemand, …, V. Croquette. 1998. Behavior of supercoiled DNA. *Biophys. J.* 74:2016–2028.
22. Strick, T. R., J.-F. Allemand, …, V. Croquette. 1996. The elasticity of a single supercoiled DNA molecule. *Science.* 271:1835–1837.
23. Vilfan, I. D., J. Lipfert, …, N. H. Dekker. 2009. Handbook of Single-Molecule Biophysics. P. Hinterdorfer and A. van Oijen, editors. Springer, New York.
24. Smith, S. B., L. Finzi, and C. Bustamante. 1992. Direct mechanical measurements of the elasticity of single DNA molecules by using magnetic beads. *Science.* 258:1122–1126.
25. Bouchiat, C., M. D. Wang, …, V. Croquette. 1999. Estimating the persistence length of a worm-like chain molecule from force-extension measurements. *Biophys. J.* 76:409–413.
26. McGhee, J. D., and P. H. von Hippel. 1974. Theoretical aspects of DNA-protein interactions: co-operative and non-co-operative binding of large ligands to a one-dimensional homogeneous lattice. *J. Mol. Biol.* 86:469–489.
27. Paik, D. H., and T. T. Perkins. 2012. Dynamics and multiple stable binding modes of DNA intercalators revealed by single-molecule force spectroscopy. *Angew. Chem. Int. Ed. Engl.* 51:1811–1815.
28. Petty, J. T., J. A. Bordelon, and M. E. Robertson. 2000. Thermodynamic characterization of the association of cyanine dyes with DNA. *J. Phys. Chem. B.* 104:7221–7227.
29. Kleimann, C., A. Sischka, …, D. Anselmetti. 2009. Binding kinetics of bisintercalator Triostin a with optical tweezers force mechanics. *Biophys. J.* 97:2780–2784.
30. Williams, L. D., M. Egli, …, A. Rich. 1992. Structure & Function, Vol. 1. Adenine Press, New York, pp. 107–125.
31. Vladescu, I. D., M. J. McCauley, …, M. C. Williams. 2007. Quantifying force-dependent and zero-force DNA intercalation by single-molecule stretching. *Nat. Methods.* 4:517–522.
32. Lipfert, J., S. Klijnhout, and N. H. Dekker. 2010. Torsional sensing of small-molecule binding using magnetic tweezers. *Nucleic Acids Res.* 38:7122–7132.
33. Salerno, D., D. Brogioli, …, F. Mantegazza. 2010. Magnetic tweezers measurements of the nanomechanical properties of DNA in the presence of drugs. *Nucleic Acids Res.* 38:7089–7099.
34. Strick, T. R., M.-N. Dessinges, …, V. Croquette. 2003. Stretching of macromolecules and proteins. *Rep. Prog. Phys.* 66:1.

Biophysical Journal, Volume *111*

Supplemental Information

Nanomechanics of Fluorescent DNA Dyes on DNA Investigated by Magnetic Tweezers

Ying Wang, Andy Sischka, Volker Walhorn, Katja Tönsing, and Dario Anselmetti

Supporting Information

Fig 1.

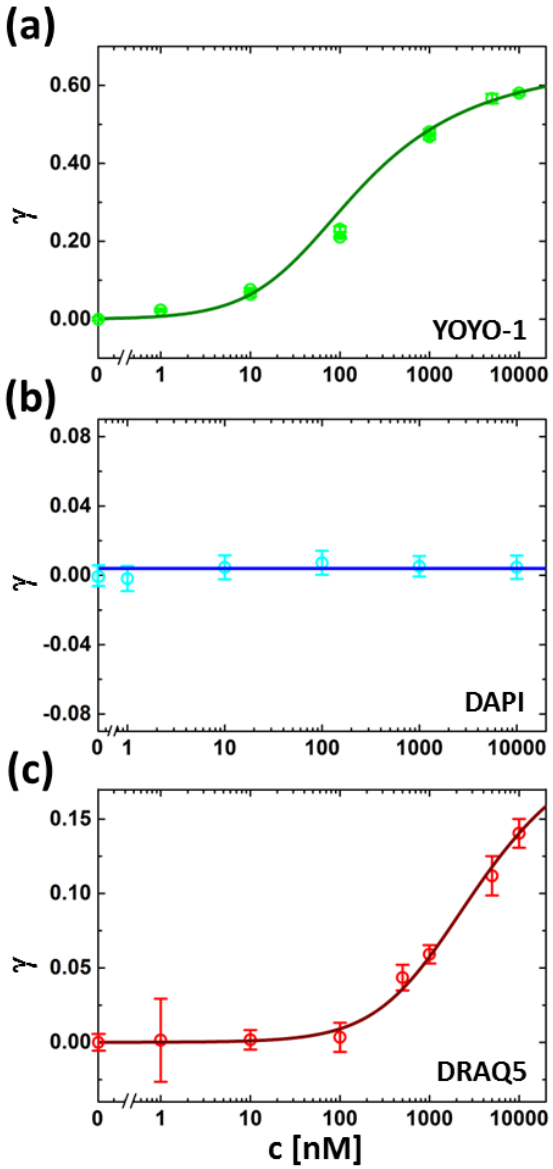

Fractional elongation $\gamma(c)$ of **(a)** YOYO-1, **(b)** DAPI and **(c)** DRAQ5. Very same data as presented in the paper in Fig. 3, yet in a semi-logarithmic representation.

Fig 2.

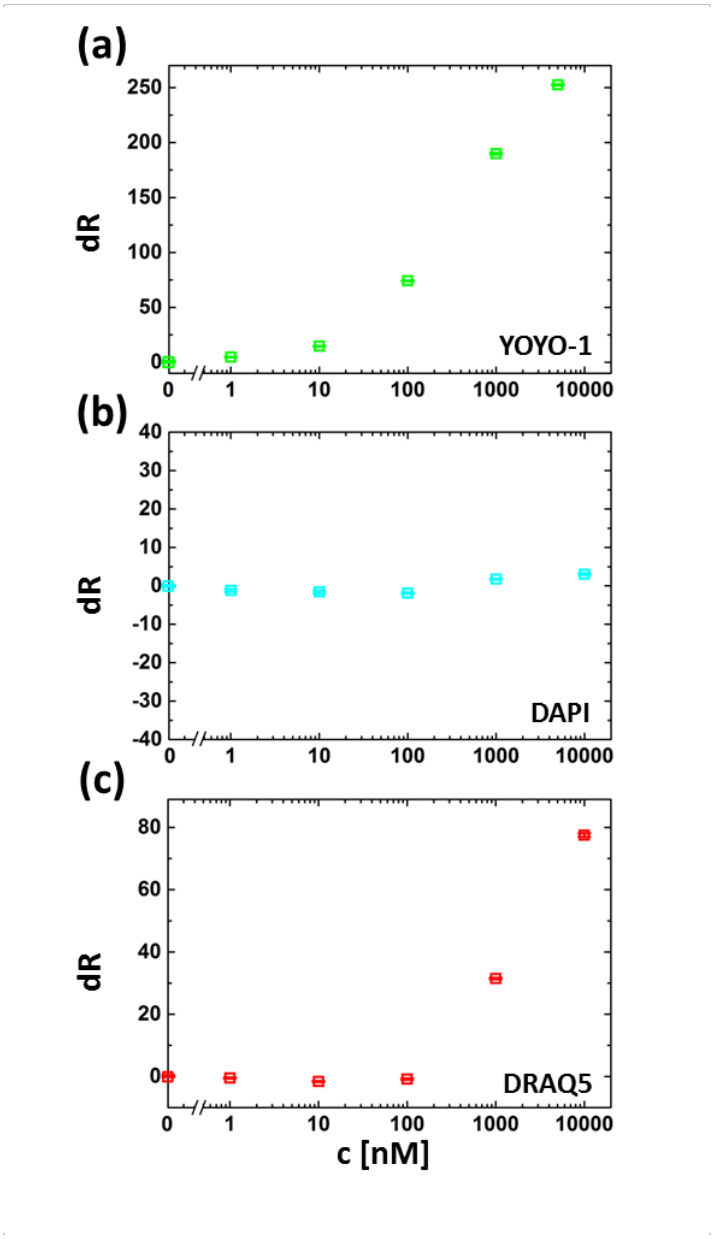

Superspiralization as a function of dye concentration of **(a)** YOYO-1, **(b)** DAPI and **(c)** DRAQ5. $dR=R(c)-R_0$.

Table 1.

coefficient of determination R^2 for	YOYO-1	DAPI	DRAQ5
WLC-fitting	0.96670	0.93838	0.95560
Mc Ghee-von Hippel fitting	0.98995	—	0.99763
dR-dL (linear fitting)	0.93296	—	0.99417

Fit quality by means of the coefficient of determination.

Paper III

Binding Mechanism of Fluorescent Dyes to DNA Characterized by Magnetic Tweezers

Y. Wang, H. Schellenberg, V. Walhorn, K. Tönsing and D. Anselmetti. *Materials Today: Proceedings.* 7th NRW Nano-Conference, Münster. 2017 (Accepted, in press).

Abstract: Fluorescent dyes are widely used for detecting and visualizing DNA molecules in many biotechnological applications. However their binding to DNA alters the structural and nanomechanical properties of DNA and thus impacts also the associated biological processes. In this work we employed magnetic tweezers to investigate the influence of four fluorescent dyes (YOYO-1, DAPI, DRAQ5 and PicoGreen) on DNA in a concentration dependent manner. Via extending and overwinding single, torsionally constrained, nick-free λ dsDNA molecules, we measured the DNA extensions and the pulling forces, which allow the further estimation of the DNA contour-, persistence length and other thermodynamic binding parameters as well. Whereas YOYO-1 and DAPI are well known as bis-intercalator and minor-groove binder, respectively, DRAQ5 and PicoGreen exhibit a bimodal, concentration-dependent binding mode.

Authors' contributions:
Design of the study: D.A.
Preparation of samples: K.T., ***Y.W.*** *and H.S.*
Design and performance of experiments, data-analysis: ***Y.W.***
Writing the manuscript: ***Y.W.****, V.W. and D.A.*

Available online at www.sciencedirect.com

ScienceDirect

Materials Today: Proceedings XX (2016) XXX–XXX

materialstoday: PROCEEDINGS

www.materialstoday.com/proceedings

NRW 2016

Binding Mechanism of Fluorescent Dyes to DNA Characterized by Magnetic Tweezers ☆

Ying Wang, Helene Schellenberg, Volker Walhorn, Katja Tönsing, Dario Anselmetti*

Experimental Biophysics and Applied Nanoscience, Physics Department,
Bielefeld University, Universitätsstrasse 25, 33615 Bielefeld, Germany
Bielefeld Institute for Nanoscience (BINAS)

Abstract

Fluorescent dyes are widely used for detecting and visualizing DNA molecules in many biotechnological applications. However their binding to DNA alters the structural and nanomechanical properties of DNA and thus impacts also the associated biological processes. In this work we employed magnetic tweezers to investigate the influence of four fluorescent dyes (YOYO-1, DAPI, DRAQ5 and PicoGreen) on DNA in a concentration dependent manner. Via extending and overwinding single, torsionally constrained, nick-free λ dsDNA molecules, we measured the DNA extensions and the pulling forces, which allow the further estimation of the DNA contour-, persistence length and other thermodynamic binding parameters as well. Whereas YOYO-1 and DAPI are well known as bis-intercalator and minor-groove binder, respectively, DRAQ5 and PicoGreen exhibit a bimodal, concentration-dependent binding mode.

Selection and Peer-review under responsibility of 7th North Rhine-Westphalian Nano-Conference.

Keywords: PicoGreen; DNA; magnetic tweezers; intercalator; minor-groove binder.

1. Introduction

Fluorescent dyes are widely used nowadays to detect or image DNA in many biotechnological areas. However their binding affects the structural and nanomechanical properties of DNA and consequently associated biological processes such as replication and transcription. In order to elucidate the binding mechanisms of these dyes to DNA,

* Corresponding author. Tel.: +49-521-106-5391; fax: +49-521-106-2959.
E-mail address: dario.anselmetti@physik.uni-bielefeld.de

Selection and Peer-review under responsibility of 7th North Rhine-Westphalian Nano-Conference.

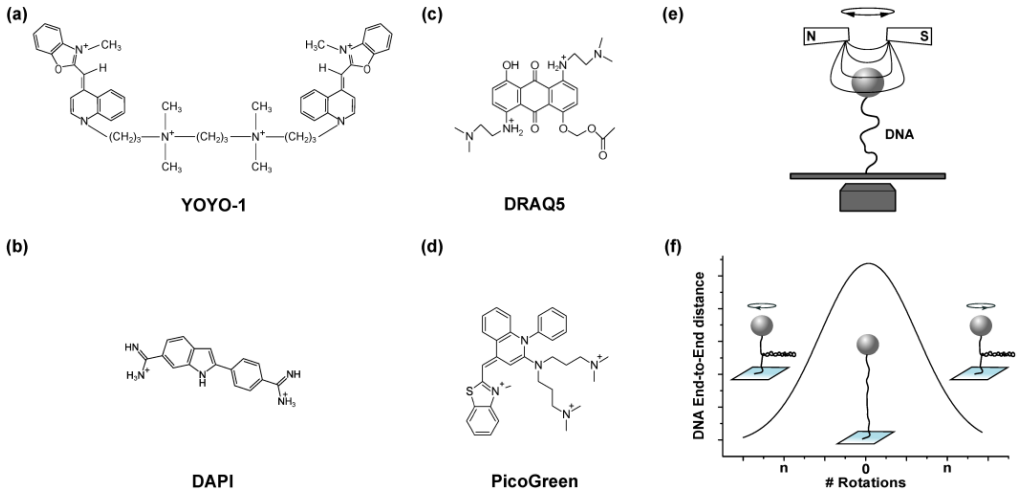

Fig. 1. Chemical structure of (a) YOYO-1, (b) DAPI, (c) DRAQ5 and (d) PicoGreen. (e) Schematic of MT-experiment. A single dsDNA molecule is attached between the surface and a micrometer-sized superparamagnetic bead. The bead can be trapped by a magnetic field and thus longitudinal as well as torsional forces with a full control of the DNA helical twist can be applied. (f) By rotating the bead, mechanical torque is applied to the DNA molecule where its end-to-end distance decreases due to plectonemic supercoiling. This extension-rotation relation can be recorded as a "hat curve".

effects like softening of the DNA strands, induced DNA elongation and partial helical unwinding are studied. In this work we focus on four DNA binding dyes YOYO-1, DAPI, DRAQ5 and PicoGreen (PG) whose chemical structure are known (Fig. 1(a-d)) [1–4]. Employing magnetic tweezers (MT) allowed us to investigate and quantify the nanomechanical effects of these dyes when binding to DNA.

YOYO-1 is a tetracationic homodimer of oxazole yellow belonging to the monomethine cyanine family. It is one of the most widely used dyes due to its little background and photobleaching-resistance. Once bound to DNA YOYO-1 exhibits an over 1000-fold stronger fluorescence emission [1]. YOYO-1 is known as a bis-intercalator, which locally unwinds the DNA double helix and thus causes a DNA elongation. Still, its influence on DNA persistence length is under debate [5].

Because of the cell-impermeability, YOYO-1 cannot be used in fixed or live cell experiments. In contrast, the classical also financially beneficial blue dye DAPI, which belongs to the indol family, is often chosen to stain chromosomes in the nucleus. A 20-fold increase of fluorescence is shown when DAPI binds to DNA [6]. Since the excitation of the dye lies in UV spectral range, detecting live samples with DAPI can lead to cell death which limits the accessible observation time. DAPI is known as a minor-groove binder that binds selectively on AT-rich regions and decreases the bending rigidity of DNA [6–9].

DRAQ5 is also a membrane-permeable dye, which compared to DAPI, can be excited by red light and therefore is less harmful for living cells. Furthermore, it can be combined with many other fluorescent dyes and thus makes it more and more applicable, especially for live cell experiments. However, the binding mode of this dye is still unclear. DRAQ5 was found to intercalate or bind to the minor groove of AT-rich regions [7,10]. In theoretical simulations, a bi-mechanistic interaction was also suggested [11]. We recently categorized DRAQ5 as a concentration dependent intercalator and a minor-groove binder [5].

PG can be used as an alternative of the cyanine dye YOYO-1, which exhibits some similar characteristics. It can be excited with a green light (λ_{ex} = 500 nm) and shows an emission maximum at a wavelength of 523 nm. The free dye yields virtually no fluorescence in solution but an over 1000-fold stronger emission once bound to DNA. Moreover, it can cover a wide range of DNA concentration applying one single dye concentration. PG is also found sequence-insensitive. The suggested incubation time of 2-5 minutes is much shorter than by other fluorescent dyes [12]. Yet, the binding mode and the other influences of PG on DNA are not well understood. Dragan et al. suggested an intercalation as well as minor-groove binding mode [13]. Japaridze et al. concluded a concentration-related co-binding mode [7].

Here, we present our experimental results of the above described fluorescent dyes. Upon studying YOYO-1 and DAPI binding to dsDNA, we defined the binding characteristics of intercalator and minor-groove binder as a

reference. On this basis we interpreted and quantified the influence of the association of DRAQ5 and PG, respectively, and categorized both as bimodal binder.

Nomenclature

c	dye concentration
$L(c)$	DNA contour length as a function of dye concentration c
L_0	contour length of bare DNA
P	DNA persistence length
F	pulling force applied from magnetic field produced by MT
k_BT	thermal energy
d	DNA end to end distance
γ	fractional elongation of DNA
K_a	equilibrium constant of association
n	binding site size per dye molecule
Δx	DNA elongation due to per binding site of one intercalated dye molecule
a	dimensionless factor, equivalent 1 for mono-intercalator and 2 for bis-intercalator
R	rotation number
θ	untwisting angle

2. Materials and methods

To perform the MT-experiments we used a previously described commercial MT system (PicoTwist, France) with custom-made flow cells [14–18]. A glass coverslip was cleaned and coated covalently with sigmacote (Sigma-Aldrich) in a desiccator to produce a homogeneous hydrophobic surface. Together with a transparent polyester film (85 mm × 60 mm, Avery-Zweckform), a double-sided adhesive tape (acrylate, 70 µm thick, cut in the middle for a 5 mm × 52 mm chamber, X-film) and two reservoirs (polymethylmethacrylat, PMMA), a flow cell was assembled. Next, an aqueous solution of anti-digoxigenin (200 µg/ml, Roche) was flushed into the chamber and bound non-specifically to the surface after incubation at 37°C for at least 2 hours. Finally, the chamber was passivated with a buffer containing 10 mM PBS with 137 mM NaCl and 2.7 mM KCl, 0.2% BSA, 0.1% Tween 20, 5 mM EDTA and 10 mM NaN_3, in order to prevent from all possible non-specific adhesion during the experiments.

For the MT experiments the used λ-DNA fragments were functionalized at one end with several biotins and at the other end with several digoxigenins according to a published protocol as described in previous work [5,17,19]. Via these specific bonds the single nick-free dsDNA molecules were attached between an anti-dig coated surface and streptavidin-coated superparamagnetic beads (Dynabeads MyOne Streptavidin C1, Thermo Fisher Scientific) (Fig. 1(e)). As reference, we verified for each probed DNA molecule the contour- and the persistence length through analyzing the stretching experiment with worm-like-chain (WLC) polymer elasticity model [20,21]:

$$\frac{FP}{k_BT} = \frac{1}{4}\left(\left(1 - \frac{d}{L(c)}\right)^{-2} - 1\right) + \frac{d}{L(c)} \tag{1}$$

where F, P, $L(c)$, k_BT and d denote applied force, the DNA persistence length, contour length as functions of the dye concentration c, the thermal energy and the molecular extension of DNA (end-to-end distance), respectively. In addition, “hat curves” were also taken by overwinding DNA in order to ensure the nick-free structure of the samples (Fig. 1(f)).

YOYO-1 iodide (1 mM), DAPI (1 mg/500 µl), DRAQ5 (5 mM) and Quant-iT PicoGreen dsDNA Reagent (concentration of stock solution unknown, proprietary) were purchased from Sigma-Aldrich and Thermo Fisher Scientific, respectively. The concentration of the PG stock solution was estimated measuring the absorption of the solution. By using an extinction coefficient of E_{500} = 70000 M^{-1} at room temperature the concentration of the stock

solution was determined as 0.3 mM [12,13], corresponding to the result from Japaridze et al. (0.2 mM) [7]. All dyes were diluted with MT buffer (10 mM PBS containing 137 mM NaCl and 2.7 mM KCl, 0.1 mg/ml BSA and 0.1% Tween 20, pH 7.4 at 25°C) to concentrations from 1 nM up to 10 µM.

After performing the reference experiments, the fluorescent dye solutions were flushed into the chamber of the flow cell stepwise increasing the concentration. After each step the system was incubated for 20 minutes to reach thermodynamic equilibrium. For each concentration, force-extension experiments were performed with forces up to 10 pN and DNA contour- and persistence lengths were fitted. Furthermore, by employing the transformed McGhee-von Hippel model:

$$\frac{\gamma}{c} = K_a \frac{a\Delta x}{x_{bp}} \cdot \frac{\left(1 - \frac{n\,\gamma\,x_{bp}}{a\Delta x}\right)^n}{\left(1 - \frac{(n-1)\,\gamma\,x_{bp}}{a\Delta x}\right)^{n-1}} \tag{2}$$

the relation between the fractional elongation of DNA γ and the added dye concentration has been analyzed [5,22–24]. Here K_a is the equilibrium constant of association for intercalation, n is the binding site size per dye molecule, x_{bp} is the reference distance between two base pairs which is equal to 0.34 nm, Δx is the DNA elongation due to one binding site of a dye molecule and a is a dimensionless geometrical factor equivalent to 1 for mono-intercalators or 2 for bis-intercalators. The fractional elongation γ can be written as

$$\gamma = \frac{L(c) - L_0}{L_0} \tag{3}$$

where L_0 is the contour length of a bare DNA.

All overwinding experiments were taken with a preset force of 0.2 pN. The data are presented as “hat curves” where the peak positions denote a rotational relaxed state of the DNA double helix. The change of the peak position of the “hat curves” and the corresponding increase of the DNA contour length are plotted as ΔR-ΔL curves and linearly fitted. Combining the slope of the linear approximation and the DNA elongation due to one dye molecule $a\Delta x$, the dye induced untwisting angle was determined by:

$$\theta = \frac{\Delta R}{\#_{\mathrm{dye}}} = \Delta R \frac{a\Delta x}{\Delta L} \tag{4}$$

where θ is the untwisting angle induced by one dye molecule, ΔR is the change of the rotation number recorded at the peak position of hat curves, $\#_{\mathrm{dye}}$ is the number of dye bound to DNA which can be calculated by the ratio between the increase of DNA contour length and the DNA elongation introduced by each dye molecule ($\Delta L/a\Delta x$), respectively.

All experiments were performed at 25°C. The preparation and experiments of DRAQ5 and PG were performed in total darkness to avoid photo bleaching effects. After every experimental series, the flow cell was replaced by a new one to avoid crosstalk of different dyes.

3. Results and discussions

3.1. Extension-experiments

We started all measurements with dye concentrations as low as 1 nM to inhibit artifacts due to unspecific adhesion. The results of the extension-experiments of stained DNA molecules are shown in Fig. 2(a-d). The force-extension data are fitted with the WLC model to estimate contour- and persistence length of the sample molecules (Fig. 2(e-h)).

In case of YOYO-1, upon raising the dye concentration we observed a successive shift of the force-extension curves corresponding to an elongation of the DNA contour length, which was caused by the YOYO-1 bis-intercalation (Fig. 2(a)). In contrast, the persistence length of the DNA of P = 50 nm remained unaffected (Fig. 2(e)). The dye intercalation to the double helix stiffened the DNA while the electrostatic bond between the positive charged binding sites and DNA backbone softened the bending rigidity. We assume that both effects cancel each other out, leading to a constant persistence length of DNA. Therefore, it can be summarized that the intercalator elongates the DNA contour length but does not influence the bending stiffness of DNA. Plotting the fractional elongation of DNA as a function of dye concentration and fitting the curves with the McGhee-von Hippel model allowed a further analysis of the thermodynamic binding parameters (Fig. 2(i-l)). Considering our experimental environment, YOYO-1 exhibits an equilibrium constant of association of K_a = (3.6±0.1)×10^6 M^{-1} together with a binding site size of n = 3.2±0.3 bp per dye (Fig. 2(i)). Each intercalated YOYO-1 molecule extends the double helix

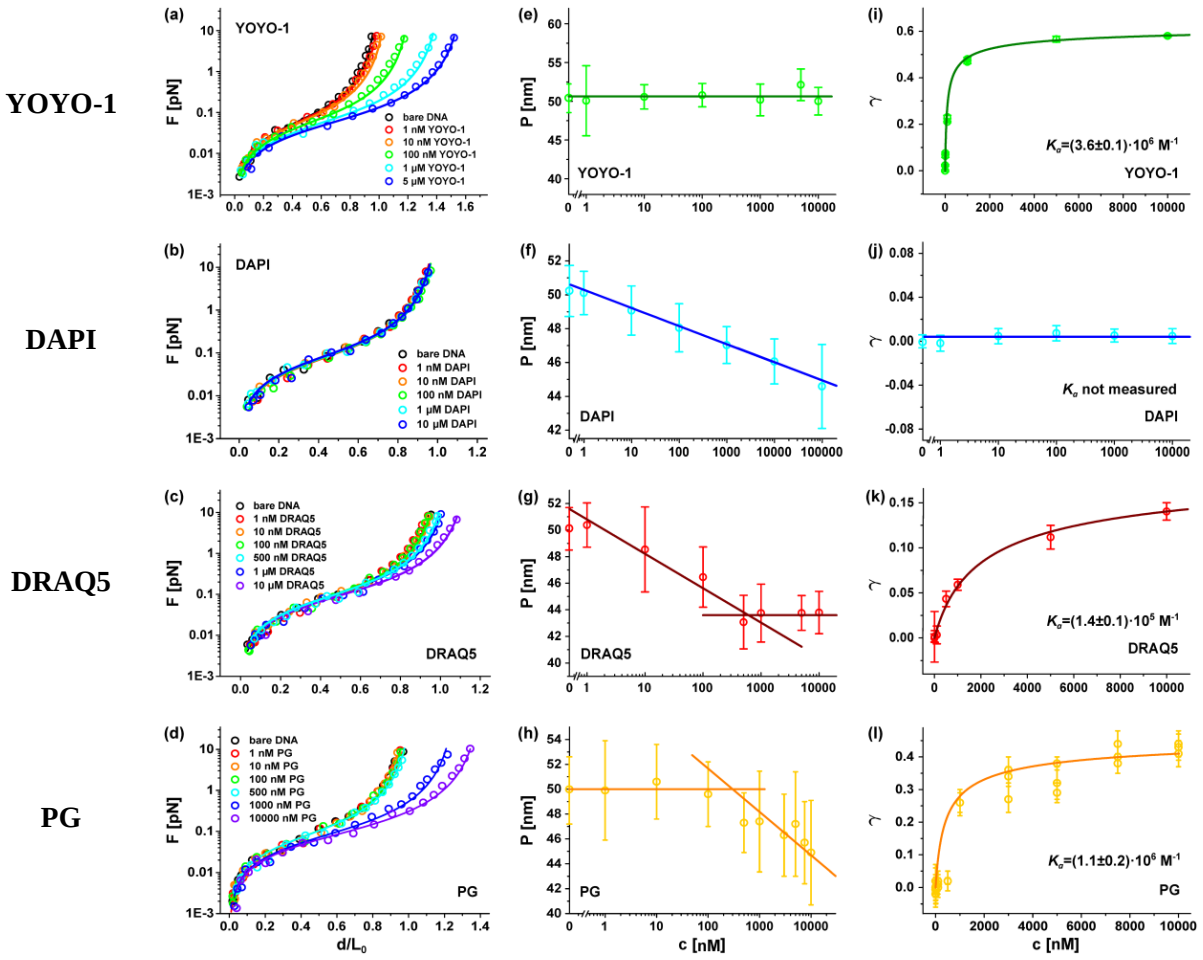

Fig. 2. (a-d) Extension-experiments of DNA with stepwise increasing dye concentrations. Opened circles represent the experimental data and solid lines for the fitting with WLC model; (e-h) DNA persistence length in dependence of dye concentrations; (i-l) Plot of fractional elongation of DNA γ with dye concentrations. Open circles show the experimental data which were approximated to the McGhee-von Hippel model (solid line).

by 0.72±0.08 nm. In contrast, for DAPI we detected only a gradual reduction of the persistence length with increased dye concentration but no change of the contour length which matched the expectation of DAPI as a minor-groove binder(Fig. 2(b, f)). Since DAPI does not intercalate, its thermodynamic parameters could not be determined with the McGhee-von Hippel model.

Next, we investigated the alteration of nanomechanical properties of DRAQ5 stained DNA. At low concentrations of DRAQ5 (<0.5 µM), we only detected a reduction of the DNA persistence length (Fig. 2(g)). Upon further increasing the dye concentration, a DNA elongation was merely observed (Fig. 2(c)). Based on our previous findings how intercalator and minor-groove binder affect the elasticity and structure of DNA, we suggest that DRAQ5 yields a concentration dependent, bimodal binding mode: at low concentrations (<0.5 µM), DRAQ5 binds preferentially on the minor-groove and intercalates to the double strands at high concentrations (>0.5 µM). Also, we determined that DRAQ5 exposes an association constant of $(1.4\pm0.1)\times10^5$ M^{-1} where each intercalated DRAQ5 induces a DNA elongation of 0.24±0.02 nm. The binding site size of 3.1±0.3 bp/dye is slightly larger than for a typical monointercalator like ethidium bromide [24,25], since the favored minor-groove binding hinders a high binding density of intercalation [5].

At last we studied PG stained DNA. Interestingly, we found an overlap of the force-extension curves at dye concentrations up to 100 nM (Fig. 2(d)). Approximating the data to the WLC-model, no change of the DNA contour- and persistence length was observed, indicating that the applied concentration was too low. This finding is in line with Japaridze and coworkers who observed no change of the DNA contour- or persistence length until the concentration ratio between PG and DNA (c(PG):c(DNA)) reached 0.67 [7]. Upon further increasing the dye concentration, an obvious shift of the extension curve was detected, suggesting an increase of the contour length and thus an intercalating binding mode. Moreover, the persistence length decreased at the same time which could be associated to a minor-groove binding (Fig. 2(h)). This result matches the hypothesis from Dragan et al. in their publication who state that PG intercalates with its phenyl quinolinium aromatic system to DNA while the dimethylaminopropyl group associates into the minor-groove [13]. Considering the chemical structure of PG and according to the previously described binding characteristics of both binding modes, we assume that PG intercalation and minor-groove binding co-exist in the same concentration regime. Furthermore, we fitted our data with McGhee-von Hippel equilibrium model and obtained a PG induced elongation of Δx = 0.38±0.04 nm/dye, which corresponds to the distance between two base pairs of DNA. Analogously, we achieved an association constant of $K_a = (1.1\pm0.2)\times10^6$ M^{-1} . The binding site size n was determined as n = 2.3±0.2 bp, which is typical for a monointercalator and matches the *nearest neighbor exclusion principle* [26]. However, using Tris buffer with 100 mM NaCl as the experimental environment, Dargan et al. measured an equilibrium constant of association of about $K_a \sim 10^7$ M^{-1} and a binding site size of n = 5.2±0.1 bp, which were both larger than our results [13]. Singer and coworkers found that the ionic strength, proteins, organic solutions etc. can influence the fluorescent intensity of PG significantly [12]. Considering the experimental conditions, BSA and monovalent cations in our buffer could also affect PG binding to DNA.

3.2. Overwinding-experiments

Williams and coworkers suggested in 1992 that DNA intercalation of dye molecules can cause unwinding of the DNA helix [27]. Since MT can apply forces with a full control of the DNA helical twist, we performed overwinding-experiments to estimate the untwisting angle induced by one intercalated dye molecule. In case of YOYO-1, DRAQ5 (>0.5 µM) and PG, the intercalation of dye molecules generated a shift of the supercoiling curves to negative rotation numbers, which can be attributed to a gradual unwinding of the DNA double helix (Fig. 3(a-d)). The correlation between the change of the rotation numbers and the elongation of the contour length are plotted in ΔR-ΔL diagrams (Fig. 3(e-h)). According to Eq. (4), using the slope of the linear approximation of ΔR-ΔL curves and the DNA elongation induced by one dye molecule $a\Delta x$, the untwisting angle of a dye molecule can be estimated [5,25,28]. Accordingly, we determined an untwisting angle of YOYO-1 of 0.088±0.041 turns/dye corresponding to 32±15° per dye. DRAQ5 intercalates in DNA strands at concentrations larger than 500 nM and unwinds the double helix for 0.036±0.013 turns/dye which equals 13±5° per dye. For PG, we observed an untwisting angle of 0.058±0.040 turns/dye equivalent to 21±14° per dye. As a minor-groove binder, DAPI does not intercalate to DNA and thus exhibits an unwinding angle of 0°.

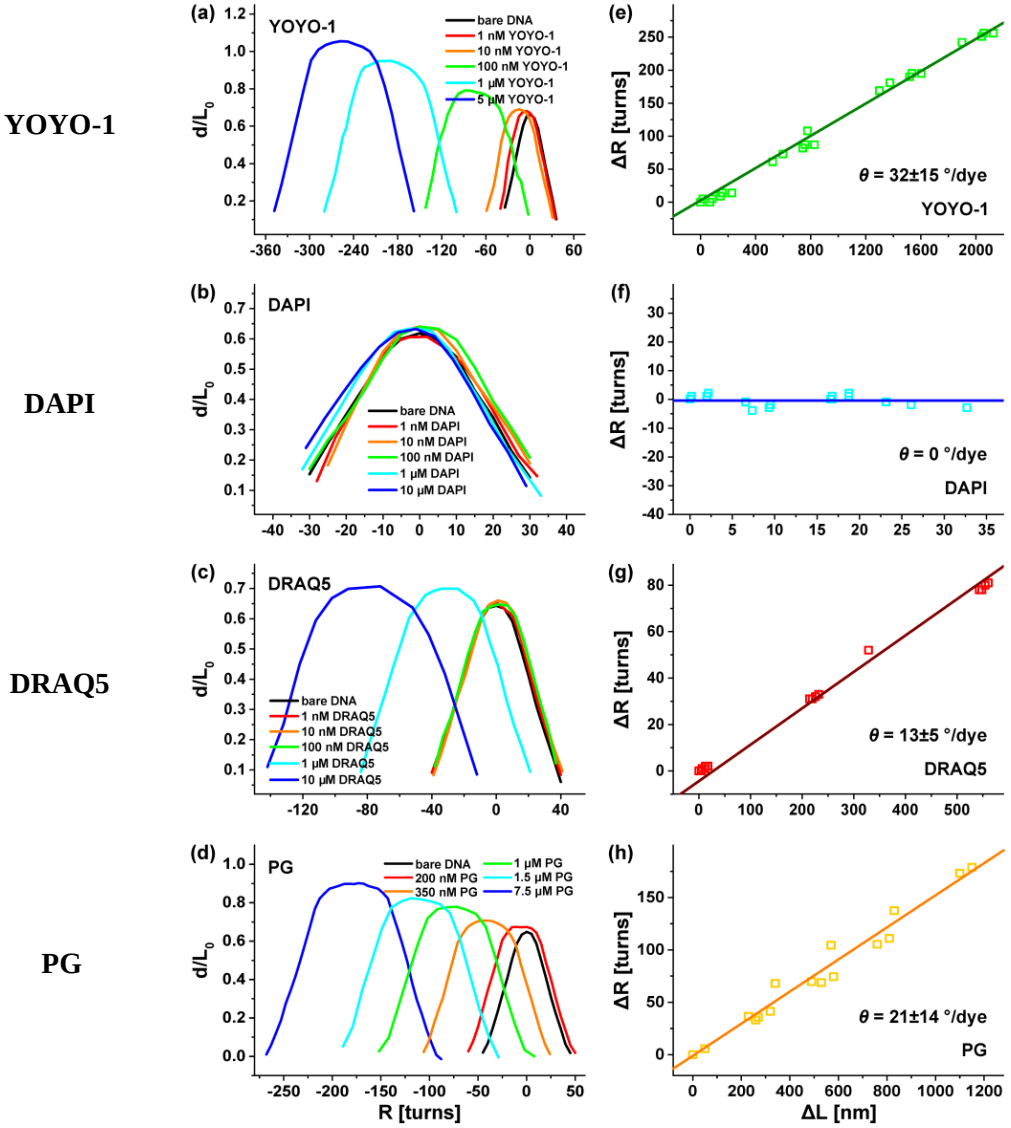

Fig. 3. (a) MT overwinding experiments of nick-free dsDNA molecule with stepwise increased dye concentration at a preset force of 0.2 pN; (b) Linear approximation (solid lines) of the change of the rotation number ΔR with the elongation of the DNA contour length ΔL (opened squares) which allows to estimate the unwinding angle per intercalated dye molecule.

4. Conclusion

In summary, we investigated the binding mechanism of YOYO-1, DAPI, DRAQ5 and PG to dsDNA with magnetic tweezers force mechanics at room temperature under buffer conditions. By means of extending and overwinding stained DNA using magnetic tweezers, we studied the impact of dye association on the nanomechanical properties of dsDNA in a concentration dependent manner. We have determined and referenced the characteristic phenomena of intercalation and minor-groove binding by studying YOYO-1 and DAPI that bind in a monomodal manner. On the basis of these results, we suggested that both, DRAQ5 and PG present a bimodal binding mode. For DRAQ5 we determined minor groove binding as primary binding mode whereas beyond a threshold concentration of 0.5 µM DRAQ5 intercalates to DNA. In contrast, PG binds as an intercalator and minor groove binder simultaneously at concentration larger than 100 nM. Furthermore we determined the unwinding of the DNA double helix upon single dye intercalation of YOYO-1, DRAQ5 and PG, yielding untwisting angles per dye of 32°, 13° and 21°, respectively.

Acknowledgements

We gratefully acknowledge technical support from Christoph Pelargus.

References

[1] H.S. Rye, S. Yue, D.E. Wemmer, M.A. Quesada, R.P. Haugland, R.A. Mathies, A.N. Glazer, Nucleic acids research 20 (1992) 2803–2812.
[2] M. Kubista, B. Aakerman, B. Norden, Biochemistry 26 (1987) 4545–4553.
[3] J.A. Thomas, Chemical Society reviews 44 (2015) 4494–4500.
[4] H. Zipper, H. Brunner, J. Bernhagen, F. Vitzthum, Nucleic acids research 32 (2004) e103.
[5] Y. Wang, A. Sischka, V. Walhorn, K. Tönsing, D. Anselmetti, Biophysical Journal 111 (2016) 1604–1611.
[6] M.L. Barcellona, G. Cardiel, E. Gratton, Biochemical and Biophysical Research Communications 170 (1990) 270–280.
[7] A. Japaridze, A. Benke, S. Renevey, C. Benadiba, G. Dietler, Macromolecules 48 (2015) 1860–1865.
[8] S. Eriksson, S.K. Kim, M. Kubista, B. Norden, Biochemistry 32 (1993) 2987–2998.
[9] F.A. Tanious, J.M. Veal, H. Buczak, L.S. Ratmeyer, W.D. Wilson, Biochemistry 31 (1992) 3103–3112.
[10] R.M. Martin, H. Leonhardt, M.C. Cardoso, Cytometry A 67 (2005) 45–52.
[11] S.A. Islam, S. Neidle, B.M. Gandecha, M. Partridge, L.H. Patterson, J.R. Brown, J. Med. Chem. 28 (1985) 857–864.
[12] V.L. Singer, L.J. Jones, S.T. Yue, R.P. Haugland, Analytical biochemistry 249 (1997) 228–238.
[13] A.I. Dragan, J.R. Casas-Finet, E.S. Bishop, R.J. Strouse, M.A. Schenerman, C.D. Geddes, Biophysical Journal 99 (2010) 3010–3019.
[14] T.R. Strick, J.-F. Allemand, D. Bensimon, A. Bensimon, V. Croquette, Science 271 (1996) 1835–1837.
[15] T.R. Strick, J.-F. Allemand, D. Bensimon, V. Croquette, Biophysical Journal 74 (1998) 2016–2028.
[16] I.D. Vilfan, J. Lipfert, D.A. Koster, S.G. Lemay, N.H. Dekker, Handbook of single-molecule biophysics, Hinterdorfer, Peter; van Oijen, Antoine, Eds; Springer Science+Business Media, 2009.
[17] T. Jany, A. Moreth, C. Gruschka, A. Sischka, A. Spiering, M. Dieding, Y. Wang, S.H. Samo, A. Stammler, H. Bogge, G. Fischer von Mollard, D. Anselmetti, T. Glaser, Inorganic chemistry 54 (2015) 2679–2690.
[18] T. Glaser, G. Fischer von Mollard, D. Anselmetti, Inorganica Chimica Acta 452 (2016) 62–72.
[19] W. Cheng, Protocol to generate half Lambda DNA for optical/magnetic tweezer, (2006) http://tweezerslab.unipr.it/cgi-bin/mt/documents.pl/Show?_id=ab03&sort=DEFAULT&search=&hits=23, accessed 05.09.2008.
[20] S. Smith, L. Finzi, C. Bustamante, Science 258 (1992) 1122–1126.
[21] C. Bouchiat, M.D. Wang, J.-F. Allemand, T. Strick, S.M. Block, V. Croquette, Biophysical Journal 76 (1999) 409–413.
[22] J.D. McGhee, P.H. von Hippel, Journal of Molecular Biology 86 (1974) 469–489.
[23] C. Kleimann, A. Sischka, A. Spiering, K. Tonsing, N. Sewald, U. Diederichsen, D. Anselmetti, Biophysical Journal 97 (2009) 2780–2784.
[24] I.D. Vladescu, M.J. McCauley, M.E. Nunez, I. Rouzina, M.C. Williams, Nature methods 4 (2007) 517–522.
[25] J. Lipfert, S. Klijnhout, N.H. Dekker, Nucleic acids research 38 (2010) 7122–7132.
[26] D.M. Crothers, Biopolymers 6 (1968) 575–584.
[27] L.D. Williams, M. Egli, Q. Gao, A. Rich, Structure & function, Adenine Press, New York, 1992; Vol. 1, p107-125.
[28] K. Günther, M. Mertig, R. Seidel, Nucleic acids research 38 (2010) 6526–6532.

Paper IV

Binding Mechanism of PicoGreen to DNA characterized by Magnetic Tweezers and Fluorescence Spectroscopy

Y. Wang, H. Schellenberg, V. Walhorn, K. Toensing and D. Anselmetti.
European Biophysics Journal. 2017 (Online first).

Abstract: Fluorescent dyes are broadly used in many biotechnological applications to detect and visualize DNA molecules. However, their binding to DNA alters the structural and nanomechanical properties of DNA and thus interferes with the associated biological processes. In this work we employed magnetic tweezers and fluorescence spectroscopy to investigate the binding of PicoGreen to DNA at room temperature in a concentration dependent manner. PicoGreen is an ultrasensitive quinolinium nucleic acid stain exhibiting hardly any background signal from unbound dye molecules. By means of stretching and overwinding single, torsionally constrained, nick-free double-stranded DNA molecules, we acquired force-extension and supercoiling curves which allow to quantify DNA contour length, persistence length and other thermodynamical binding parameters, respectively. The results of our magnetic tweezers single-molecule binding study were well supported through analyzing the fluorescent spectra of the stained DNA. On the basis of our work, we could identify a concentration-dependent bimodal binding behavior, where apparently, PicoGreen associates to DNA as an intercalator and minor-groove binder simultaneously.

Authors' contributions:
Design of the study: D.A.
Preparation of samples: K.T., ***Y.W.*** *and H.S.*
Design of experiments (MT and FS): ***Y.W.***
Performance of experiments (MT): ***Y.W.***
Performance of experiments (FS): H.S.
Data-analysis: ***Y.W.***
Writing the manuscript: ***Y.W.****, V.W. and D.A.*

European Biophysics Journal, 2017 (Online First). DOI 10.1007/s00249-017-1204-z

Binding Mechanism of PicoGreen to DNA characterized by Magnetic Tweezers and Fluorescence Spectroscopy

Ying Wang, Helene Schellenberg, Volker Walhorn, Katja Tönsing, Dario Anselmetti

Experimental Biophysics and Applied Nanoscience, Physics Department,
Bielefeld Institute for Nanoscience (BINAS),
Bielefeld University, Universitätsstrasse 25, 33615 Bielefeld, Germany

Corresponding author: Prof. Dr. Dario Anselmetti

Experimental Biophysics and Applied Nanoscience
Physics Faculty
Bielefeld University
Universitaetsstr. 25
D-33615 Bielefeld
Germany

Tel: +49-521-106-5391
Fax: +49-521-106-2959
dario.anselmetti@physik.uni-bielefeld.de

Abstract

Fluorescent dyes are broadly used in many biotechnological applications to detect and visualize DNA molecules. However, their binding to DNA alters the structural and nanomechanical properties of DNA and thus interferes with associated biological processes. In this work we employed magnetic tweezers and fluorescence spectroscopy to investigate the binding of PicoGreen to DNA at room temperature in a concentration dependent manner. PicoGreen is an ultrasensitive quinolinium nucleic acid stain exhibiting hardly any background signal from unbound dye molecules. By means of stretching and overwinding single, torsionally constrained, nick-free double-stranded DNA molecules, we acquired force-extension and supercoiling curves which allow to quantify DNA contour length, persistence length and other thermodynamical binding parameters, respectively. The results of our magnetic tweezers single-molecule binding study were well supported through analyzing the fluorescent spectra of stained DNA. On the basis of our work, we could identify a concentration-dependent bimodal binding behavior, where apparently, PicoGreen associates to DNA as an intercalator and minor-groove binder simultaneously.

Keywords: PicoGreen; DNA; magnetic tweezers; intercalator; minor-groove binder.

Introduction

Fluorescent dyes are nowadays widely used to detect or visualize DNA in many biotechnological areas. As there are already many different dyes on the market, developing new and better DNA reagents is challenging. In this work, we focused on the comparatively new ultrasensitive fluorescent dye PicoGreen (PG) (Fig. 1b). PG can be seen as an alternative to a cyanine dye like YOYO-1, which shares some similar characteristics. It can be excited with green light at a wavelength of 500 nm and shows an emission maximum at 523 nm. The free dye exhibits virtually no fluorescence in solution but an over 1000-fold stronger signal once bound to DNA, which allows to apply a single dye concentration to a wide range of DNA concentrations. A major benefit of PG is a short incubation time of 2 to 5 minutes, which is much shorter than for other fluorescent dyes. However, this cell membrane impermeable dye is also expected to bind in an unselective manner (Singer et al. 1997).

Notably, staining DNA significantly affects its structural and mechanical properties and therefore interferes with biological processes such as replication and transcription. On the molecular level, dye association to DNA induces nanomechanical effects like softening, elongation and often unwinding which commonly remains unknown.

The binding mode of PG and its impact on DNA are not well understood. Dragan et al. suggested an intercalation as well as minor-groove binding mode with an equilibrium constant of association of 10^7-$10^8\,\mathrm{M}^{-1}$. Furthermore, they found a dependence between the binding site size and the ionic strength of Tris buffer by means of fluorescent spectra of PG-stained DNA (Dragan et al. 2010). Japaridze et al. used AFM to probe the dye induced impact of PG and observed no change in the DNA nanomechanical properties until PG reached a 0.67 fold

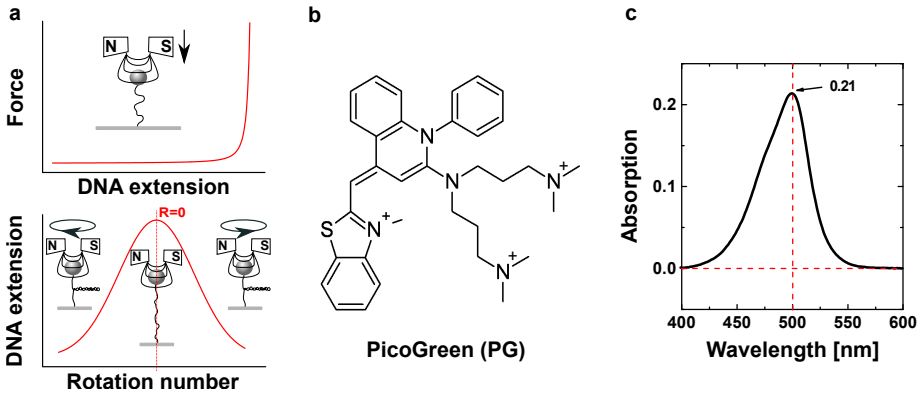

Figure 1: **a.** Schematic of the MT experiment and measuring principle for extending and supercoiling single DNA molecules; **b.** Chemical structure of PicoGreen (Zipper et al. 2004); **c.** Absorption spectrum of 100-fold diluted PG solution (in distilled water) to determine the concentration of the stock solution c_0.

concentration with respect to the DNA. Furthermore, no softening of DNA in the entire experiment was detected. Therefore, they proposed a bimodal binding mode where PG acts as a minor-groove binder at low dye concentrations and as an intercalator at higher dye concentrations (Japaridze et al. 2015). Singer and coworkers discovered that the labeling or the fluorescent sensitivity of the dye was affected when salt, protein or other organic solution were present (Singer et al. 1997). In this work, we present a joint magnetic tweezers (MT) and fluorescence spectroscopy (FS) to study and quantify the binding characteristics of PG to dsDNA in PBS buffer at a NaCl concentration of about 140 mM. We performed several MT extension and overwinding experiments within a force range from 5×10^{-3} pN up to 10 pN and analyzed these within the theoretical framework of the worm-like chain model (WLC) and the McGhee-von Hippel model (Kleimann et al. 2009). Moreover, fluorescence spectroscopy was used to estimate the equilibrium constant of association. Our results suggest that PG simultaneously binds as a minor-groove binder and intercalator.

Materials and methods

To perform the MT-experiments (Fig. 1a) we used a previously described commercial MT system (PicoTwist, Lyon, France) with a custom-made flow cell (Strick et al. 1996; Strick et al. 1998; Vilfan et al. 2009; Jany et al. 2015; Glaser et al. 2016). Briefly, a glass coverslip was cleaned and covalently functionalized with sigmacote (Sigma-Aldrich, St. Louis, USA) in a desiccator to produce a homogeneously hydrophobic surface. Together with a 100 µm thick transparent polyester film (85 mm×60 mm, mod. 3560, Avery-Zweckform, Oberlaindern, Germany), a double-sided adhesive tape (acrylate, 70 µm thick, cut in the middle for a 5 mm×52 mm chamber, X-film, Lindlar, Germany) and two reservoirs (polymethylmethacrylat, PMMA), a flow cell was assembled. Next, anti-digoxigenin (200 µg ml^{-1}, Roche, Penzberg, Germany) was immersed into the flow cell at 37 °C for at least 2 hours and allowed to non-specifically adsorb to the glass surface. Finally, the chamber was passivated with a buffer contain-

ing 10 mM PBS with 137 mM NaCl and 2.7 mM KCl, 0.2 % BSA, 0.1 % Tween 20, 5 mM EDTA and 10 mM NaN_3, in order to prevent all possible non-specific adhesion during the experiments.

For the MT experiments we used λ-DNA fragments that were functionalized at one end with several biotins and at the other end with several digoxigenins, according to a published protocol as described in former work (Cheng 2006; Jany et al. 2015; Wang et al. 2016). Via the specific bonds a single nick-free dsDNA molecule was attached between the anti-digoxigenin coated glass surface and a streptavidin coated 1 µm superparamagnetic microbead (Dynabeads MyOne, Thermo Fisher Scientific, Waltham, USA). As a reference and control prior to every experiment, we measured the contour- and persistence length for each probed DNA molecule by means of stretching experiments and subsequent approximation of the extension curves to the worm-like-chain (WLC) polymer elasticity model (Smith et al. 1992; Bouchiat et al. 1999):

$$\frac{FP}{k_{\mathrm{B}}T} = \frac{1}{4}\left(\left(1 - \frac{d}{L(c)}\right)^{-2} - 1\right) + \frac{d}{L(c)} \tag{1}$$

Here, F, P, $L(c)$, $k_{\mathrm{B}}T$ and d denote the applied force, DNA persistence length, contour length as functions of the dye concentration c, thermal energy and molecular extension of the DNA (end-to-end distance), respectively. In addition MT "hat curves" were also acquired by overwinding DNA in order to ensure the nick-free nature of the probed DNA molecule.

Quant-iT PicoGreen dsDNA reagent was purchased (Thermo Fisher Scientific, Waltham, USA) and delivered in DMSO. The proprietary concentration of the stock solution was determined using UV-VIS spectroscopy by measuring the absorption of the solution (Fig. 1c). Assuming an extinction coefficient of $E_{500} = 70\ 000\,\mathrm{M}^{-1}$ at room temperature (Singer et al. 1997; Dragan et al. 2010), the concentration of the stock solution was estimated as mM, which corresponds to a recent measurement by Japaridze et al. (0.2 mM) (Japaridze et al. 2015). Consequently, the dye was diluted with MT buffer (10 mM PBS with 137 mM NaCl and 2.7 mM KCl, 0.1 mg ml^{-1} BSA and 0.1 % Tween 20, pH 7.4 at 25 °C) to concentrations from 1 nM up to 10 µM.

Subsequent to the reference experiments, the fluorescent dye was flushed into the microfluidic flow cell by stepwise increasing the concentration followed by an incubation of 20 minutes to achieve thermodynamical equilibrium. For each concentration single-molecule MT force-extension experiments were performed with forces up to 10 pN where the DNA contour- and persistence lengths were measured. All experiments were repeated with at least three individual DNA molecules for each dye concentration and the data were approximated with the WLC model. The resulting fitting errors as well as contour- and persistence lengths were averaged. Furthermore, by employing the transformed Mc Ghee-von Hippel model for thermal equilibrium (Vladescu et al. 2007):

$$\frac{\gamma}{c} = K_a \frac{\Delta x}{x_{\mathrm{bp}}} \cdot \frac{\left(1 - \dfrac{n\gamma x_{\mathrm{bp}}}{\Delta x}\right)^{n}}{\left(1 - \dfrac{(n-1)\,\gamma x_{\mathrm{bp}}}{\Delta x}\right)^{n-1}} \tag{2}$$

the relation between the fractional elongation of DNA γ and the dye concentration c have been determined (McGhee and von Hippel 1974). Here, K_a is

the equilibrium constant of association for intercalation, n is the binding site size per dye molecule, x_{bp} is the reference distance between two base pairs ($x_{\mathrm{bp}} = 0.34\,\mathrm{nm}$) and Δx is the DNA elongation due to one intercalated dye. The fractional elongation γ can be written as

$$\gamma = \frac{L(c) - L_0}{L_0} \tag{3}$$

where L_0 is the contour length of a bare DNA. The fitting errors of $L(c)$ and L_0 contribute to the uncertainty of γ, Δx and K_a by means of propagation of uncertainty. The overwinding experiments were all taken with a preset force of 0.2 pN. The dye preparation and all experiments were performed at 25 °C in total darkness to avoid photo bleaching.

Results and discussion

Extension- and overwinding experiments

In order to investigate the impact of PG association on the nanomechanic properties of DNA we used MT based extension and overwinding experiments. MT allow the exact determination of the DNA end-to-end distance, contour and persistence length at full control of the DNA helical twist. Firstly, we performed extension experiments while the twist was adjusted in such a way that the DNA remained in the torsionally relaxed state, in which it exposes the maximum end-to-end length.

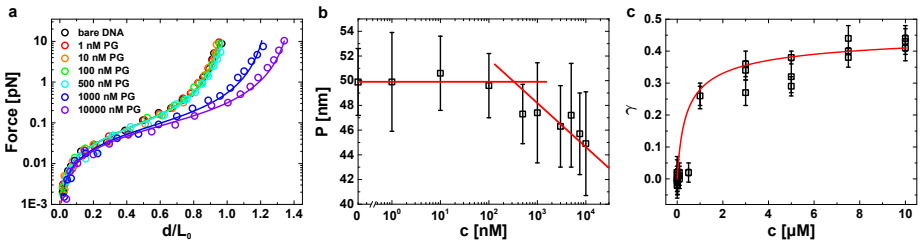

Figure 2: a. Extension-experiments of DNA with stepwise increased dye concentrations. Opened circles represent the experimental data and solid lines for the fitting with WLC model; **b.** DNA persistence length in dependence of dye concentrations. The regimes beneath and beyond the threshold concentration were approximated by a zero slope line (<100 nM) and a straight line (>100 nM) **c.** Plot of fractional elongation of DNA γ with dye concentrations. Opened squares show the experimental data which were approximated to McGhee-von Hippel model (solid lines).

We started the measurements with dye concentrations as low as 1 nM to inhibit artifacts due to unspecific binding and stepwise increased the dye concentration up to 10 µM. The results of the extension-experiments of PG-stained DNA molecules are shown in Fig. 2a. The force-extension data were approximated to the WLC model to estimate the contour- and the persistence length of the sample molecules (Fig. 2b). Interestingly, we found that the force-extension curves did not change significantly at dye concentrations up to 100 nM. By analyzing the data no change of the DNA contour- or persistence length was

observed, which suggests that the applied dye concentrations were too low to observe any effect. Japaridze and coworkers also observed no change of the DNA contour- or persistence length until the dye base pair concentration ratio ($c_{\mathrm{PG}} : c_{\mathrm{DNA}}$) reached 0.67 (Japaridze et al. 2015). These findings consistently suggest, that PG only binds to DNA beyond a certain threshold concentration/dye base pair ratio. Upon further increasing the dye concentration, a successive shift of the force extension curves to larger contour lengths was detected (Fig. 2a). Moreover, the persistence length decreased at the same time (Fig. 2b).

We found earlier for other fluorescent dyes that intercalation induces an increase of the contour length at more or less constant persistence length (Wang et al. 2016). In contrast, minor groove binding induces a reduction of the persistence length leaving the contour length virtually unchanged. This leads to the conclusion that PG DNA binding exhibits a bimodal binding mechanism: intercalation and minor groove binding at the same time. This also matches with results by Dragan et al. who suggested that the PG phenyl quinolinium aromatic system intercalates into the DNA while dimethylaminopropyl simultaneously binds to the minor-groove (Dragan et al. 2010).

Furthermore, we approximated the fractional elongation data to the Mc Ghee-von Hippel model (Fig. 2c) and quantified the elongation per intercalated dye as $\Delta x = 0.38 \pm 0.04$ nm/dye. The binding site size n was calculated as 2.32 ± 0.21 bp which is a typical value for a mono-intercalator and is compliant with the nearest neighbor exclusion principle (Crothers 1968; Vladescu et al. 2007; Lipfert et al. 2010). Analogously, we achieved an equilibrium constant of association of $K_a = (1.06 \pm 0.20) \times 10^6\,\mathrm{M}^{-1}$. Using Tris buffer with 100 mM NaCl as experimental environment, Dargan et al. estimated a binding site size of 5.2 ± 0.1 bp (Dragan et al. 2010) which is twice as large as our result. Yet, the experimental conditions have a significant influence on PG association. Assuming that the fluorescence signal intensity linearly correlates with the degree of binding, Singer and co-workers reported on substantial changes of the fluorescence intensity upon changing the buffer conditions. Consequently, BSA and the monovalent cations apparently alter the electrostatic shielding which in turn affects the PG binding mode (Singer et al. 1997).

Fluorescence spectroscopy

In addition, we estimated the equilibrium constant of association K_a in a series of fluorescence spectroscopy experiments. Firstly, we prepared a DNA solution with a defined concentration of base pairs (100 nM) and successively added small amounts of dye in such a way that the dye concentration increased by 5 nM steps. Due to the large surplus of DNA almost all dye molecules bind to the DNA and therefore contribute to the fluorescence signal I_{b} (Fig. 3a). Consequently, the fluorescence intensity exhibits a linear increase (Fig. 3c). In a second series the dye was similarly added to DNA, however, the DNA base pair concentration was reduced to 0.4 nM. Therefore, we observed a saturation of the fluorescence intensity I (Fig. 3b, c) and applied the McGhee-von Hippel model

$$\frac{\nu}{c_{\mathrm{PG,free}}} = K_a \frac{(1 - n\nu)^n}{(1 - n\nu + \nu)^{n-1}} \tag{4}$$

to estimate K_a and the binding site size per dye molecule n (Fig. 3d, McGhee and von Hippel 1974). Here, ν denotes the binding density of PG which is equal to $\frac{I \cdot c}{I_\mathrm{b} \cdot c_{\mathrm{DNA(bp)}}}$ and $c_{\mathrm{PG,free}} = \left(1 - \frac{I}{I_\mathrm{b}}\right) \cdot c$ (Dragan et al. 2010). We estimated a PG association constant as $(5.05 \pm 0.38) \times 10^6 \mathrm{M}^{-1}$ and the binding site size of 2.31 ± 0.04 bp, which fully complies with our results of the MT experiments. However, as PG apparently exposes a non-trivial bimodal binding mode, the McGhee-von Hippel model might be of limited applicability.

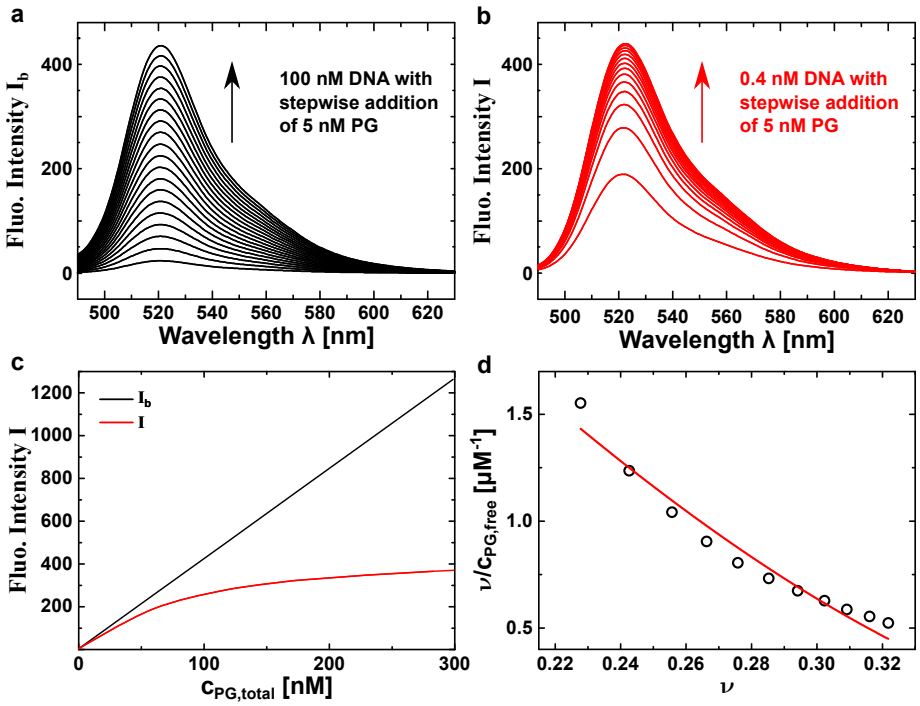

Figure 3: **a.** Fluorescence spectra of PG successively added with an increment of 5 nM to λ-DNA with a base pair concentration of **a.** 100 nM and **b.** 0.4 nM. **c.** Plots of fluorescence signals from **a.** and **b.** as a function of PG concentration; **c.** Approximating the data to McGhee-von Hippel model to achieve K_a and n.

Overwinding-experiments

MT overwinding-experiments allow twisting of single molecules in a well-defined manner. Supercoiling experiments of nick-free DNA are commonly presented as "hat curves" (Fig. 4a). The peaks of these curves denote the rotational relaxed state of the DNA double helix. In contrast, overwinding nicked DNA would result in free rotation (idle state) around the intact strand so no supercoiling could be detected. To further support the results of our extension experiments, we acquired overwinding curves at pulling forces of 0.2 pN. PG was immersed with stepwise increasing concentrations. We found that the "hat curves" shifted to negative rotation numbers, which can be attributed to intercalation (Williams et al. 1992; Vol. 1, pp. 107-125). Evidently, PG binding

induces supercoiling which can only be removed by applying rotations in the counter direction. Additionally, the intercalation yields an elongation due to the untwisting of the DNA double helix, which is in full agreement with our extension experiments (Williams et al. 1992; Vol. 1, pp. 107-125).

Moreover, we estimated the change of the rotation number ΔR and the elongation of the DNA contour length ΔL and approximated the data linearly (Fig. 4b). We obtained a slope of 0.153 ± 0.004 turns/nm. The untwisting angle per intercalated PG molecule θ was then estimated with the following correlation $\theta = \dfrac{\Delta R}{\#_{\mathrm{dye}}}$ where the number of intercalated dye molecules $\#_{\mathrm{dye}}$ was calculated from $\#_{\mathrm{dye}} = \dfrac{\Delta L}{\Delta x}$ (Lipfert et al. 2010; Günther et al. 2010; Wang et al. 2016). Combining the slope of the linear fit and the previously calculated lengthening per dye molecule Δx, we determined an untwisting angle of 0.058 ± 0.040 turns/dye corresponding to 21 ± 14 °/dye, which is comparable to the value for typical mono-intercalators such as ethidium bromide (Hayashi and Harada 2007; Lipfert et al. 2010).

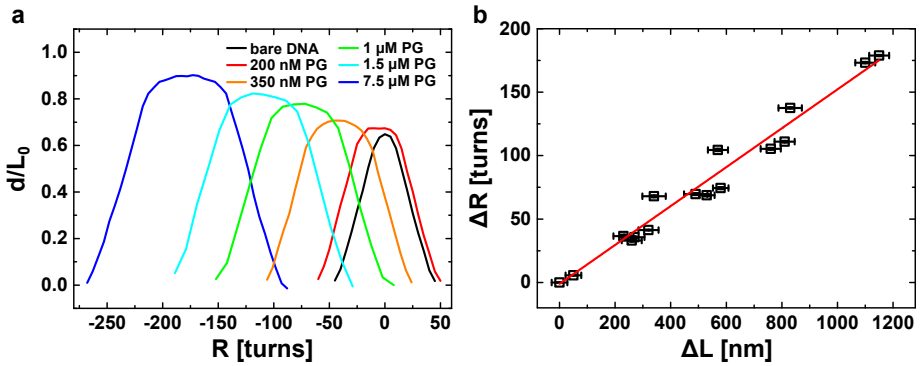

Figure 4: a. Rotational overwinding experiments of DNA molecule with stepwise increased PG concentration with a preset force of 0.2 pN; **b.** Linear approximation (solid line) of the change of rotation number ΔR with the elongation of the DNA contour length ΔL which allows to estimate the unwinding angle per intercalated PG molecule.

Conclusion

In summary, we investigated and quantified the nanomechanical binding mechanism of PicoGreen to dsDNA at room temperature in PBS buffer. Upon extending and overwinding single stained DNA molecules, we found an elongation, softening and untwisting of the DNA double helix depending on the dye concentration. These results suggest that PG simultaneously binds as an intercalator and minor-groove binder, which complies with data published elsewhere (Dragan et al. 2010). Furthermore, the elongation and unwinding per intercalated dye molecule was estimated as 0.38 nm/dye and approximately 21°/dye, respectively.

By means of MT extension experiments and fluorescence spectroscopy, we consistently estimated a binding site size of 2.3 bp, which is within the typical range of mono-intercalators. In contrast, Dargan and co-workers reported 3.8 bp

and 5.2 bp, yet at differing experimental conditions (Dragan et al. 2010). As the PG fluorescence intensity and therefore its association to DNA are subjected to variations in different buffer solutions, we can conclude that the PG-DNA binding exhibits a non-trivial binding behavior that is substantially influenced by the experimental conditions (Singer et al. 1997).

Finally, the equilibrium constant of association was estimated in the range of $10^6\,\mathrm{M}^{-1}$ with both force extension curves and fluorescence spectroscopy, respectively.

Acknowledgements

We gratefully acknowledge technical support from Christoph Pelargus.

References

Bouchiat, C.; Wang, M. D.; Allemand, J. F.; Strick, T.; Block, S. M.; Croquette, V. (1999) Estimating the Persistence Length of a Worm-Like Chain Molecule from Force-Extension Measurements. Biophysical Journal 76 (1), 409–413. DOI: 10.1016/S0006-3495(99)77207-3.

Cheng, W. (2006) Protocol to generate half Lambda DNA for optical/magnetic tweezer.
http://tweezerslab.unipr.it/cgi-bin/mt/documents.pl/Show?_id=ab03&sort=DEFAULT&search=&hits=23. Accessed 05.09.2008.

Crothers, D. M. (1968) Calculation of binding isotherms for heterogenous polymers. Biopolymers 6 (4), 575–584. DOI: 10.1002/bip.1968.360060411.

Dragan, A. I.; Casas-Finet, J. R.; Bishop, E. S.; Strouse, R. J.; Schenerman, M. A.; Geddes, C. D. (2010) Characterization of PicoGreen interaction with dsDNA and the origin of its fluorescence enhancement upon binding. Biophysical Journal 99 (9), 3010–3019. DOI: 10.1016/j.bpj.2010.09.012.

Glaser, T.; Fischer von Mollard, G.; Anselmetti, D. (2016) Rational design of dinuclear complexes binding at two neighboring phosphate esters of DNA. Inorganica Chimica Acta 452, 62–72. DOI: 10.1016/j.ica.2016.02.013.

Günther, K.; Mertig, M.; Seidel, R. (2010) Mechanical and structural properties of YOYO-1 complexed DNA. Nucleic acids research 38 (19), 6526–6532. DOI: 10.1093/nar/gkq434.

Hayashi, M.; Harada, Y. (2007) Direct observation of the reversible unwinding of a single DNA molecule caused by the intercalation of ethidium bromide. Nucleic acids research 35 (19), e125. DOI: 10.1093/nar/gkm529.

Jany, T.; Moreth, A.; Gruschka, C.; Sischka, A.; Spiering, A.; Dieding, M.; Wang, Y.; Haji Samo, S.; Stammler, A.; Bögge,H.; Fischer von Mollard, G.; Anselmetti, D.; Glaser, T. (2015) Rational design of a cytotoxic dinuclear Cu2 complex that binds by molecular recognition at two neighboring phosphates of the DNA backbone. Inorganic chemistry 54 (6), 2679–2690. DOI: 10.1021/ic5028465.

Japaridze, A.; Benke, A.; Renevey, S.; Benadiba, C.; Dietler, G. (2015) Influence of DNA Binding Dyes on Bare DNA Structure Studied with Atomic Force Microscopy. Macromolecules 48 (6), 1860–1865. DOI: 10.1021/ma502537g.

Kleimann, C.; Sischka, A.; Spiering, A.; Tonsing, K.; Sewald, N.; Diederichsen, U.; Anselmetti, D. (2009) Binding kinetics of bisintercalator Triostin a with optical tweezers force mechanics. Biophysical Journal 97 (10), 2780–2784. DOI: 10.1016/j.bpj.2009.09.001.

Lipfert, J.; Klijnhout, S.; Dekker, N. H. (2010) Torsional sensing of small-molecule binding using magnetic tweezers. Nucleic acids research 38 (20), 7122–7132. DOI: 10.1093/nar/gkq598.

McGhee, J. D.; von Hippel, P. H. (1974) Theoretical aspects of DNA-protein interactions. Co-operative and non-co-operative binding of large ligands to a one-dimensional homogeneous lattice. Journal of Molecular Biology 86 (2), 469–489. DOI: 10.1016/0022-2836(74)90031-X.

Singer, V. L.; Jones, L. J.; Yue, S. T.; Haugland, R. P. (1997) Characterization of PicoGreen reagent and development of a fluorescence-based solution assay for double-stranded DNA quantitation. Analytical biochemistry 249 (2), 228–238. DOI: 10.1006/abio.1997.2177.

Smith, S.; Finzi, L.; Bustamante, C. (1992) Direct mechanical measurements of the elasticity of single DNA molecules by using magnetic beads. Science 258 (5085), 1122–1126. DOI: 10.1126/science.1439819.

Strick, T. R.; Allemand, J. F.; Bensimon, D.; Bensimon, A.; Croquette, V. (1996) The Elasticity of a Single Supercoiled DNA Molecule. Science 271 (5257), 1835–1837. DOI: 10.1126/science.271.5257.1835.

Strick, T. R.; Allemand, J. F.; Bensimon, D.; Croquette, V. (1998) Behavior of Supercoiled DNA. Biophysical Journal 74 (4), 2016–2028. DOI: 10.1016/S0006-3495(98)77908-1.

Vilfan, I. D.; Lipfert, J.; Koster, D. A.; Lemay, S. G.; Dekker, N. H. (2009) Handbook of single-molecule biophysics. Hinterdorfer, P.; van Oijen, A., Eds; Springer Science+Business Media.

Vladescu, I. D.; McCauley, M. J.; Nunez, M. E.; Rouzina, I.; Williams, M. C. (2007) Quantifying force-dependent and zero-force DNA intercalation by single-molecule stretching. Nature methods 4 (6), 517–522. DOI: 10.1038/nmeth1044.

Wang, Y.; Sischka, A.; Walhorn, V.; Tönsing, K.; Anselmetti, D. (2016) Nanomechanics of Fluorescent DNA Dyes on DNA Investigated by Magnetic Tweezers. Biophysical Journal 111 (8), 1604–1611. DOI: 10.1016/j.bpj.2016.08.042.

Williams, L. D.; Egli, M.; Gao, Q.; Rich, A. (1992) Structure & function (1), 107-125. Sarma, R. H., Sarma, M. H., Eds. New York. Adenine Press.

Zipper, H.; Brunner, H.; Bernhagen, J.; Vitzthum, F. (2004) Investigations on DNA intercalation and surface binding by SYBR Green I, its structure determination and methodological implications. Nucleic acids research 32 (12), e103. DOI: 10.1093/nar/gnh101.

4.3 Paper V

As one of the basic proteins in the cell, histones play an important role. They help to pack the DNA polymer within the nucleus. Core histones, consisting of each of two H2A, H2B, H3 and H4 histone proteins, are wrapped by 147 base pairs of DNA strands, resulting in nucleosomes. The linker protein H1 further contributes to an even more compact structure, eventually leading to the highly packed chromosome. However, in biological processes like replication and transcription, the DNA polymer must first be freed from the chromosome conformation to the linear double strands, followed by a transition to a single-stranded form. This unpacking mechanism inevitably results in a dissociation of the histones from the DNA. The action of histones afterwards is still unknown. A possible hypothesis is that the free histones bind to the ssDNA. Theoretically, these proteins should be able to associate with ssDNA due to the electrostatic interaction between the positively charged proteins and the negatively charged DNA backbone. However, this is hardly explored. Therefore in this paper, the interaction between histone proteins and single-stranded DNA was investigated experimentally.

Via both bulk and single-molecule studies, the association of histones to ssDNA was proved. In magnetic tweezers assays, this phenomenon was observed with respect to two different aspects. Firstly, performing the force-extension experiments with different concentrations of histone proteins (core proteins with linker proteins), a reduction of the DNA length was observed. This fact can be explained with the topological wrapping of the ssDNA around histone cores which causes a decrease of the effective DNA length. Combined with the TEM- (transmission electron microscopy) and AFM-imaging of the ssDNA-histone complexes, a nucleosome-like conformation was detected. Secondly, no opening of the secondary structure of the ssDNA could be observed with the presence of histone proteins (10 nM). With adding histones at a large concentration (500 nM), ssDNA exhibited a negligible contour length. This result supports the hypothesis that histones and ssDNA form some type of compact and organized nucleosome-like structures.

In addition, histones were found to bind cooperatively to both ds- and ssDNA with a similar binding affinity by an equilibrium constant of association of $10^7\,\mathrm{M}^{-1}$ in a physiological environment. Furthermore, the associ-

ation of histones with ssDNA is suggested to happen spontaneously during replication and transcription processes of chromatin. The conclusion that core histones preferentially bind to one DNA strand, leads to a concrete understanding of the construction of nucleosomes.

Paper V

Biophysical Characterization of the Association of Histones with Single-stranded DNA

Y. Wang, L. van Merwyk, K. Toensing, V. Walhorn, D. Anselmetti and X. Fernàndez-Busquets. *Biochimica et Biophysica Acta*. 2017 (Submitted).

Abstract: Despite the profound current knowledge of the architecture and dynamics of nucleosomes, little is known about the structures generated by the interaction of histones with single-stranded DNA (ssDNA), which is widely present during replication and transcription. Non-denaturing gel electrophoresis reveals that histones have a high affinity for ssDNA at physiological salt concentrations, with an apparent binding constant similar to that calculated for their association with double-stranded DNA (dsDNA). The length of DNA (number of nucleotides in ssDNA or base pairs in dsDNA) associated with a histone octamer is the same for both ssDNA and dsDNA. Whereas histone-ssDNA complexes show a high tendency to aggregate in 0.2M NaCl, at lower ionic strength nucleosome-like structures are observed in electron microscope images. Core histones are able to protect ssDNA from digestion by micrococcal nuclease, and magnetic tweezers assays indicate a shortening of ssDNA upon its interaction with histones. Finally, the purified (+) strand of a cloned DNA fragment of nucleosomal origin has a higher affinity for histones than the purified complementary strand. Taken together, these data suggest that histones and ssDNA associate into some type of nucleosome-like assembly that may facilitate the participation of histones in the replication and transcription of chromatin.

Authors' contributions:
Design of the study: X.F-B. and D.A.
Preparation of samples: K.T., ***Y.W.*** *and L.vM.*
Design and performance of experiments, data-analysis (MT): ***Y.W.***
Design of experiments (AFM): V.W.
Performance of experiments, data-analysis (AFM): L.vM. and V.W.
Writing the manuscript: X.F-B., ***Y.W.****, V.W. and D.A.*

Submitted to: Biochimica et Biophysica Acta

Biophysical Characterization of the Association of Histones with Single-stranded DNA

Ying Wang[1], Luis van Merwyk[1], Volker Walhorn[1], Katja Toensing[1], Dario Anselmetti[1], Xavier Fernández-Busquets[2,3,4]

1 Experimental Biophysics and Applied Nanoscience, Faculty of Physics, Bielefeld University, Bielefeld 33615, Germany

2 Nanomalaria Group, Institute for Bioengineering of Catalonia (IBEC), Barcelona 08028, Spain

3 Barcelona Institute for Global Health (ISGlobal), Hospital Clinic-Universitat de Barcelona, Barcelona 08036, Spain

4 Nanoscience and Nanotechnology Institute (IN2UB), University of Barcelona, Barcelona 08028, Spain

ABSTRACT

Despite the profound current knowledge of the architecture and dynamics of nucleosomes, little is known about the structures generated by the interaction of histones with single-stranded DNA (ssDNA), which is widely present during replication and transcription. Non-denaturing gel electrophoresis reveals that histones have a high affinity for ssDNA at physiological salt concentrations, with an apparent binding constant similar to that calculated for their association with double-stranded DNA (dsDNA). The length of DNA (number of nucleotides in ssDNA or base pairs in dsDNA) associated with a histone octamer is the same for both ssDNA and dsDNA. Whereas histone-ssDNA complexes show a high tendency to aggregate in 0.2 M NaCl, at lower ionic strength nucleosome-like structures are observed in electron microscope images. Core histones are able to protect ssDNA from digestion by micrococcal nuclease, and magnetic tweezers assays indicate a shortening of ssDNA upon its interaction with histones. Finally, the purified (+) strand of a cloned DNA fragment of nucleosomal origin has a higher affinity for histones than the purified complementary strand. Taken together, these data suggest that histones and ssDNA associate into some type of nucleosome-like assembly that may facilitate the participation of histones in the replication and transcription of chromatin.

INTRODUCTION

Nucleosomes are present even in chromatin regions where replication and transcription are taking place [1];[2]. In spite of the detailed knowledge of its three-dimensional structure [3], the nucleosome is no longer viewed as a single static entity: rather, it is a family of particles varying in their structural and dynamic properties, leading to different functionalities [4]. It seems clear that the precise positioning of nucleosomes on particular DNA sequences is directly related to the regulation of chromatin activity (reviewed in [5];[6]), but the detailed knowledge of the molecular processes that allow the elongation of DNA and RNA chains in eukaryotic genes containing nucleosomes is still limited. The linker histones H1 and H5 are partially displaced from active genes [7], but results coming from several laboratories have indicated different fates for core histones during transcription, suggesting various mechanisms for transcription elongation [2];[8]. The remarkable comformational flexibility of nucleosome cores detected using various physicochemical techniques [1];[9];[10] could facilitate the passage of RNA polymerase without modification of histone composition. However, during transcription the DNA template is extensively distorted as it passes through the narrow active center of RNA polymerase [11], which makes it unlikely for transcription to occur without drastic nucleosomal disruption. Indeed, *in vitro* transcription assays with nucleosomal templates showed that RNA polymerase II cannot traverse through nucleosomes [12]. On moderately active genes, histones H2A/H2B are exchanged at a much higher rate that H3/H4 histones, suggesting that only H2A/H2B are displaced during transcription [13];[14], whereas during intense transcription all core histones are displaced/exchanged at the transcribed regions [15]. Nucleosome dissociation could be produced either by the direct contact of the polymerase molecule with the nucleosome core, or indirectly by the DNA topological stress generated during transcription [16]. The high concentration of chromatin in the nucleus and the well-known high affinity of excess histones for nucleosomes [17], had suggested in early studies the possibility that the displaced histones H2A, H2B (and even H3, H4) could be transiently associated with the nucleosomes of chromatin regions located near the transcribed genes [18]. The spontaneous reactions of transfer of H2A, H2B and H3, H4 from nucleosomes containing excess histones to DNA [18], between partially dissociated nucleosomes [19], and to histone chaperones [20] could be involved in the mechanism of nucleosome reassembly after the passage of the RNA polymerase.

Depletion of H2A/H2B dimers has been also suggested to occur during DNA replication and repair [21];[22]. Time-resolved small angle X-ray scattering was used to determine transient structures of protein and DNA constituents of nucleosome core particles during salt-induced disassembly [23], which revealed asymmetric release of DNA from disrupted nucleosome cores, displaying different patterns of protein dissociation. Such kinetic intermediates have been suggested to be biologically important elements for gene regulation. In pioneering classic assays it had been reported that the purified replication proteins of bacteriophage T4 allowed the *in vitro* replication of a nucleosome-containing DNA template without histone displacement [24], and that nucleosomes (or at least H3/H4 tetramers) of SV40 minichromosomes remained associated with DNA during the replication with eukaryotic enzymes [25]. On the other hand, from yeast *in vivo* studies it had been concluded that during chromatin replication the

bulk of core histone octamers within old nucleosomes were dissociated [26]; the newly synthesized nucleosomes contained random mixtures of two H2A/H2B dimers (new or old) and one H3/H4 tetramer (new or old). More recently, it has been shown that the yeast histone H3 variant Cse4 undergoes *de novo* replacement in S phase [27].

Summarizing, despite the existence of a large amount of data reporting on the dynamic eviction of histones from DNA during replication and transcription [28], there is also compelling evidence that a complete dissociation of nucleosome cores might not always occur. However, even in these cases, it is reasonable to assume that the normal structure of the nucleosome must be strongly perturbed to allow the transient formation of single-stranded DNA (ssDNA). This implies that the histones remaining bound to DNA may interact with ssDNA. Moreover, a temporary interaction between ssDNA and the histones released from nucleosomes involved in replication or transcription cannot be excluded. Little is known about these possibilities because only a few early reports have been devoted to the study of the interaction of histones with ssDNA [29-32]. In this work we have used different techniques to carry out a detailed analysis of the association of core histones with the ssDNA of bacteriophage M13. We have also investigated the interaction of histones with the purified (+) and (-) strands of a cloned DNA fragment from nucleosomal origin.

MATERIALS AND METHODS

Materials

Except where otherwise indicated, reactions were performed at room temperature (20 °C) and reagents were purchased from Sigma-Aldrich Corporation (St. Louis, MO, USA).

Preparation of nucleosomes, histones, and M13 ssDNA and dsDNA

Core histones, oligonucleosomes and core particles were obtained from chicken erythrocyte nuclei as previously described [19]. Circular ssDNA and dsDNA from bacteriophage M13mp18 were isolated and analyzed by conventional procedures [33]. The concentrations of DNA solutions were determined spectrophotometrically, using an A_{260} of 20 and 28 for solutions of $1\,\mathrm{mg\,ml^{-1}}$ of dsDNA and ssDNA [34], respectively.

Linearization of ssM13mp18 and dsM13mp18 DNAs

Digestion with *EcoRI* (Roche Diagnostics GmbH, Mannheim, Germany), which has a single recognition site in M13mp18, was the strategy chosen to linearize the circular DNA forms. To generate a double strand region around the *EcoRI* site in the ssDNA species, 100 µg of ssM13mp18 (7,250 bases) were mixed with 0.54 µg of the 20-base oligonucleotide 5'- CGAGCTCGAATTCGTAATCA-3' (approximate molar ratio 1:2), and left to hybridize at room temperature for 30 min prior to restriction enzyme digestion and analysis in agarose gels (Figure 1).

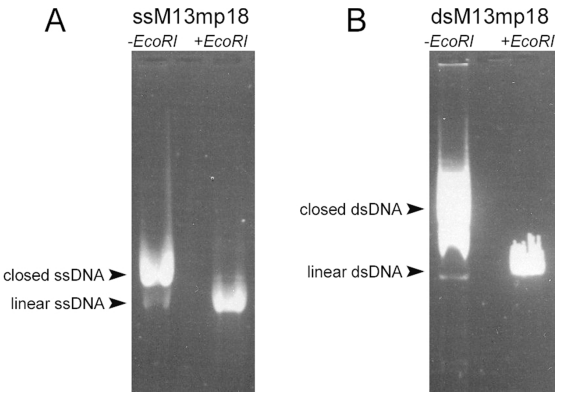

Figure 1: Analysis in 1.4 % agarose gels of the linearization products of M13 **(A)** ssDNA and **(B)** dsDNA.

Purification of the (+) and (-) strands of the core NX1 DNA fragment

The NX1 DNA insert [35] was excised from the M13 vector by digestion with *EcoRI* and *BamHI* (Roche Diagnostics GmbH) and further amplified using the pBluescript SK(+) vector (Stratagene). Finally, *EcoRI* and *BamHI* were used to remove the insert from this plasmid. The linear plasmid was separated from the NX1 fragment by precipitation with 7.5 % polyethylene glycol in TE buffer (1 mM EDTA, 10 mM Tris-HCl, pH 7.5) containing 0.55 M NaCl. The resulting NX1 DNA was phenol-extracted twice, precipitated with isopropanol, and washed with 70 % ethanol. The (+) and (-) strands of NX1 DNA were purified by polyethylene glycol precipitation as described elsewhere [36].

Electrophoretic analysis of DNA-histone complexes

All titrations were performed in the presence of TE buffer at the NaCl concentrations indicated in the corresponding figure legends. In those experiments involving NX1 DNA the buffer contained 6.6 % sucrose and BSA at the same concentration as histones. Histones were mixed with DNA, incubated at room temperature for at least 30 min and finally loaded onto the indicated gels. NX1 DNA samples were analyzed in nondenaturing, 15 cm long 6 % polyacrylamide-TBE gels, as described previously [18]. Samples containing M13 DNA were electrophoresed in nondenaturing, 25 cm long 1.4 % agarose-TBE gels, at 250 V for 3 h in an ice bath. The DNA was stained with ethidium bromide and the gel was photographed over an ultraviolet light. Photographic negatives were scanned with a Shimadzu CS-9000 densitometer.

Transmission electron microscopy

M13 ssDNA or linearized M13 dsDNA was mixed at room temperature with core histones (histone to DNA weight ratio was 1.2 for dsDNA and 2.4 for ssDNA) in a buffer containing 2 M NaCl, 0.2 mM EDTA, and 5 mM triethanolamine hydrochloride, pH 7.4. The NaCl concentration was progressively decreased by dilution: 1.6 M (30 min), 1.2 M (1 h), 0.85 M (1 h), 0.75 M (1 h), 0.6 M (1 h), 0.45 M (1 h), and 0.2 M (2 h). The final DNA concentrations were 24 µg ml^{-1} (dsDNA) and 21 µg ml^{-1} (ssDNA). Spread preparations of the resulting samples and oligonucleosomes were prepared as previously described [18]. All samples were fixed by treatment with 0.2 % glutaraldehyde (Merck) for about 15 h at 4 °C in the presence of 0.2 M NaCl, 0.2 mM EDTA, and 5 mM triethanolamine hydrochloride, pH 7.4. Fixed samples were diluted with the fixation buffer containing 10 mM NaCl to a final concentration of 2-0.8 µg DNA/ml.

Atomic force microscopy (AFM)

Highly oriented pyrolytic graphite (HOPG) substrates (ZYB-SS-2; TipsNano, Estonia) were coated with octadecylamine (ODA) by means of vapor deposition according to a method published elsewhere [37];[38]. Briefly, ca. 5 µg ODA on a microscope slide was placed on a heater plate at a temperature of 100 °C. After melting of the ODA, freshly cleaved HOPG was placed 4 cm above the ODA droplet face down for 5-20 sec while capped with a beaker. Prior to the application of DNA the modified substrates were analyzed by AFM in order to select those that exposed large ($< 100 \times 100\,\mathrm{nm}^2$) crystalline domains. For free DNA images, 10 µl of M13 ssDNA (0.5 ng µl^{-1} deionized water) was applied to the ODA-functionalized HOPG substrates, which after 10 min incubation were gently dried with filter paper under N_2 flow. For histone-DNA samples, 0.9 ng µl^{-1} ssDNA was incubated with 2.6 ng histone/µl and allowed to react for 15 min. Finally, 10 µl of M13 ssDNA-histone solution was applied to the ODA-functionalized HOPG substrates, which after 10 min incubation were gently dried with filter paper under N_2 flow.

Magnetic tweezers (MT) assays

We used a commercial MT instrument (Pico Twist, Lyon, France) with a custom-made flow cell that is briefly described below. A glass coverslip was first cleaned and covalently coated with Sigmacote in a desiccator to achieve a hydrophobic surface. With 70 µm thick, double-adhesive tape (Montex DX1, X-film, Lindlar, Germany) and a 100 µm thick polyester cover (3570, Zweckform, Oberlaindern, Germany) we then built a flow cell with 5 mm wide, 50 mm long and 70 µm thick chamber. Next, a 200 µg ml^{-1} anti-digoxigenin (anti-dig, Roche, Penzberg, Germany) solution was flushed into the flow cell and allowed to non-specifically adsorb onto the hydrophobic glass surface during incubation for at least 2 hours at 37 °C. Finally, the flow cell was rinsed with 10 mM PBS, pH 7.4, containing 137 mM NaCl and 2.7 mM KCl, and supplemented with 0.2 % BSA, 0.1 % Tween® 20, 5 mM EDTA and 10 mM NaN_3 in order to block and passivate further non-specific bonds during the experiments. The resulting flow cell was stored at 4 °C.

For MT experiments with dsDNA, λ DNA fragments (New England BioLabs, Frankfurt, Germany) were functionalized following existing protocols [39], at one end with several biotins (Biotin-14-dCTP, Meta-Bion, Steinkirchen, Germany) and at the other end with several digoxigenins (Dig-11-dUTP, Hoffmann-LaRoche, Penzberg, Germany), and stored in 10 mM PBS buffer (+137 mM NaCl, +2.7 mM KCl, pH 7.4 at 25 °C) at 4 °C. This dsDNA was linked via anti-dig to the surface of the custom-made flow cell. As a magnetic handle, streptavidin-coated magnetic beads (Dynabeads® MyOne™ Streptavidin C1, Life Technologies, Carlsbad, USA) were bound to the biotin-functionalized DNA end. For that, the magnetic beads (10 mg ml^{-1}) were gently mixed with 60 pM λ DNA in MT buffer (10 mM PBS containing 137 mM NaCl and 2.7 mM KCl, supplemented with 0.1 mg ml^{-1} BSA and 0.1 % Tween® 20, pH 7.4 at 25 °C) and incubated for 15 min. Prior to every experiment the structural integrity of each probed DNA molecule (nick-free) and its torsionally constrained immobilization were verified, a reference hat-curve was acquired by MT overwinding experiments, and the DNA contour length was finally determined by means of stretching experiments.

For MT experiments with ssDNA, and following the removal of the two short oligonucleotide fragments resulting from *EcoRI* digestion (Figure 2A), M13 ssDNA was functionalized with a biotinylated oligonucleotide (5'-B-CTGTGTGAAAT-B-3'; B=biotin, C/T=dC/dT-biotin, Meta-Bion) at the 3' end and with two digoxigenin-labeled oligonucleotides (5'-D-AGCTCGAATT-D-3' and 5'-D-ATCCCCGGGT-D-3'; D=digoxigenin, Meta-Bion) at the 5' end (Figure 2B), and stored until use at 4 °C in 10 mM PBS, pH 7.4, containing 137 mM NaCl and 2.7 mM KCl.

Figure 2: Scheme depicting **(A)** the strategy followed to linearize circular M13 ssDNA through *EcoRI* digestion and **(B)** the binding sites on the resulting linear DNA of (green, 3' end) biotinylated and (red, 5' end) digoxigenin-labeled oligonucleotides.

For single-molecule experiments, M13 ssDNA was attached in a separate vial to streptavidin-coated 2.8 µm M280 superparamagnetic microbeads (Dynabeads, 10 mg ml^{-1}, Thermo Fisher, Waltham, USA) via the specific biotin-streptavidin bond. When flushed into the flow cell, ssDNA-microbeads were allowed to bind the anti-dig coated surface through the specific digoxigenin-anti-dig interaction. Properly immobilized M13-microbead constructs were trapped in the magnetic field and stretched for functional control. These force-extension (F-d) experiments were performed from 0.3 pN up to about 30 pN. In addition, double stranded (ds) λ DNA (NEB, Frankfurt, Germany) was used in control assays, following a functionalization protocol described in a former work [39]; dsDNA F-d experiments were performed from 10^{-3} pN up to 10 pN. To estimate the DNA contour and persistence lengths, the experimental data were fitted to the (extended) worm-like-chain model [40-42].

WLC:

$$\frac{FL_{\mathrm{P}}}{k_{\mathrm{B}}T} = \frac{1}{4}\left(\left(1-\frac{d}{L_0}\right)^{-2} - 1\right) + \frac{d}{L_0} \tag{1}$$

extended WLC:

$$d = L_0\left[1 - \frac{1}{2}\left(\frac{k_{\mathrm{B}}T}{FL_{\mathrm{P}}}\right)^{1/2} + \frac{F}{K_0}\right] \tag{2}$$

Preset forces were 0.4 pN and 15 pN for overwinding and extension-time experiments, respectively. Histone solution (10 µM) was diluted to the applied concentrations with MT buffer, flushed into the chamber and incubated for 15 minutes to achieve thermodynamic equilibrium. All experiments were performed in MT buffer.

Micrococcal nuclease digestion

M13 dsDNA or ssDNA at a concentration of 68 µg ml^{-1} was digested with micrococcal nuclease (3.6 or 0.5 UWµg^{-1} dsDNA or ssDNA, respectively) in the absence or in the presence of core particle histones at a w/w ratio histone:DNA of 1:1 or 2:1 for dsDNA and ssDNA, respectively. The samples were incubated for 5 h in TE buffer containing 0.2 M NaCl and 10 mM $CaCl_2$ before adding micrococcal nuclease and incubating for the times indicated (1, 11, 20, and 45 min). To stop the reaction, nuclease-treated samples were digested with proteinase K in the presence of 0.2 % SDS, and the DNA EtOH-precipitated and resuspended in 50 µl of deionized formamide. After heating for 2 min at 100 °C the resulting DNA was analyzed in a 7 % polyacrylamide/formamide denaturing gel stained with ethidium bromide as described elsewhere [43].

RESULTS

Binding of core histones to high molecular mass ssDNA

The binding of core histones to M13 ssDNA and dsDNA was initially monitored by measuring in agarose gels the decrease in intensity of the corresponding DNA bands with the addition of increasing histone amounts (Figure 3A). These titration studies showed the expected sigmoidal profiles characteristic of a cooperative binding between histones and DNA (Figure 3B), where at higher concentrations the equilibrium was more displaced towards the formation of nucleoproteic complexes. Together with results derived from turbidimetric analyses (Figure 3C), the data obtained revealed that considering equal DNA masses, ssDNA required twice as much histone than dsDNA for equal association dynamics. When the data are represented considering the molar concentration of histone octamers vs. nucleotides or base pairs for ssDNA and dsDNA respectively, the titration curves are coincident (Figure 3C). This suggested that the length of DNA (expressed in number of ssDNA nucleotides and dsDNA base pairs) associated with a histone octamer is the same for both ssDNA and dsDNA.

The observed binding cooperativity permitted the calculation of thermodynamic parameters such as the nucleation constant K [44], and the cooperativity factor ω, which expresses the relative affinity of a ligand for a contiguous binding

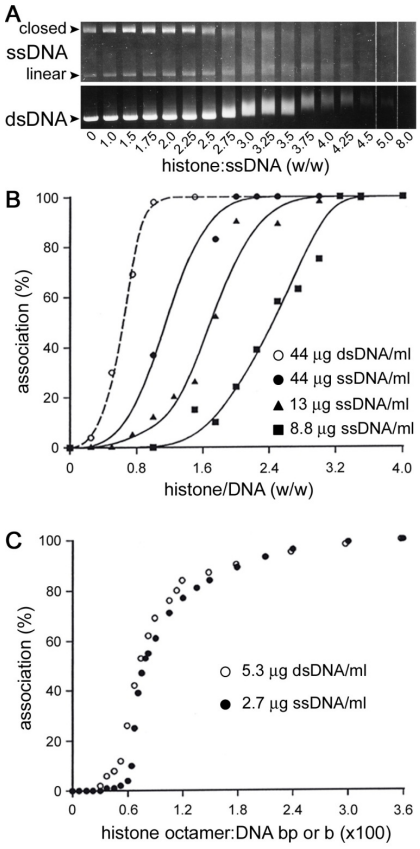

Figure 3: Association of core particle histones with M13 ssDNA and dsDNA. **(A** and **B)** Agarose gel studies. **(A)** Equimolar amounts of M13 ssDNA and dsDNA (9.6 and 19.2 µg ml^{-1} respectively) were mixed and titrated with increasing amounts of core particle histones in TE buffer supplemented with 0.15 M NaCl. **(B)** In similar assays performed at different DNA concentrations, the resulting ethidium bromide-stained bands were densitometered and the inverse of band intensity relative to t_0 was represented as % DNA-histone association. **(C)** Turbidimetric studies. After 10 min incubation A_{320} was measured. The represented histone/DNA mass ratio corresponds to histone octamers (1.09×10^5 Da/octamer) vs. base pairs (6.50×10^2 Da/bp) or nucleotides (3.25×10^2 Da/b) for dsDNA and ssDNA respectively.

site. Thus, when the next binding site is already occupied the binding constant K' becomes the association constant $K\omega$. In the case of a cooperative binding the product $K\omega$ is related with the ligand concentration at the titration midpoint, $L_{T,1/2}$, according to the following equation:

$$\frac{1}{K\omega} = L_{T,1/2} - \left(\frac{N}{2n}\right) \tag{3}$$

where n is the binding site size (168 nucleotides or base pairs per histone octamer) and N its concentration. Application of the equation (3) to the titration curves from Figure 3C provided similar $K\omega$ values for dsDNA and ssDNA (2.5×10^7 and $2.0 \times 10^7\,\mathrm{M}^{-1}$, respectively). The separate values for K and ω can be obtained by fitting the experimental data to the following theoretical equation (4) for the quantitative analysis of the cooperative binding of proteins to nucleic acids (Figure 4) [45]:

$$\frac{\nu}{L} = K\left(1 - n\nu\right)\left[\frac{\left(2\omega - 1\right)\left(1 - n\nu\right) + \nu - R}{2\left(\omega - 1\right)\left(1 - n\nu\right)}\right]^{n-1}\left[\frac{1 - \left(n + 1\right)\nu + R}{2\left(1 - n\nu\right)}\right]^{2} \tag{4}$$

where $R = \left[\left[1 - \left(n + 1\right)\nu\right]^2 + 4\omega\nu\left(1 - n\nu\right)\right]^{1/2}$, ν is the binding density of the ligand (in moles of histone octamer per mole of nucleotide residue or base pair), and L is the free octamer concentration (in mol l^{-1}). The resulting values for

K and ω are $5 \times 10^3\,\mathrm{M}^{-1}$ and 5×10^3 for dsDNA and $3 \times 10^3\,\mathrm{M}^{-1}$ and 7×10^3 for ssDNA, respectively.

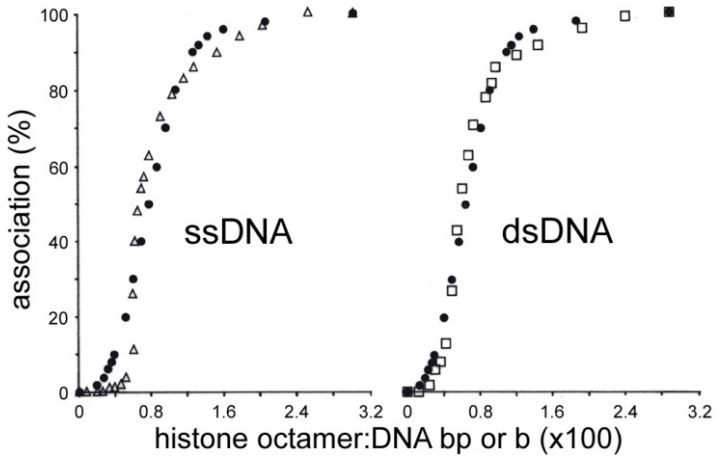

Figure 4: Fitting of the titration curves from Figure 3C according to McGhee and Von Hippel [45]. Theoretical values are represented by solid circles and experimentally obtained values by empty symbols.

To explore whether the interaction of histones with ssDNA is the result of molecular adsorption or of a nucleosome-like association, we characterized the resulting structures by electron microscopy and nuclease protection assays. Transmission electron microscope images of histone-ssDNA samples showed the presence of nucleosome-like particles that were undistinguishable from those observed in histone-dsDNA or native chromatin samples (Figure 5). Micrococcal nuclease digestion studies indicated that in the presence of histones there was a significant protection of M13 ssDNA in front of the DNase (Figure 6).

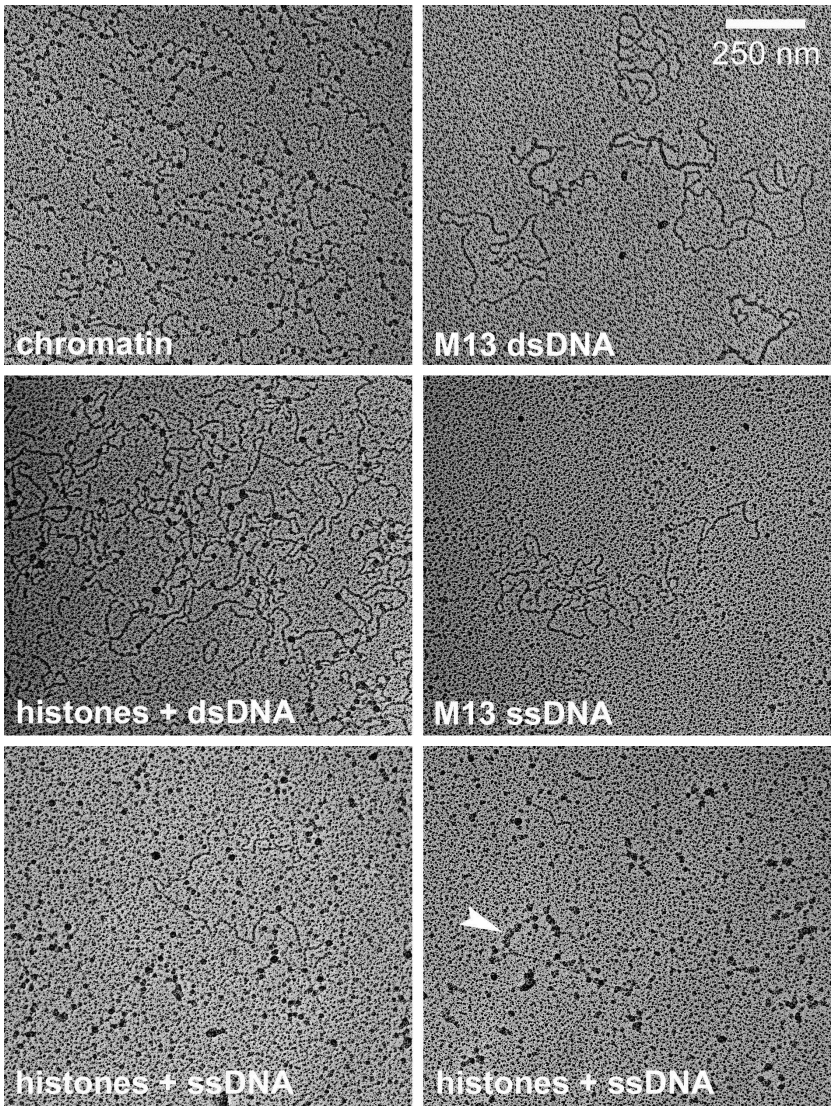

Figure 5: Transmission electron microscopy analysis of the structures formed between core particle histones and M13 ssDNA. Native chicken erythrocyte oligonucleosomes (chromatin) and histone+M13 dsDNA samples are included as controls. The arrowhead indicates an example of nucleosome-like structures on the histone+ssDNA sample.

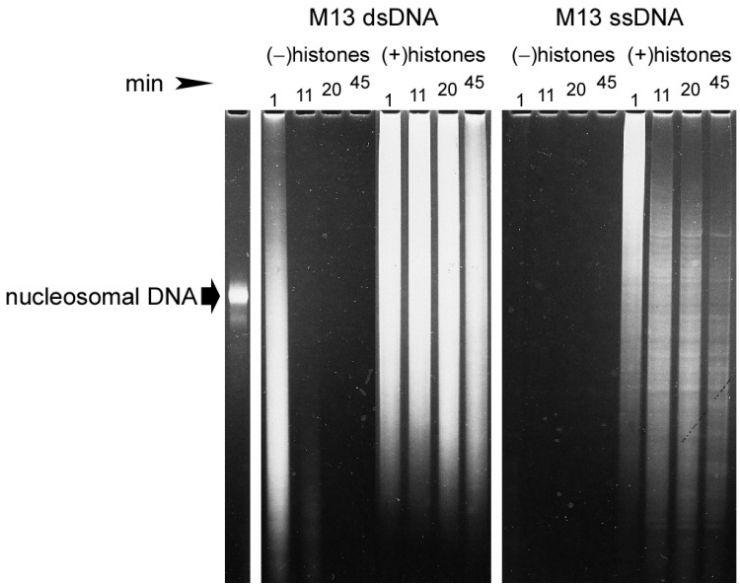

Figure 6: Micrococcal nuclease digestion of M13 ssDNA and dsDNA complexed with core particle histones. The electrophoretic mobility of native mononucleosomal DNA is shown as a control.

Atomic force microscopy of ssDNA and ssDNA-histone complexes

Because TEM images and DNase protection assays suggested the presence of nucleosomelike structures in ssDNA-histone samples, single-molecule AFM and MT assays were performed to further investigate this interaction. The structure and integrity of the M13 ssDNA to be used in MT assays were first analyzed by AFM imaging, following a protocol whereby the DNA was immobilized on ODA-modified HOPG and imaged under ambient conditions. Typical AFM topography images showed highly ordered domains of parallel oriented ODA on HOPG that interacted via their positively charged amine groups with the negatively charged M13 ssDNA, resulting in stretched and axially oriented ssDNA molecules (Figure 7A and B). Without the counterionic ODA surfactant layer the ssDNA exhibited a featureless random coil-like structure due to self-hybridization effects (data not shown). In contrast, AFM images of preassembled histone-M13 ssDNA complexes immobilized on ODA-modified HOPG did not show individual and stretched ssDNA molecules, revealing instead the presence of globular structures (Figure 7C) of dimensions similar to those observed in TEM images of histone-ssDNA samples.

Magnetic tweezers analysis of ssDNA-histone interaction

MT assays were done to explore histone-DNA interactions in more detail. In histone-free control and reference experiments, stretching and overwinding curves of double-standed λ DNA resulted in polymer elasticity and torsional

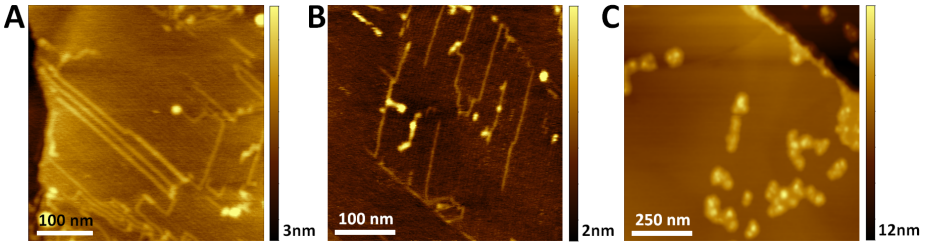

Figure 7: Typical AFM topography images on ODA modified graphite of **(A** and **B)** M13 ssDNA and **(C)** histone-M13 ssDNA complexes. Note the much larger z-scaling of the histone-ssDNA image in **C** compared to **A** and **B**.

curves as expected for linear, nick-free dsDNA (Figure 8A and B), e.g. yielding a persistence length of $L_\mathrm{p} = 48\,\mathrm{nm}$ and the plectonemic overwinding of the molecule associated with a shortening of the molecular end-to-end distance ("hat curve"). In contrast, MT experiments with single-stranded M13 DNA exhibited considerably softer elastic properties with a persistence length of only $L_\mathrm{p} = 7\,\mathrm{nm}$ in molecular stretching experiments (Figure 8C). In addition, torsional overwinding experiments with ssDNA led to a rotation-independent constant end-to-end distance since the DNA polymer can rotate around its sugar backbone in idle state (Figure 8D).

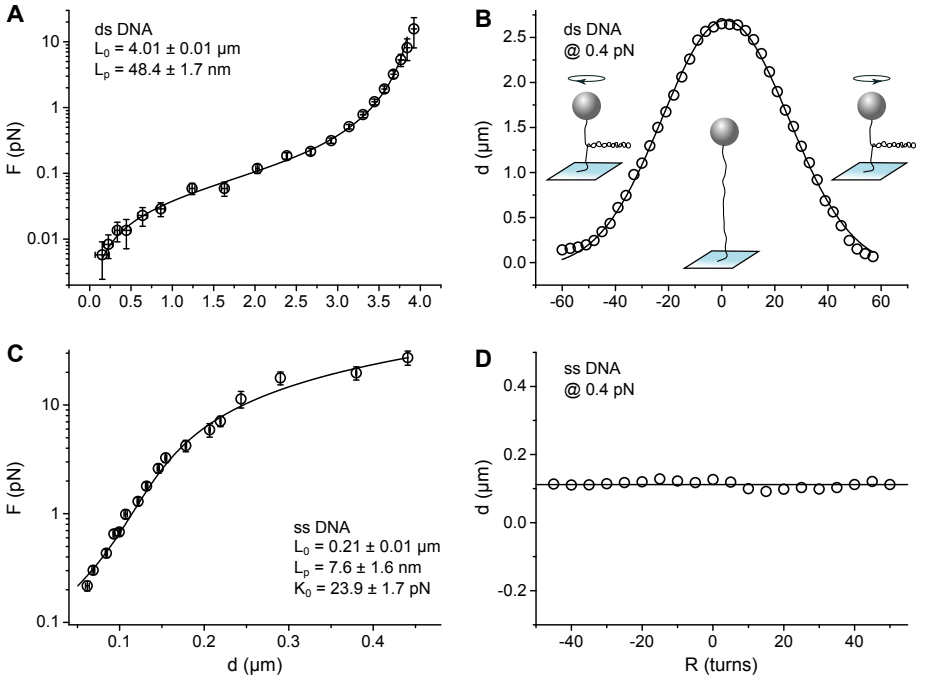

Figure 8: Magnetic tweezers stretching and overwinding analysis of dsDNA and ssDNA. The single-molecule force-extension elasticity curves of **(A)** dsDNA and **(C)** ssDNA are fitted with WLC and extended WLC models, respectively (solid lines). Torsional unwinding curves under a preset force of 0.4 pN are shown for **(B)** dsDNA and **(D)** ssDNA.

The addition of 5 nM histone to a single dsDNA molecule held in the MT trap at a preset force of 0.5 pN resulted in a shortening of the dsDNA along time with distinct ca. 100 nm-steps (Figure 9A). This step size can be rationalized by the fact that nucleosome formation is realized by wrapping 147 bp $\times$ 0.34 nm/bp $\approx$ 50.0 nm of dsDNA around the histone octamer complex and therefore steps of 100 nm would correspond to the formation of a distinct nucleosome pair. The observation of nucleosome pair formation can be topologically explained since the wrapping of a torsionally constrained dsDNA molecule (as we have in the MT) around a histone core induces torsional twists that can be released by the formation of two counterrotating nucleosome wrappings. A similar experiment with ssDNA could not be conducted since ssDNA undergoes self-hybridization under such low external forces leading to shortening of the molecular end-to-end distance in the absence of histones.

In contrast, ssDNA was found to be amenable to analysis in single-molecule stretching experiments performed under higher forces of up to 20 pN (Figure 9B and C). In the presence of 10 nM core histones plus linker H1 histone, MT stretching assays clearly indicated a significantly shorter end-to-end ssDNA length (Figure 9B), suggesting interaction of histones with ssDNA accompanied by the formation of three-dimensional nucleoprotein structures. In a different MT assay, where the ssDNA fragments were kept at a constant preset force of 15 pN over time (Figure 9C), bare M13 ssDNA exhibited discrete end-to-end distance jumps that can be attributed to partial disentangling of ssDNA secondary structure. In contrast, ssDNA-histone complexes containing 10 nM protein that were kept at a constant force of 15 pN, exhibited a stable and constant end-to-end DNA distance. The presence of 500 nM histone led to a fully compacted ssDNA with negligible contour length that could not be disentangled (data not shown). These results support the hypothesis that ssDNA and histones form some type of organized nucleosome-like structure.

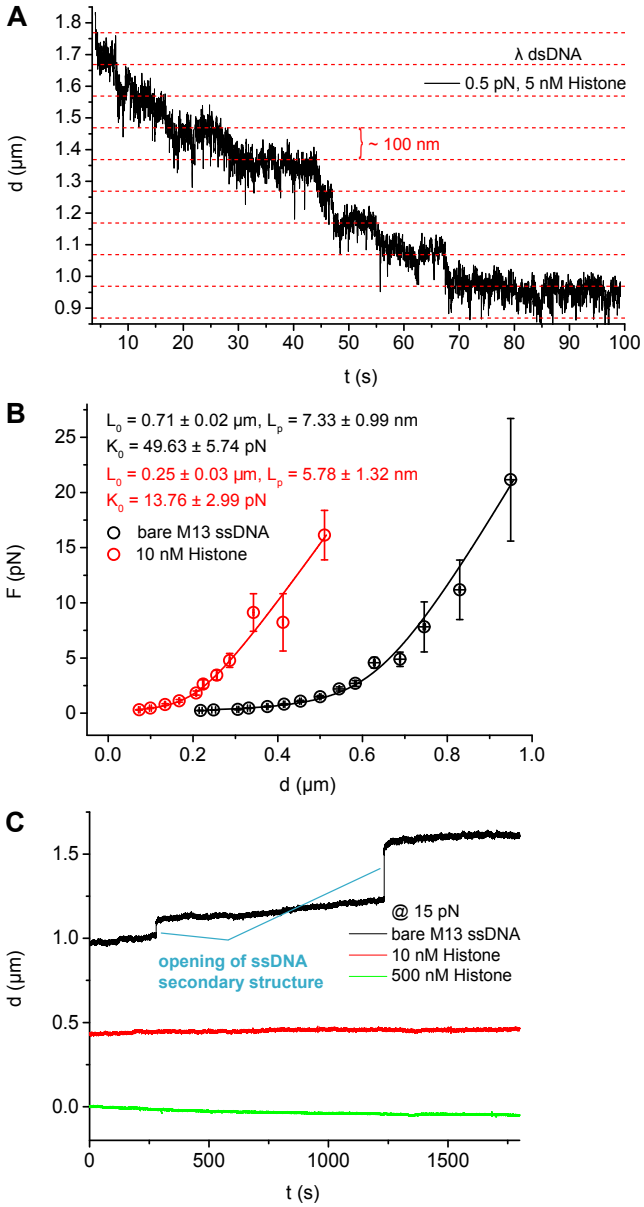

Figure 9: MT stretching experiments of λ dsDNA and M13 ssDNA in the presence and absence of histones. **(A)** End-to-end distance shortening in the presence of 5 nM core histones of a single λ dsDNA molecule held at a preset force of 0.5 pN. **(B)** Force-extension curves of M13 ssDNA in the absence (black, right) and in the presence of 100 nM histone (red, left). Solid lines show the extended WLC fit on the experimental data. **(C)** Real-time ssDNA extension measurement with a preset force of 15 pN. Black (upper), red (middle) and green (lower) solid lines exhibit the temporal extensions of M13 ssDNA in the presence of 0 nM, 10 nM and 500 nM histone, respectively. Steps in the black line indicate the opening of ssDNA secondary structure.

Competitive association of ssDNA and dsDNA with core histones

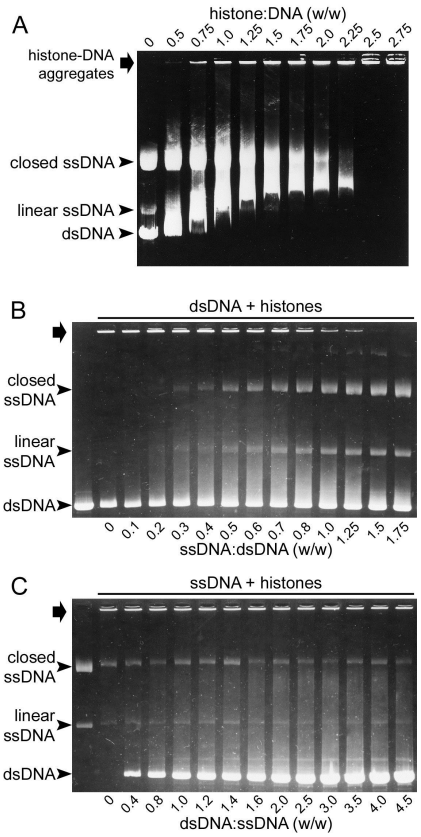

Figure 10: Competitive association of histones with M13 ssDNA and dsDNA. Samples were prepared in TE buffer supplemented with 0.15 M NaCl and analyzed in 1.4 % agarose gels. **(A)** Increasing amounts of histones were added to a solution containing 52 µg ml^{-1} of each DNA form. **(B)** M13 dsDNA (20 µg ml^{-1}) was complexed with histones (22 µg ml^{-1}) and titrated with increasing amounts of M13 ssDNA. Uncomplexed dsDNA is shown in the first lane. **(C)** M13 ssDNA (9.2 µg ml^{-1}) was complexed with histones (22.1 µg ml^{-1}) and titrated with increasing amounts of M13 dsDNA. Uncomplexed ssDNA is shown in the first lane. Arrows indicate histone-DNA aggregates not entering the gel.

Competition experiments were done where increasing core histone amounts were added to a solution containing equal masses of ssDNA and dsDNA (i.e. a molar ratio ssDNA:dsDNA 2:1). The electrophoretic mobility of the resulting DNA/histone complexes was analyzed in non-denaturing agarose gels (Figure 10A). In agreement with the association results obtained separately with each DNA form (Figure 3B), at a histone:DNA ratio of 0.75 (w/w) all the dsDNA was complexed with histones whereas the ssDNA was not associated to histones as indicated by their respective electrophoretic mobilities. At a histone:DNA ratio of 2.25 (w/w) all the ssDNA was associated to histones; when subtracting the 0.75 histone equivalents bound to dsDNA, the remaining 1.5 equivalents are consistent with the histone amount required to complex the twice as high molar amount of ssDNA relative to dsDNA present in the solution. The addition of large amounts of ssDNA to aggregated dsDNA-core histone complexes induced the complete release of the dsDNA previously associated with histones (Figure 10B). In contrast, dsDNA could not dissociate core histones from ssDNA (Figure 10C). Taking into account that the apparent association constant is essentially the same for both ssDNA- and dsDNA-histone complexes, these observations suggest that the kinetic stability is higher in the case of the complexes containing ssDNA.

Binding of core histones to the purified (+) and (–) strands of a cloned nucleosome core DNA

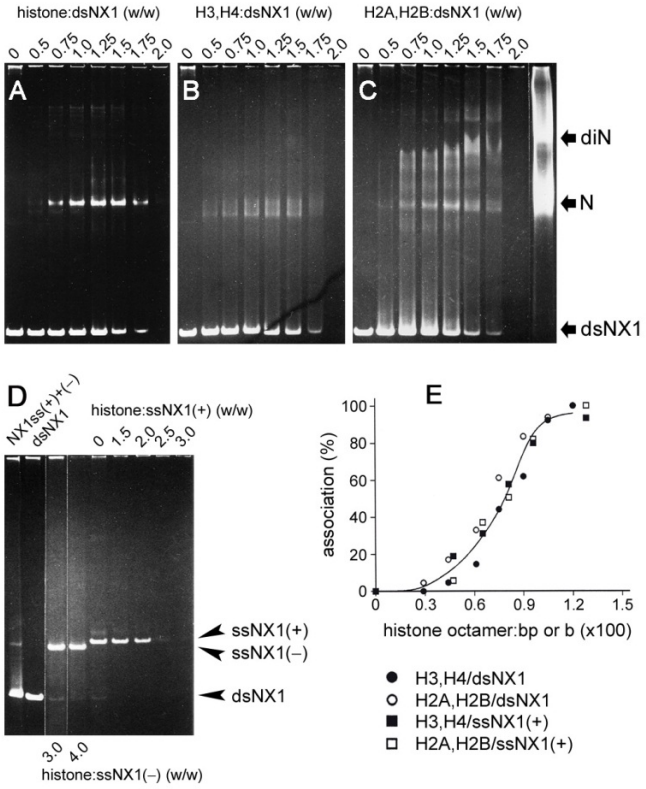

Figure 11: Titration with histones of the different forms of NX1 fragment. Samples were prepared in TE buffer supplemented with 0.2 M NaCl, 6.6 % sucrose, and an amount of BSA equal to the indicated histone content. Each lane contains 0.4 µg of NX1 dsDNA or 0.2 µg of NX1 ssDNA (+) or (–) strands. NX1 dsDNA was titrated with **(A)** core particle histones, **(B)** H3,H4, and **(C)** H2A,H2B. The electrophoretic mobility of mononucleosomes (N) and dinucleosomes (diN) is indicated as control. **(D)** Titration with core particle histones of NX1 ssDNA (–) and (+) strands. As controls are shown a sample containing 0.2 µg of each NX1 (+) and (–) strands and a lane containing 0.4 µg of NX1 dsDNA. **(E)** Titration of NX1 dsDNA and ssDNA(+) with the histone pairs H2A,H2B and H3,H4. The histone/DNA ratio is expressed as in Figure 3B.

To characterize more in detail the type of structure formed by histones on ssDNA we performed titration studies in non-denaturing 6 % polyacrylamide gels using the cloned 158 bp NX1 DNA sequence that was forming a nucleosome in vivo [36] (Figure 11). dsNX1 was complexed with a similar kinetics by core particle histones (Figure 11A) and by the pairs H3,H4 (Figure 11B) and H2A,H2B (Figure 11C). Nucleosome and nucleosome-like bands were observed at about half the electrophoretic mobility than naked nucleosomal dsDNA. The two strands of the NX1 fragment were purified by polyethylene glycol differential precipitation [36], through a protocol involving treatment of the (–) strand with HCl (pH 1.8). Since it had been described that DNA can be partially

depurinated with acid and then cleaved at depurination sites with 0.5 M NaOH [46], we examined whether the purified (–) strand used in this study was depurinated. The (–) st rand was incubated at room temperature for 15 min with 0.5 M NaOH in the presence of 1 M NaCl [46] and the resulting sample was analyzed in a polyacrylamide gel. The intensity of the band corresponding to the (–) strand was unchanged by the alkaline treatment (not shown) , indicating that the extent of depurination was negligible. As expected, the (–) and (+) strands used in this study reassociated rapidly to form the typical band corresponding to NX1 DNA (Figure 11D).

The association of core histones with NX1 dsDNA in the presence of 0.2 M NaCl produced a decrease in the intensity of the free DNA band, a well-defined nucleosome band, and aggregated material that did not enter the gel (Figure 11A). Under the same ionic strength conditions, increasing amounts of core histones caused a progressive decrease in the intensity of the band corresponding to the (+) strand of the NX1 fragment. These titration results obtained for the (+) strand were consistent with the data obtained with M13 DNA, according to which an amount (w/w) of core particle histones double than that needed for dsDNA was required in order to complex ssDNA. As previously reported [35] the (+) strand had a significantly greater affinity for histones than the (–) strand (Figure 11D), probably as a result of their different sequences. NX1 ssDNA-histone titrations did not reveal the appearance of nucleosome-like bands. This is probably due to the neutralization of the negative charges of the 158-base NX1 ssDNA fragment, which are almost completely cancelled by the 148 positive charges of a histone octamer [47], resulting in a species with virtually no electrophoretic mobility. Similar results were obtained for the H2A,H2B and H3,H4 pairs (Figure 11E).

DISCUSSION

Our binding assays demonstrate that histones have high affinity for ssDNA at physiological ionic strength. These studies and the competitive association results indicate that the binding constant is roughly the same for both M13 dsDNA and M13 ssDNA, strongly suggesting that in the cell nucleus histones may interact with ssDNA. The association constant determined for histone-ssDNA binding does not differ significantly from those obtained for other molecules binding dsDNA [48];[49] and ssDNA [50]. Although our results indicate that the ssDNA-histone complexes have a high tendency to aggregate under physiological salt concentrations, at lower ionic strength structures resembling nucleosome core particles can be detected in the electron microscope, and the interaction with histones protects ssDNA from micrococcal nuclease digestion. Since the present knowledge on the replication and transcription of chromatin suggests that the interaction of histones with ssDNA can take place only transiently and in some cases only before the partial or complete removal of histones induced by these processes, *a priori* it seems unlikely that histones can interact *in vivo* with ssDNA stretches long enough to produce complete nucleosomal structures. However, the structural studies of other authors have shown that the binding of core histones to ssDNA can produce nucleosome-like complexes [29-32], in agreement with the conclusions that can be obtained from the data presented here. Optical/magnetic tweezers have been used to study the force-induced

dynamic response of canonical nucleosomes to different mechanical constraints [51-53], but this powerful technique had not been applied so far to the study of histone-ssDNA interactions. The pioneering magnetic tweezers results presented here support the hypothesis that histones do not merely adsorb on ssDNA, but they induce the formation of some type of structure leading to shortening of the DNA and stabilization of its secondary structure; both observations are consistent with the existence in histone-ssDNA complexes of a nucleosome-like entity.

The finding that the length of DNA covered by each histone octamer is the same for both ssDNA and dsDNA, suggests that histones can be bound to either one of these DNA forms without extensive modification of the nucleosome structure. This could be related to the sequential arrangement of histones along DNA in the nucleosome core particle inferred from DNA-histone crosslinking experiments and from the structural analysis of core particle and histone octamer crystals [54]. It has been reported that this histone organization is maintained even when the nucleosome structure is perturbed with denaturing agents [55] and when nucleosomes are located within transcriptionally active heat-shock *Drosophila* genes [56]. Repositioning of histone octamers during transcription has been described to occur along the same DNA segment by sliding [57], a process only considered so far for dsDNA but which can also unfold on ssDNA regions of transcribed genes. The association of histones with a constant length of either dsDNA or ssDNA may facilitate transcription without alteration of the linear order of histones along DNA.

In contrast to the well-established fact that the dsDNA sequences in a genome are a determinant of nucleosome organization and positioning [57];[58], to the best of our knowledge there are no studies on the possible differential affinity of ssDNA sequences for histones. Our results obtained with M13 ssDNA are unable to show any preference of histones for specific nucleotide sequences. However, we have detected significant differences in histone binding between the (+) and (–) strands of the nucleosome DNA fragment used in this study. Although the observed binding energy difference is relatively small (ca. $1\,\mathrm{kcal\,mol^{-1}}$), it is high enough to produce a preferential association of histones with one of the strands. Comparable energy differences allow the preferential binding of histones to dsDNA containing nucleosome positioning sequences in competitive reconstitution experiments [59]. From a kinetic point of view, low energy differences may be useful for functional processes involving nucleosomes. Our observations are compatible with crosslinking results indicating that core histones in the nucleosome are bound within discrete DNA segments mainly to one DNA strand, but can occasionally jump to bind the complementary strand [60], and suggest that the association of histones with ssDNA could occur spontaneously during replication and transcription of chromatin.

ACKNOWLEDGEMENTS

We thank the staffs of the Servei de Seqüenciació de DNA (Centre d'Investigació i Desenvolupament, CSIC) and of the Servei de Microscòpia Electrònica (Universitat Autònoma de Barcelona) for their assistance. We acknowledge technical support from Helene Schellenberg and Christoph Pelargus. We are indebted to Prof. Joan-Ramon Daban for valuable discussions regarding the

biophysical characterization of the interaction of histones with ssDNA.

FUNDING

This work was supported in part by grants BIO2002-00128 from the Ministerio de Economía y Competitividad, Spain, which included Fondo Europeo de Desarrollo Regional funds, and 2009SGR-760 from the Generalitat de Catalunya, Spain.

REFERENCES

1. Deniz,Ö., Flores,O., Aldea,M., Soler-López,M. and Orozco,M. (2016) Nucleosome architecture throughout the cell cycle. Sci. Rep., 6, 19729.

2. Kulaeva,O.I., Hsieh,F.K., Chang,H.W., Luse,D.S. and Studitsky,V.M. (2013) Mechanism of transcription through a nucleosome by RNA polymerase II. Biochim. Biophys. Acta, 1829, 76-83.

3. Zhu,P. and Li,G. (2016) Structural insights of nucleosome and the 30 nm chromatin fiber. Curr. Opin. Struct. Biol., 36, 106-115.

4. Zlatanova,J., Bishop,T.C., Victor,J.M., Jackson,V. and van Holde,K. (2009) The nucleosome family: dynamic and growing. Structure, 17, 160-171.

5. Bannister,A.J. and Kouzarides,T. (2011) Regulation of chromatin by histone modifications. Cell Res., 21, 381-395.

6. Wolffe,A.P. and Hayes,J.J. (1999) Chromatin disruption and modification. Nucleic Acids Res., 27, 711-720.

7. Flanagan,T.W. and Brown,D.T. (2016) Molecular dynamics of histone H1. Biochim. Biophys. Acta, 1859, 468-475.

8. Wunsch,A. and Jackson,V. (2005) Histone release during transcription: acetylation stabilizes the interaction of the H2A-H2B dimer with the H3-H4 tetramer in nucleosomes that are on highly positively coiled DNA. Biochemistry, 44, 16351-16364.

9. Sivolob,A. and Prunell,A. (2004) Nucleosome conformational flexibility and implications for chromatin dynamics. Philos. Trans. R. Soc. Lond. A Math. Phys. Eng. Sci., 362, 1519-1547.

10. Nam,G.M. and Arya,G. (2016) Free-energy landscape of mono- and dinucleosomes: enhanced rotational flexibility of interconnected nucleosomes. Phys. Rev. E, 93, 032406.

11. Liu,X., Bushnell,D.A., Wang,D., Calero,G. and Kornberg,R.D. (2010) Structure of an RNA polymerase II-TFIIB complex and the transcription initiation mechanism. Science, 327, 206.

12. Chang,C.H. and Luse,D.S. (1997) The H3/H4 tetramer blocks transcript elongation by RNA polymerase II in vitro. J. Biol. Chem., 272, 23427-23434.

13. Kulaeva,O.I., Gaykalova,D.A. and Studitsky,V.M. (2007) Transcription through chromatin by RNA polymerase II: histone displacement and exchange. Mutat. Res., 618, 116-129.

14. Kimura,H. and Cook,P.R. (2001) Kinetics of core histones in living human cells: little exchange of H3 and H4 and some rapid exchange of H2b. J. Cell Biol., 153, 1341-1354.

15. Katan-Khaykovich,Y. and Struhl,K. (2011) Splitting of H3-H4 tetramers at transcriptionally active genes undergoing dynamic histone exchange. Proc. Natl. Acad. Sci. U.S.A., 108, 1296-1301.

16. Clark,D.J. and Leblanc,B.P. (2015) Analysis of DNA supercoiling induced by DNA-protein interactions. In Leblanc,B.P. and Rodrigue,S. (eds.), DNA-Protein Interactions: Principles and Protocols. Springer, New York, NY, pp. 161-172.

17. Eisenberg,H. and Felsenfeld,G. (1981) Hydrodynamic studies of the interaction between nucleosome core particles and core histones. J. Mol. Biol., 150, 537-552.

18. Aragay,A.M., Fernàndez-Busquets,X. and Daban,J.R. (1991) Different mechanism for in vitro formation of nucleosome core particles. Biochemistry, 30, 5022-5032.

19. Aragay,A.M., Diaz,P. and Daban,J.R. (1988) Association of nucleosome core particle DNA with different histone oligomers. J. Mol. Biol., 204, 141-154.

20. Gurard-Levin,Z.A., Quivy,J.P. and Almouzni,G. (2014) Histone chaperones: assisting histone traffic and nucleosome dynamics. Ann. Rev. Biochem., 83, 487-517.

21. MacAlpine,D.M. and Almouzni,G. (2013) Chromatin and DNA replication. Cold Spring Harb. Perspect. Biol., 5, a010207.

22. Arimura,Y., Tachiwana,H., Oda,T., Sato,M. and Kurumizaka,H. (2012) Structural analysis of the hexasome, lacking one histone H2A/H2B dimer from the conventional nucleosome. Biochemistry, 51, 3302-3309.

23. Chen,Y., Tokuda,J.M., Topping,T., Sutton,J.L., Meisburger,S.P., Pabit,S.A., Gloss,L.M. and Pollack,L. (2014) Revealing transient structures of nucleosomes as DNA unwinds. Nucleic Acids Res., 42, 8767-8776.

24. Bonne-Andrea,C., Wong,M.L. and Alberts,B.M. (1990) In vitro replication through nucleosomes without histone displacement. Nature, 343, 719-726.

25. Krude,T. and Knippers,R. (1991) Transfer of nucleosomes from parental to replicated chromatin. Mol. Cell. Biol., 11, 6257-6267.

26. Jackson,V. (1990) In vivo studies on the dynamics of histone-DNA interaction: evidence for nucleosome dissolution during replication and transcription and a low level of dissolution independent of both. Biochemistry, 29, 719-731.

27. Wisniewski,J., Hajj,B., Chen,J., Mizuguchi,G., Xiao,H., Wei,D., Dahan,M. and Wu,C. (2014) Imaging the fate of histone Cse4 reveals de novo replacement in S phase and subsequent stable residence at centromeres. eLife, 3, e02203.

28. Das,C. and Tyler,J.K. (2013) Histone exchange and histone modifications during transcription and aging. Biochim. Biophys. Acta, 1819, 332-342.

29. Palter,K.B. and Alberts,B.M. (1979) The use of DNA-cellulose for analyzing histone-DNA interactions. Discovery of nucleosome-like histone binding to single-stranded DNA. J. Biol. Chem., 254, 11160-11169.

30. Palter,K.B., Foe,V.E. and Alberts,B.M. (1979) Evidence for the formation of nucleosome-like histone complexes on single-stranded DNA. Cell, 18, 451-467.

31. Caffarelli,E., De Santis,P., Leoni,L., Savino,M. and Trotta,E. (1983) Interactions of the histone octamer with single-stranded DNA. Sedimentation analysis and low-angle X-ray diffraction. Biochim. Biophys. Acta, 739, 235-243.

32. Caffarelli,E., Leoni,L. and Savino,M. (1985) Folding of single-stranded DNA on the histone octamer. FEBS Lett., 181, 69-73.

33. Sambrook,J.F. and Russell,D.W. (2001) Molecular Cloning: A Laboratory Manual. Cold Spring Harbor Laboratory Press, Cold Spring Harbor, New York.

34. Brenner,S.L., Mitchell,R.S., Morrical,S.W., Neuendorf,S.K., Schutte, B.C. and Cox,M.M. (1987) recA protein-promoted ATP hydrolysis occurs throughout recA nucleoprotein filaments. J. Biol. Chem., 262, 4011-4016.

35. Gallego,F., Fernàndez-Busquets,X. and Daban,J.R. (1995) Mechanism of nucleosome dissociation produced by transcription elongation in a short chromatin template. Biochemistry, 34, 6711-6719.

36. Fernàndez-Busquets,X. and Daban,J.R. (1992) Purification of the two strands of a DNA fragment by polyethylene glycol precipitation. Biotechniques, 13, 686-688.

37. Dubrovin,E.V., Speller,S. and Yaminsky,I.V. (2014) Statistical analysis of molecular nanotemplate driven DNA adsorption on graphite. Langmuir, 30, 15423-15432.

38. Dubrovin,E.V., Gerritsen,J.W., Zivkovic,J., Yaminsky,I.V. and Speller,S. (2010) The effect of underlying octadecylamine monolayer on the DNA conformation on the graphite surface. Colloids Surf. B Biointerfaces, 76, 63-69.

39. Wang,Y., Sischka,A., Walhorn,V., Tönsing,K. and Anselmetti,D. (2016) Nanomechanics of fluorescent DNA dyes on DNA investigated by magnetic tweezers. Biophys. J., 111, 1604-1611.

40. Smith,S.B., Finzi,L. and Bustamante,C. (1992) Direct mechanical measurements of the elasticity of single DNA molecules by using magnetic beads. Science, 258, 1122.

41. Bustamante,C., Smith,S.B., Liphardt,J. and Smith,D. (2000) Single-molecule studies of DNA mechanics. Curr. Opin. Struct. Biol., 10, 279-285.

42. Bouchiat,C. and Mézard,M. (2000) Elastic rod model of a supercoiled DNA molecule. Eur. Phys. J. E, 2, 377-402.

43. Maniatis,T. and Efstratiadis,A. (1980) Fractionation of low molecular weight DNA or RNA in polyacrylamide gels containing 98 % formamide or 7 M urea. Methods Enzymol., 65, 299-305.

44. Schwarz,G. and Watanabe,F. (1983) Thermodynamics and kinetics of co-operative protein-nucleic acid binding. J. Mol. Biol., 163, 467-484.

45. McGhee,J.D. and von Hippel,P.H. (1974) Theoretical aspects of DNA-protein interactions: co-operative and non-co-operative binding of large ligands to a onedimensional homogeneous lattice. J. Mol. Biol., 86, 469-489.

46. Wahl,G.M., Stern,M. and Stark,G.R. (1979) Efficient transfer of large DNA fragments from agarose gels to diazobenzyloxymethyl-paper and rapid hybridization by using dextran sulfate. Proc. Natl. Acad. Sci. U.S.A., 76, 3683-3687.

47. Mirzabekov,A.D. and Rich,A. (1979) Asymmetric lateral distribution of unshielded phosphate groups in nucleosomal DNA and its role in DNA bending. Proc. Natl. Acad. Sci. U.S.A., 76, 1118-1121.

48. Cesconetto,E.C., Junior,F.S.A., Crisafuli,F.A.P., Mesquita,O.N., Ramos,E.B. and Rocha,M.S. (2013) DNA interaction with Actinomycin D: mechanical measurements reveal the details of the binding data. Phys. Chem., 15, 11070-11077.

49. Duan,Y., Gao,Z., Wang,L., Wang,H., Zhang,H. and Li,H. (2016) Selection and identification of chloramphenicol-specific DNA aptamers by mag-SELEX. Appl. Biochem. Biotechnol., 1-13.

50. Uchiyama,S., Kawahara,K., Hosokawa,Y., Fukakusa,S., Oki,H., Nakamura,S., Kojima,Y., Noda,M., Takino,R., Miyahara,Y. et al. (2015) Structural basis for dimer formation of human condensin structural maintenance of chromosome proteins and its implications for single-stranded DNA recognition. J. Biol. Chem., 290, 29461-29477.

51. Mihardja,S., Spakowitz,A.J., Zhang,Y. and Bustamante,C. (2006) Effect of force on mononucleosomal dynamics. Proc. Natl. Acad. Sci. U.S.A., 103, 15871-15876.

52. Recouvreux,P., Lavelle,C., Barbi,M., Conde e Silva,N., Le Cam,E., Victor,J.M. and Viovy,J.L. (2011) Linker histones incorporation maintains chromatin fiber plasticity. Biophys. J., 100, 2726-2735.

53. Bancaud,A., Conde e Silva,N., Barbi,M., Wagner,G., Allemand,J.F., Mozziconacci,J., Lavelle,C., Croquette,V., Victor,J.M., Prunell,A. et al. (2006) Structural plasticity of single chromatin fibers revealed by torsional manipulation. Nat. Struct. Mol. Biol., 13, 444-450.

54. Luger,K., Mader,A.W., Richmond,R.K., Sargent,D.F. and Richmond, T.J. (1997) Crystal structure of the nucleosome core particle at 2.8 Å resolution. Nature, 389, 251-260.

55. Zayetz,V.W., Bavykin,S.G., Karpov,V.L. and Mirzabekov,A.D. (1981) Stability of the primary organization of nucleosome core particles upon some conformational transitions. Nucleic Acids Res., 9, 1053-1068.

56. Studitsky,V.M., Belyavsky,A.V., Melnikova,A.F. and Mirzabekov,A.D. (1988) The structure of nucleosomal core particles within transcribed and repressed gene regions. Nucleic Acids Res., 16, 11187-11205.

57. Gutiérrez,J., Paredes,R., Cruzat,F., Hill,D.A., van Wijnen,A.J., Lian,J.B., Stein,G.S., Stein,J.L., Imbalzano,A.N. and Montecino,M. (2007) Chromatin remodeling by SWI/SNF results in nucleosome mobilization to preferential positions in the rat osteocalcin gene promoter. J. Biol. Chem., 282, 9445-9457.

58. Yazdi,P.G., Pedersen,B.A., Taylor,J.F., Khattab,O.S., Chen,Y.H., Chen,Y., Jacobsen,S.E. and Wang,P.H. (2015) Nucleosome organization in human embryonic stem cells. PLoS ONE, 10, e0136314.

59. Battistini,F., Hunter,C.A., Moore,I.K. and Widom,J. (2012) Structure-based identification of new high-affinity nucleosome binding sequences. J. Mol. Biol., 420, 8-16.

60. Shick,V.V., Belyavsky,A.V., Bavykin,S.G. and Mirzabekov,A.D. (1980) Primary organization of the nucleosome core particles sequential arrangement of histones along DNA. J. Mol. Biol., 139, 491-517.

Chapter 5

Concluding discussion and outlook

This thesis is motivated by the importance and necessity of understanding the binding of ligands to DNA by molecular recognition. The main aim of this work was to investigate the binding mechanisms of different ligands to DNA and furthermore their association induced influences on the structural and nanomechanical properties as well as related behavior of the DNA polymer. Since the application of ligands is broadly distributed in many different areas, this work selectively explored several ligands covering three key biological research fields:

1) fundamental research of life science (Paper V);

2) biotechnological applications (Papers II-IV);

3) medical applications (Paper I).

Already since the 19th century the cell nucleus has been widely explored as the location of many DNA involved important biological and genetic processes taking place. Although the main mechanisms of DNA replication and transcription are already known, some details still remain unclear and debatable. To answer such questions, Paper V deals with a family of the most important basic proteins, histones, as DNA-binding ligands. This paper offers an imagination and understanding of the functionality which histones may have during replication and transcription of chromatin.

Histone proteins are well known as packaging proteins which organize the long DNA polymer chain into a compact structure resulting in the for-

mation of a chromosome. However, in order to realize the replication and transcription processes of chromatin, the normal structure of the chromosome and nucleosome must be strongly destructed to allow the temporary formation of single-stranded DNA. Therefore, a dissociation of the bound histones from the DNA chain can be expected. Yet, the action of these dissociated histone proteins remains a question. This implies the possibility that the excess histones may interact with the single-stranded DNA. A further hypothesis is that this interaction may even be involved in replication and transcription. To prove this hypothesis, several *in vitro* studies were performed in this paper to investigate the interaction between histones and single-stranded DNA.

Via electrophoretic bulk studies, the association between histones and ssDNA was observed. Furthermore, the equilibrium constant of association of this binding was determined as $10^7\,\mathrm{M}^{-1}$. Since the binding of histones to dsDNA exhibits a similar equilibrium constant of association, histones were suggested to have an equally strong binding affinity to both ds- and ssDNA. In addition, from the TEM- and AFM-imaging one can see that in the presence of histones, a nucleosome formation was generated. Via single-molecule studies with magnetic tweezers, with the addition of histones, the observed DNA length reduction indicated also the nucleosome-like structure on the DNA strand. These results suggest that in replication and transcription processes, dissociated histones bind to ssDNA. Furthermore, histones were proved to protect ssDNA against DNase. Therefore, it seems valid to suggest that the binding of histones to ssDNA occurs in basic biological processes.

Apart from fundamental research, DNA-ligands are also widely involved in biotechnological applications. In order to better investigate and understand the real time behaviors and properties of biological objects, e.g. DNA, the cell nucleus or even the whole cell, these probes are often observed under microscopes. Unfortunately, most of the probes are too small or too limpid to be seen. In this case, the employment of technological additives and tools becomes necessary. A great example of such an application is the fluorescence microscopy and its appropriate dyes. Mostly used are fluorescent DNA binding dyes generating a “luminescence” of the DNA polymers and thereby parts of the cell nucleus as well. However, mechanical behavior and properties of the DNA are more or less influenced by the binding of dyes and

consequently the validity of the studies with such dyes is at stake. In Papers II-IV, the impacts of four widely used dyes (YOYO-1, DAPI, DRAQ5 and PicoGreen) on DNA were investigated.

In the case of YOYO-1, this green dye has a strong photo-bleaching resistance which is very practical for relatively long-term experiments with high illumination, e.g. electrophoretic analysis with microfluidics. A very little background helps to observe the absolute fluorescence of the dyes bound to DNA. In this case, applying a high concentration of YOYO-1 might be considered unharmful. However, the investigations indicate the opposite. Since YOYO-1 is a bis-intercalator, upon binding, the dye molecules elongate and unwind the DNA double strands. This means that the natural DNA B-conformation with an overwinding angle of 36° does not exist any more. In addition, the rise of a base pair is extended to about 0.7 nm due to the intercalation of a YOYO-1 molecule. Applying YOYO-1 concentrations over the saturation concentration, the binding of dye molecules to DNA even influences the elastic characteristic of the DNA polymer. Therefore, in order to reduce the dye induced impacts on DNA to a negligible level, staining DNA samples with a relatively low concentration of YOYO-1 is advisable.

An alternative of YOYO-1 is PicoGreen. These two dyes share many similar characteristics, i.e. they are both cell-impermeable, have little background and can be excited with green light. Unlike YOYO-1, PicoGreen does not have a strong photo-bleaching resistance. However, its extremely short incubation time of 2-5 min is a large benefit. In addition, PicoGreen binds to DNA in an unselective manner. In the study, the association between PicoGreen and DNA was observed after increasing the dye concentration over a threshold value (100 nM) at the experimental conditions (about 150 mM cation and in the presence of the protein BSA). Once bound to DNA, PicoGreen elongates, softens and unwinds the polymer at the same time due to its simultaneous bimodal binding mode. Furthermore, an elongation per bound dye molecule was determined as 0.38 nm with an untwisting angle of 21°. In this case, using a high concentration of PicoGreen relatively strongly affects the DNA properties.

The financially beneficial blue dye DAPI is favored in cell experiments due to its cell-permeability. It can be excited by UV-light and thus is widely used in fixed-cell experiments. Since DAPI binds to the minor-groove of DNA, the original structure of the DNA polymer remains unaffected. How-

ever, the bending- and torsional elasticity of the DNA molecule is reduced, which should be considered when using DAPI to stain the DNA samples.

Another dye which can be well used in cell experiments is DRAQ5. DRAQ5 can be excited with red light. Compared to DAPI, which is excited by UV-light, DRAQ5 is much less harmful for living cells during long-term experiments. The investigations suggested that DRAQ5 binds to the minor-groove of DNA at low concentrations ($< 0.5\,\mu M$), resulting in a softening of the DNA polymer. At high concentrations ($> 0.5\,\mu M$), DRAQ5 (mono-)intercalates into the double strands of DNA. Therefore, the natural B-conformation of DNA is changed with an unwinding of 13° per bound dye. In addition, the intercalation of DRAQ5 enlarges the basepair distance to about 0.6 nm. Since DRAQ5 possesses a bimodal binding mode inducing completely different mechanical influences on the DNA polymer, it is important to choose an appropriate concentration range considering the aim of the study. Besides, DRAQ5 is relatively sensitive to photo-bleaching. Therefore, working with DRAQ5 in darkness is advisable, especially when combining it with other fluorescent dyes.

Notably, all four DNA binding dyes affect either the structural or the mechanical properties of DNA to a certain extent, and therefore interfere with the biological processes like replication and transcription. Observing such processes by staining DNA with fluorescent dyes, some unwanted effects can be expected. In addition, all four dyes have a good binding affinity of about 10^5-$10^6\,M^{-1}$. Therefore, an application with large excess is not necessary.

With the advancement of the biotechnology, more and more new dyes are developed and brought into the market. Besides, the binding of many familiar dyes is not well studied yet. Exploring them and finding better dyes with less effects on DNA properties stays a hot topic of biophysical research. As a next step, the binding studies of other widely used fluorescent dyes like SYBR Green I ([2-[N-(3-dimethylaminopropyl)-N-propylamino]-4-[2,3-dihydro-3-methyl-(benzo-1,3-thiazol-2-yl)-methylidene]-1-phenyl-quinolinium], [123]) and Acridine Orange (3,6-bis(dimethylamino)acridine, [119]) are also worth to be conducted. Moreover, in order to prevent the above mentioned effects due to the binding of dyes in the biological studies, designing dyes with totally new binding modes might be promising as well.

In fact, besides biotechnological interest, binding modes different from

groove-binding or intercalation can also benefit other biological research. Focused on medical applications, Paper I describes a new design of a potential anticancer drug using an unspecific binding mode. The existing anticancer drugs work more or less via specific binding to DNA. For example, anthracyclines like mitoxantrone intercalate into the DNA double strands and the platinum-based agent cisplatin must bind to the nucleobases of DNA. Such binding mechanisms restrict the efficiency of the cytotoxic function to a certain extent and consequently the healing efficacy. Respecting these facts, designing a drug with an unspecific and unselective binding mode seems to be rational. With this in mind, a new (metal) complex serving as the functional core of a potential drug was designed and synthesized.

The rational design of the metal complex is based on the molecular recognition of DNA-ligand systems. The complex contains two positively charged copper ions which are able to bind to the negatively charged DNA backbone through electrostatic interaction. The Cu_2 ions are held by a rigid backbone made from MOM_21 so that they bind to two neighboring phosphate groups of the DNA backbone simultaneously. Two sterical blockers, made from DPA^{Me} on two (left and right) sides the complex, prevent a possible association between the Cu_2 complex and DNA nucleobases, which is less efficient compared to the unselective electrostatic binding.

After synthesizing the $Cu_2(OAc)_2$ complex, its binding to DNA polymers was tested and proved. Serving as a sterical hindrance, the copper complex prevents the interaction between DNA and DNA polymerases, consequently restraining the DNA synthesis. In addition, the successful and, notably, permanent association of the Cu_2 complex with DNA guarantees its strong cytotoxic effect (proved by *living cell* studies) in a long term. Its cell-permeability was also verified by *living cell* studies, which is one of the prerequisites to develop an anticancer drug. According to these results, the new Cu_2 complex exhibits a very promising potential for oncogenic applications.

Based on the same principle, the influence, binding and cytotoxicity of other complexes from the $[(tom^{Me})M_2]^{n+}$ family (with other metal ions like cobalt and nickel) for binding to DNA are now under investigation. Their potentials as anticancer drugs are also worth looking forward to. In addition, studies on the binding nanomechanics of drugs applied in present therapies and their induced effects should be executed (e.g. mitoxantrone). However,

besides improving and speeding up the healing efficacy, the reduction of the side-effects of anticancer drugs remains a serious issue. In therapies at present, healthy normal cells are attacked as well. On the one hand, reducing the dose of drugs without weakening the healing efficacy is a solution. On the other hand, improving the specific recognition of drugs for cancer/tumor cells will largely progress the quality of cancer therapies.

In the studies mentioned above, magnetic tweezers are employed as the major tool due to their unique advantages compared to other single-molecule techniques. The extremely high force resolution of a few femto newton extends the low-force region of single-molecule stretching experiments, leading to a more precise analysis of the elasticity of DNA polymers. In addition, the lack of force-clamp measurements at very low forces is filled. The ability of twisting DNA molecules allows to observe the structural properties of the double strands. Furthermore, different from AFM or optical tweezers, the "multi-molecules" mode enables the detection of several single molecules simultaneously. This improves the efficiency of statistical measurements to a large degree.

Certainly, as a relatively young technique, magnetic tweezers can be further developed. In the original setup (see Section 2.3.1), due to the low frame rate of the video camera (60 Hz) and limited oversampling, the spatial resolution of the probed single molecule is restricted to a few nanometers. As a solution, the advanced high-speed magnetic tweezers using a camera with a frame rate of 10 kHz allows for high oversampling resulting in an Å spatial resolution [141, 142].

Further new members of the family of magnetic tweezers are the magnetic torque tweezers (MTT) and the electromagnetic torque tweezers (eMTT) [17, 19, 20, 143]. Thanks to the supplementary elements (small secondary magnet for MTT and electromagnet for eMTT) to the original setup, direct measurements of the applied torque (magnitude and direction) during rotation experiments can be gained. Based on all these respects, magnetic tweezers make themselves a powerful and promising tool in single-molecule studies.

With the technical development, magnetic tweezers have grown into a powerful tool beyond the single-molecular level. Extending the research to protein and cell studies, protein-protein interactions, i.e. the protein folding and unfolding, can be observed by magnetic tweezers as well [17, 21].

Apart from single-molecule applications, magnetic tweezers are also able to measure the elasticity of a cell membrane with a non-contact modus combined with appropriate paramagnetic (nano)particles [17, 22]. A thorough understanding of the cell-contact can be achieved via studying the protein-cell interaction [144]. Injecting magnetic particles into a probed cell, the mechanical manipulation of a certain part of the cell is also realizable [145, 146]. Combining magnetic tweezers with other techniques like fluorescence microscopy, a simultaneous mechanical and optical observation of a biomolecular system in real time is possible. In fact, the largest challenge here is to decrease the influence of the high illumination intensity of the MT setup on the fluorophore lifetime. A spectral separation of the illumination sources for magnetic tweezers and the fluorescence excitation realizes a normal image tracking of MT without a damage of fluorophores. Thereby, a bimodal measuring methodology at the same time is realistic. Furthermore, using TIRFM (total internal reflection fluorescence microscope) for the fluorescence observation, only the fluorophores in a small region of the sample surface are excited, resulting in a high resolution of the fluorescence [23, 24].

References

[1] K. Pearson. *The grammar of science*. Cosmo Classics: Science. New York NY: Cosimo, 2007. 416 pp.

[2] A. S. Tijsseling and A. Anderson. *Thomas Young's Research on Fluid Transients: 200 Years On. Proceedings 10th International Conference on Pressure Surges (Edinburgh, UK, 14-16.05.2008)*. Ed. by S.Hunt. BHR Group Limited, Cranfield, UK, 2008, pp. 21–33.

[3] I. Glynn. *Elegance in science. The beauty of simplicity*. Oxford and New York: Oxford University Press, 2010. 271 pp.

[4] E. Sackmann and R. Merkel. *Lehrbuch der Biophysik*. Lehrbuch Physik. Weinheim: Wiley-VCH, 2010. XXIX, 958 S.

[5] S. Smith, L. Finzi, and C. Bustamante. "Direct mechanical measurements of the elasticity of single DNA molecules by using magnetic beads". In: *Science* 258 (5085 1992), pp. 1122–1126.

[6] E. V. Sokurenko, V. Vogel, and W. E. Thomas. "Catch-bond mechanism of force-enhanced adhesion: counterintuitive, elusive, but ... widespread?" In: *Cell host & microbe* 4 (4 2008). Journal Article Research Support, N.I.H., Extramural Review, pp. 314–323.

[7] A. Harder, A.-K. Moller, F. Milz, P. Neuhaus, V. Walhorn, T. Dierks, and D. Anselmetti. "Catch bond interaction between cell-surface sulfatase Sulf1 and glycosaminoglycans". In: *Biophysical journal* 108 (7 2015). Journal Article Research Support, Non-U.S. Gov't, pp. 1709–1717.

[8] K. Günther, M. Mertig, and R. Seidel. "Mechanical and structural properties of YOYO-1 complexed DNA". In: *Nucleic acids research* 38 (19 2010), pp. 6526–6532.

[9] Y. Wang, A. Sischka, V. Walhorn, K. Tönsing, and D. Anselmetti. "Nanomechanics of Fluorescent DNA Dyes on DNA Investigated by Magnetic Tweezers". In: *Biophysical Journal* 111 (8 2016), pp. 1604–1611.

[10] T. Strick. "Twisting and stretching single DNA molecules". In: *Progress in Biophysics and Molecular Biology* 74 (1-2 2000), pp. 115–140.

[11] T. R. Strick, M.-N. Dessinges, G. Charvin, N. H. Dekker, J.-F. Allemand, D. Bensimon, and V. Croquette. "Stretching of macromolecules and proteins". In: *Reports on Progress in Physics* 66 (1 2003), pp. 1–45.

[12] S. Smith, L. Finzi, and C. Bustamante. "Direct mechanical measurements of the elasticity of single DNA molecules by using magnetic beads". In: *Science* 258 (5085 1992), pp. 1122–1126.

[13] T. R. Strick, J.-F. Allemand, D. Bensimon, A. Bensimon, and V. Croquette. "The Elasticity of a Single Supercoiled DNA Molecule". In: *Science* 271 (5257 1996), pp. 1835–1837.

[14] T. R. Strick, J.-F. Allemand, D. Bensimon, and V. Croquette. "Behavior of Supercoiled DNA". In: *Biophysical Journal* 74 (4 1998), pp. 2016–2028.

[15] I. D. Vilfan, J. Lipfert, D. A. Koster, S. G. Lemay, and N. H. Dekker. *Handbook of single-molecule biophysics*. Ed. by P. Hinterdorfer and A. van Oijen. Springer Science+Business Media, 2009. 371-395.

[16] J. Lipfert, S. Klijnhout, and N. H. Dekker. "Torsional sensing of small-molecule binding using magnetic tweezers". In: *Nucleic acids research* 38 (20 2010). Journal Article Research Support, Non-U.S. Gov't, pp. 7122–7132.

[17] R. Sarkar and V. V. Rybenkov. "A Guide to Magnetic Tweezers and Their Applications". In: *Frontiers in Physics* 4 (1 Pt 1 2016), p. 491.

[18] A. Celedon, D. Wirtz, and S. Sun. "Torsional mechanics of DNA are regulated by small-molecule intercalation". In: *The journal of physical chemistry. B* 114 (50 2010). Journal Article Research Support, Non-U.S. Gov't, pp. 16929–16935.

[19] J. Lipfert, J. W. J. Kerssemakers, T. Jager, and N. H. Dekker. "Magnetic torque tweezers: measuring torsional stiffness in DNA and RecA-DNA filaments". In: *Nature methods* 7 (12 2010). Journal Article, pp. 977–980.

[20] X. J. A. Janssen, J. Lipfert, T. Jager, R. Daudey, J. Beekman, and N. H. Dekker. "Electromagnetic torque tweezers: a versatile approach for measurement of single-molecule twist and torque". In: *Nano letters* 12 (7 2012). Journal Article, pp. 3634–3639.

[21] H. Chen, S. Chandrasekar, M. P. Sheetz, T. P. Stossel, F. Nakamura, and J. Yan. "Mechanical perturbation of filamin A immunoglobulin repeats 20-21 reveals potential non-equilibrium mechanochemical partner binding function". In: *Scientific reports* 3 (2013). Journal Article Research Support, N.I.H., Extramural Research Support, Non-U.S. Gov't, p. 1642.

[22] R. J. Saphirstein, Y. Z. Gao, M. H. Jensen, C. M. Gallant, S. Vetterkind, J. R. Moore, and K. G. Morgan. "The focal adhesion: a regulated component of aortic stiffness". In: *PloS one* 8 (4 2013). Journal Article Research Support, N.I.H., Extramural, e62461.

[23] M. Swoboda, M. S. Grieb, S. Hahn, and M. Schlierf. "Measuring two at the same time: combining magnetic tweezers with single-molecule FRET". In: *EXS* 105 (2014). Journal Article Research Support, Non-U.S. Gov't Review, pp. 253–276.

[24] F. E. Kemmerich, M. Swoboda, D. J. Kauert, M. S. Grieb, S. Hahn, F. W. Schwarz, R. Seidel, and M. Schlierf. "Simultaneous Single-Molecule Force and Fluorescence Sampling of DNA Nanostructure Conformations Using Magnetic Tweezers". In: *Nano letters* 16 (1 2016). Journal Article Research Support, Non-U.S. Gov't, pp. 381–386.

[25] T. A. Brown. *Genomes 2.Ed.* New York and Chichester: Wiley, 2002. 520 pp.

[26] F. Miescher. "Über die chemische Zusammensetzung der Eiterzellen". In: *Med.-Chem. Unters.* 4 (1871), pp. 441–460.

[27] O. T. Avery, C. M. MacLeod, and M. McCarty. "Studies on the Chemical Nature of the Substance Induding Transformation of Pneumococcal Types. Induction of Transformation by a Desoxyribonucleic Acid Fraction Isolated from Pneumococcus Type III". In: *The Journal of Experimental Medicine* 79 (2 1944), pp. 137–158.

[28] J. D. Watson and F. H. Crick. "Molecular structure of nucleic acids; a structure for deoxyribose nucleic acid". In: *Nature* 171 (4356 1953). Journal Article, pp. 737–738.

[29] R. E. Franklin and R. G. Gosling. "Molecular Configuration in Sodium Thymonucleate". In: *Nature* 171 (4356 1953), pp. 740–741.

[30] B. R. Wood. "The importance of hydration and DNA conformation in interpreting infrared spectra of cells and tissues". In: *Chemical Society reviews* 45 (7 2016). Journal Article Research Support, Non-U.S. Gov't Review, pp. 1980–1998.

[31] J. F. Allemand, D. Bensimon, R. Lavery, and V. Croquette. "Stretched and overwound DNA forms a Pauling-like structure with exposed bases". In: *Proceedings of the National Academy of Sciences of the United States of America* 95 (24 1998), pp. 14152–14157.

[32] R. E. Franklin and R. G. Gosling. "Evidence for 2-chain helix in crystalline structure of sodium deoxyribonucleate". In: *Nature* 172 (4369 1953). Journal Article, pp. 156–157.

[33] D. A. Marvin, M. Spencer, M. H. F. Wilkins, and L. D. Hamilton. "A New Configuration of Deoxyribonucleic Acid". In: *Nature* 182 (4632 1958), pp. 387–388.

[34] F. M. Pohl and T. M. Jovin. "Salt-induced co-operative conformational change of a synthetic DNA: equilibrium and kinetic studies with poly (dG-dC)". In: *Journal of Molecular Biology* 67 (3 1972). Journal Article, pp. 375–396.

[35] N. Ramaswamy, M. Bansal, G. Gupta, and V. Sasisekharan. "Structure of D-DNA: 8-fold or 7-fold helix?" In: *The EMBO Journal* 2 (9 1983), pp. 1557–1560.

[36] J. M. Vargason, B. F. Eichman, and P. S. Ho. "The extended and eccentric E-DNA structure induced by cytosine methylation or bromination". In: *Nature structural biology* 7 (9 2000). Journal Article Research Support, Non-U.S. Gov't Research Support, U.S. Gov't, Non-P.H.S., pp. 758–761.

[37] D. Ussery. "DNA structure: A-, B- and Z-DNA helix families". In: *Encyclopedia of Life Sciences* (2002).

[38] G. Hayashi, M. Hagihara, and K. Nakatani. "Application of L-DNA as a molecular tag". In: *Nucleic acids symposium series (2004)* (49 2005). Journal Article, pp. 261–262.

[39] P. Ho and M. Carter. "DNA Structure: Alphabet Soup for the Cellular Soul". In: *DNA replicatio. Current advances*. Ed. by H. Seligmann. Rijeka, Croatia: InTech, 2011.

[40] K. Nakamoto, M. Tsuboi, and G. D. Strahan. *Drug-DNA Interactions. Structures and Spectra*. John Wiley & Sons, Inc, Sept. 12, 2008.

[41] F. DiMaio, X. Yu, E. Rensen, M. Krupovic, D. Prangishvili, and E. H. Egelman. "Virology. A virus that infects a hyperthermophile encapsidates A-form DNA". In: *Science (New York, N.Y.)* 348 (6237 2015). Journal Article Research Support, N.I.H., Extramural, pp. 914–917.

[42] B. Basham, G. P. Schroth, and P. S. Ho. "An A-DNA triplet code: thermodynamic rules for predicting A- and B-DNA". In: *Proceedings of the National Academy of Sciences of the United States of America* 92 (14 1995). Comparative Study Journal Article Research Support, Non-U.S. Gov't Research Support, U.S. Gov't, Non-P.H.S., pp. 6464–6468.

[43] D. R. Whelan, T. J. Hiscox, J. I. Rood, K. R. Bambery, D. McNaughton, and B. R. Wood. "Detection of an en masse and reversible B- to A-DNA conformational transition in prokaryotes in response to desiccation". In: *Journal of the Royal Society, Interface* 11 (97 2014). Journal Article Research Support, Non-U.S. Gov't, p. 20140454.

[44] A. Rich and S. Zhang. "Timeline: Z-DNA: the long road to biological function". In: *Nature reviews. Genetics* 4 (7 2003). Historical Article Journal Article Review, pp. 566–572.

[45] X. Liang, H. Kuhn, and M. D. Frank-Kamenetskii. "Monitoring single-stranded DNA secondary structure formation by determining the topological state of DNA catenanes". In: *Biophysical journal* 90 (8 2006). Journal Article Research Support, N.I.H., Extramural, pp. 2877–2889.

[46] R. P. Bowater. "Supercoiled DNA: Structure". In: *Encyclopedia of life sciences*. Ed. by J. W. &. S. Ltd. London et al.: Nature Pub. Group and Wiley, 2002-2010, pp. 1–11.

[47] C. R. Calladine. *DNA. Das Molekül und seine Funktionsweise*. 3. Aufl. [der engl. Ausg.] = 1. [dt.] Aufl. München: Elsevier Spektrum Akad. Verl., 2006. VII, 294 S.

[48] P. J. Hagerman. "Flexibility of DNA". In: *Annual review of biophysics and biophysical chemistry* 17 (1988). Journal Article Research Support, U.S. Gov't, P.H.S. Review, pp. 265–286.

[49] C. G. Baumann, S. B. Smith, V. A. Bloomfield, and C. Bustamante. "Ionic effects on the elasticity of single DNA molecules". In: *Proceedings of the National Academy of Sciences* 94 (12 1997), pp. 6185–6190.

[50] Y. Lu, B. Weers, and N. C. Stellwagen. "DNA persistence length revisited". In: *Biopolymers* 61 (4 2001-2002). Journal Article Research Support, U.S. Gov't, P.H.S., pp. 261–275.

[51] C. Storm and P. C. Nelson. "The bend stiffness of S-DNA". In: *EPL (Europhysics Letters)* 62.5 (2003), p. 760.

[52] P. Cluzel, A. Lebrun, C. Heller, R. Lavery, J.-L. Viovy, D. Chatenay, and F. o. Caron. "DNA. An Extensible Molecule". In: *Science* 271 (5250 1996), pp. 792–794.

[53] S. B. Smith, Y. Cui, and C. Bustamante. "Overstretching B-DNA: the elastic response of individual double-stranded and single-stranded DNA molecules". In: *Science (New York, N.Y.)* 271 (5250 1996). Journal Article Research Support, Non-U.S. Gov't Research Support, U.S. Gov't, Non-P.H.S. Research Support, U.S. Gov't, P.H.S., pp. 795–799.

[54] A. Lebrun and R. Lavery. "Modelling Extreme Stretching of DNA". In: *Nucleic Acids Research* 24 (12 1996), pp. 2260–2267.

[55] I. Rouzina and V. A. Bloomfield. "Force-Induced Melting of the DNA Double Helix 1. Thermodynamic Analysis". In: *Biophysical journal* 80 (2 2001), pp. 882–893.

[56] N. Bosaeus, A. H. El-Sagheer, T. Brown, S. B. Smith, B. Akerman, C. Bustamante, and B. Norden. "Tension induces a base-paired overstretched DNA conformation". In: *Proceedings of the National Academy of Sciences of the United States of America* 109 (38 2012). Journal Article Research Support, Non-U.S. Gov't, pp. 15179–15184.

[57] G. Ramachandran and T. Schlick. "Buckling transitions in superhelical DNA. Dependence on the elastic constants and DNA size". In: *Biopolymers* 41 (1 1997), pp. 5–25.

[58] M. Daune. *Molekulare Biophysik*. Vieweg-Lehrbuch. Braunschweig and Wiesbaden: Vieweg, 1997. XVIII, 546 S.

[59] I. Johnson. *The molecular probes handbook. A guide to fluorescent probes and labeling technologies*. 11.ed. Carlsbad, Calif.: Life Technologies, 2010. 1060 pp.

[60] K. A. Connors. *Chemical kinetics. The study of reaction rates in solution*. New York, N.Y.: VCH, 1990. xiii, 480.

[61] A. F. Holleman, E. Wiberg, and N. Wiberg. *Lehrbuch der Anorganischen Chemie*. 102., stark umgearb. u. verb. Aufl. / von Nils Wiberg. Berlin u.a.: de Gruyter, 2007. XXXIX, 2149 S.

[62] E. Fischer. "Einfluss der Configuration auf die Wirkung der Enzyme". In: *Berichte der deutschen chemischen Gesellschaft* 27 (3 1894), pp. 2985–2993.

[63] N. M. Green. "Avidin". In: *Advances in protein chemistry* 29 (1975). Journal Article, pp. 85–133.

[64] G. Neuert, C. Albrecht, E. Pamir, and H. E. Gaub. "Dynamic force spectroscopy of the digoxigenin-antibody complex". In: *FEBS letters* 580 (2 2006). Journal Article Research Support, Non-U.S. Gov't, pp. 505–509.

[65] R. Janissen, B. A. Berghuis, D. Dulin, M. Wink, T. van Laar, and N. H. Dekker. "Invincible DNA tethers: covalent DNA anchoring for enhanced temporal and force stability in magnetic tweezers experiments". In: *Nucleic Acids Research* 42 (18 2014). Journal Article Research Support, Non-U.S. Gov't, e137.

[66] C. Le Grimellec, P. E. Milhiet, E. Perez, F. Pincet, J. P. Aime, V. Emiliani, O. Thoumine, T. Lionnet, V. Croquette, J. F. Allemand, and D. Bensimon. *Nanoscience. Nanobiotechnology and nanobiology.* Ed. by P. Boisseau, P. Houdy, and M. Lahmani. Berlin: Springer, 2010. Chap. 8, 447-467.

[67] E. J. G. Peterman and G. J. L. Wuite, eds. *Single Molecule Analysis. Methods and Protocols.* Vol. 783. SpringerLink Bücher. Totowa, NJ: Springer Science+Business Media LLC, 2011, Chap. 15, 265–293.

[68] G. U. Lee, L. A. Chrisey, R. J. Colton, et al. "Direct Measurement of the Forces between Complementary Strands of DNA". In: *Science-New York Then Washington-* (1994), pp. 771–771.

[69] U. Dammer, M. Hegner, D. Anselmetti, P. Wagner, M. Dreier, W. Huber, and H. J. Güntherodt. "Specific antigen/antibody interactions measured by force microscopy". In: *Biophysical Journal* 70 (5 1996), pp. 2437–2441.

[70] F. Pincet and J. Husson. "The solution to the streptavidin-biotin paradox: the influence of history on the strength of single molecular bonds". In: *Biophysical Journal* 89 (6 2005). Comparative Study Evaluation Studies Journal Article Research Support, Non-U.S. Gov't Validation Studies, pp. 4374–4381.

[71] C. Gosse and V. Croquette. "Magnetic Tweezers. Micromanipulation and Force Measurement at the Molecular Level". In: *Biophysical Journal* 82 (6 2002), pp. 3314–3329.

[72] G. Charvin, J. F. Allemand, T. Strick, D. Bensimon, and V. Croquette. "Twisting DNA. Single molecule studies". In: *Contemporary Physics* 45 (5 2004), pp. 383–403.

[73] P. A. Tipler, G. Mosca, and J. Wagner. *Physik. Für Wissenschaftler und Ingenieure.* 7. Aufl. 2015. Berlin Heidelberg: Springer Berlin Heidelberg, 2015. XXXVI, 1454 S. 1600 Abb., 650 Abb. in Farbe.

[74] J. E. Mark. *Physical properties of polymer handbook*. 2nd ed. New York: Springer, 2006. 1 online resource (xix, 1076).

[75] H. Kuhn, H.-D. Försterling, and D. H. Waldeck. *Principles of physical chemistry*. 2. ed. Hoboken NJ u.a.: Wiley, 2009. XLII, 1032 S.

[76] M.-N. Dessinges, B. Maier, Y. Zhang, M. Peliti, D. Bensimon, and V. Croquette. "Stretching single stranded DNA, a model polyelectrolyte". In: *Physical review letters* 89 (24 2002). Journal Article Research Support, Non-U.S. Gov't, p. 248102.

[77] G. Francius, D. Alsteens, V. Dupres, S. Lebeer, S. d. Keersmaecker, J. Vanderleyden, H. J. Gruber, and Y. F. Dufrene. "Stretching polysaccharides on live cells using single molecule force spectroscopy". In: *Nature protocols* 4 (6 2009). Journal Article Research Support, Non-U.S. Gov't, pp. 939–946.

[78] A. Bosco, J. Camunas-Soler, and F. Ritort. "Elastic properties and secondary structure formation of single-stranded DNA at monovalent and divalent salt conditions". In: *Nucleic Acids Research* 42 (3 2014). Journal Article Research Support, Non-U.S. Gov't, pp. 2064–2074.

[79] P. J. Flory. *Principles of polymer chemistry*. 1. publ. Ithaca NY u.a.: Cornell Univ. Pr, 1953. XVI, 672 S.

[80] O. Kratky and G. Porod. "Röntgenuntersuchung gelöster Fadenmoleküle". In: *Recueil des Travaux Chimiques des Pays-Bas* 68.12 (1949), pp. 1106–1122.

[81] C. Bustamante, J. Marko, E. Siggia, and S. Smith. "Entropic Elasticity of Lambda-phage DNA". In: *Science* 265 (5178 1994), pp. 1599–1600.

[82] T. Odijk. "Stiff Chains and Filaments under Tension". In: *Macromolecules* 28 (20 1995), pp. 7016–7018.

[83] C. Bustamante, S. B. Smith, J. Liphardt, and D. Smith. "Single-molecule studies of DNA mechanics". In: *Current opinion in structural biology* 10 (3 2000). Journal Article Journal Article, pp. 279–285.

[84] A. Ahsan, J. Rudnick, and R. Bruinsma. "Elasticity Theory of the B-DNA to S-DNA Transition". In: *Biophysical Journal* 74 (1 1998), pp. 132–137.

[85] O. A. Saleh, D. B. McIntosh, P. Pincus, and N. Ribeck. "Nonlinear low-force elasticity of single-stranded DNA molecules". In: *Physical review letters* 102 (6 2009). Journal Article Research Support, U.S. Gov't, Non-P.H.S., p. 068301.

[86] P.-G. d. Gennes. *Scaling concepts in polymer physics*. 7. print. Ithaca, NY: Cornell Univ. Press, 2004. 324 pp.

[87] D. DeRossi, K. Kajiwara, Y. Osada, and A. Yamauchi. *Polymer Gels. Fundamentals and Biomedical Applications*. Boston, MA: Springer US, 1991.

[88] A. V. Dobrynin, R. H. Colby, and M. Rubinstein. "Scaling Theory of Polyelectrolyte Solutions". In: *Macromolecules* 28 (6 1995), pp. 1859–1871.

[89] J. P. Cohen Addad, ed. *Physical properties of polymeric gels*. Chichester u.a.: Wiley, 1996. XII, 311 S.

[90] S. K. Sukumaran and G. Beaucage. "A structural model for equilibrium swollen networks". In: *Europhysics Letters (EPL)* 59 (5 2002), pp. 714–720.

[91] A. Dobrynin and M. Rubinstein. "Theory of polyelectrolytes in solutions and at surfaces". In: *Progress in Polymer Science* 30 (11 2005), pp. 1049–1118.

[92] S. M. Bhattacharjee, A. Giacometti, and A. Maritan. "Flory theory for polymers". In: *Journal of Physics: Condensed Matter* 25.50 (2013), p. 503101.

[93] Y. Zhang, H. Zhou, and Z.-C. Ou-Yang. "Stretching Single-Stranded DNA: Interplay of Electrostatic, Base-Pairing, and Base-Pair Stacking Interactions". In: *Biophysical journal* 81 (2 2001), pp. 1133–1143.

[94] P. Pincus. "Excluded Volume Effects and Stretched Polymer Chains". In: *Macromolecules* 9 (3 1976), pp. 386–388.

[95] J. L. Barrat and J. F. Joanny. "Persistence Length of Polyelectrolyte Chains". In: *EPL (Europhysics Letters)* 24.5 (1993), p. 333.

[96] B. Y. Ha and D. Thirumalai. "A mean field model for semiflexible chains". In: *The Journal of Chemical Physics* 103 (21 1995), pp. 9408–9412.

[97] U. Micka and K. Kremer. “Persistence length of the Debye-Hückel model of weakly charged flexible polyelectrolyte chains”. In: *Physical Review E* 54 (3 1996), pp. 2653–2662.

[98] W. Kuhn. “Über die Gestalt fadenförmiger Moleküle in Lösungen”. In: *Kolloid-Zeitschrift* 68 (1 1934), pp. 2–15.

[99] M. Rubinstein and R. H. Colby. *Polymer physics*. Reprinted. Colby, Ralph H. (VerfasserIn). Oxford: Oxford Univ. Press, 2010. 440 pp.

[100] J. D. McGhee and P. H. v. Hippel. “Theoretical aspects of DNA-protein interactions. Co-operative and non-co-operative binding of large ligands to a one-dimensional homogeneous lattice”. In: *Journal of Molecular Biology* 86 (2 1974), pp. 469–489.

[101] D. M. Crothers. “Calculation of binding isotherms for heterogenous polymers”. In: *Biopolymers* 6 (4 1968), pp. 575–584.

[102] L. D. Williams, M. Egli, Q. Gao, and A. Rich. *Structure & function*. In collab. with Sarma. R. H., Sarma. M. H., Eds. New York: Adenine Press, 1992; Vol. 1, p107-125.

[103] I. D. Vladescu, M. J. McCauley, M. E. Nuñez, I. Rouzina, and M. C. Williams. “Quantifying force-dependent and zero-force DNA intercalation by single-molecule stretching”. In: *Nature methods* 4 (6 2007). Journal Article Research Support, N.I.H., Extramural Research Support, Non-U.S. Gov’t Research Support, U.S. Gov’t, Non-P.H.S., pp. 517–522.

[104] C. Kleimann, A. Sischka, A. Spiering, K. Tönsing, N. Sewald, U. Diederichsen, and D. Anselmetti. “Binding kinetics of bisintercalator Triostin a with optical tweezers force mechanics”. In: *Biophysical Journal* 97 (10 2009). Journal Article Research Support, Non-U.S. Gov’t, pp. 2780–2784.

[105] G. Schwarz and F. Watanabe. “Thermodynamics and kinetics of co-operative protein-nucleic acid binding”. In: *Journal of Molecular Biology* 163 (3 1983), pp. 467–484.

[106] A. Hershey. *The bacteriophage lambda. (Conference on lambda; Cold Spring Harbor - N.Y., September 1970)*. Vol. [2]. Cold Spring Harbor monograph series. Cold Spring Harbor - N.Y: Cold Spring Harbor Laboratory, 1971. 792 pp.

[107] K. Dose and A. Bieger-Dose. *Biochemie: Eine Einführung*. Springer Berlin Heidelberg, 2013.

[108] F. Sanger, A. R. Coulson, G. F. Hong, D. F. Hill, and G. B. Petersen. "Nucleotide sequence of bacteriophage lambda DNA". In: *Journal of Molecular Biology* 162 (4 1982). Journal Article Research Support, Non-U.S. Gov't, pp. 729–773.

[109] J. R. Dawson and J. A. Harpst. "Light scattering and hydrodynamic properties of linear and circular bacteriophage lambda DNA". In: *Biopolymers* 10 (12 1971). Journal Article, pp. 2499–2508.

[110] D. P. Clark and N. J. Pazdernik. *Molecular Biology*. Academic Press, 2013.

[111] W. Cheng. *Protocol to generate half Lambda DNA for optical/magnetic tweezer*. 2006. URL: `http://tweezerslab.unipr.it/cgi-bin/mt/documents.pl/Show?_id=ab03&sort=DEFAULT&search=&hits=23` (visited on 09/05/2008).

[112] J. Messing, B. Gronenborn, B. Müller-Hill, and P. Hans Hopschneider. "Filamentous coliphage M13 as a cloning vehicle: insertion of a HindII fragment of the lac regulatory region in M13 replicative form in vitro". In: *Proceedings of the National Academy of Sciences of the United States of America* 74 (9 1977), pp. 3642–3646.

[113] Q. Chi, G. Wang, and J. Jiang. "The persistence length and length per base of single-stranded DNA obtained from fluorescence correlation spectroscopy measurements using mean field theory". In: *Physica A: Statistical Mechanics and its Applications* 392 (5 2013), pp. 1072–1079.

[114] C. Yanisch-Perron, J. Vieira, and J. Messing. "Improved M13 phage cloning vectors and host strains: nucleotide sequences of the M13mp18 and pUC19 vectors". In: *Gene* 33 (1 1985). Journal Article Research Support, U.S. Gov't, Non-P.H.S. Research Support, U.S. Gov't, P.H.S., pp. 103–119.

[115] R. Ebright, Q. Dong, and J. Messing. "Corrected nucleotide sequence of M13mp18 gene III". In: *Gene* 114 (1 1992). Journal Article Research Support, U.S. Gov't, P.H.S. Published Erratum, pp. 81–83.

[116] *National Center for Biotechnology Information, PubChem Compound Database, https://pubchem.ncbi.nlm.nih.gov/compound/441203*. CID =441203, accessed 22.02.2017.

[117] T. Jany, A. Moreth, C. Gruschka, A. Sischka, A. Spiering, M. Dieding, Y. Wang, S. H. Samo, A. Stammler, H. Bogge, G. Fischer von Mollard, D. Anselmetti, and T. Glaser. "Rational design of a cytotoxic dinuclear Cu2 complex that binds by molecular recognition at two neighboring phosphates of the DNA backbone". In: *Inorganic chemistry* 54 (6 2015). Journal Article Research Support, Non-U.S. Gov't, pp. 2679–2690.

[118] T. Glaser and I. Liratzis. "A Streamlined Synthesis for 2,7-Diformyl-1,8-naphthalenediol". In: *Synlett* (4 2004), pp. 735–737.

[119] R. W. Sabnis. *Handbook of Fluorescent Dyes and Probes*. Hoboken, NJ, USA: John Wiley & Sons, Inc, 2015.

[120] H. S. Rye, S. Yue, D. E. Wemmer, M. A. Quesada, R. P. Haugland, R. A. Mathies, and A. N. Glazer. "Stable fluorescent complexes of double-stranded DNA with bis-intercalating asymmetric cyanine dyes: properties and applications". In: *Nucleic acids research* 20 (11 1992), pp. 2803–2812.

[121] M. L. Barcellona, G. Cardiel, and E. Gratton. "Time-resolved fluorescence of DAPI in solution and bound to polydeoxynucleotides". In: *Biochemical and Biophysical Research Communications* 170 (1 1990), pp. 270–280.

[122] J. A. Thomas. "Optical imaging probes for biomolecules: an introductory perspective". In: *Chemical Society reviews* 44 (14 2015). Journal Article Review, pp. 4494–4500.

[123] H. Zipper, H. Brunner, J. Bernhagen, and F. Vitzthum. "Investigations on DNA intercalation and surface binding by SYBR Green I, its structure determination and methodological implications". In: *Nucleic acids research* 32 (12 2004). Journal Article Research Support, Non-U.S. Gov't, e103.

[124] V. L. Singer, L. J. Jones, S. T. Yue, and R. P. Haugland. "Characterization of PicoGreen reagent and development of a fluorescence-based

solution assay for double-stranded DNA quantitation". In: *Analytical biochemistry* 249 (2 1997). Journal Article, pp. 228–238.

[125] A. I. Dragan, J. R. Casas-Finet, E. S. Bishop, R. J. Strouse, M. A. Schenerman, and C. D. Geddes. "Characterization of PicoGreen interaction with dsDNA and the origin of its fluorescence enhancement upon binding". In: *Biophysical Journal* 99 (9 2010). Journal Article Research Support, Non-U.S. Gov't, pp. 3010–3019.

[126] D. P. Melters, J. Nye, H. Zhao, and Y. Dalal. "Chromatin Dynamics in Vivo: A Game of Musical Chairs". In: *Genes* 6 (3 2015). Journal Article Review, pp. 751–776.

[127] "Epigenetics—A New Frontier for Alcohol Research". In: *Alcohol Alert of Alcohol Research: Current Reviews* 86 (2013).

[128] C. Crane-Robinson, S. E. Dancy, E. M. Bradbury, A. Garel, A. M. Kovacs, M. Champagne, and M. Daune. "Structural studies of chicken erythrocyte histone H5." In: *European journal of biochemistry* 67.2 (1976). Quelldatenbank: info:sid/sfx:ULBD, pp. 379–388.

[129] L. Fan and V. A. Roberts. "Complex of linker histone H5 with the nucleosome and its implications for chromatin packing". In: *Proceedings of the National Academy of Sciences of the United States of America* 103 (22 2006). Journal Article Research Support, N.I.H., Extramural Research Support, U.S. Gov't, Non-P.H.S., pp. 8384–8389.

[130] J. Ausio. "Histone variants–the structure behind the function". In: *Briefings in functional genomics & proteomics* 5 (3 2006). Journal Article Research Support, Non-U.S. Gov't Review, pp. 228–243.

[131] P. Oudet, M. Gross-Bellard, and P. Chambon. "Electron microscopic and biochemical evidence that chromatin structure is a repeating unit". In: *Cell* 4 (4 1975). Journal Article, pp. 281–300.

[132] K. E. van Holde, J. R. Allen, K. Tatchell, W. O. Weischet, and D. Lohr. "DNA-histone interactions in nucleosomes". In: *Biophysical Journal* 32 (1 1980), pp. 271–282.

[133] K. Rippe, J. Mazurkiewicz, and N. Kepper. *DNA interactions with polymers and surfactants*. Ed. by B. Lindman and R. Dias. Hoboken, N.J: John Wiley, 2008, Chap. 6, Chap. 6.

[134] J. D. Watson and T. A. Baker. *Molecular biology of the gene*. 7. ed., international ed. Always learning. Boston, Mass. and Cold Spring Harbor, NY: Pearson and Cold Spring Harbor Laboratory Press, 2014. 872 pp.

[135] K. Luger, A. W. Mader, R. K. Richmond, D. F. Sargent, and T. J. Richmond. "Crystal structure of the nucleosome core particle at 2.8 A resolution". In: *Nature* 389 (6648 1997). Journal Article Research Support, Non-U.S. Gov't, pp. 251–260.

[136] R. D. Kornberg. "Structure of chromatin". In: *Annual review of biochemistry* 46 (1977). Journal Article Review, pp. 931–954.

[137] A. T. Annunziato. "DNA Packaging: Nucleosomes and Chromatin". In: 1 (1 2008), p. 26.

[138] M. Amouyal. "Use of Histones to Increase the Frequency of Recombinant Plasmid Formation during Molecular Cloning". In: *Advances in Gene, Molecular and Cell Therapy* 1 (2 2007), pp. 192–197.

[139] *National Center for Biotechnology Information, PubChem Compound Database, https://pubchem.ncbi.nlm.nih.gov/compound/4212*. CID= 4212, accessed 22.02.2017.

[140] C. Panousis and D. R. Phillips. "DNA sequence specificity of mitoxantrone". In: *Nucleic Acids Research* 22 (8 1994), pp. 1342–1345.

[141] B. M. Lansdorp, S. J. Tabrizi, A. Dittmore, and O. A. Saleh. "A high-speed magnetic tweezer beyond 10,000 frames per second". In: *The Review of scientific instruments* 84 (4 2013). Journal Article Research Support, Non-U.S. Gov't Research Support, U.S. Gov't, Non-P.H.S., p. 044301.

[142] A. Huhle, D. Klaue, H. Brutzer, P. Daldrop, S. Joo, O. Otto, U. F. Keyser, and R. Seidel. "Camera-based three-dimensional real-time particle tracking at kHz rates and Angstrom accuracy". In: *Nature communications* 6 (2015). Journal Article Research Support, Non-U.S. Gov't, p. 5885.

[143] J. Lipfert, M. Lee, O. Ordu, J. W. J. Kerssemakers, and N. H. Dekker. "Magnetic tweezers for the measurement of twist and torque". In: *Journal of visualized experiments : JoVE* (87 2014). Journal Article Research Support, Non-U.S. Gov't Video-Audio Media.

[144] E. Bazellieres, V. Conte, A. Elosegui-Artola, X. Serra-Picamal, M. Bintanel-Morcillo, P. Roca-Cusachs, J. J. Munoz, M. Sales-Pardo, R. Guimera, and X. Trepat. "Control of cell-cell forces and collective cell dynamics by the intercellular adhesome". In: *Nature cell biology* 17 (4 2015). Journal Article Research Support, N.I.H., Extramural Research Support, Non-U.S. Gov't, pp. 409–420.

[145] A. H. B. d. Vries, B. E. Krenn, R. van Driel, V. Subramaniam, and J. S. Kanger. "Direct observation of nanomechanical properties of chromatin in living cells". In: *Nano letters* 7 (5 2007). Journal Article Research Support, Non-U.S. Gov't, pp. 1424–1427.

[146] H. Ebrahimian, M. Giesguth, K.-J. Dietz, G. Reiss, and S. Herth. "Magnetic tweezers for manipulation of magnetic particles in single cells". In: *Applied Physics Letters* 104 (6 2014), p. 063701.

List of abbreviations

AFM	atomic force microscopy
ATP	adenosine triphosphate
CCD	charge-coupled device
conf. I, II	configuration I, II
cos site	cohesive site
DNA	deoxyribonucleic acid
dsDNA	double-stranded DNA
E.Coli	Escherichia coli
eMTT	electromagnetic magnetic tweezers
FJC	freely jointed chain
F-plasmid	fertility plasmid
FRC	freely rotating chain
IBEC	Institute for Bioengineering of Catalonia
IgG	immunoglobulin G
LamB receptor	Maltoporin, or LamB porin
LED	light-emitting diode
MT	magnetic tweezers
MTT	magnetic torque tweezers
NEB	New England BioLabs
OT	optical tweezers
PCR	polymerase chain reaction
RNA	ribonucleic acid
SIRV2	Sulfolobus islandicus rod-shaped virus 2
ssDNA	single-stranded DNA
TEM	transmission electron microscopy
TIRFM	total internal reflection fluorescence microscope
UV light	ultraviolet light

WLC	worm-like chain

Components of nucleic acids

A	adenine
C	cytosine
G	guanine
T	thymine
U	uracil
dA	deoxyadenylate (nucleotide)
	deoxyadenosine (nucleoside)
dC	deoxycytidylate (nucleotide)
	deoxycytidine (nucleoside)
dG	deoxyguanylate (nucleotide)
	deoxyguanosine (nucleoside)
dT	deoxythymidylate (nucleotide)
	deoxythymidine (nucleoside)
dU	deoxyuridylate (nucleotide)
	deoxyuridine (nucleoside)
dNTP	deoxynucleoside (dA, dC, dG, dT, dU) triphosphate
P-group	phosphate group

Chemical compounds

AO	Acridine Orange, 3,6-bis(dimethylamino)acridine
BSA	bovine serum albumins
DAPI	4',6-diamidine-2-phenylindole dihydrochloride
dig	digoxigenin
DMSO	dimethyl sulfoxide, $(CH_3)_2SO$
DPA^{Me}	di((6-methylpyridin-2-yl)-methyl)amine
DRAQ5	deep red fluorescent antraquinone dye Nr.5, 1,5-bis[2-(di-methylamino)ethyl]amino-4,8-dihydroxy-anthracene-9,10-dione
EDTA	ethylenediaminetetraacetic acid

mitoxantrone	1,4-dihydroxy-5,8-bis[2-(2-hydroxyethylamino)ethyl-amino]anthracene-9,10-dione
$MOM_2$1	2,7-diformyl-1,8-bis(methoxymethoxy)naphthalene
PBS	phosphate buffered saline
PG	PicoGreen, [2-[N-bis-(3-dimethylaminopropyl)-amino]-4-[2,3-dihydro-3-methyl-(benzo-1,3-thiazol-2-yl)-methyl-idene]-1-phenyl-quinolinium]+
PMMA	polymethylmethacrylat
SYBR Green I	[2-[N-(3-dimethylaminopropyl)-N-propylamino]-4-[2,3-dihydro-3-methyl-(benzo-1,3-thiazol-2-yl)-methylidene]-1-phenyl-quinolinium]
tom	tri-iso-propylsilyloxymethyl
YOYO-1	1,1'-(4,4,7,7-tetramethyl-4,7-diazaundecamethylene)-bis-4-[3-methyl-2,3-dihydro-(benzo-1,3-oxazole)-2-methyl-idene]-quinolinium tetraiodide

Acknowledgments

First as a master and then a PhD student, I have spent five and a half years in the working group "Experimental Biophysics and Applied Nanoscience". All these years, I have been surrounded with so many lovely and amazing people. They have not only created an excellent and stimulating scientific environment, but also built a wonderful social atmosphere. Therefore, I am sincerely grateful for all the support they have given to me.

First of all, I would like to express my immense gratitude to my supervisor Professor Dario Anselmetti for giving me the opportunity to join his working group. His fantastic suggestions, his support and professional guidance were indispensable throughout my whole research process. I really appreciate him always motivating me to travel to conferences and to present the results of my work.

Secondly, I want to thank Professor Thomas Huser for appraising my thesis.

I am indebted to Dr. Volker Walhorn for his great coworking and amounts of meaningful discussions concerning my papers. I also owe him special thanks for proofreading my thesis. I very much appreciate the help of Dr. Katja Tönsing for proofreading my thesis and helpful discussions about my research. Without her chemistry knowledge, my work would have been much tougher. I also want to thank Christoph Pelargus and Helene Schellenberg. Their technical support has been very valuable.

I would like to thank all of my former and current colleagues for making working with them so enjoyable and for the exchange of knowledge and experience. Especially, I want to express my thanks to my office colleague Dr. Mareike Dieding. She has been willing to read my work at any time and has always been happy to give advice. I would like to thank Niklas Biere for designing the title page of my dissertation.

I am grateful to my parents for their constant support in all matters.

Finally, I want to thank my husband Dr. Martin Venker. I thank him for proofreading my thesis with a scientific perspective from another major and his support in all respects.

10.03.2017, Bielefeld